COMMISSION OF INQUIRY INTO THE AIR ONTARIO CRASH AT DRYDEN, ONTARIO

Final Report

Technical Appendices

The Honourable Virgil P. Moshansky
Commissioner

COMMISSION OF INQUIRY INTO THE AIR ONTARIO CRASH AT DRYDEN, ONTARIO

The Final Report consists of three volumes: I (Parts One–Four), II (Part Five), and III (Parts Six–Nine and the General Appendices); and this volume of Technical Appendices. The contents of volumes I, II, and III of the Final Report are found at the end of this volume.

COMMISSION OF INQUIRY INTO THE AIR ONTARIO CRASH AT DRYDEN, ONTARIO

Final Report

Technical Appendices

The Honourable Virgil P. Moshansky
Commissioner

CONTENTS

PREFACE

Independent research and analysis were conducted by Fokker Aircraft B.V., the manufacturer of the Fokker F-28 Mk1000 aircraft; and, with Fokker, by the Canadian Aviation Safety Board. On behalf of this Commission, research and analysis were carried out by individuals with expertise in the areas of aerodynamics, physics, meteorology, and psychology.

This volume of Technical Appendices contains the reports used by this Commission of Inquiry in analysing the performance of Fokker Aircraft F-28 Mk1000, C-FONF, during its last takeoff from Dryden Municipal Airport, on March 10, 1989. It also contains an analysis relating to the human factors aspects surrounding the accident. What follows is a brief description of each of the reports contained in this volume.

1 **Structures/Site Survey Group Report LP 38/89: Accident: Fokker F28, Mk 1000, Registration C-FONF, 10 March 1989 Occurrence No. 825-89-C0048: Canadian Aviation Safety Board**

The Structures/Site Survey Group Report was entered as Exhibit 484 through Mr James W. Hutchinson, chief, engineering analysis, Canadian Aviation Safety Board. It represents an analysis of the final flight path of the aircraft, a fire damage analysis of the aircraft wreckage, and the crashworthiness aspects of the accident. This report was spoken to by Mr Hutchinson during his testimony before this Commission on April 9, 1990.

2 **Fokker Aircraft B.V. Amsterdam, Fokker Aerodynamics, Report No. L-28-222: Note on the Aircraft Characteristics as Affected by Frost, Ice or Freezing Rain Deposits on Wings**

Fokker Aircraft Report No. L-28-222, dated December 16, 1969, was the result of wind tunnel tests and studies conducted by Fokker Aircraft dealing with the effects of sandpaper roughness on the wings of both jet- and propeller-powered aircraft. The report specifically describes the degradation in takeoff lift and acceleration characteristics of the F-28 aircraft caused by surface roughness on the wings due to contamination such as frost, ice, or freezing rain. This report was entered as part of Exhibit 532 and was spoken to by Mr Jack van Hengst, chief aerodynamic analyst, Fokker Aircraft B.V., during his testimony before this Commission on May 1, 1990.

3 **Fokker Aircraft B.V. Amsterdam, Report No. VS-28-25: Flight Simulator Investigation on the Take-off Performance Effects of Slush on the Runway and Ice on the Wings of a Fokker 100**

Fokker Aircraft Report No. VS-28-25 was the result of simulation flights conducted by Fokker Aircraft and Commission investigators using Fokker Aircraft's Fokker 100 engineering flight simulator, adjusted to approximate the flight characteristics of an F-28 Mk1000 aircraft. It summarizes Fokker's data and

findings used to assess the takeoff performance of a Fokker F-28 Mk 1000 aircraft with contamination on the aircraft wings and on the runway. The report was entered as Exhibit 544 and was spoken to by expert witnesses Mr Gary Wagner and Mr J. Murray Morgan, and by Mr Jack van Hengst, during their respective testimony before this Commission on May 4, May 3, and May 2, 1990.

4 A Report on the Flight Dynamics of the Fokker Mk 1000 as They Pertain to the Accident at Dryden, Ontario, March 1989

The flight dynamics report was researched and prepared by Mr J. Murray Morgan of National Aeronautics Establishment, National Research Council Canada; Mr Gary A. Wagner, Air Canada pilot, physicist, and aeronautical engineer; and Mr Richard H. Wickens, National Research Council Canada. The objective of the flight dynamics report was to develop a range of possible flight path scenarios in order to approximate that flown by C-FONF on its last flight, on March 10, 1989. The report contains an aerodynamic analysis to support simulation work and to provide background for the accident analysis and investigation. This report was spoken to by Messrs Wickens, Morgan, and Wagner during their respective testimony before this Commission on April 30, May 3, and May 4, 1990.

5 Wind Tunnel Investigation of a Wing-Propeller Model Performance Degradation due to Distributed Upper-Surface Roughness and Leading Edge Shape Modification

The report on propeller performance degradation is based on research conducted by Mr Richard H. Wickens and Mr V.D. Nguyen of the National Research Council Canada relating to the effects of performance degradation on propeller-driven aircraft due to wing contamination. This report was spoken to by Mr Wickens during his testimony before this Commission on April 30, 1990.

6 Freezing Precipitation on Lifting Surfaces

This report was prepared by Dr Myron M. Oleskiw of the National Research Council Canada to determine the effects of snow on the wings of aircraft C-FONF on March 10, 1989, and the possibility of snow turning to ice through such factors as adiabatic and evaporation cooling caused by airflow over the wing and the possibility of snow adhering to the wings due to wing surface cooling. This report was entered as Exhibit 521 and was spoken to by Dr Oleskiw during his testimony before this Commission on April 26, 1990.

7 Human Factors Aspects of the Air Ontario Crash at Dryden, Ontario: Analysis and Recommendations to the Commission of Inquiry

The human factors aspects analysis, prepared by Dr Robert L. Helmreich of the University of Texas, was based on the evidence and information before this Commission and on previous research in the area of human performance in flight operations. The report was entered as Exhibit 1270 and was spoken to by expert witnesses Dr Robert L. Helmreich, Dr Charles O. Miller, and Mr David Adams during their testimony before this Commission on December 17, 18, 19, and 20, 1990.

Appendix 1

Occurrence No. 825-89-C0048
Structures/Site Survey Group Report
LP 38/39
Accident: Fokker F28, Mk 1000, Registration C-FONF, 10 March 1989

Canadian Aviation Safety Board
Investigation Team:
J.W. Hutchinson, Structures Chairperson
J.E. Foot, Site Security and Survey Chairperson

Occurrence No. 825-89-C0048

STRUCTURES/SITE SURVEY

GROUP REPORT

LP 38/89

Accident: Fokker F28,Mk 1000
Registration C-FONF
10 March 1989

Structures Chairperson: _J.W. Hutchinson_
J.W. Hutchinson, P. Eng.
Chief, Engineering Analysis
Canadian Aviation Safety Board
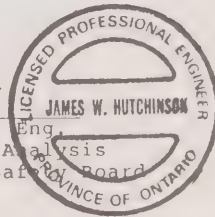
Site Survey Chairperson: _J.E. Foot_
J.E. Foot
Elec/Mech Engineering Specialist
Canadian Aviation Safety Board

TABLE OF CONTENTS

FIGURES

Figure 10– Tree model showing aircraft attitude as viewed from the front.

Figure 11– Infrared aerial photograph looking back along the wreckage trail towards the airport. The extent of the fire damage to the trees is represented by the darker coloured trees.

APPENDICES

Appendix A – Wreckage Catalogue (initial search)
Appendix B – Wreckage Catalogue (2nd ground search)
Appendix C – Wreckage Retrieval & Layout Reconstruction
Appendix D – Aircraft Flight Path Computer Reconstruction

1.0   INTRODUCTION

1.1   Fokker F28-Mk 1000, registration C-FONF crashed shortly
after take-off near the end of runway 29 from Dryden
Municipal airport, Dryden Ontario. The accident occurred
at 12:11 hours CST on March 10, 1989. The aircraft crashed
in heavily wooded terrain in one to two metres (m) of snow.
The aircraft was operated by Air Ontario on a scheduled
commercial flight (number 363) from Thunder Bay to Winnipeg
with a stop at Dryden. Of the 65 passengers and four crew
members on board, 22 received fatal injuries at impact and
two more severely injured passengers died later in
hospital.

1.2   The aircraft path was considered in three segments. The
first segment from the end of runway 29 for a distance of
726 metres (m), on a heading of 290 degrees magnetic. In
this segment the aircraft struck the tops of eighteen
trees, the first one being 126 m off the end of the runway.
The second segment is identified as the upper half of the
wreckage trail and represents the aircraft striking a
substantial number of trees near the top of a knoll and
begin its descent through the trees a further distance of
144 m remaining on approximately the same heading of 290
degrees. The third segment is identified as the lower half
of the wreckage trail and represents the aircraft making
primary impact with the ground and sliding about 80 m to a
stop against a stand of trees.

1.3   A three view drawing of the F28-Mk 1000 is depicted in
Figure 1 showing the general overall dimensions.

2.0   FINDINGS

2.1   The aircraft first contacted a single tree top 126 m off
        the end of runway 29 (293 magnetic), 3 degrees to the left
        of the runway centre line. The tree top was broken off at
        an elevation of 413.1 m above sea level (ASL). The
        elevation at the end of runway 29 is 413 m ASL.

2.2   The aircraft clipped the tops of eighteen trees over the
        next 600 m prior to striking a substantial number of trees
        near the top of a knoll. The heights of the broken tops of
        all the trees contacted between the first tree and the top
        of the knoll remained relatively constant at 413 metres
        (+-1.5 m).

2.3   The aircraft descended into the trees, cutting a swath for
        224 m in length. The terrain elevation at the top of the
        knoll was 404 m and sloped downwards to 390 m ASL.
        Aircraft wreckage was scattered along the entire swath of
        cut trees. The majority of the wreckage came to rest at a
        Latitude of 49 degrees 45 minutes 11 seconds and Longitude
        92 degrees 46 minutes 8 seconds (UTM 5520300 N, 516650 E).

2.4   The initial pieces of wreckage found consisted of pieces of
        the red lens cap from the rotating beacon, which was broken
        off the belly of the fuselage. These pieces were found in
        the vicinity of the first tree strike off the end of runway
        29.

2.5   The next pieces of wreckage were located at the main tree
        strikes and consisted of the left wing tip, main landing
        gear doors (MLG) and pieces of the radome. The majority of
        the fuselage, right wing and the empennage stayed
        relatively intact until the aircraft came to rest.

2.6   Approximately 50 m after contacting the more heavily treed
        area, a fire developed which traveled down the length of
        the wreckage trail and culminated in the almost total
        destruction of the cockpit and fuselage area aft to the
        rear pressure bulkhead. The empennage and engines were
        superficially sooted and remained relatively unburnt.

2.7   All major control surfaces, doors, and hatches were found
        in the main wreckage scatter zone. Except for the MLG
        doors the remaining doors and hatches were determined to be
        in the closed and locked position prior to impact.

2.8   It was determined that the landing gear was in transit up
        when major tree contact occurred.

2.9   Reconstruction of the wreckage and examination of the
        break-up patterns showed that they were consistent with
        either tree or ground impact damage.

2.10   The initial evidence of fire was noted to be approximately 50 m after the aircraft struck trees at the top of the knoll which was consistent with the rupturing of the left fuel tank. There was no evidence of an in-flight fire prior to the aircraft striking the trees.

3.0   WRECKAGE SURVEY AND BREAK-UP SEQUENCE

3.1   During the ground searches carried out as part of the
          on-site investigation, most pieces of aircraft wreckage
          were located, tagged, assigned an item number and staked.
          The majority of these pieces were identified with
          assistance from the manufacturer and the operator of the
          aircraft. In some cases, when a number of pieces of
          wreckage were found in close proximity to each other, they
          were grouped together under the same item and stake number.
          The position of each stake was then surveyed by ground
          survey and incorporated into a wreckage distribution plot
          shown in Figure 2. A Wreckage Catalogue listing the
          wreckage items surveyed along with a brief description is
          contained in Appendix 'A'. A second ground search was also
          carried out in May 1989 when the ground was clear of snow.
          A number of wreckage pieces were found and tagged. The
          locations of these items relative to the accident site were
          then recorded using a standard police grid search method.
          The Wreckage Catalogue in Appendix 'B' identifies the
          location along with a brief description all of the pieces
          of wreckage found during the second ground search.

3.2   During the second search phase, numerous pieces of the red
          lens from the rotating beacon were found just beyond the
          first tree strike, 126 m off the end of Runway 29. This
          beacon is normally mounted on the belly, in the centre of
          the fuselage, just aft of the main landing gear inboard
          doors. Figures 3 and 4 show the location of the rotating
          beacon on the belly of the fuselage of another F28, C-FONG.
          Figure 5 shows the numerous pieces of the broken red lens
          recovered from the vicinity of the first tree strikes. All
          other pieces of wreckage found during the second search
          were located within either the upper or lower part of the
          wreckage trail.

3.3   As the aircraft began striking a substantial number of
          trees near the top of the knoll, the aircraft started to
          receive major structural damage. The wreckage distribution
          plot (Figure 2) shows to scale the location of all the main
          pieces of wreckage recovered.

3.4   Among the first items recovered near the top of the knoll
          were the left and right outboard main landing gear (MLG)
          doors, both essentially intact, and various pieces of both
          inboard MLG doors, including the gear access panels. The
          inboard MLG doors are normally stowed when the gear is
          either fully up or down. When the gear is selected up after
          take-off, the inboard gear doors will open down and in,
          hinged to the fuselage at the inboard end of the doors.
          They will remain open while the gear is in transit. Due to
          the location of these doors near the beginning of the

wreckage trail, it is considered that they were open when
the aircraft entered the trees. The nature of the impact
damage to the MLG doors was consistent with them having
been opened normally, as opposed to being forced open due
to tree strikes, etc.

3.5   A review of the wreckage distribution shows that as the
aircraft proceeded through the trees, it shed most of its
left wing in the upper half of the wreckage trail, due to
impact damage with trees. Near the top of the knoll, on the
left side near the start of the wreckage trail, the left
wing tip navigation light holder and a small piece of the
red lens were found. Only the stub section of the left wing
inboard from lift dumper (spoiler) #2, remained attached to
the fuselage structure after the aircraft came to a stop.
The lift dumpers are numbered 1 to 5 on each wing from the
inboard end outward.

3.6   Sections of all the major control surfaces were accounted
for at the wreckage site between the top of the knoll and
where the aircraft finally came to a stop. Found along the
wreckage trail were sections of the left elevator, the left
inboard and outboard flaps and sections of the flap leading
edge vanes, the flap shroud doors, the left aileron and
trim tab, and lift dumpers 3, 4, and 5 from the left wing.
The remaining control surfaces, including the majority of
the right wing were found still attached to the fuselage
structure, or in close proximity to the main wreckage.
Figure 6 shows an aerial photograph of the main wreckage
trail with overlays depicting the outline of the tree cut
swath (overlay 1), an outline of the tree fire damage
(overlay 2), location of wreckage items identified as
coming from the left wing or left elevator (overlay 3),
location of wreckage items identified as coming from the
main and nose landing gear doors (overlay 4).

3.7   The main wreckage consisted of three major pieces. There
were two major breaks in the fuselage, one just aft of the
main passenger door, and the second through the fuselage
at approximately seat row 12. The first major piece of
wreckage consisted of the tail section, which was facing
forward on the right side and approximately in line with
the lower half of the wreckage trail. The vertical fin and
both mounted engines were essentially intact. The complete
speed brake assembly (doors, frame, support structure) had
separated from the tail of the aircraft and was found in a
reversed position just behind the tail section. The right
horizontal stabilizer and elevator were intact. The left
elevator had separated from the horizontal stabilizer and
the tip of the stabilizer had been torn away. The main
section of fuselage between the two major breaks was turned
approximately 130 degrees to the left with respect to the

tail section. The right wing had remained attached to the
fuselage structure until it came to rest, and became
partially separated during the post-impact ground fire. The
cockpit section forward of the break had rotated a further
90 degrees to the left with respect to the fuselage, such
that the main wreckage formed an approximate 'U-shape'.

3.8   Reconstruction and examination of the wreckage are detailed
in Appendix 'C'.

4.0   AIRCRAFT PATH

4.1   The aircraft flight path was reconstructed based upon the
physical evidence of the clipped tree tops and the location
of wreckage. A total of eighteen tree tops were clipped
starting at 126 m from the end of runway 29. Pieces of the
red lens from the rotating beacon were found adjacent to
the first tree. The position and elevation of the eighteen
clipped trees were determined during the ground survey and
recorded in UTM co-ordinates and heights ASL. The tree
positions were then plotted on a Dryden Site Plan (Figure
7) and the heading was determined to be 290 degrees
magnetic based on the fact that the aircraft had to contact
each tree. The aircraft maintained this heading or ground
track for 600 m until it came into contact with a
substantial number of trees at the top of a small knoll. A
profile (Figure 8) of the flight path showed that the
elevation of the eighteen tree tops remained relatively
constant at 413 m (+- 1.5 m).

4.2   The attitude of the aircraft as it passed through the
eighteen trees prior to the major tree strike was
reconstructed using computer modeling to scale of the
aircraft and the cut trees. Appendix 'D' depicts the
aircraft attitude at the various locations along the
flight path. The flight path was estimated based on the
location of the first pieces of wreckage found (rotating
beacon red lens) and the possible positions of the aircraft
required to strike all eighteen trees. The assumption was
made that the aircraft was not yawed, that is, its heading
and ground track remained essentially constant. The
accuracy of the aircraft attitude varies with the number of
trees cut at any one time and the attitudes depicted are
considered to be the best possible fit.

4.3   The cut tree canopy starting at the top of the knoll was
documented by aerial photography in conjunction with the
deployment of numerous target blankets. The target
blankets were surveyed and tied into the original UTM
co-ordinate system. Photogrammetric analysis of the aerial
photographs determined the position of each of the
individual cut trees in terms of UTM co-ordinates and their
height ASL. A scale model (1:72) of the cut trees, over
the first 45 m through the tree canopy, was built based
upon this survey information, to determine the aircraft
attitude at this point. A model aircraft (1:72) of an
F-28-3000 was obtained for this purpose. A model 1000 was
not available but the only difference between the two is
that the 3000 model has a 1.5 m longer wing span; all other
dimensions are the same. Flaps were scaled and glued onto
the model aircraft at the 25 degree position. This
position had been determined from the examination of the

flap track screw jacks. Landing gear was scaled and added
to the model in the full down position. It had been
determined that the gear was in transit at this time but
the exact location had not been determined.

4.4   The aircraft was then fitted to the cut tree model which
showed that the aircraft was in a left bank (angle between
the lateral axis of the aircraft and the horizontal
estimated to be 7 degrees (+- 2 degrees) which increased to
15 degrees over the next 45 m. This was consistent with
the pieces of left wing located in this area. There was no
distinct path which would indicate that the main landing
gear was fully extended at this point. The aircraft pitch
angle (angle between the longitudinal axis of the aircraft
fuselage and the horizontal) was determined to be nose-down
approximately 1-3 degrees. This appeared to remain
relatively constant over the next 45 m. Figures 9 and 10
show the model depicting the aircraft as it entered the
tree canopy at the top of the knoll.

4.5   As the aircraft proceeded into the trees at the top of the
knoll it began to receive major structural damage,
primarily to the left wing. The width of the swath cut
through the trees was about 20 - 25 m, but began to narrow
to about 12 m, which indicates that the aircraft continued
to roll to the left and finally impacted the ground
predominantly on the left side. The primary ground impact
was at about 144 m from the top of the knoll. The aircraft
then yawed to the left with the right wing dropping and the
aircraft sliding about 80 m to a stop against a stand of
trees.

5.0   CRASHWORTHINESS

5.1   FIRE DAMAGE

The initial pieces of wreckage that exhibited fire damage,
were items number 11, outboard wing leading edge and number
12, LH piece outboard wing structure containing a hot-air
anti-ice exhaust louvre and part of the fuel tank (Appendix
'A'). Both items were found in close proximity to each
other on the left side of the wreckage trail approximately
50 m from the first major tree strikes near the top of the
knoll. Both items exhibited small areas of superficial
charring and sooting and were adjacent to burnt trees. The
remaining pieces of wreckage from this point forward until
the main wreckage all exhibited some form of burn damage
such as charring or sooting. It appears that as the left
wing started to break apart fuel was lost and was ignited
almost immediately. The ignition point of the fuel was not
determined but may have been the result of electrical
arcing as the wires in the wing were torn out or by fuel
vapours being ignited by the engines. The ensuing fire
traveled or followed the aircraft path until the aircraft
finally came to rest. The post crash fire was confined to
the trees down and adjacent to the wreckage trail with
many of the trees exhibiting superficial charring. Figure
11 is an infrared aerial photograph showing the wreckage
trail looking back towards the airport. The use of
infrared photography clearly displays the fire damage to
the trees as depicted by the outline of darker coloured
trees.

The fuselage from the interior of the cockpit back to the
rear pressure bulkhead was gutted by post crash fire.
Although the fuselage was gutted the fire appeared to have
been more intense on the left side than the right. This is
based upon the observation that part of the right side of
the fuselage (containing the overwing exit and nine
windows) was still in place and the exterior paint scheme,
although charred, was still recognizable. The exterior
nose of the aircraft was relatively free of fire damage.
The cockpit floor was burnt away revealing the remains of
the nose gear and steel belts from the tires. The left
side of the instrument panel was completely burnt out
whereas the centre (engine panel) and right panel were
relatively intact although they were also burnt and
physically damaged. The engines, tail section and
empennage exhibited superficial sooting and the interior of
the tail section was in good condition.

There was no evidence of an in-flight fire prior to the
aircraft striking the trees near the top of the knoll.

F28 ENGINEERS GUIDE
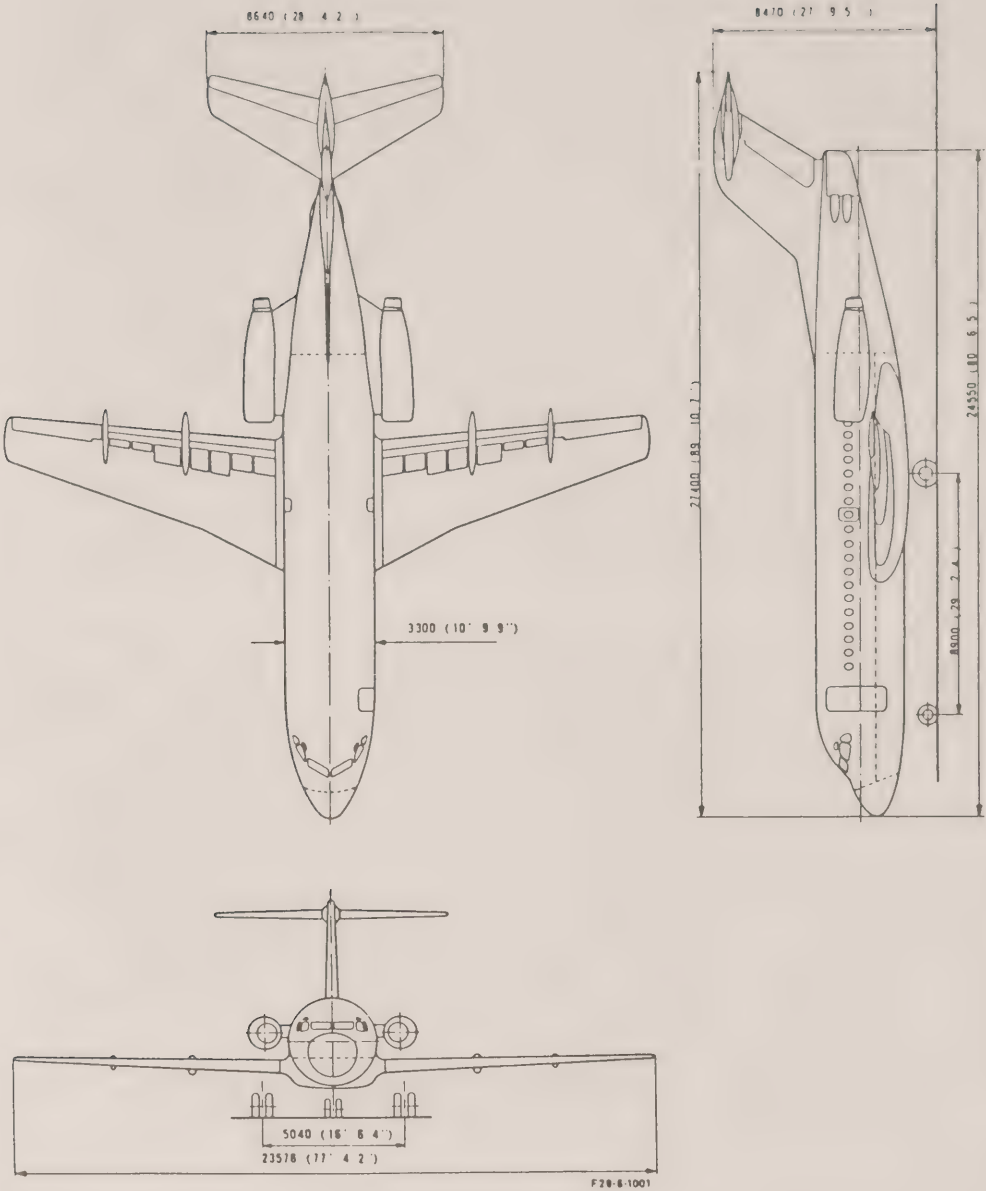
FIG. 1   GENERAL ARRANGEMENT

Figure 2

Wreckage Distribution Plot

Tree Cut Outline
Main Wreckage Trail
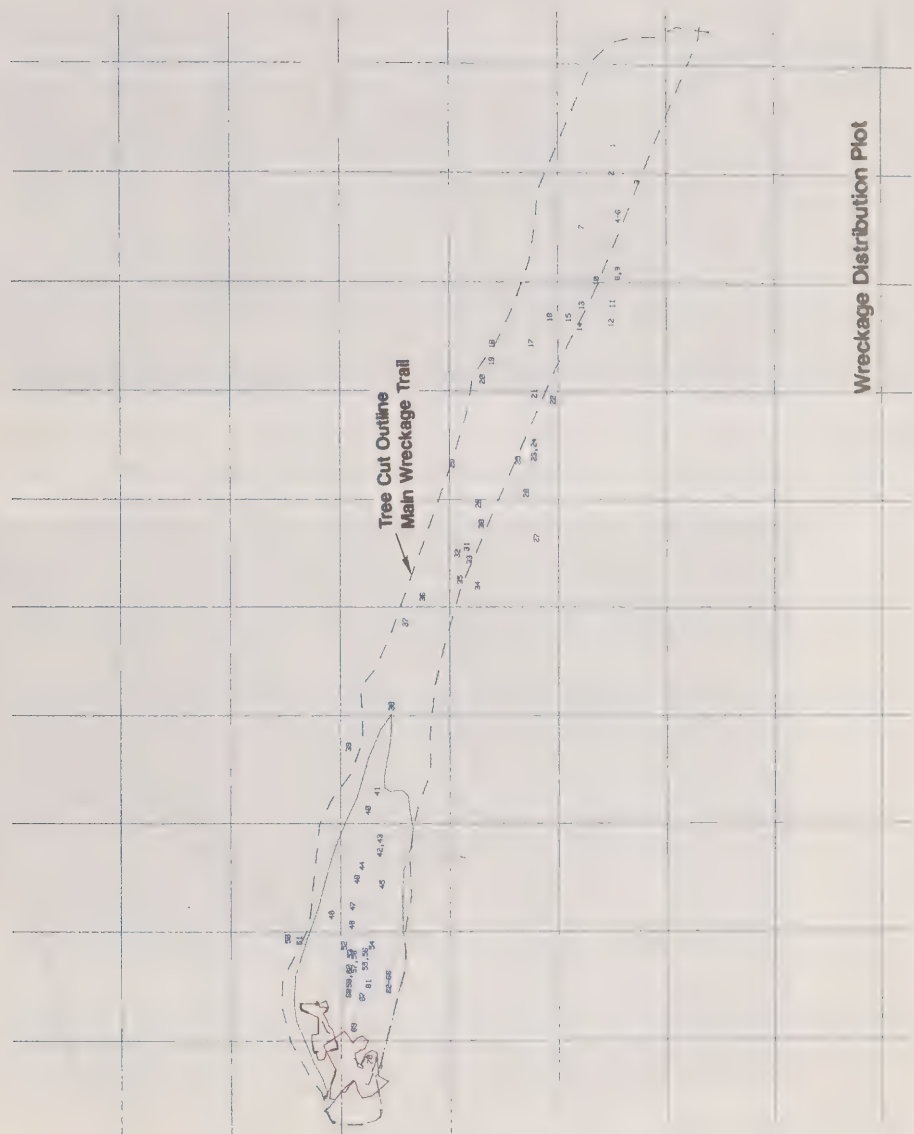
Figure 3 - **View of Fokker F28, C-FONG, showing the location of the anti-collision light mounted on the fuselage belly (arrow).**

Figure 4 **- As in Figure 3, close-up view.**

Figure 5 - Photo of all the pieces of the red lens from the anti-collision light recovered from the vicinity of the first clipped trees off the end of Runway 29.
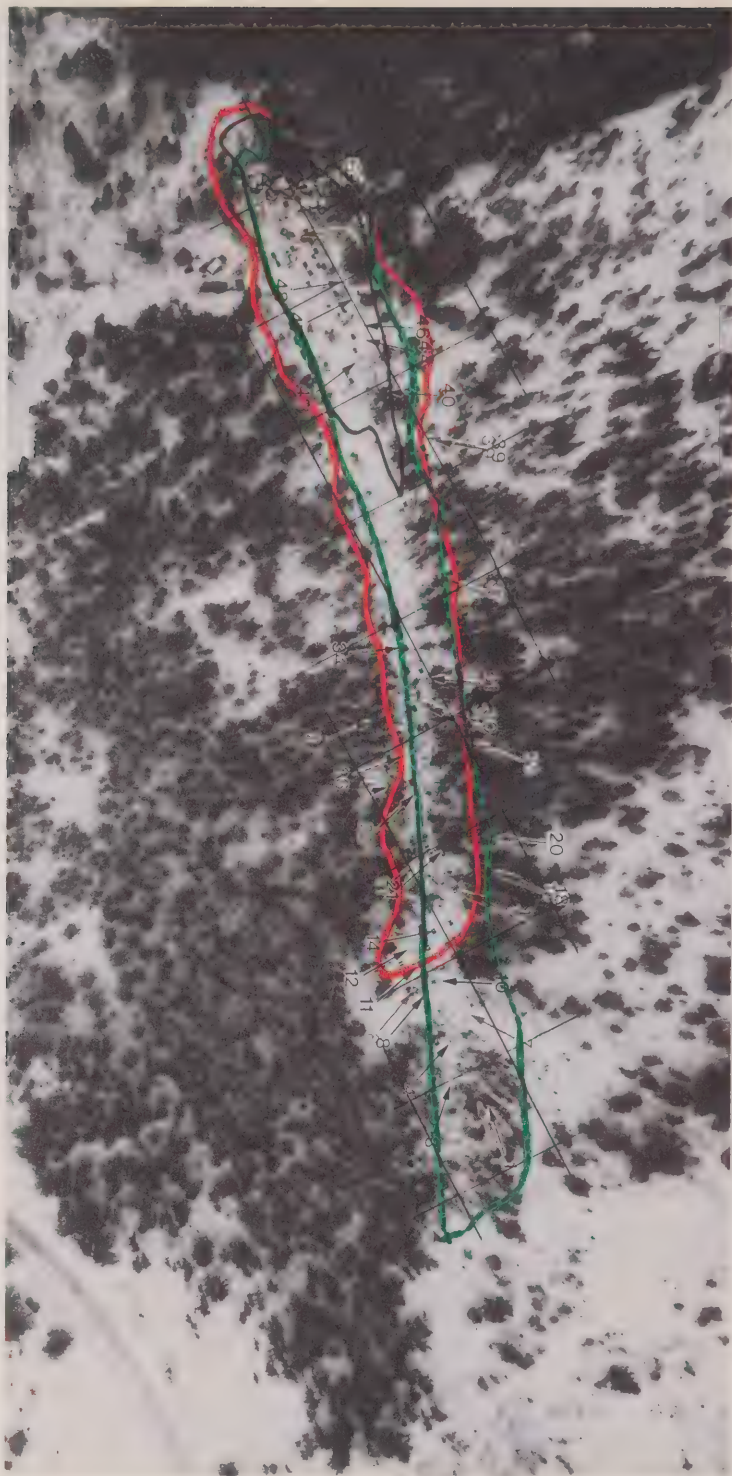
Figure 6

Overlay 1: Tree Cut Swath

Overlay 2: Tree-Fire Damage

Overlay 3: Left Wing and Left Elevator

Overlay 4: Main and Nose Landing Gear Doors

Figure 7

TREE STRIKES ●

Figure 8

Aircraft Flight Path Profile

Tree Strikes : ●

RED LENS

RNY

RNY

25m

250 m

FIGURE 9

FIGURE 10

Figure 11

Tree Fire Damage

WRECKAGE CATALOGUE   APPENDIX 'A'

ITEM #   DESCRIPTION

1   A) RH inboard main landing gear
                  (MLG) door.
               B) Small piece red lens cover from
                  left Nav light amoung freshly broken
                  spruce branches.
               C) ADF Sense antenna.

2   A) RH outbord (MLG) door P/N A11440-420,
                  S/N CH 52.

3   A) Piece of LH wing leading edge
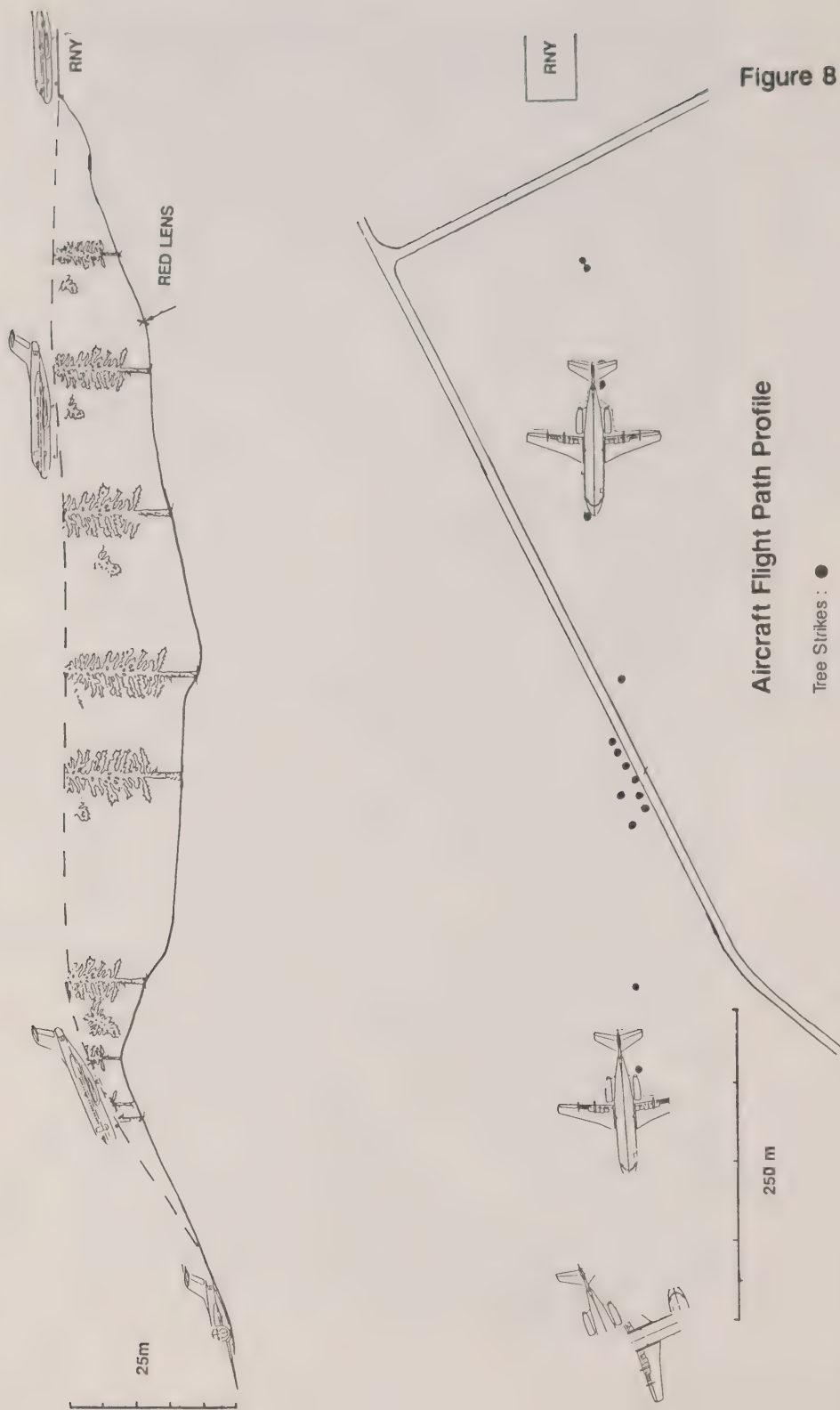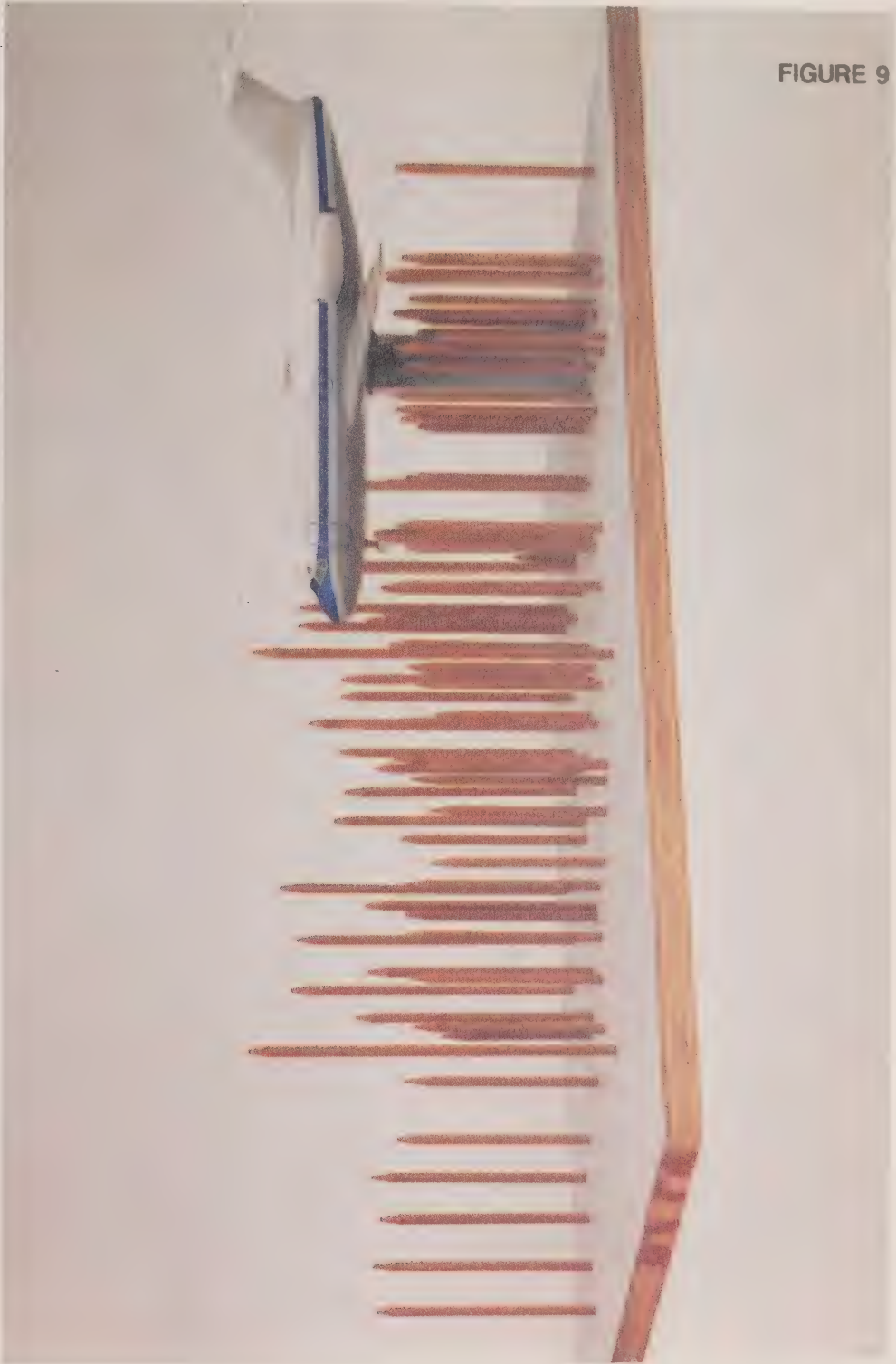   P/N A143124401.
               B) Left wing tip navigation light
                  holder.

4   A) Piece of LH wing tip structure with
                  static discharge wick.
               B) Piece of leading edge duct for
                  anti-ice.

5   A) LH wing tip piece (trailing).

6   A) Extendable light (flare or taxi
                  light).
               B) Wing ribs/stringers.

7   A) LH inboard gear access door (red on
                  inside) 2 pin latches in "out"
                  position

8   A) LH outboard MLG door A11440-423.
               B) Piece of wing skin.

9   A) LH wing skin.

10   A) LH outboard wing structure with
                  aileron fitting. Number 75F stenciled
                  on panel. Top panel exhibits black
                  strip with "Ne pas Marcher" written
                  on it. Access panel numbered "1" for
                  fuel quantity probe.

11   A) LH outboard wing structure.

12   A) LH outboard wing structure number 75E
                  contains outboard aileron hinge
                  and flux valve.

– A2 –

13   A) Piece wing leading edge A12430-001.

14   A) Mid section of LH aileron and aileron
                               tab.
                            B) Vent float valve.

15   A) Stringers.
                            B) Piece wing skin.
                            C) Piece of radome.

16   A) VHF comm. antenna.

17   A) RH inboard MLG access door.
                            B) Piece of radome

18   A) Section of LH inboard MLG door.

19   A) Top centre piece of nose above
                               radome.

20   A) LH outboard end of aileron (number
                               83W).

21   A) Section of LH inboard MLG door.
                            B) LH wing fence.

22   A) Piece of wing fence.
                            B) Stringers.

23   A) Piece of wing skin – fuel cell.

24   A) Middle section of LH outboard flap
                               vane.

25   A) Piece of wing leading edge with heat
                               duct.
                            B) Piece of radome.

26   A) Section of LH wing skin with access
                               panel numbered 5. Fuel quantity
                               probe.

27   A) Piece of wing skin with inboard end
                               rib (fuel cell).

28   A) Part of flaptrack fairing (1 of 8).
                            B) Piece of wing skin.

29   A) RH nose gear door with number 281,
                               (see item #305 Appendix B for LH
                               door)
                            B) Glideslope antenna.
                            C) Pieces of radome.

– A3 –

30	A) Outboard flap with flap vane.
	B) Piece of lower wing skin.
	C) Section of RH inboard MLG door
31	A) Inner aft shroud door of LH flap.
	B) Piece of wing skin.
32	A) Landing light.
	B) Flap track fairing.
33	A) Inner forward shroud door of RH flap
	B) Pieces of wing skin.
34	A) Pieces of wing skin, fuel cell area.
35	A) Flap fairing.
	B) Wing panel, A-frame support.
36	A) Piece of wing skin.
	B) Oil service door.
37	A) Section of RH MLG door
	P/N A11320-4LP, S/N 5H51.
	B) Drive cap.
	C) Air valve temperature sensor.
	D) Piece wing skin – fuel cap number 4.
	E) Bellcrank W.S. 8056.
38	A) Piece of trailing edge of wing
	number 52B.
	B) Landing light.
39	A) Flap shroud panel – 2 pieces outer
	O/B aft L.H.
	B) Small piece of LH nosegear door, red
	number 28.
40	A) LH outboard flap track with trailing
	edge wing structure and inboard
	section of aileron and trim tab.
	B) Trailing edge upper wing fairing flap
	with abrasíve strip and shroud door
	damper.
41	A) Piece fuselage skin with green
	insulation.
	B) Piece wing skin.
42	A) LH inboard flap track canoe.
	B) Piece of radome.
43	A) LH inboard flap track with section of
	wing structure attached.

– A4 –

44
A) Mid section of LH inboard flap vane.
B) Piece of flap fairing.
C) Piece of engine nacelle.
D) LH lift dumper #4 (counting from inboard out).
E) Leading edge of horizontal stabilizer A03507-401, S/N 066.

45
A) Piece of wing skin number 52E, 50C, 45A.
B) Piece of leading edge of LH stabilizer P/N A03507-401, S/N 066.
C) Support flap – A-frame.

46
A) Inner and outer forward shroud doors from LH outboard flap.

47
A) Piece of LH elevator P/N A04-001-415, S/N 064.
B) Piece of engine cowling.

48
A) LH Wing structure with #5 lift dumper attached.
B) Flap rod torque tube.
C) Fuel quantity transmitter.

49
A) Piece of flap.
B) Main wheel well structure.

50
A) Transmitter and pressure switch, located in wheel well.

51
A) Piece of tail cone.

52
A) Engine cowling and lock.

53
A) Leading edge of wing root.

54
A) Piece of fuselage skin with antenna mount.

55
A) Lower fuselage skin P/N A128 30-401.

56
A) Engine fuel drain.

57
A) Piece of wing skin.

58
A) Shroud door bellcrank.

59
A) Skin with number 91L.

60
A) Wing fillet skin-lift dumper line.

– A5 –

61   A) LH inboard flap with flap vane (mid section of vane missing).

62   A) ADF loop antenna.

63   A) Bell

64   A) Seat frame.

65   A) Static inverter P/N 601698-2.

66   A) Piece of cabin floor.

67   A) Piece of engine support beam carry-through P/N 13103003-2.

68   A) Piece of engine cowl.

69   A) LH inboard wing structure with lift dumper #3 attached.

70   A) Main wreckage.

FOKKER F-28, C-FONF
2ND GROUND SEARCH
WRECKAGE SURVEY

In May 1989, after the snow had melted from the ground, a ground
search was carried out with the assistance of an OPP Search and
Rescue Team and three members of the CASB Investigation Team.

A datum line was established from the end of runway 29 through the
centre of the accident site to the edge of the beacon road, on a
heading of 290 (see survey drawing).

Two search paths were laid out, one north of the datum (North Team)
and one south of the datum (South Team). The first search was from
the beacon road eastward to the airport fence, with the return
search westward back to the beacon road. Each search path was
approximately 15 metres wide, with the total search width about 60
metres wide.

Item locations were identified by distance measured along datum
line from point 0,0 at the edge of the beacon road, and distance
north or south of datum line. Items 200-223 located north of datum,
items 300-322 located south of datum. All measurements in metres
translated from the standard OPP grid search method of Tally's and
Paces, where;

                63 paces   = 1 tally
                10 tallys = 1 kilometre
                (average pace estimated to be 1.3 metres)

– B2 –

ITEM #	IDENTIFICATION	LOCATION
200	Skid control valve, Ass'y # 9543466	118, 9 (NORTH)
201	Skid control valve, Unit # 9542718	134, 14
202	Structure w/door lock bar	140, 13
203	Wing structure	166, 7
204	Skid control valve (see item 200)	169, 12
205	Right I/B skid control gen. drive	169, 9
206	Piece of door hinge	177, 9
207	Small piece of casting	177, 4
208	Small AC induction motor	192, 9
209	Torque tube	211, 12
210	Small piece of structure	216, 13
211	Pressure transmitter P/N 3567645-3701	220, 12
212	Hydraulic valve	248, 5
213	Small bracket	270, 7
214	Lift dumper hydraulic accumulator	282, 9
215	Low inertia motor	324, 9
216	Fuel guage transmitter P/N 391067-06098	334, 4
217	Piece of trailing edge aileron (6"x6")	346, 3
*	Group of tree tops knocked off	282, 0
218	Pieces of red lens (anti-collision light, lower)	772, 5 785, 5
219	Pieces of red lens (anti-collision light, lower)	841, 9 865, 0

-------------------RETURN SWEEP-------------------------

220	AC motor	260, 20
221	Access panel 95A	231, 17
222	Access panel frame 95D	213, 21
223	piece of wing skin	165, 21

– B3 –

ITEM #	IDENTIFICATION	LOCATION
300	Piece of wing panel (burned)	143, 3 (SOUTH)
301	Piece of wing structure	143, 5
302	Service door 21A (fwd of nose gear bay)	155, 14
303	AC motor & landing light G/B see #220	158, 6
304	weather radar unit P/N 2067568-0501	176, 7
305	Section of LH nose gear door	200, 2
306	Tube	222, 0
307	Small gearbox	229, 1
308	Electrical conector	235, 6
309	Landing light pot	242, 3
310	Fuel guage transmitter 391057-06097	283, 7
311	small bushing	298, 9
312	Fuel tank supply fitting	306, 0
313	Pieces of landing light glass	458, 6
314	Piece of ADF antenna	486, 0
315	Pieces of red lens (anti-collision light, lower)	686, 6
316	Pieces of red lens (anti-collision light, lower)	780, 0
317	Pieces of red lens (anti-collision light, lower)	792, 0

-------------------------RETURN SWEEP-------------------------

318	Piece of fuel tank w/cap	402, 21
319	Piece of engine structure	272, 26
320	Tube fitting	216, 14
321	Servo motor	185, 18
322	Servo motor	172, 0
323	Aircraft manual	109, 20

WRECKAGE RETRIEVAL AND

LAYOUT RECONSTRUCTION

A.   RETRIEVAL

Upon completion of the site survey, all of the wreckage
along the wreckage trail was retrieved and slung out of the
site by helicopter to a secure area at Dryden airport,
where it was loaded onto enclosed trailers, sealed and
shipped by rail to the CASB Engineering Lab in Ottawa. The
remaining pieces of the main wreckage required some
sectioning to allow removal from the site by truck. The
main fuselage was separated by a longitudinal cut through
the middle section of the floor. The right stabilizer and
elevator were separated from the vertical fin, as was the
reamaining section of the left stabilizer. Both engines had
already been removed from the aircraft by the Powerplants
Group and removed from the site.

The nose section of the aircraft, both halves of the
fuselage, the right wing , the tail section and sectioned
pieces of the stabilizer were removed from the site by
truck and shipped to Ottawa by rail.

B.   LAYOUT RECONSTRUCTION

FUSELAGE

All of the wreckage was sorted and a partial reconstruction
of the major pieces was carried out. In this manner, the
break-up patterns and fire damage could be examined, and
all major components of the fuselage and wings could be
identified. The tail section was essentially intact, and
although the cockpit area was gutted due to post-impact
fire, it was roughly in one main piece. A general photo of
the burned out cabin area of the fuselage is shown in
Figure C-1.

LEFT WING

The wreckage of the left wing is shown laid out in Figure
C-2. The middle and outboard left flap tracks were
recovered from the wreckage trail, but the flap screw jack
for the middle track was not recovered. The mounting points
where the middle screw jack was attached to the track were
examined. There was evidence of severe impact damage to the
track adjacent to the rear mounting point and the mounting
bracket was found to have failed due to overload. The
translating nut had broken in two due to overload and the
front mounting point was deformed due to bending. These
failures allowed the screw jack to separate from the track.
The middle flap track (survey item #43) was found near the

bottom of the wreckage trail adjacent to a large
outcropping of rocks. It is considered that the screw jack
likely separated from the track due to impact with the
ground at this point, and was projected forward, becoming
buried under the snow and debris near the main wreckage.
During the retrieval of the main wreckage, this area was
cleared away to the edge of the wreckage zone and the screw
jack may have been trapped in the debris at this time.

RIGHT WING

The right wing is shown laid out in Figure C-3. The right
wing was found essentially in its proper orientation in the
field on the right side of the aircraft where it had come
to rest. Much of the destruction to the right wing occurred
due to the post-crash ground fire. All the major control
surfaces of the right wing were identified.

PASSENGER/EMERGENCY AND CARGO DOORS

There is one main passenger door, located on the forward
left side of the aircraft, and a service/emergency door on
the forward right side (Refer to Figures C-4 and C-5). The
passenger door is hinged at the bottom and is kept closed
by a latching mechanism which has two hook latches in the
door lintel engaging into the latch fittings of the door.
The door was found in place, still attached to the
fuselage. Both hook latches had separated from the door
lintel due to fire damage, but they were recovered and
found in the locked position. The service/emergency door is
a plug-type door which is kept in the closed position by
four wedge -shaped latch pins engaging into holes recessed
into the door aperture. The door was found free of the
fuselage, but was recovered in the immediate vicinity of
the main wreckage. The four latch pins were in the out
(locked) position. Both of these doors were damaged due to
impact and fire.

There are two cargo doors, both on the right side, one on
the lower forward fuselage and one on the lower aft
fuselage (Refer to Figures C-6 and C-7). Both cargo doors
are hinged at the bottom to the main structure and both
were found still attached by their hinges. The doors are
normally held in the closed position by two hook latches
engaging onto latch fittings in the door lintel. For the
forward cargo door both latch hooks were still on the door
in the locked position, although the door lintel had been
destroyed by the fire. The forward half of the rear cargo
door was consumed by fire as was the door lintel. One latch
hook was still attached to the door and was found in the
locked position. The other latch hook had separated, but
was also found in the locked position.

- C3 -

There is one over-wing emergency exit window on each side
of the aircraft at seat row 8. Only two small pieces of
exit window were recovered (Figure C-8), both pieces found
in the main wreckage zone. Although not determined
positively, both pieces were likely from the same exit
window on the right side of the aircraft. The remainder of
the right exit window, as well as the left exit window,
were most probably consumed by the post-impact ground fire.

LANDING GEAR DOORS

Most pieces of the nose gear doors, and the left and right
main gear doors were identified. Figures C-9, C-10 and C-11
show the doors laid out during reconstruction.

Fuselage view from rear showing burnt out cabin area.

Wreckage of left wing laid out during reconstruction

Figure C-3

Wreckage of right wing laid out during reconstruction

Figure C-4

Main Passenger Door

Figure C-5

Service/Emergency Door

Figures C-6, C-7

Right Front Cargo Door

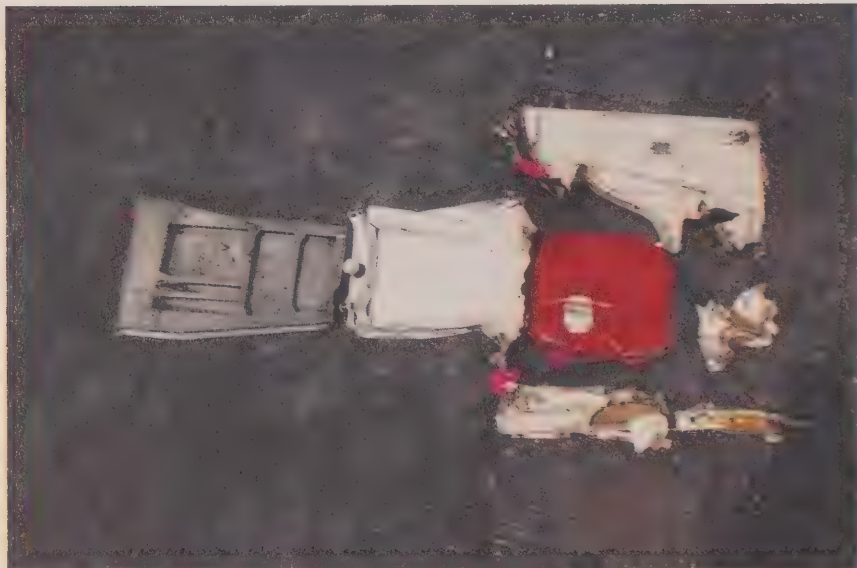**Right Rear Cargo Door**

Figures C-8, C-9

Exit Window

Nose Gear Doors and Service Doors 21A, 23A, 24A

Figure C-10, C-11

Left Main Gear Door

Right Main Gear Door

Appendix D
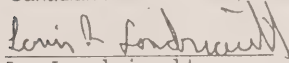
Occurrence No. 825-89-C0048
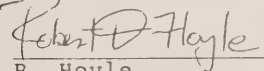
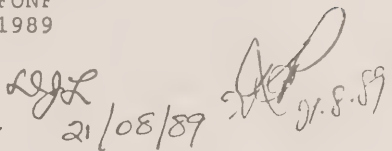FLIGHT PATH RECONSTRUCTION REPORT

LP 97/89

Accident: Fokker F-28-1000
Reg. # C-FONF
10 March 1989

Prepared by:

M.R. Poole, P.Eng.
Superintendent, Computer Systems Engineering
Engineering Branch
Canadian Aviation Safety Board

R. Hoyle,
Computer Scientist/Analyst
Engineering Branch
Canadian Aviation Safety Board

L. Landriault,
Systems Manager/Technologist
Engineering Branch
Canadian Aviation Safety Board

1.0   INTRODUCTION

1.1   On Friday, March 10, 1989, a Fokker F28 (C-FONF)
        crashed in a wooded area shortly after take-off.

1.2   In support of the overall investigation, a three-di-
        mensional flight reconstruction was requested by the
        Engineering Branch technical coordinator for the Dry-
        den Accident. The flight reconstruction associated
        with this paper is depicted on standard VHS video
        tape (reference LP097/89). The video tape depicts a
        few sample views chosen to demonstrate the recon-
        struction.   It should be realized that any desired
        view (including witness location views) can easily be
        generated.

1.3   Normally, flight reconstructions of this nature are
        based largely on flight recorder information. As no
        flight recorder data was available, the reconstruc-
        tion was based on a review of the witness statements,
        the physical evidence of the trees cut by the air-
        craft on its trajectory, and past flight recorder
        data for this particular aircraft (reference LP040/97
        - Flight Recorders Group Report).

1.4   The runway and surrounding geographical information
        were modeled in UTM grid coordinates from maps and
        photographs of Dryden Municipal Airport. Tree data
        was input as supplied by the Site Survey Group for
        the Dryden accident. Figure 1 shows an overall view
        of the airport and trees.

1.5   The F-28 aircraft was modeled from engineering draw-
        ings provided by Fokker.

1.6   It is important to note that this reconstruction de-
        picts an approximation of the aircraft's flight path
        and behavior from the limited data available.   The
        results are qualitative and should not be used for
        quantitative analysis. Any conclusions based on this
        reconstruction should be reviewed in light of the
        manner in which the reconstruction was produced.

2.0   INVESTIGATION

2.1.0   Assumptions for the Reconstruction

2.1.1   In order to reconstruct the estimated flight path,
the following basic assumptions were made:

1   The aircraft does not begin to rotate until
3400 feet of distance (taxi-way alpha) based on
witness statements.

2   The aircraft reaches Vref (126 knots indicated
air speed as determined by the Operations
Group) at 3400 feet of consumed runway (con-
stant acceleration) and continues at Vref for
the remainder of the flight.

3   The first rotation is at a 'typical' pitch rate
based on previous flight data from C-FONF. The
pitch attitude is allowed to reach 13 degrees.
Thirteen degrees represents the maximum pitch
attitude the aircraft may have reached
(reference Performance Group Report).

4   At 13 degrees of pitch attitude the aircraft is
rotated back down to an arbitrary attitude of
five degrees. This was done so that the air-
craft had two noticeable rotations as per wit-
ness statements.

5   The aircraft is then rotated for the second
time to 11 degrees of pitch attitude (consis-
tent with Performance Group scenarios).

6   The aircraft reaches an altitude of six feet
during the first rotation and ten feet during
the second rotation. Both altitudes are com-
pletely arbitrary.

7   The aircraft does not yaw or drift throughout
the flight.

8   All tree cuts represent the point at which the
aircraft contacted the tree. In other words,
the trees did not bend or break off at a point
lower than the point of contact.

9   The breakup sequence is not considered in the
final group of trees.

10   The trees do not affect the flight path of the
aircraft due to the relative mass of the air-
craft and that of the trees.

– 3 –

11   The flaps were set at 25 degrees for the
        purpose of fitting the aircraft through the
        trees. (refer to the Systems Group Report).

12   The landing gear was assumed to be in the down
        position (refer to Structures Group Report).

- 4 -

2.2.0   Take-off Roll

2.2.1   The constant acceleration required to accelerate the
aircraft to Vref at 3400 feet was determined as fol-
lows:

Vref = at
d = 0.5 at^2
Hence,   212.5 ft/s = at
            0.5 at^2 = 3400 ft

            0.5 (212.5)t = 3400 ft
            t = 32.0 s

            a = 212.5 ft/s /32.0 s
            a = 6.64 ft/s/s (.21 g)

2.2.2   Take-off fifteen (LP040/89) had an average accelera-
tion of approximately .25 g. Higher take-off weight
and runway slush would contribute to the lower ac-
celeration level calculated above.

2.3.0   Tree-cut Path and Attitude Determination

2.3.1   A linear regression was initially fit through the x-y
tree location data.   The aircraft was then placed
along this regression path at discrete locations
(Figure 2).   At each discrete location, a fit of
roll, pitch, and altitude were attempted. In some
cases, it was required to move the aircraft slightly
off the regression to obtain a good fit. A smooth
spline was then fit through the refined locations, as
well as the take-off roll. This spline was then used
as the flight path.   This spline produced a smooth
curve from the time the aircraft was assumed airborne
during the second rotation to the heading determined
from the regression through the trees.

2.3.2   In general, roll attitudes were more apparent than
pitch attitudes due to the fact that pitch is in the
same direction as the direction of flight.   It was
discovered that a number of different fits were pos-
sible, especially during the first tree locations
where there were very few trees. In general, the
solutions which yielded the least attitude deviations
from level flight were chosen to estimate the flight
path.

2.3.3   The attitudes and altitude (with respect to the mean
         runway elevation) for each of the eight fit locations
         were determined as follows (figures 3 through 10):

Location	Time (sec)	Roll (degrees)	Pitch (degrees)	Altitude (feet)
1(see note)	47.2	6.4	5.5	-1.3
2	48.6	-1.1	5.5	2.0
3	50.0	6.0	5.5	-2.3
4	53.2	6.4	3.1	-5.5
5	56.2	-10.1	-1.0	-10.8
6	56.3	-10.3	-1.3	-10.5
7	56.4	-10.5	-1.3	-11.1
8	56.5	-13.9	-3.6	-10.5

Note: For the first location, it was reported that
the anti-collision light on the belly of the aircraft
was   struck off by one of the two trees.   Due to the
geometry of the aircraft, the aircraft would have to
have been pitched up a least 5.5 degrees such that
the nose gear would clear the top of the clipped
tree.   If the aircraft were level, for instance, the
nose gear would have clipped the tree and the tree
would have then been too short to hit the anti-col-
lision light.

– 6 –

2.4.0   Data Generation Summary

2.4.1   A graphical representation of the ground velocity, heading, roll, pitch and altitude data used in the reconstruction is shown in Figure 11.

2.4.2   Once the reconstruction is generated, the 'camera' positions, perspectives and orientations the computer system can generate are infinite. Typical orientations are chase plane views, cockpit views and fixed views in space. Since the witness locations were plotted in the reconstruction, it was possible to place the observer at a witness location to view the sequence. A 'knob box' input device allowed the user to rotate the observer's head from left to right or up and down. This view revealed the relative size of the aircraft, given the distances involved. In general, views generated from the witness locations demonstrated that the aircraft would have been difficult to see due to the distances involved, even in the best of environmental conditions.

2.4.3   The tree-fit data where available was considered more reliable than witness information. The physics and geometry of the circumstances of the Dryden accident do not allow for a great deal of flexibility in the reconstruction. For example, the aircraft could not have reached much altitude when clearing the end of the runway in order to hit the first trees and continue on a fairly flat altitude. Similarly, roll and pitch attitude rates are generally limited by the mass and consequent momentum of the aircraft.

2.4.4   The positive pitch attitudes determined through the initial trees correlate with the relatively flat altitude history. A positive pitch attitude would likely have been required to maintain the altitude displayed through the trees.

3.0   EVALUATION

3.1   The flight reconstruction represents an approximate
        depiction of the aircraft's flight path and attitudes
        during the accident sequence. The reconstruction is
        based on the physical evidence of the tree strikes,
        witness information and past empirical flight re-
        corder data.

3.2   For the purposes of this flight reconstruction, wit-
        ness information was considered very subjective and
        qualitative. The physical evidence of the tree
        strikes was considered to have relatively good re-
        liability. The data provided many possible flight
        attitudes. In general, attitudes were chosen which
        deviated the least from level flight. The recon-
        struction should therefore be viewed with caution.
        Any conclusions drawn based on the flight recon-
        struction should be made with full cognizance of its
        method of production, assumptions and approximations.
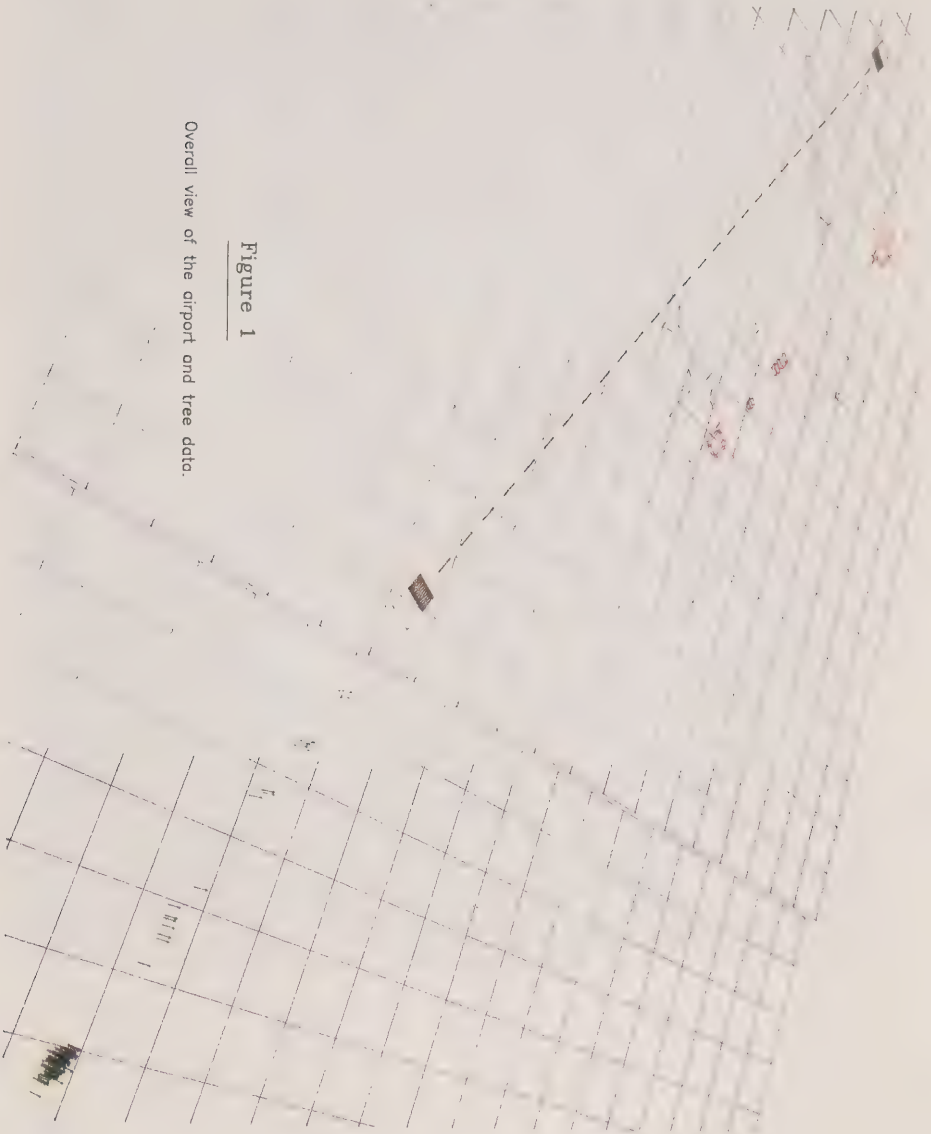
Figure 1

Overall view of the airport and tree data.

Tree Group No. 5
Time: 56.2 sec
Altitude: -10.8 ft
Roll: -10.1 deg
Pitch: -1.0 deg

Tree Group No. 6
Time: 56.3 sec
Altitude: -10.5 ft
Roll: -10.3 deg
Pitch: -1.3 deg

Tree Group No. 7
Time: 56.4 sec
Altitude: -11.1 ft
Roll: -10.5 deg
Pitch: -1.3 deg

Tree Group No. 8
Time: 56.5 sec
Altitude: -10.5 ft
Roll: -13.9 deg
Pitch: -3.6 deg

Tree Group No. 4
Time: 53.2 sec
Altitude: -5.5 ft
Roll: 6.4 deg
Pitch: 3.1 deg

Tree Group No. 3
Time: 50.0 sec
Altitude: -2.3 ft
Roll: 6.0 deg
Pitch: 5.5 deg

Tree Group No. 2
Time: 48.6 sec
Altitude: 2.0 ft
Roll: -1.1 deg
Pitch: 5.5 deg

Tree Group No. 1
Time: 47.2 sec
Altitude: -1.3 ft
Roll: 6.4 deg
Pitch: 5.5 deg *

Figure 2

Tree cut path and attitude determination locations.
Note: All altitudes are measured with respect to the mean
runway elevation at Dryden Municipal Airport which
is 1353 feet above sea level.

* — denotes minimum pitch angle at 47.2 seconds.
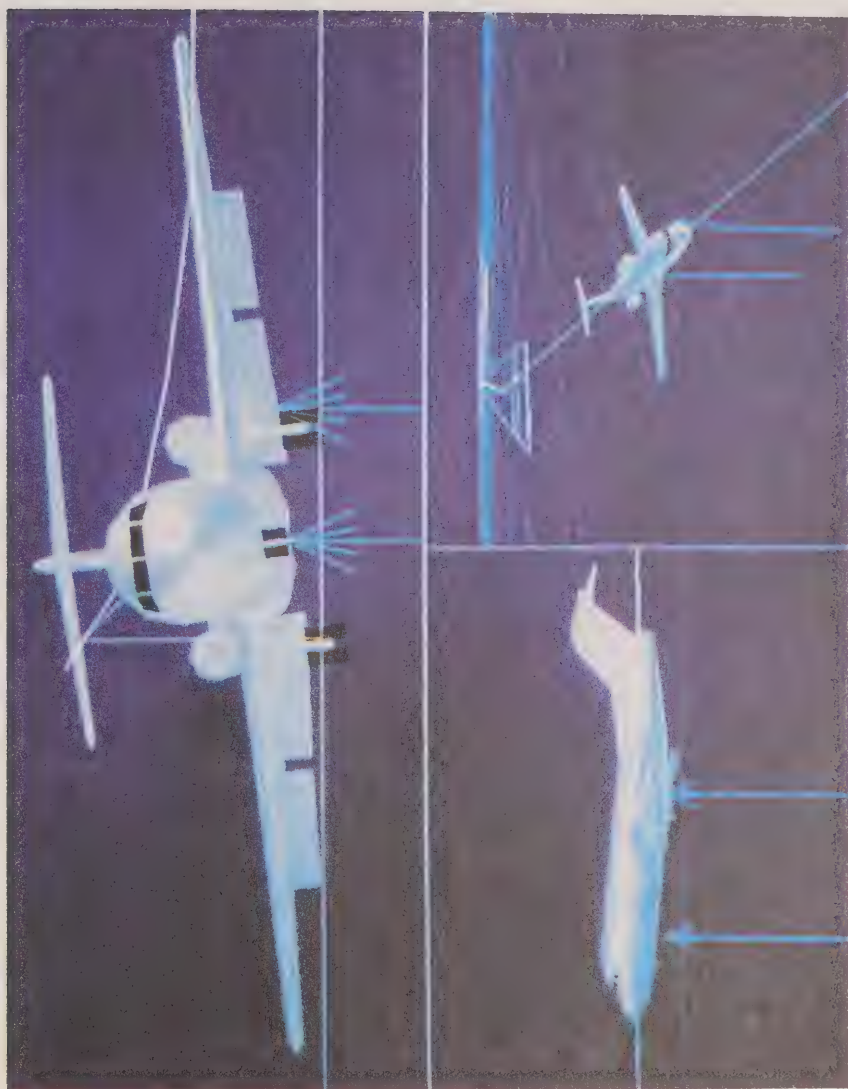
Figure 3 – Fit at location 1.

Figure 4 - Fit at location 2.

Figure 5 – Fit at location 3.
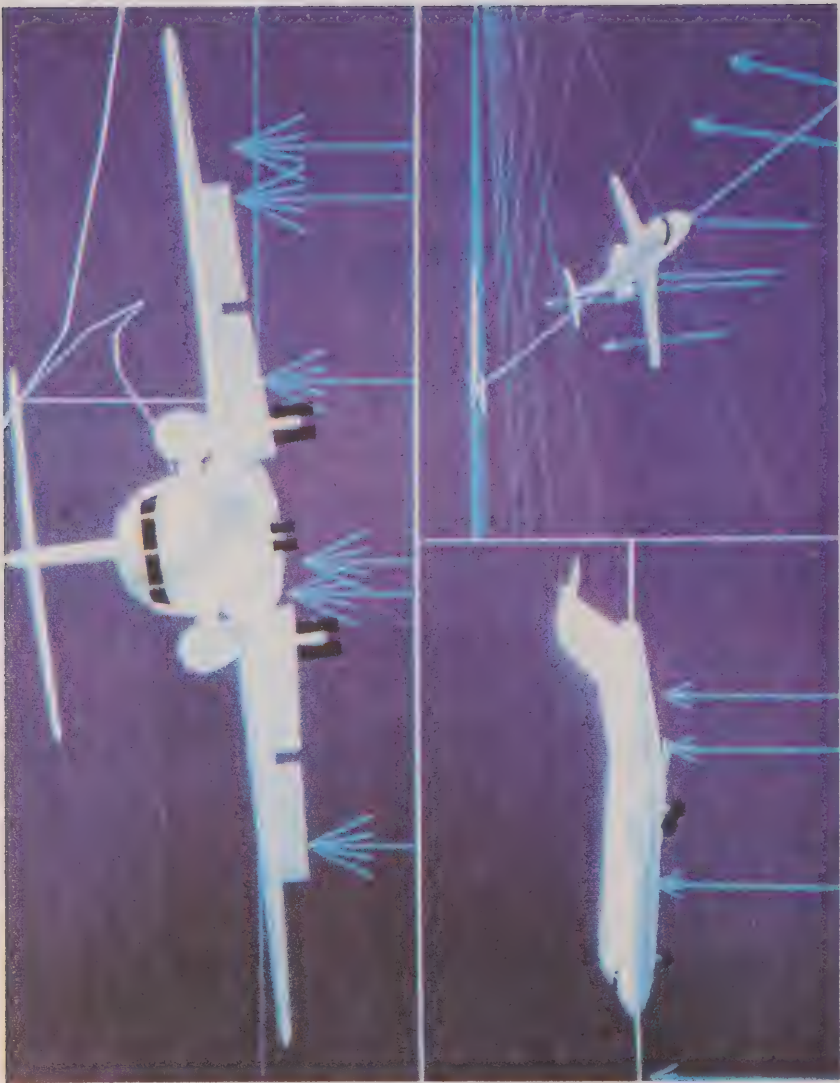
Figure 6 – Fit at location 4.

Figure 7 – Fit at location 5.

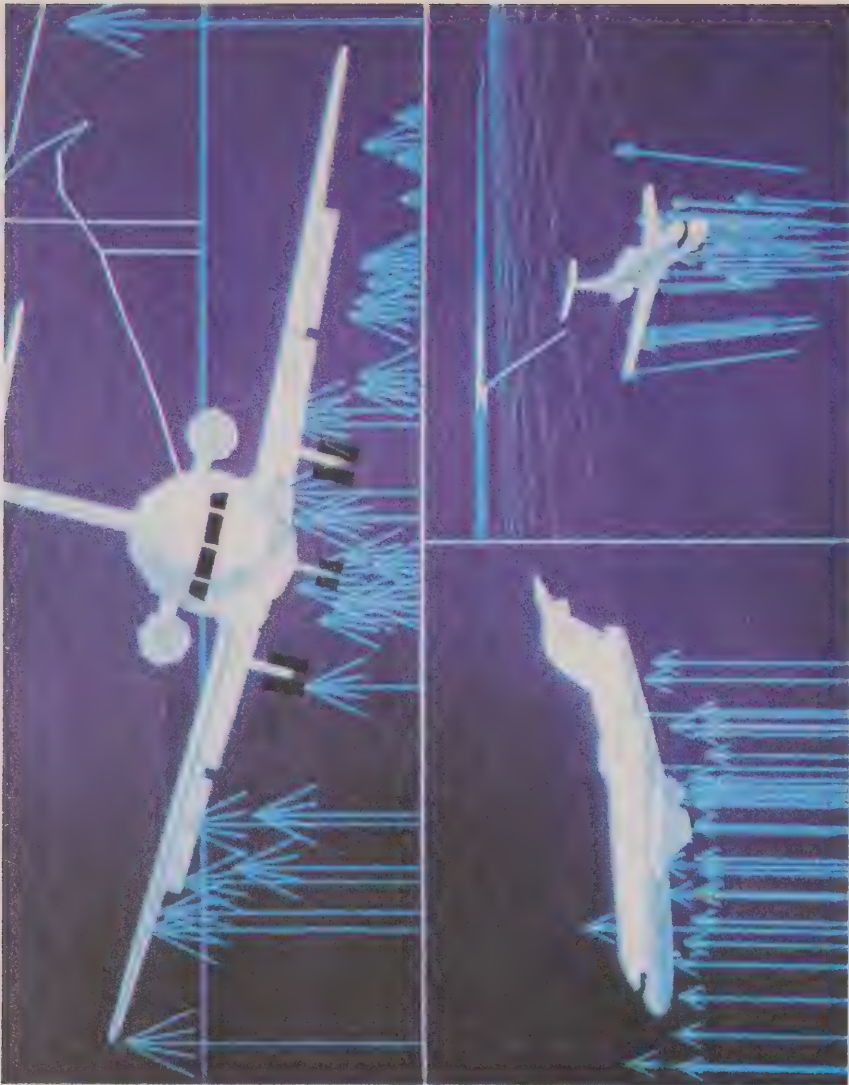Figure 8 - Fit at location 6.

Figure 9 - Fit at location 7.

Figure 10 - Fit at location 8.

CFONF Estimated Velocity, Heading, Attitude and Altitude vs. Flight Time

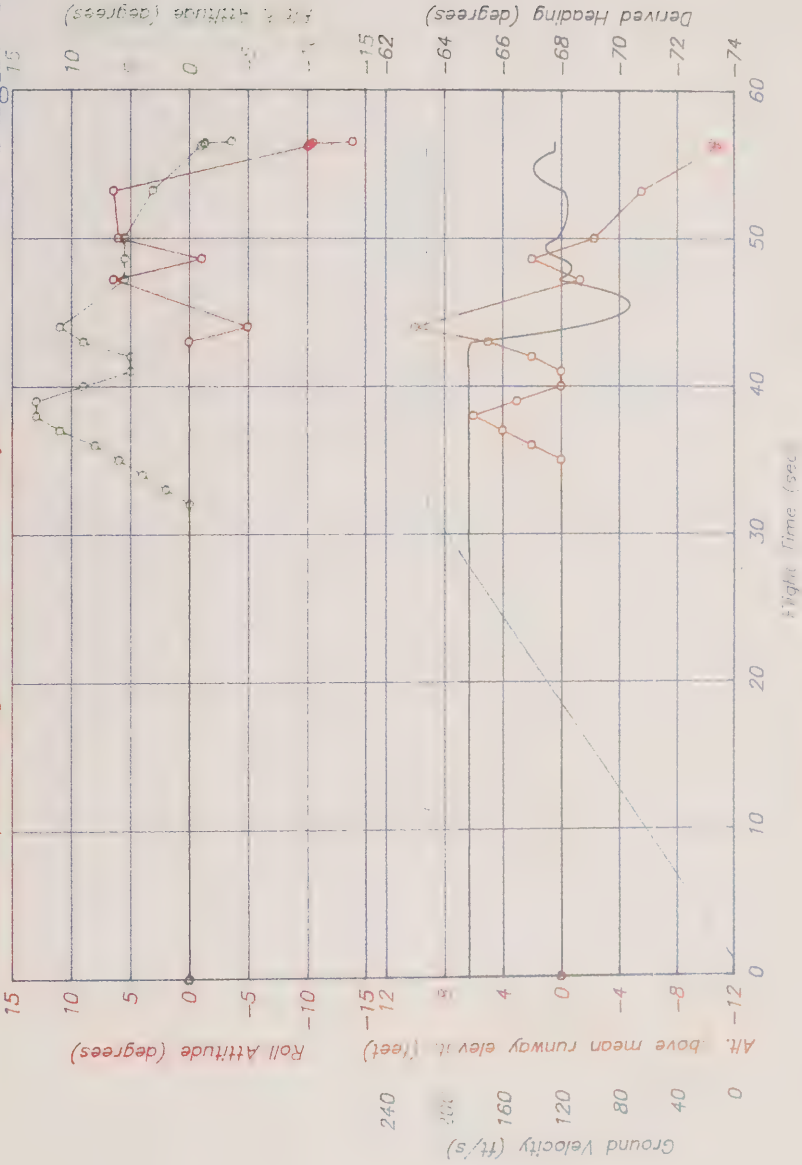— based on previous flights and tree–cut analysis

Figure 7.6

Appendix 2

Fokker Aircraft B.V. Amsterdam
Fokker Aerodynamics
Report No. L-28-222
Note on the Aircraft Characteristics as Affected by
Frost, Ice or Freezing Rain Deposits on Wings

December 16, 1969

N.V. KONINKLIJKE NEDERLANDSE VLIEGTUIGENFABRIEK FOKKER
ROYAL NETHERLANDS AIRCRAFT FACTORIES FOKKER
SCHIPHOL-ZUID   THE NETHERLANDS

RAPPORT ÷ REPORT

AFDELING DEPARTMENT Aerodynamics Department	**RAPPORT NR. REPORT NR.** L-28-222
DATUM DATE December 16th, 1969	**RUBRICERINGS KODE CLASSIFICATIONS CODE** RK

ONDERWERP ÷ SUBJECT   Note on the aircraft characteristics as affected by frost, ice or freezing rain deposits on wings.

SAMENVATTING ÷ SUMMARY

OPGESTELD ÷ PREPARED

Ir. Tj. Schuringa

J.H.D. Blom

GEZIEN ÷ APPROVED

J.H.D. Blom

GEKONTROLEERD ÷ CHECKED

AANTAL BLADEN ÷ NUMBER OF PAGES 1 + 7	**HERZIENINGS-NR ÷ RE-ISSUE NR.** **DATUM ÷ DATE**	**KOPIE AAN ÷ COPY TO**
FORMAAT ÷ SIZE A4 = 8		
A3 =		
A2 =		
A1 =		
FOTO NRS. ÷ PHOTO NRS.	**WIJZIGINGEN ÷ REVISIONS** **DATUM ÷ DATE**	
TEKENING NRS. ÷ DRAWING NRS.		

Introduction

Generally, it is well known that the contamination of
the wing and tail of parked aircraft by snow
produces a potential hazard during take-off and subsequent
flight. It is, therefore, a wisely accepted practice
to remove snow prior to take-off. However, the effects
of thin layers of deposits, resulting from e.g. frost
or light freezing rain, are often not considered to be
detrimental to the take-off characteristics.

This Note deals with these deposits, which create
some sort of sandpaper like roughness on the wing
upper surface. Firstly a general discussion is given,
secondly the take-off characteristics as
affected by precipitation will be discussed. The
Note closes with a conclusion.

1. Take-off lift as affected by sandpaper wing roughness

The effect of thin deposit layers on wing surfaces
causing sandpaper-like roughness can be shown by
comparing the lift characteristics of a contaminated
wing with those of a clean wing.

In figure 1 the relationship is depicted between lift
and incidence of a clean, thus non-contaminated wing.
The amount of lift to get the aircraft off the ground
at the lift-off speed, V_{LOF}, is less than the maximum
lift which the wing is able to deliver. This reserve
in lift is ensured by the airworthiness Requirements
on Performance used during the certification of the
aircraft.
During the take-off run the aircraft will rotate up
to an incidence at which the lift is sufficient to
get the aircraft off the ground. In the case of a
jet aircraft, see lower curve in figure 1, this occurs
at point A ensuring an incidence reserve against the
stall incidence by the margin a.

For the case of the same wing being used on a propeller
driven aircraft with the same T.O.W., this incidence
reserve is much greater as the propeller slipstream
increases the wing lift. In both cases, however, the
V_R-, V_{LOF}- and V_2-speeds are based on the same power-off
conditions.

For a typical case of a propeller driven aircraft, see upper curve in figure 1, the lift curve shows lift-off at point B and an incidence reserve against stalling of margin b.

In figure 2, which is based on windtunnel tests simulating the full scale frost or light freezing rain type roughness on the windtunnel model, a considerable reduction is shown in both maximum lift capability and stall incidence of a contaminated wing compared with the clean wing in figure 1.

The propeller aircraft, lifting off at the same incidence, B, has a considerably reduced reserve against stalling; the margin b in figure 1 is reduced to margin b' in figure 2. This situation will however escape notice in flight, at least with all engines operating, as the behaviour of the aircraft is essentially the same as with a clean wing. This is more the case as the difference in wing drag due to the assumed roughness will not be critical under these conditions.

The jet aircraft, however, will be in a stalled condition when it is rotated up to and beyond the incidence at point A. Consequently, it will show characteristics quite different from those at a "normal" take-off.

2. Take-off characteristics

In figure 3 the effects of "sandpaper" roughness on take-off characteristics are shown in more detail. The graphs of lift versus incidence and versus aerodynamic drag are based on windtunnel and flight tests of the F-28. Windtunnel tests show that comparable jet aircraft suffer similar lift and drag penalties due to the same type of roughness.

When the aircraft is rotated at V_R the body angle of incidence does not normally exceed approximately 8 degrees, leaving a 3 degrees reserve before stickshaker activation and approximately 5.5 degrees before the maximum lift is reached. This latter corresponds with a flight condition out of ground proximity.. When on the other hand "sandpaper" roughness is present on the wing top surface the probability of encountering a wing stall at the normal maximum incidence of 8 degrees is rather high. This depends somewhat on type and extent of the frost roughness.

The wing stall developed under these conditions
is particularly dangerous because the inherent
good stalling characteristics of the clean wing
are lost. An uncontrollable roll accompanies the
asymmetric stall provoked by roughness, and
in addition a tremendous increase in drag develops
upon slight overrotation of the aircraft. The
latter is very likely to happen in ground
proximity when the aircraft does not appear to
gain its customary height.
Both effects are further illustrated in figure 5.

The F-28 wing is designed for a slow progression
of flow separation towards the wing tip with
increasing incidence, thus ensuring perfect roll
control throughout a stall test manoeuvre. The
uncontaminated wing shows initial local separation
at the stickshaker incidence, 11 degrees angle of inci-
dence , the maximum lift is reached at 13 to 14
degrees angle of incidence and flow separation does
not affect roll control until an incidence of 20
degrees is reached.
In ground proximity with the main wheels in light
touch with the ground the maximum angle of incidence
which could be tested, without tail scrubbing,
was 15 degrees.
At this angle the flow separation was still
restricted to the area inboard of the kink in the
wing leading edge and perfect roll control was
preserved.
With frost roughness present on the wing upper
surface the characteristic of slow stall progression
towards the wing tip is lost and uncontrollable roll
may develop at angles of incidence as low as 10 degrees,
as indicated in the left graph of figure 5.
In the right graph of figure 5 the effects of
roughness on drag are illustrated. The drag of the
clean wing is such that the aircraft is capable of
climbing away at the required climb angle at V_2 with
one engine inoperative. In the case of a contaminated
wing the drag may, however, be doubled due to a wing
stall which occurs at an angle of incidence only slightly
greater than that for stickshaker operation.
Consequently, acceleration is lost even with all
engines operating at T.O. power.

Conclusion

In the interest of flight safety complete removal
of relatively thick layers of snow and ice from
wing and tail surfaces is very common.
However, also sandpaper-like roughness caused by
thin deposits due to frost or light freezing rain
must be completely removed prior to take-off, in
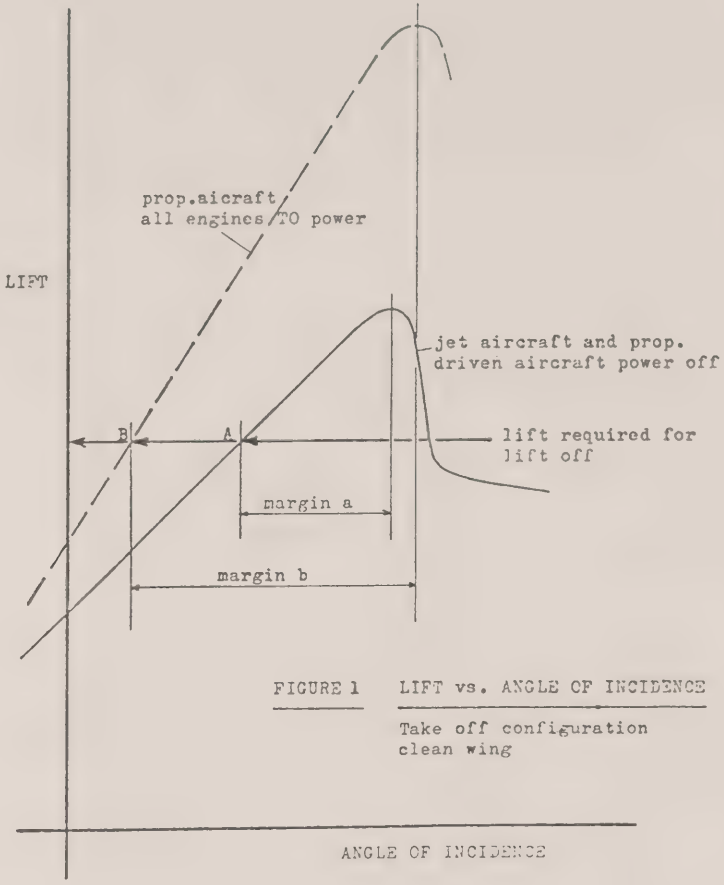particular of jet propelled aircraft.

LIFT

prop.aicraft
all engines TO power

jet aircraft and prop.
driven aircraft power off

lift required for
lift off

B   A

margin a

margin b

FIGURE 1   LIFT vs. ANGLE OF INCIDENCE

Take off configuration
clean wing

ANGLE OF INCIDENCE

FIGURE 2   LIFT vs. ANGLE OF INCIDENCE

Take off configuration
"sandpaper" roughness on
wing top surface

LIFT
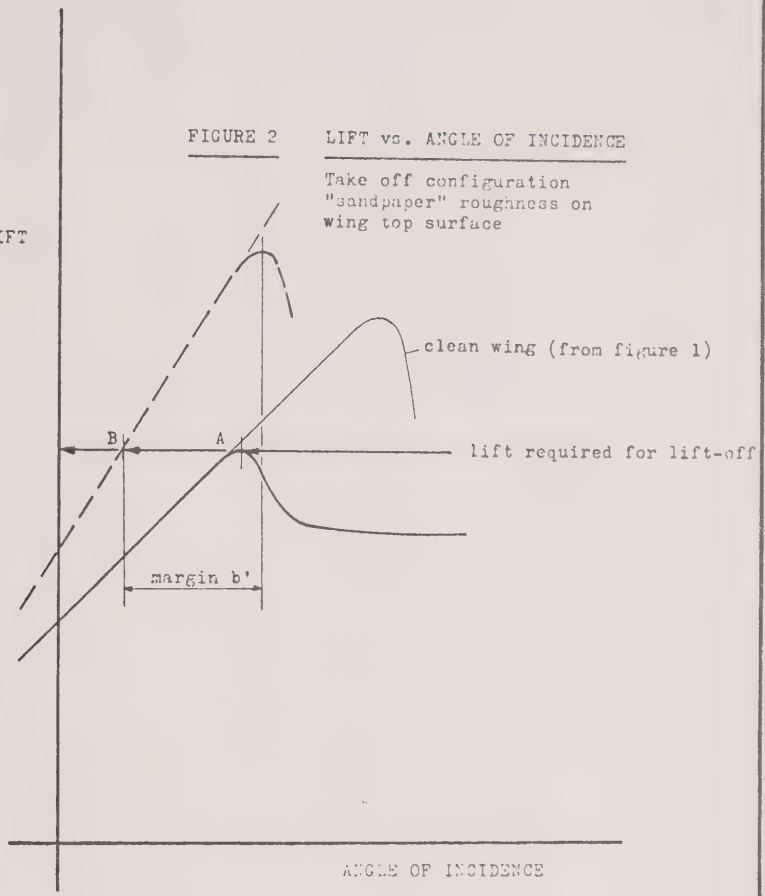
clean wing (from figure 1)

B   A   lift required for lift-off

margin b'

ANGLE OF INCIDENCE

FIGURE 3   FOKKER F28   EFFECT OF "SANDPAPER" ROUGHNESS ON TAKE OFF/CLIMB
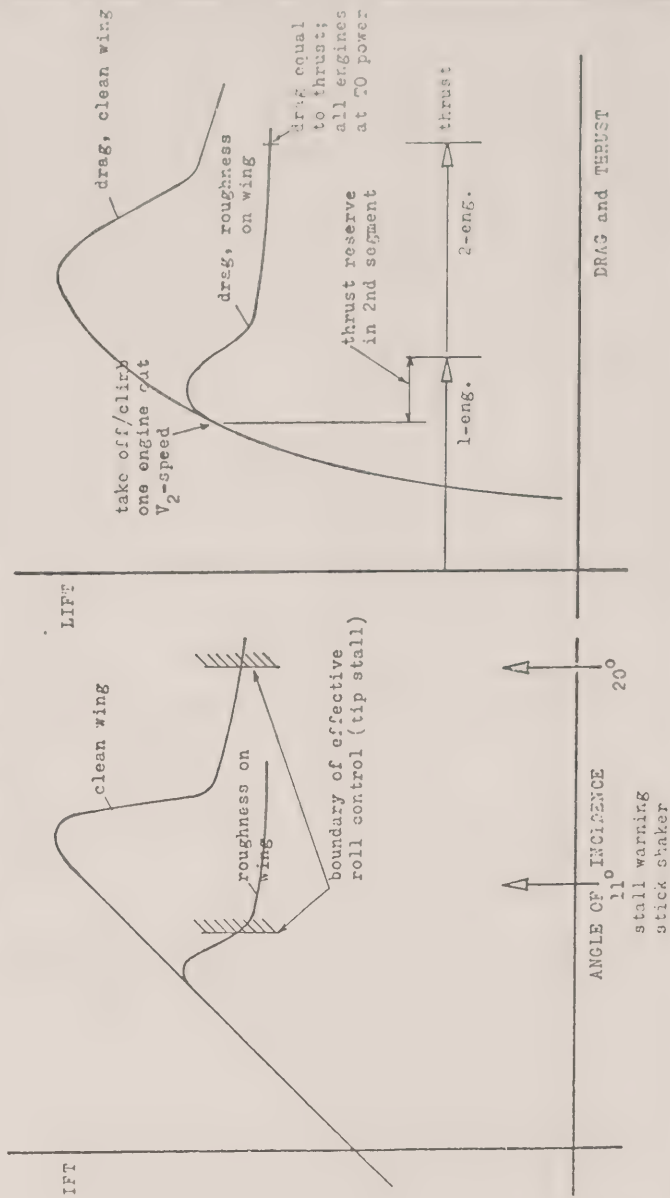
Appendix 3

Fokker Aircraft B.V. Amsterdam
Report No. VS-28-25
**Flight Simulator Investigation into the Take-off
Performance Effects of Slush on the Runway and Ice
on the Wings of a Fokker 100**

August 1989

R E P O R T
Fokker Aircraft B.V. Amsterdam
The Netherlands

issue date: August 1989   issue no: 2

---

security class   Restricted

report no. VS-28-25

---

plant/department   Schiphol/EDAA

order no. 22192

---

controlled copies

ED100	Mr. den Hertog
EQFA	Mr. Jellema
EDVP	Mr. de Boer
EDAA	Mr. van Hengst
ELTS	
CASB	via EQFA

title: Flight simulator investigation
into the take-off performance
effects of slush on the runway
and ice on the wings of a
Fokker 100.

---

enclosures:

---

summary:

Simulations have been executed on the Fokker fixed base engineering flight
simulator, in which the Fokker 100 was modelled.
Test conditions were selected to represent the take-off performance of the
F-28 Mk1000 as during the accident on Dryden Airport, Ontario, on March 10,
1989.
A comprehensive set of runway slush and wing ice conditions has been
investigated.

Issue 2: Test results for flap 25 is added.

---

prepared/department	checked/department	original issue date
B.J. Warrink/EDAA/SB BW	N. v.d. Bovenkamp/EDAA/SB	June 1989

approved/department	approval others	
J. v. Hengst/EDAA	R. Jellema/EQFA	

page 1 of 52 pages

form 1146 02-85 3 90 01

REPORT
Fokker Aircraft B.V. Amsterdam
The Netherlands

issue date: August 1989   issue no: 2

security class   Restricted   ¦ report no.   VS-28-25

LIST OF EFFECTIVE PAGES

Page	iss.date	iss.nr	Prepared	Checked	Approved
1	August´89	2	B.J. Warrink	N. v.d. Bovenkamp	J. van Hengst
2	"	2	"	"	"
3	"	2	"	"	"
4	"	2	"	"	"
5	"	2	"	"	"
6	June ´89	1	"	"	"
7	"	1	"	"	"
8	"	1	"	"	"
9	August´89	2	"	"	"
10-37	June ´89	1	"	"	"
38-49	August´89	2	"	"	"
50-51	June ´89	1	"	"	"
52	August´89	2	"	"	"

page 2 of 52 pages

form 1146 02-85 3.90.01

Introduction

In the week of June 5th-9th, 1989, a delegation of the Canadian
investigative authorities visited Fokker at Schiphol to discuss the
accident of an F-28 Mk1000 near Dryden Airport on March 10. The discussion
with respect to performance and flight handling was with:

Mr. D. Langdon   CASB
Mr. G. Wagner   Concordia University (CALPA/Advisor to Commissioner)
Mr. M. Morgan   NAE
Mr. D. Wickens   NAE

No calculation- or simulation models were available of the F28 Mk1000. To
investigate the effect of slush on the runway and ice on the wings, use has
therefore been made of the Fokker 100 simulation model. The use of this
model in stead of the F28 Mk1000 can be justified with:
- a take-off weight (87000 lbs) was selected which resulted in the same
  take-off speeds as for a Mk1000 at the weight in the Dryden accident
  (63500 lbs).
- a thrust setting was selected which gave the same thrust/weight ratio
  and thus the same take-off distance and climb performance.
- a c.g. position was used (30% mac) that gives the same rotation pitch
  response as a Mk1000 with the c.g. at 22% mac.
- the simulation of ice and ground effects is much better in the Fokker
  100 aero model than in the former F-28 Mk1000 (n.b. The Fokker 100 aero
  model is certified by the FAA to phase 2 standard).
- the Fokker 100 angles-of-attack for stall warning and stall are close
  to those of the F28 Mk1000 (flap 18, clean wing): F28 Mk1000 11.0 deg
  and 13.5 deg and Fokker 100 13.0 deg and 15.5 deg respectively.

Due to differences in lift/drag ratio etc., the representation of F28
Mk1000 by the Fokker 100 is of course not perfect, but considered close
enough for a qualitative assessment.

On request of the Canadian investigative authorities, the take-off
performance for flap 25 has been investigated by Fokker in August 1989.

The simulation results are presented in this report. They are intended to
support the investigation into the cause of the Dryden accident.

R E P O R T
Fokker Aircraft B.V. Amsterdam
The Netherlands

issue date: August 1989   issue no: 2

----

security class   Restricted   ¦ report no.   VS-28-25

Simulation model

The aerodynamic model as used in the simulations is according to
reference 2.

Ice on the wing is simulated as a change in lift-, drag- and pitching
moment coefficient. The magnitude of it has been determined in the
windtunnel, in which one inch thick horn shaped ice on the leading edge was
simulated. From tests with different ice shapes and from literature it is
known that these effects are also valid for rime ice or frozen slush in the
leading edge region. Through calculations in which static equilibrium
conditions are determined the effect of 1 inch ice (in ground- effect) on
lift, flight path angle and elevator deflection has been assessed. See
figures 1, 2 and 3.
In the simulation the effect of ice on the wing could be linearly varied
between 0 and 1.0 inch.

Slush on the runway was modelled through a rolling friction coefficient
(upto mu = .15) in the ground roll model. This coefficient depends on the
Equivalent Water Depth and the ground speed, according to reference 3.
The slush thickness was varied between 0 and 0.5 inch E.W.D. in the
simulation.

Simulator tests

Three series of simulator sessions on the fixed-base simulator were
executed, two flown by mr. G. Wagner and the third flown by mr. J. Hofstra
(Fokker test pilot).
1. June 7th. Preliminary investigations into the effect of slush and ice.
    Take-offs at ISA/SL, Flap 18.
    See table 1 for the conditions and the take-off distances.

2. June 8th. Detail investigations thru 20 take-offs at Zürich, 1500 ft
    elevation/0 C, Flap 18.
    See table 2 and the figures 4 to 22.

3. August 1. Detail investigations thru 12 take-offs at Zürich, 1500 ft
    elevation/0 C, Flap 25.
    See table 3 and the figures 23 to 34.

----

form 1146 02-85 3 90 01

R E P O R T
Fokker Aircraft B.V. Amsterdam
The Netherlands

issue date: August 1989   issue no: 2

----

security class	Restricted	report no. VS-28-25

Parameters

The following parameters are presented in the plots:

Parameter	Unit	Description
ALFA	deg	Angle of attack
CAS	kts	Calibrated airspeed
DE	deg	Elevator deflection
HRADIO	m	Radio height; equals zero for stretched undercarriage at zero pitch-angle. At lift-off HRADIO = .7 m due to pitch angle
TETA	deg	Pitch angle
XDIST	m	Distance along runway. XDIST = 0 at start of take-off roll.

Observations from the tests

1. The take-off distance without slush or ice has been approximated fairly through weight and thrust selection (at 1500 ft field elevation/0 C):

		F28 Mk1000 AFM	Fokker 100 simulation	Flap
TOD	m	1400	1455	18
	ft	4600	4770	
	m	1350	1340	25
	ft	4430	4400	

2. The increment in take-off distance (from standstill to 35 ft altitude) agrees well between simulation and AFM (no ice on wing), Flap 18 only.

Slush Depth inch EWD	F28 Mk1000 AFM ft	Fokker 100 simulation ft
0	0	0
.15	350	
.2	520	440
.25	650	850
.5	1770	1490

3. The effect of ice on the wing is considerable (see figures 35,36 and 37). Above a certain ice thickness the performance loss is so large that the aircraft cannot climb out off ground-effect (30 m) anymore.

4. Engine failure at V_1 is catastrophic when combined with slush on the runway and some ice on the wing leading edge.

5. The airfield elevation (1500 ft versus sea-level) has increased the sensitivity to ice on the wing. Compare figures 35 and 36.

----

page 5 of 52 pages

form 1146 02-85 3 90 01

REPORT
Fokker Aircraft B.V. Amsterdam
The Netherlands

issue date: August 1989   issue no: 2

---

security class   Restricted   ¦ report no. VS-28-25

References

1. Fokker report L-28-269, issue 5.
   Flight Simulator Data for the Fokker F28 Mk0100 aircraft.
   E. Obert/Dept. CB-AP/April 1973.

2. Fokker report L-28-336, issue 8.3.
   Aerodynamic data of the Fokker 100.
   EDAA/SB/Oct. 1988.

3. Fokker F28 Mk1000 Airplane Flight Manual Section 2.11.5
   "Take-off from slush covered runways".

---

page 6 of 52 pages

form 1146 02-85 3 90 01

Table 1

Take-off distances of simulations on June 7th
Fokker 100, Flaps 18 deg, W - 87000 lbs, CG = 30%, EPR = 1.62, ISA/SL,
V_1 = 124 kt, V_2 = 128 kt. (see page 2)

Run	Slush inch FWD	Ice	Rotation	TOR m	TOD (to 35 ft) m
1	.5	0	Normal	1290	1480
2	0	0	"	970	1180
3	.5	0	Nosewheel lift	1280	1460
4	.5	0	" "	1230	1450
5	0	.25	Normal	950	1180
6	0	.50	"	970	1260
7	0	.75	"	960	1640
8	0	1.00	"	980/2380	2690
9	.5	.75	"	1290	1920
10	.5	1.00	"	1330/4860	5300

----

form 1146 02-85 3 90 01

Table 2

Take-off distances of simulations on June 8th
Fokker 100, Flaps 18 deg, CG = 30%, EPR = 1.62, 1500 ft/0xC
V_1 = 124 kt, V_2 = 128 kt. (see page 2)

Run	Figure	Weight lbs	Slush inch EWD	Ice	Remark	TOR m	TOD (to 35´) m
1	4	87000	0	0		1265	1455
2	5	87000	.25	0		1500	1715
3	6	87000	.2	0		1395	1590
4	7	87000	.5	0		1730	1910
5	8	87000	.2	.5		1430	1730
6	9	87000	.15	.5		1380	1705
7	10	87000	.15	.6		1410	1870
8	11	87000	.15	.7		1575	2090
9	12	87000	.15	.75		1585	2255
10	13	87000	.15	.75		1545	2285
11	14	87000	.15	.75	Slow rotation	1555	1850
12	15	87000	.15	.8		1830	2410
13	16	89000*	.15	.75		1665	2410
14	-	89000	.15	.8			
15	17	89000	.15	.8		2260	4490
16	18	89000	.15	.825		1935	crash
17	19	89000	.15	.8		2745	crash
18	20	89000	.15	.4	Engine failure V_1	1680	crash
19	21	89000	.15	.25	Engine failure V_1	1545	crash
20	22	89000	.15	.1	Engine failure V_1	1540	crash

*   to simulate weight increment due to snow and ice on wing and fuselage

Table 3

Take-off distances of simulations on August 1
Fokker 100, Flaps 25 deg, CG = 30%, EPR = 1.62, 1500 ft/0 C
V_1 = 120 kts, V_2 = 128 kts.

Run	Figure	Weight lbs	Slush inch EWD	Ice	Remark	TOR m	TOD m
1	23	83900	0	0		1165	1340
2	24	83900	.15	.5		1300	1545
3	25	83900	.15	.6		1285	1580
4	26	83900	.15	.7		1290	1695
5	27	83900	.15	.75		1270	2360
6	28	83900	.15	.8		1250	3210
7	29	83900	.15	.9	No lift off	1270	–
8	30	85900*	.15	.5		1270	1580
9	31	85900	.15	.6		1285	1716
10	32	85900	.15	.7		1300	2015
11	33	85900	.15	.75		1300	CRASH
12	34	85900	.15	.8		1300	CRASH

*   to simulate weight increment due to snow and ice on wing and fuselage

form 1146 02-85 3 90 01

REPORT
Fokker B.V. Amsterdam
The Netherlands

ISSUE DATE   JUNE 1989   ISSUE no.:

security class

RESTRICTED

JS-28-25

TAKE-OFF WITH ICE

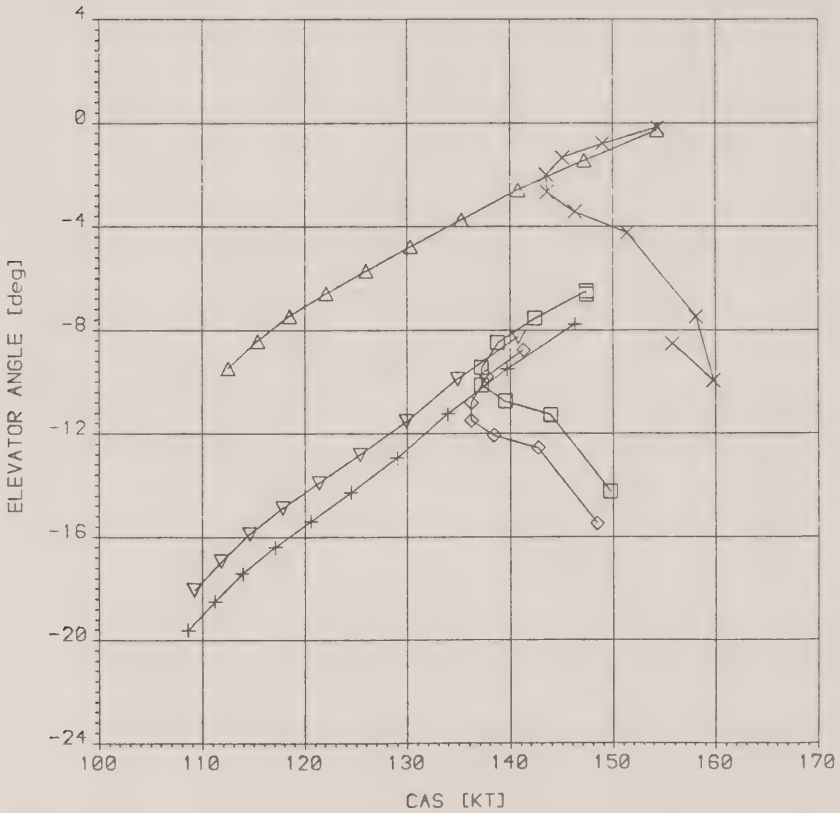FOKKER 100
W = 39500 kg
TAKE-OFF THRUST
FLAP 18

	ICE ON WING	GROUND-EFFECT
△	NO	NO
▽	NO	YES, H = 1M
+	NO	YES, H = 0
×	YES	NO
□	YES	YES, H = 1M
◇	YES	YES, H = 0

plotted: WARRINK
date   : 7-JUN-89

page 10   Fig 1

REPORT
Fokker B.V. Amsterdam
The Netherlands

security class

RESTRICTED

TAKE-OFF WITH ICE

FOKKER 100
W = 39500 kg
TAKE-OFF THRUST
FLAP 18

	ICE ON WING	GROUND-EFFECT
△	NO	NO
▽	NO	YES, H = 1M
+	NO	YES, H = 0
×	YES	NO
□	YES	YES, H = 1M
◇	YES	YES, H = 0

FLIGHT PATH ANGLE [d]

CAS [KT]
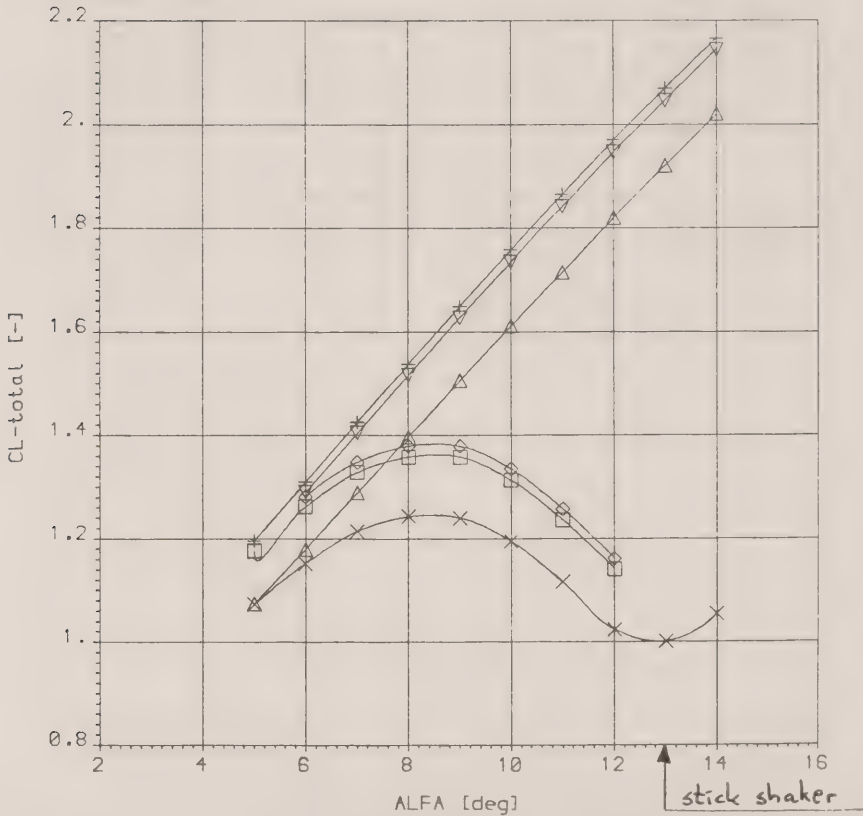
REPORT
Fokker B.V. Amsterdam
The Netherlands

issue date: JUNE 1989   issue no.:

security class   RESTRICTED   report no.:   US-28-25
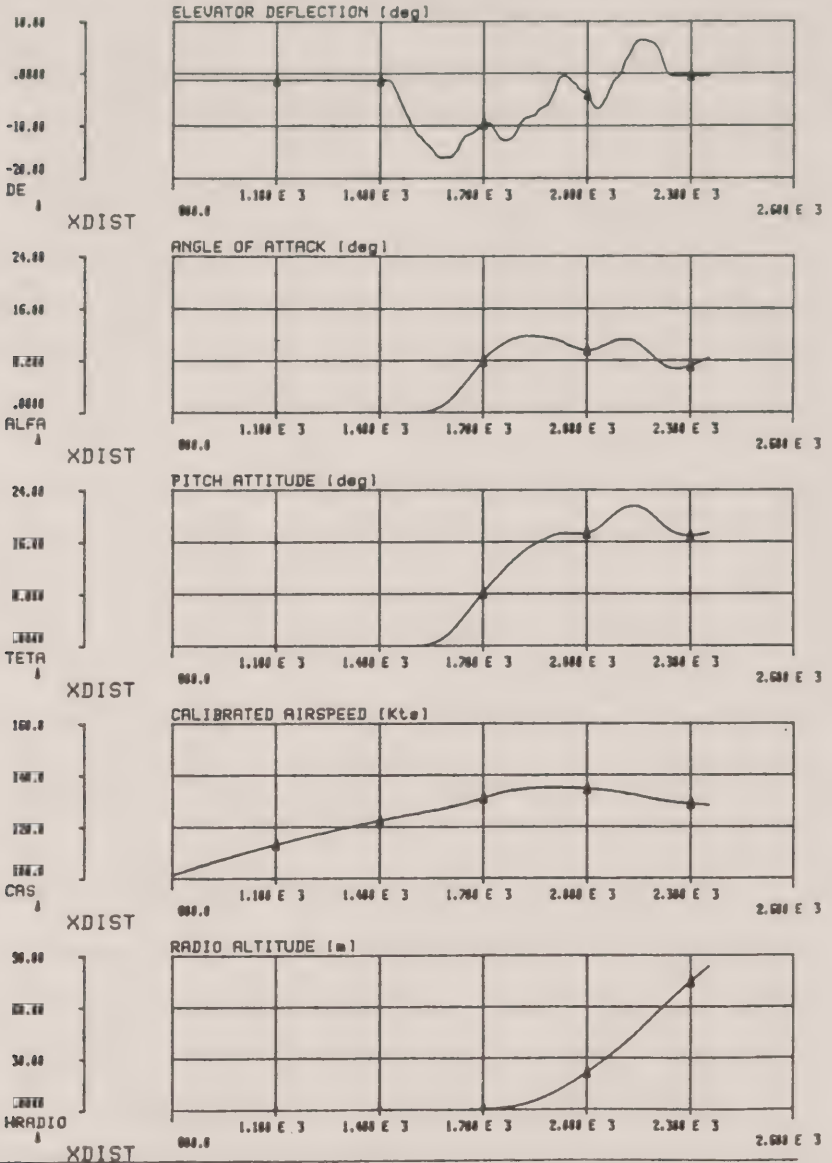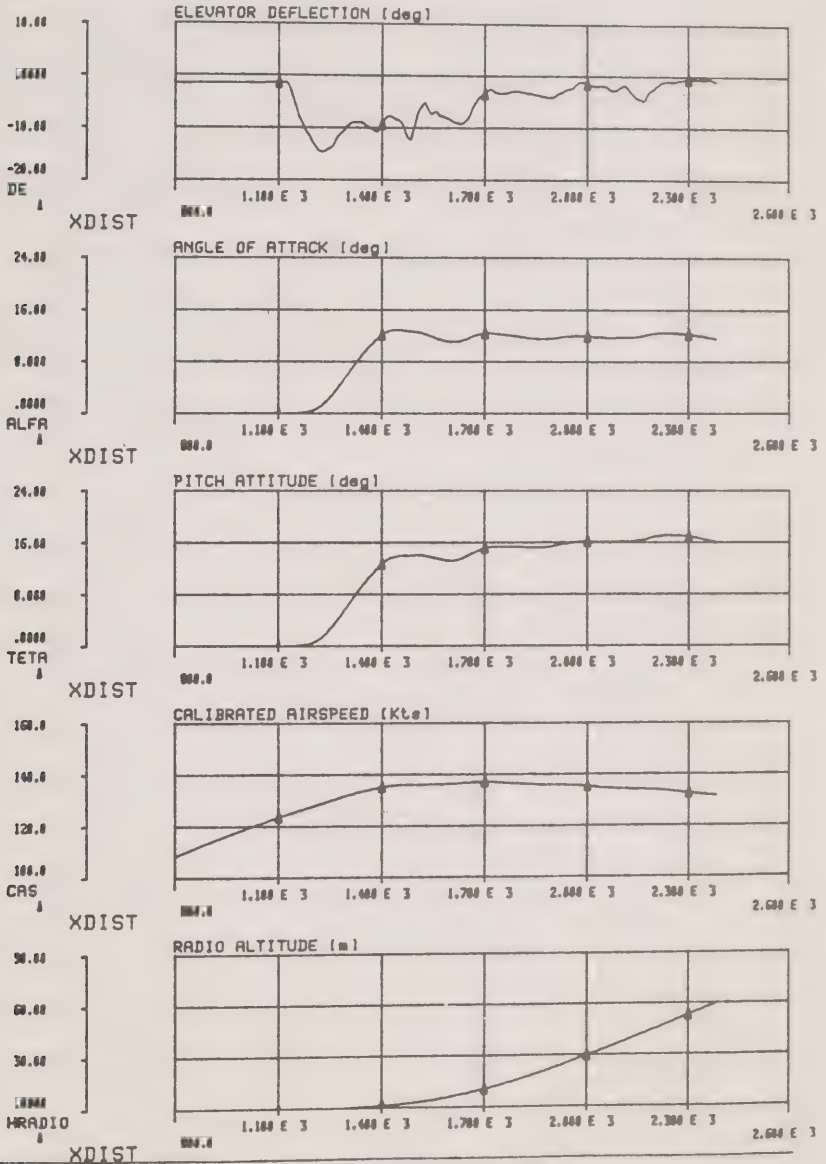
TAKE-OFF WITH ICE

FOKKER 100
W = 39500 kg
TAKE-OFF THRUST
FLAP 18

	ICE ON WING	GROUND-EFFECT
△	NO	NO
▽	NO	YES, H = 1M
+	NO	YES, H = 0
×	YES	NO
□	YES	YES, H = 1M
◇	YES	YES, H = 0

REPORT

Fokker Fokker Aircraft B.V.
Amsterdam The Netherlands

security class	report no. :
RESTRICTED	VS-28-25

Fokker 100 / TAY620   Condition 1: Ice = 0.0   Slush = 0.0

ELEVATOR DEFLECTION [deg]

ANGLE OF ATTACK [deg]

PITCH ATTITUDE [deg]

CALIBRATED AIRSPEED [Kts]

RADIO ALTITUDE [m]

REPORT

Fokker Aircraft B.V.

Amsterdam The Netherlands

Issue date:JUNE 1989   issue no.:01

security class	report no.:
RESTRICTED	VS-28-25

Fokker 100 / TAY620   Condition 2: Ice = 0.0   Slush = 0.25
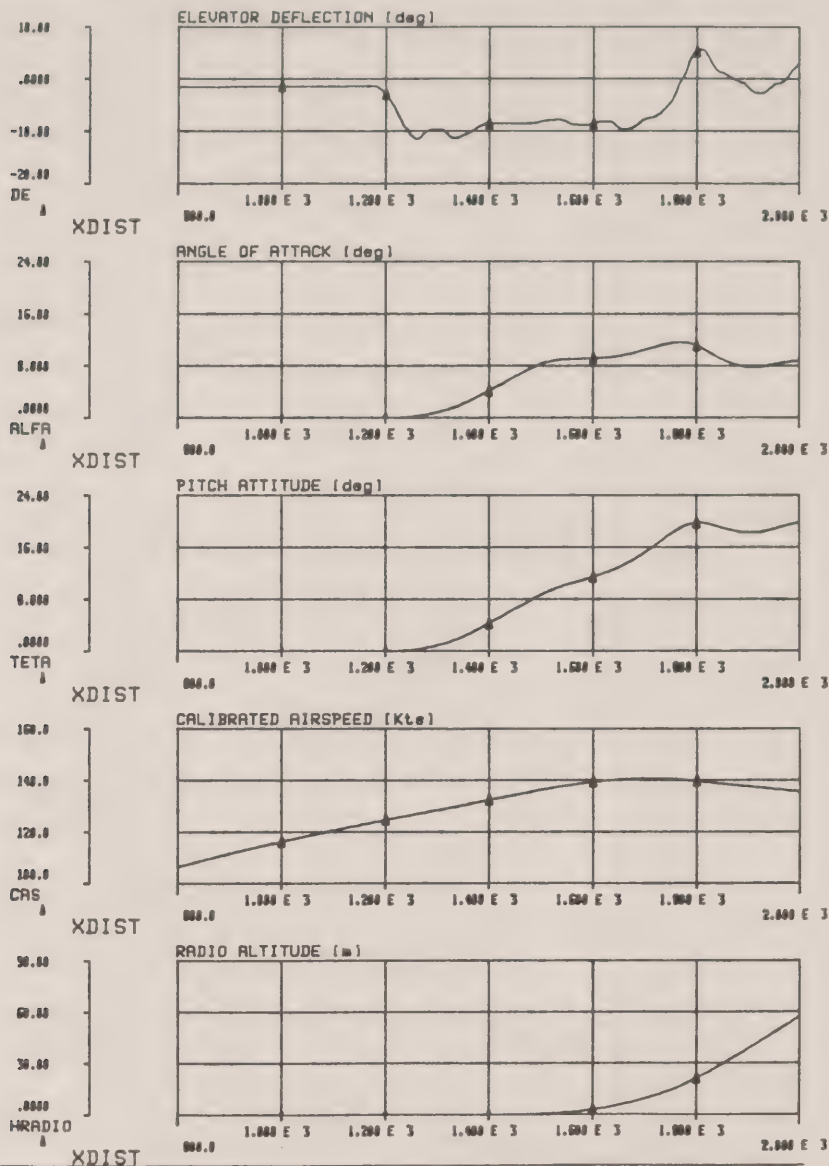
page 14   Fig 5

REPORT

(Fokker) Fokker Aircraft B.V.

Amsterdam The Netherlands

security class	report no.,
RESTRICTED	VS-28-25

Fokker 100 / TAY620   Condition 3, Ice = 0.0   Slush = 0.2
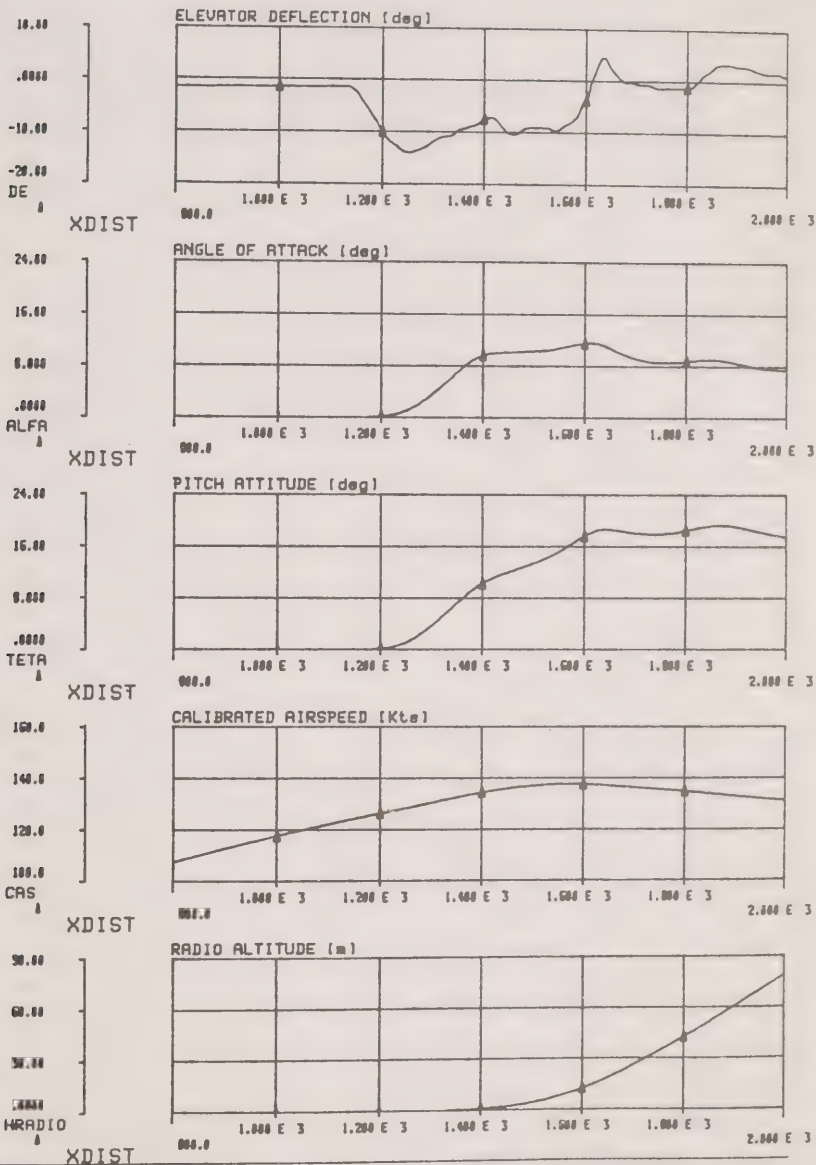
ELEVATOR DEFLECTION [deg]

ANGLE OF ATTACK [deg]

PITCH ATTITUDE [deg]

CALIBRATED AIRSPEED [Kts]

RADIO ALTITUDE [m]

Fig 6

REPORT

Fokker Fokker Aircraft B.V.
Amsterdam The Netherlands

Issue date.JUNE 1989   Issue no..01

security class	report no.:
RESTRICTED	VS-28-25

Fokker 100 / TAY620   Condition 4: Ice = 0.0   Slush = 0.5

ELEVATOR DEFLECTION [deg]

ANGLE OF ATTACK [deg]

PITCH ATTITUDE [deg]

CALIBRATED AIRSPEED [Kts]

RADIO ALTITUDE [m]

page 16   Fig 7

REPORT

Fokker Aircraft B.V.
Amsterdam The Netherlands

Issue date:JUNE 1989   Issue no.:01

security class	report no.:
RESTRICTED	VS-28-25

Fokker 100 / TAY620   Condition 6: Ice = 0.5   Slush = 0.15

page 17   Fig 8

REPORT

Fokker Aircraft B.V.
Amsterdam The Netherlands

issue date:JUNE 1989   issue no.:01
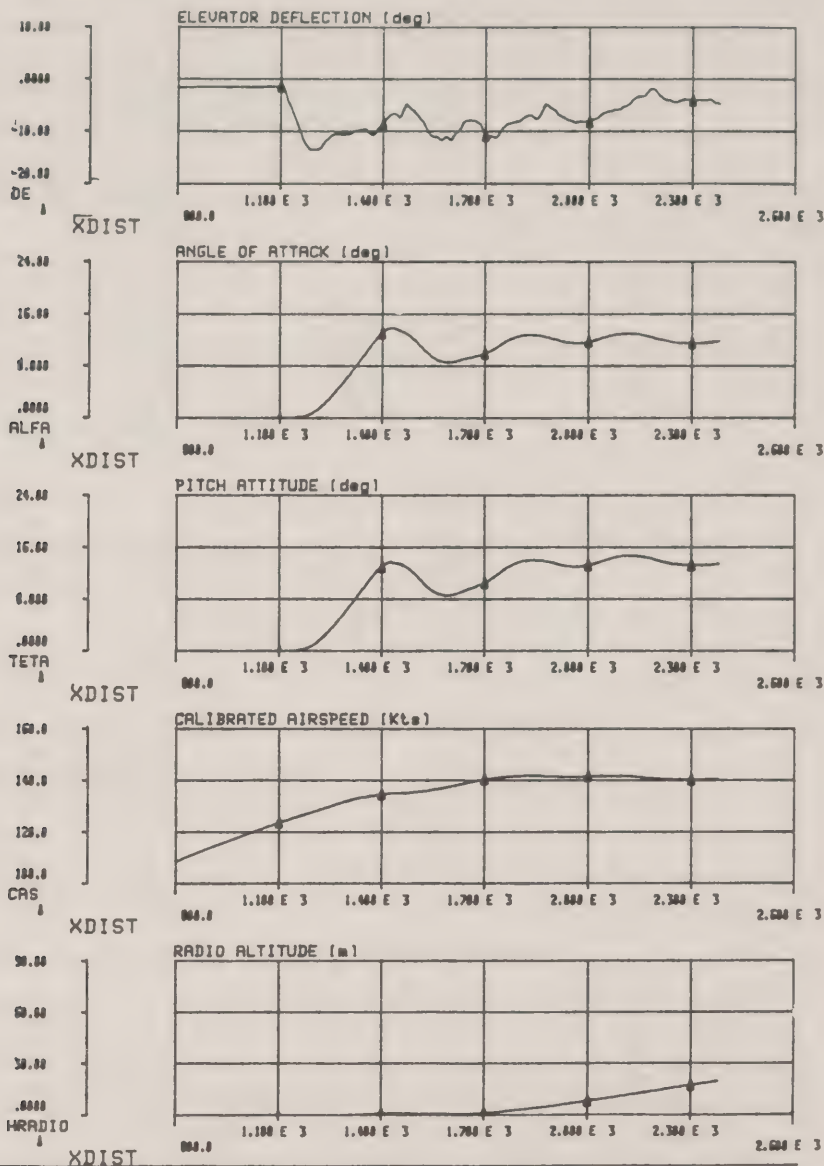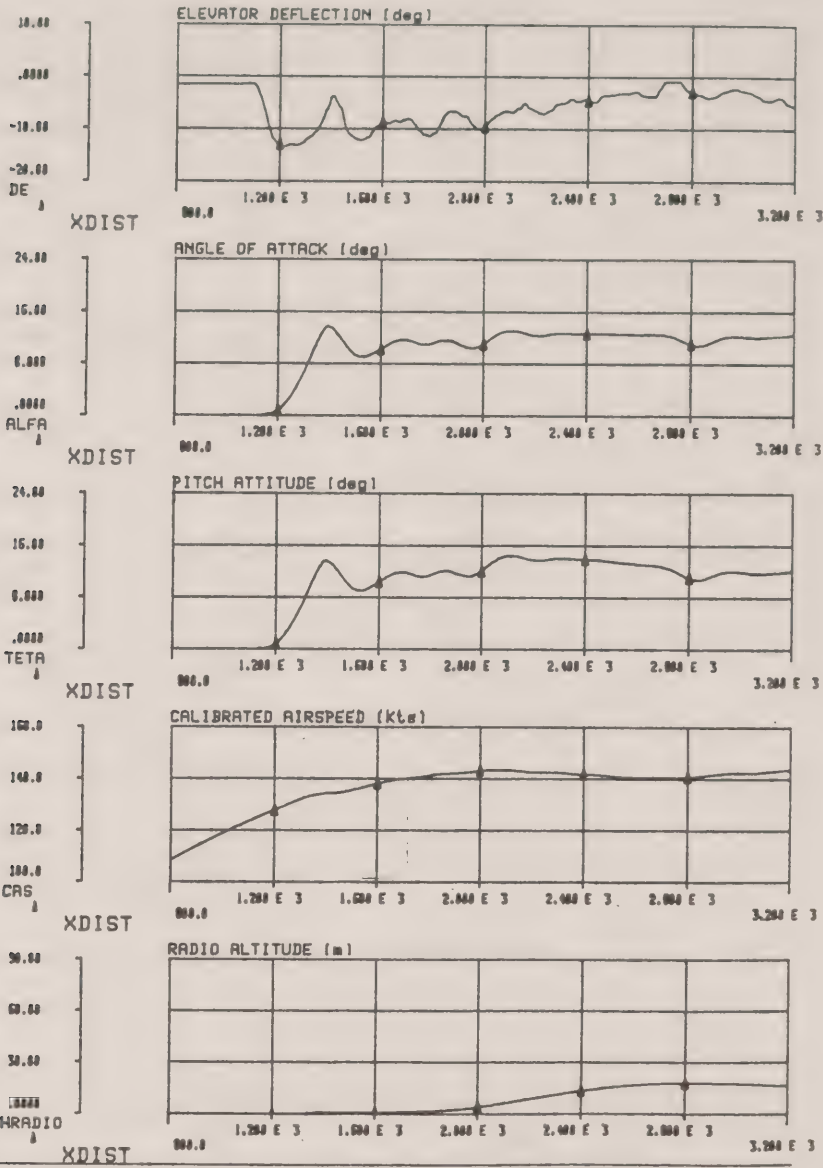
security class	report no.:
RESTRICTED	US-28-25

Fokker 100 / TAY620   Condition 5: Ice = 0.5   Slush = 0.2
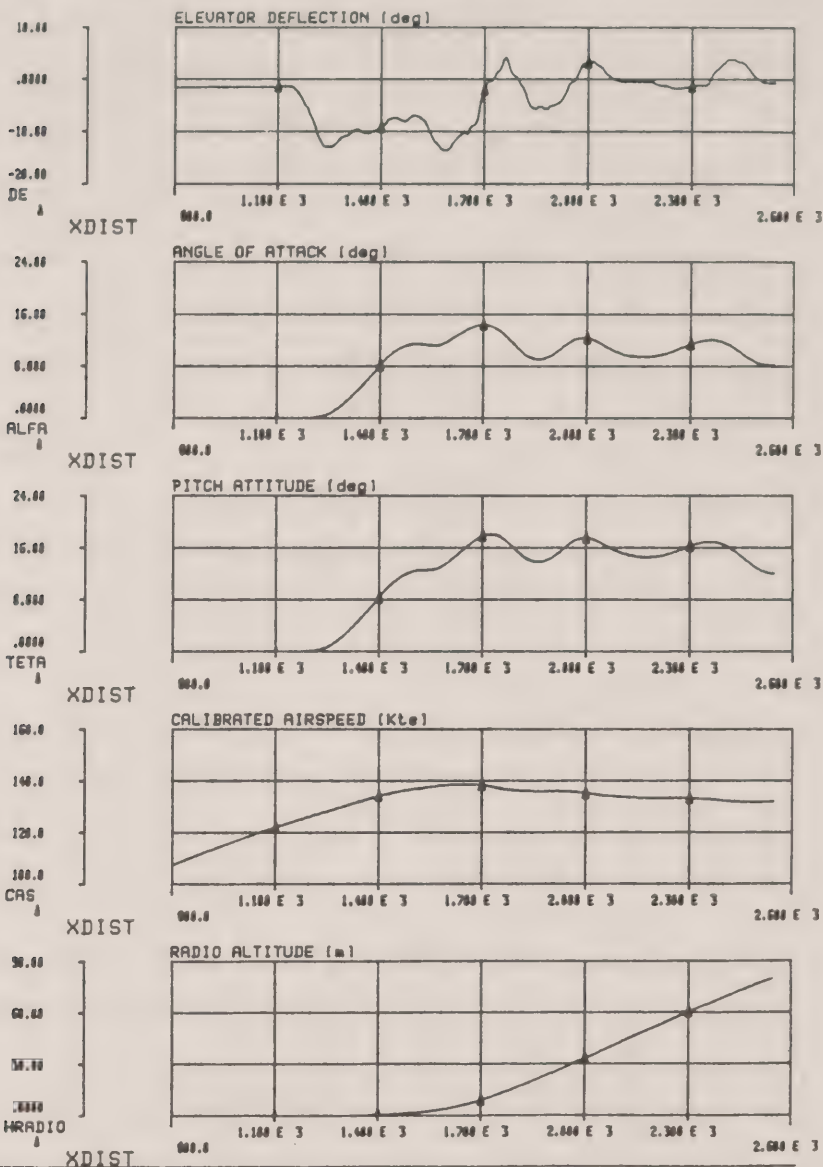
ELEVATOR DEFLECTION [deg]

ANGLE OF ATTACK [deg]

PITCH ATTITUDE [deg]

CALIBRATED AIRSPEED [Kts]

RADIO ALTITUDE [m]

page 18   Fig 9

REPORT

Fokker

Fokker Aircraft B.V.
Amsterdam The Netherlands

Issue date:JUNE 1989   Issue no.:01

security class	report no.:
RESTRICTED	VS-28-25

Fokker 100 / TAY620   Condition 7: Ice = 0.6   Slush = 0.15
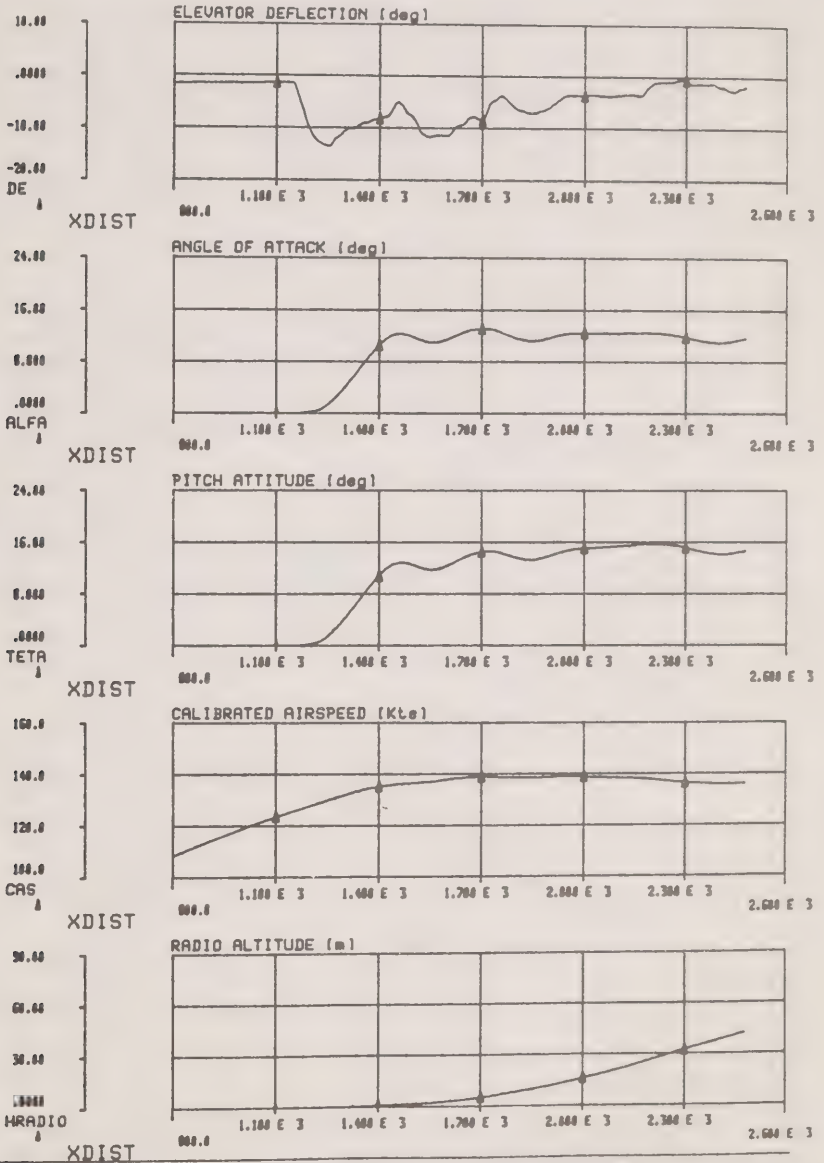
REPORT

Fokker

Fokker Aircraft B.V.
Amsterdam The Netherlands
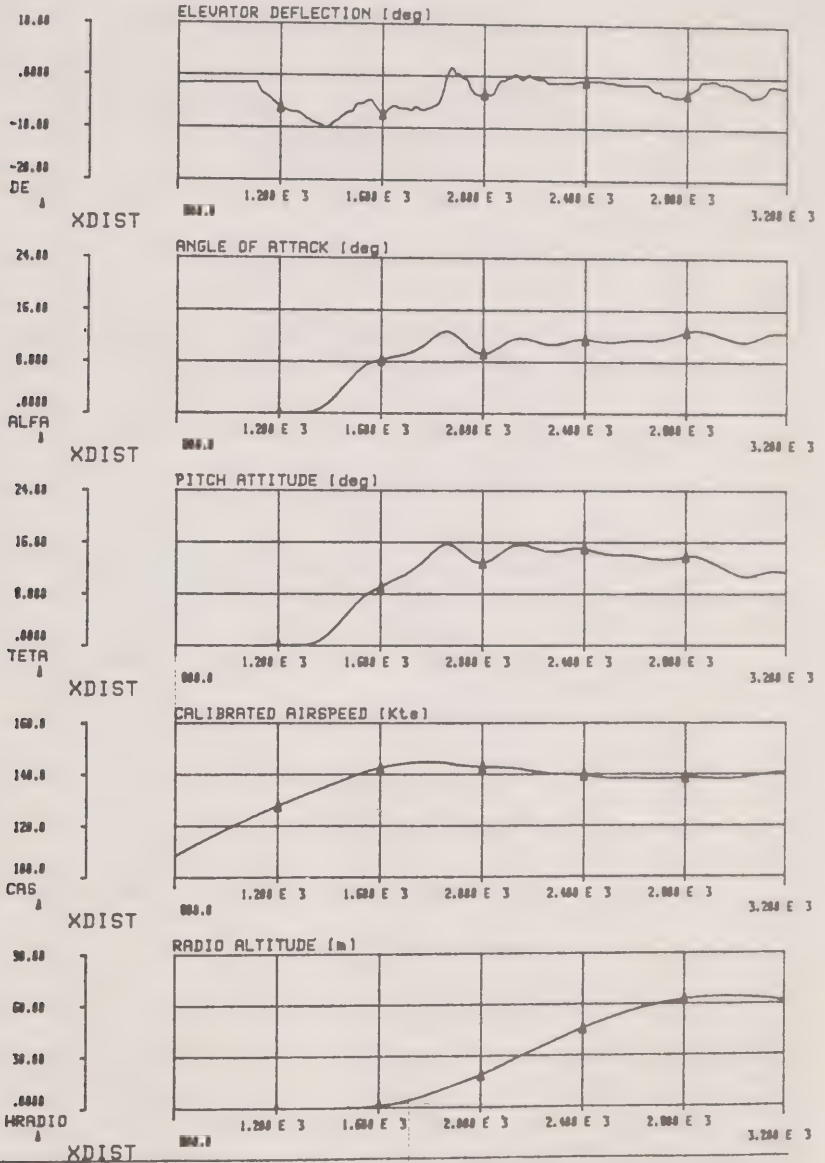
issue date.JUNE 1989   issue no..01

security class	report no..
RESTRICTED	VS-28-25

Fokker 100 / TAY620   Condition 8: Ice = 0.7   Slush = 0.15

REPORT

Fokker Aircraft B.V.

Amsterdam The Netherlands
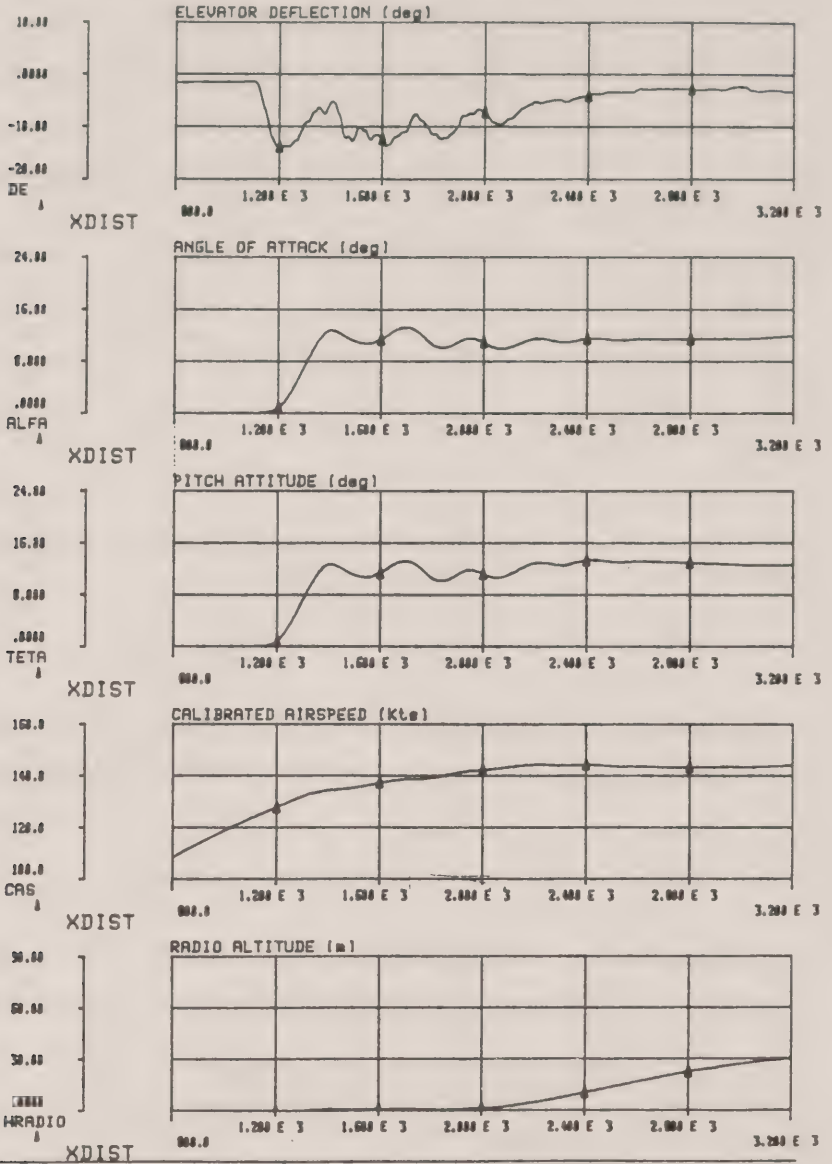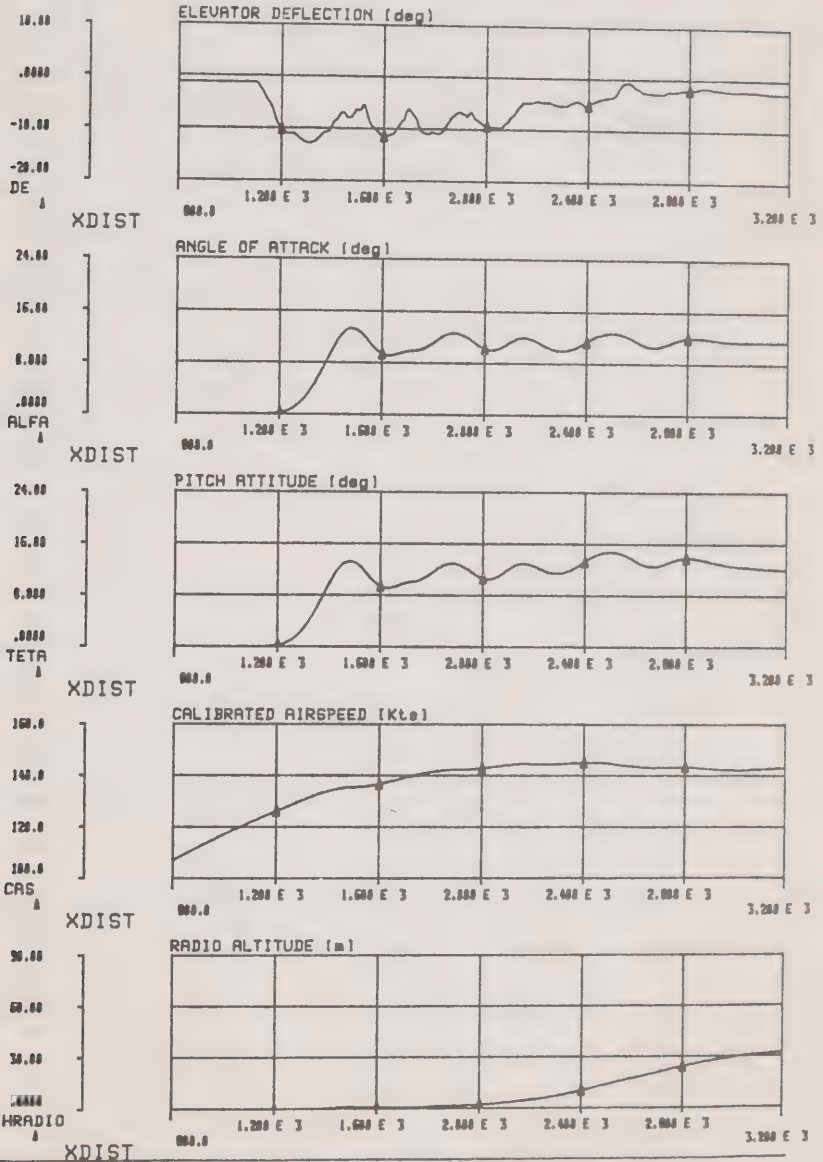
Fokker

Issue date:JUNE 1989   issue no.:01

security class	report no.:
RESTRICTED	VS-28-25

Fokker 100 / TAY620   Condition 9: Ice = 0.75   Slush = 0.15

REPORT

(Fokker) Fokker Aircraft B.V.
Amsterdam The Netherlands

security class	report no.:
RESTRICTED	VS-28-25

Fokker 100 / TAY620   Condition 10, Ice = 0.75   Slush = 0.15

REPORT

(Fokker) Fokker Aircraft B.V.
Amsterdam The Netherlands

security class	report no.:
RESTRICTED	VS-28-25

Fokker 100 / TAY620   Condition 11: Ice = 0.75   Slush = 0.15

ELEVATOR DEFLECTION [deg]

ANGLE OF ATTACK [deg]

PITCH ATTITUDE [deg]

CALIBRATED AIRSPEED [Kts]

RADIO ALTITUDE [m]

page 23   Fig 14

REPORT

Fokker

Fokker Aircraft B.V.
Amsterdam The Netherlands

issue date,JUNE 1989   issue no.,01

security class	report no.;
RESTRICTED	VS-28-25

Fokker 100 / TAY620 Condition 12, Ice = 0.8   Slush = 0.15

page 24   Fig 15

REPORT

Fokker Fokker Aircraft B.V.
Amsterdam The Netherlands

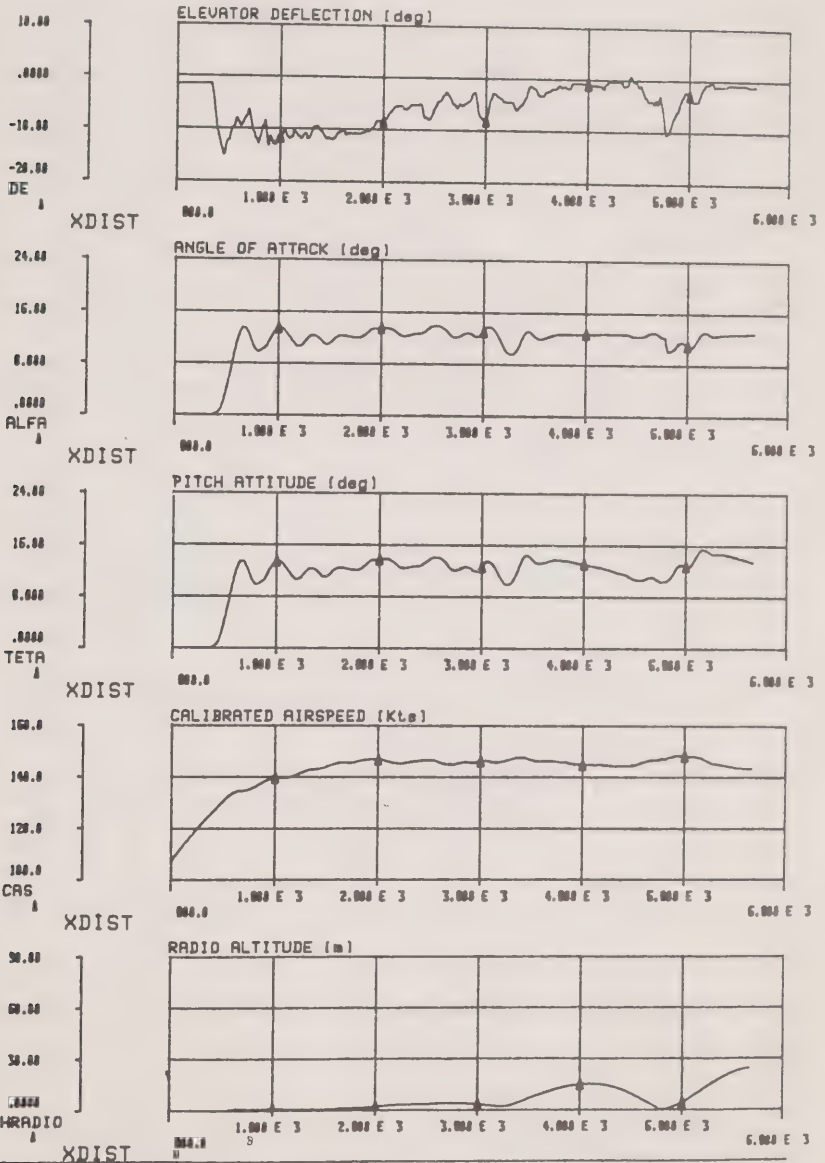|	Issue date,JUNE 1989 Issue no.,01
security class RESTRICTED	report no., VS-28-25

Fokker 100 / TAY620 Condition 13, Ice = 0.75 Slush = 0.15

page 25   Fig 16A

REPORT
Fokker Aircraft B.V.
Amsterdam The Netherlands

security class	report no.:
RESTRICTED	VS-28-25

Fokker 100 / TAY620   Condition 13; Ice = 0.75   Slush = 0.15

page 26   Fig 16 B

REPORT

(Fokker) Fokker Aircraft B.V.

Amsterdam The Netherlands

	Issue date:JUNE 1989 Issue no.:01
security class RESTRICTED	report no.: VS-28-25

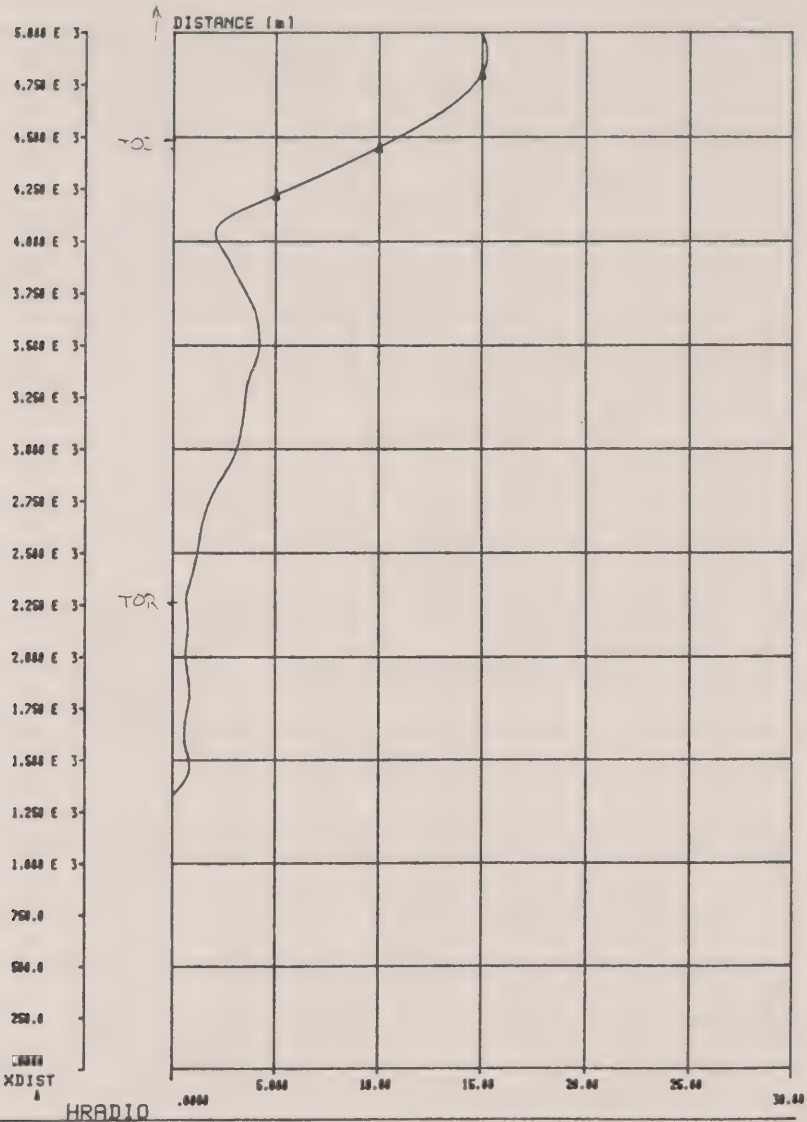Fokker 100 / TAY620   Condition 15: Ice = 0.8   Slush = 0.15

ELEVATOR DEFLECTION [deg]

ANGLE OF ATTACK [deg]

PITCH ATTITUDE [deg]

CALIBRATED AIRSPEED [Kts]

RADIO ALTITUDE [m]

page 27   Fig .7 A

REPORT

Fokker

Fokker Aircraft B.V.
Amsterdam The Netherlands

issue date:JUNE 1989   issue no.:01

security class	report no.:
RESTRICTED	US-28-25

Fokker 100 / TAY620   Condition 15: Ice = 0.8   Slush = 0.15

page 28

REPORT

Fokker
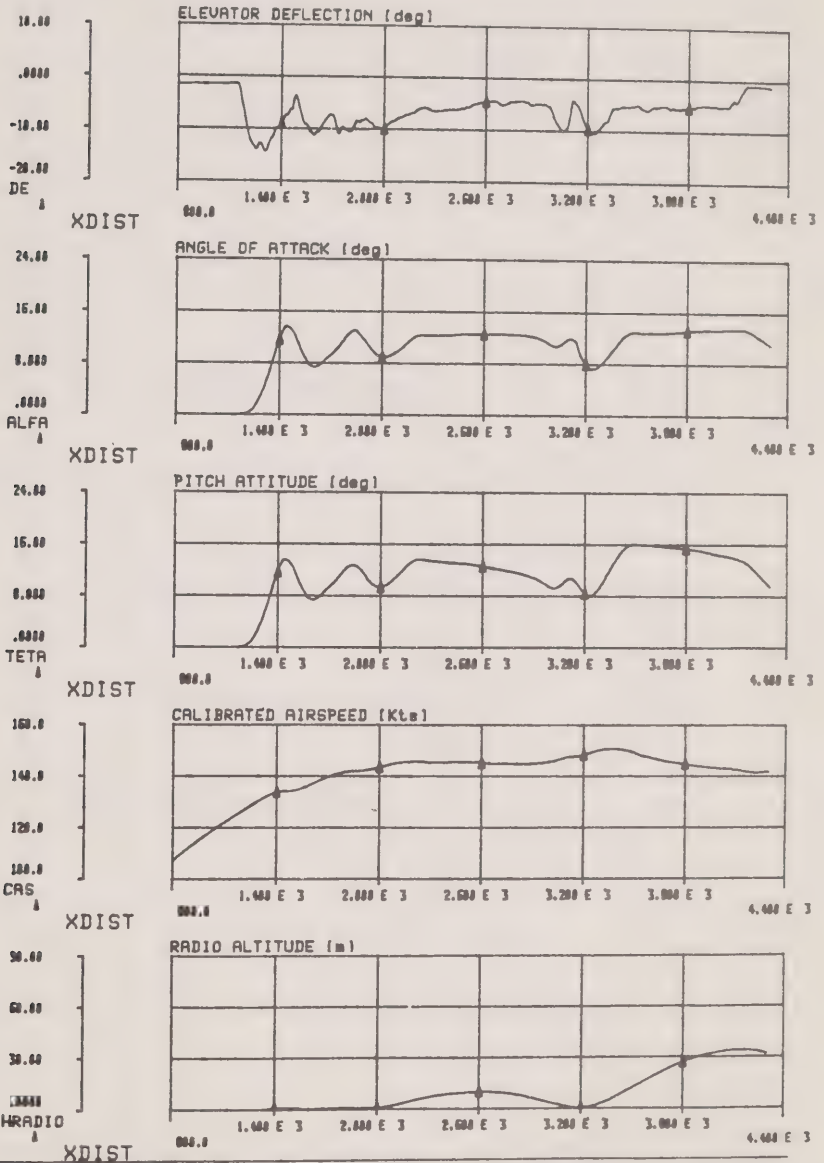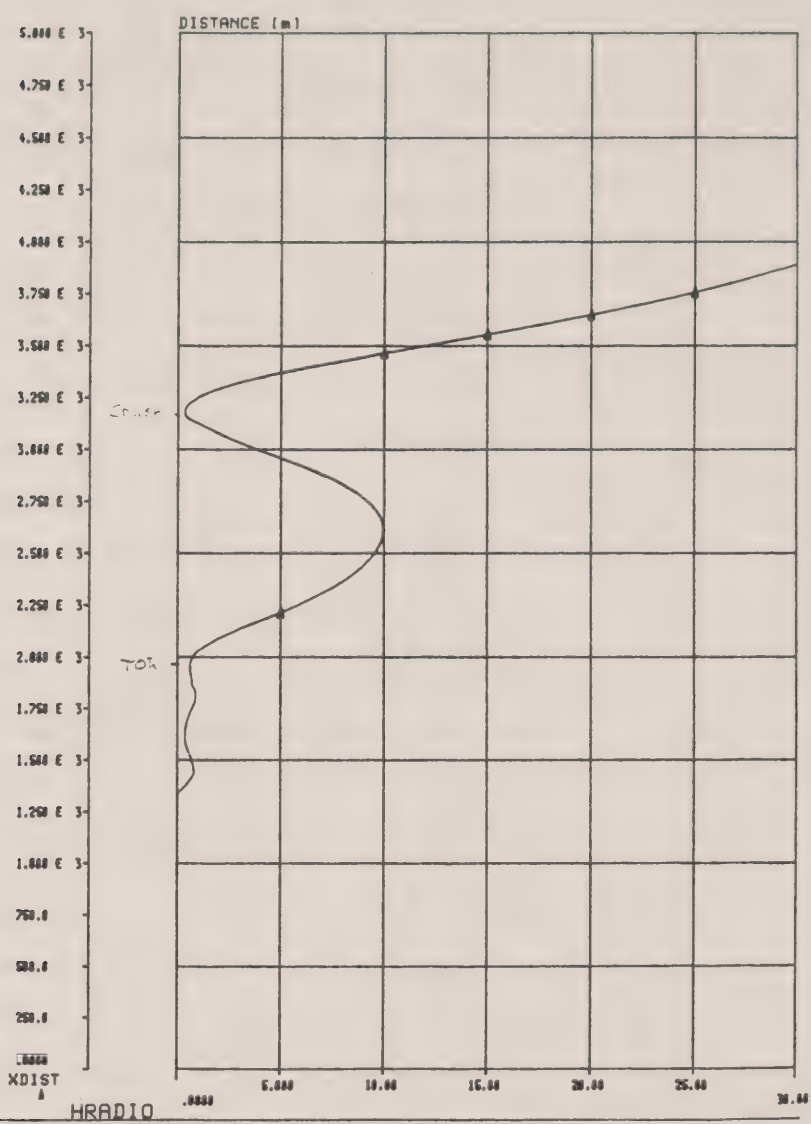
Fokker Aircraft B.V.
Amsterdam The Netherlands

Issue date: JUNE 1989   Issue no.: 01

security class	report no.:
RESTRICTED	VS-28-25

Fokker 100 / TAY620   Condition 16: Ice = 0.825   Slush = 0.15

ELEVATOR DEFLECTION [deg]

ANGLE OF ATTACK [deg]

PITCH ATTITUDE [deg]

CALIBRATED AIRSPEED [Kts]

RADIO ALTITUDE [m]

page 29   Fig 18 A

REPORT

Fokker

Fokker Aircraft B.V.
Amsterdam The Netherlands

Issue date:JUNE 1989   Issue no.:01

security class	report no.:
RESTRICTED	VS-28-25

Fokker 100 / TAY620   Condition 16; Ice = 0.825   Slush = 0.15
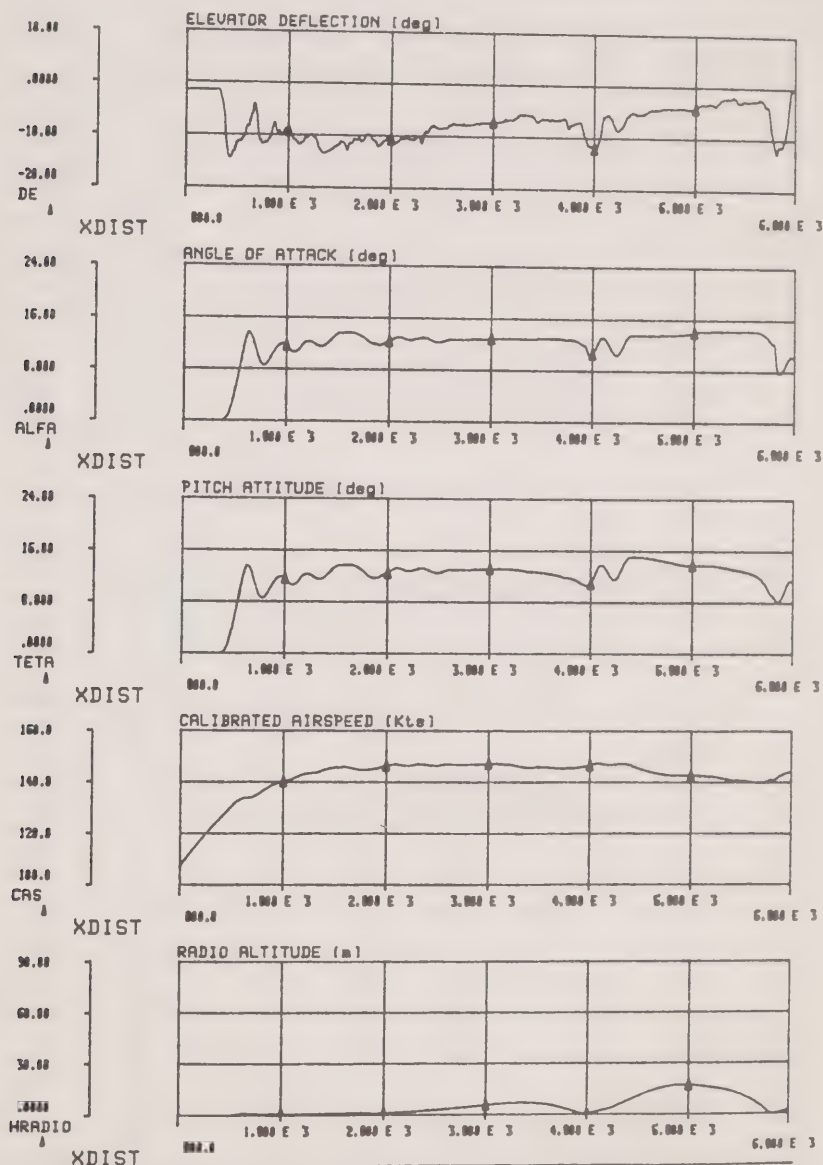
page 30   Fig 18B

REPORT

Fokker Aircraft B.V.
Amsterdam The Netherlands

security class	Issue date: JUNE 1989 Issue no.: 01
RESTRICTED	report no.: VS-28-25

Fokker 100 / TAY620 Condition 17, Ice = 0.8   Slush = 0.15

ELEVATOR DEFLECTION [deg]

ANGLE OF ATTACK [deg]

PITCH ATTITUDE [deg]

CALIBRATED AIRSPEED [Kts]

RADIO ALTITUDE [m]

page 31   Fig 19A

REPORT

Fokker

Fokker Aircraft B.V.
Amsterdam The Netherlands

issue date.JUNE 1989   issue no..01

security class	report no.:
RESTRICTED	US-28-25

Fokker 100 / TAY620   Condition 17: Ice = 0.8   Slush = 0.15
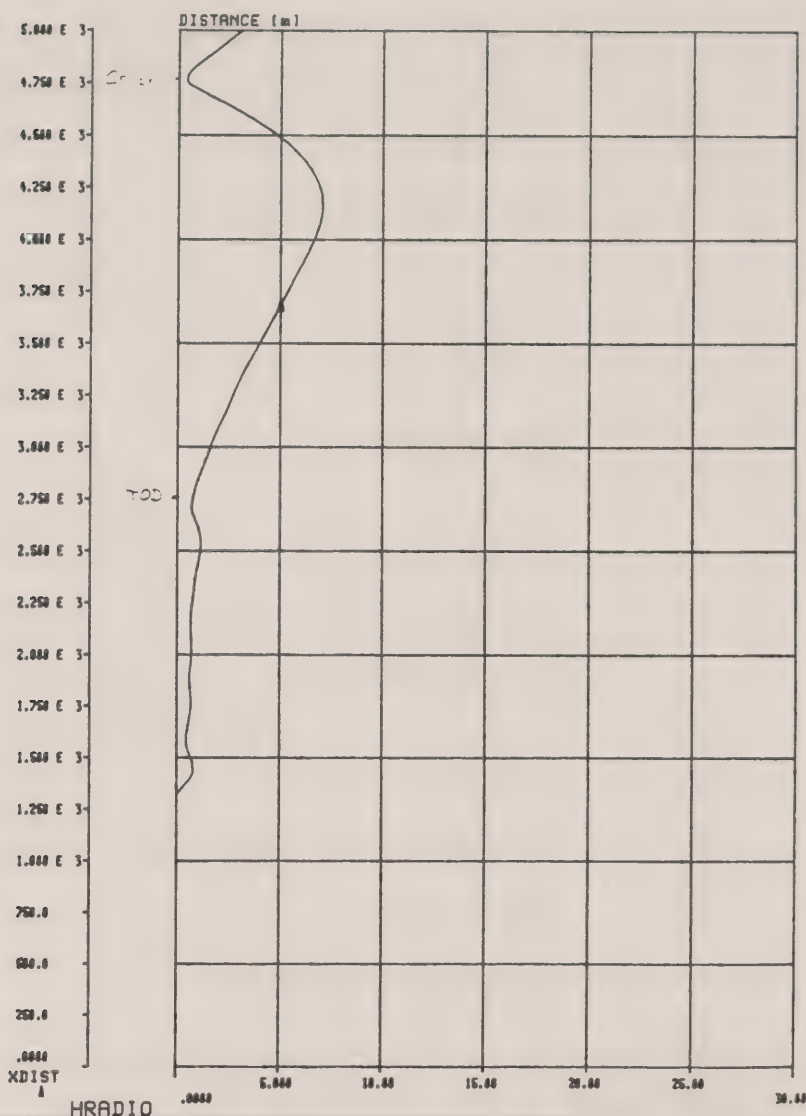
page 32   Fig 19 B

REPORT

(Fokker) Fokker Aircraft B.V.
Amsterdam The Netherlands

	Issue date.JUNE 1989	issue no..01
security class	report no..	
RESTRICTED		VS-28-25

Fokker 100 / TAY620   Condition 18. Ice = 0.4   Slush = 0.15

ELEVATOR DEFLECTION [deg]

ANGLE OF ATTACK [deg]

PITCH ATTITUDE [deg]

CALIBRATED AIRSPEED [Kts]

RADIO ALTITUDE [m]

page 33   Fig 20

REPORT
Fokker   Fokker Aircraft B.V.
Amsterdam The Netherlands

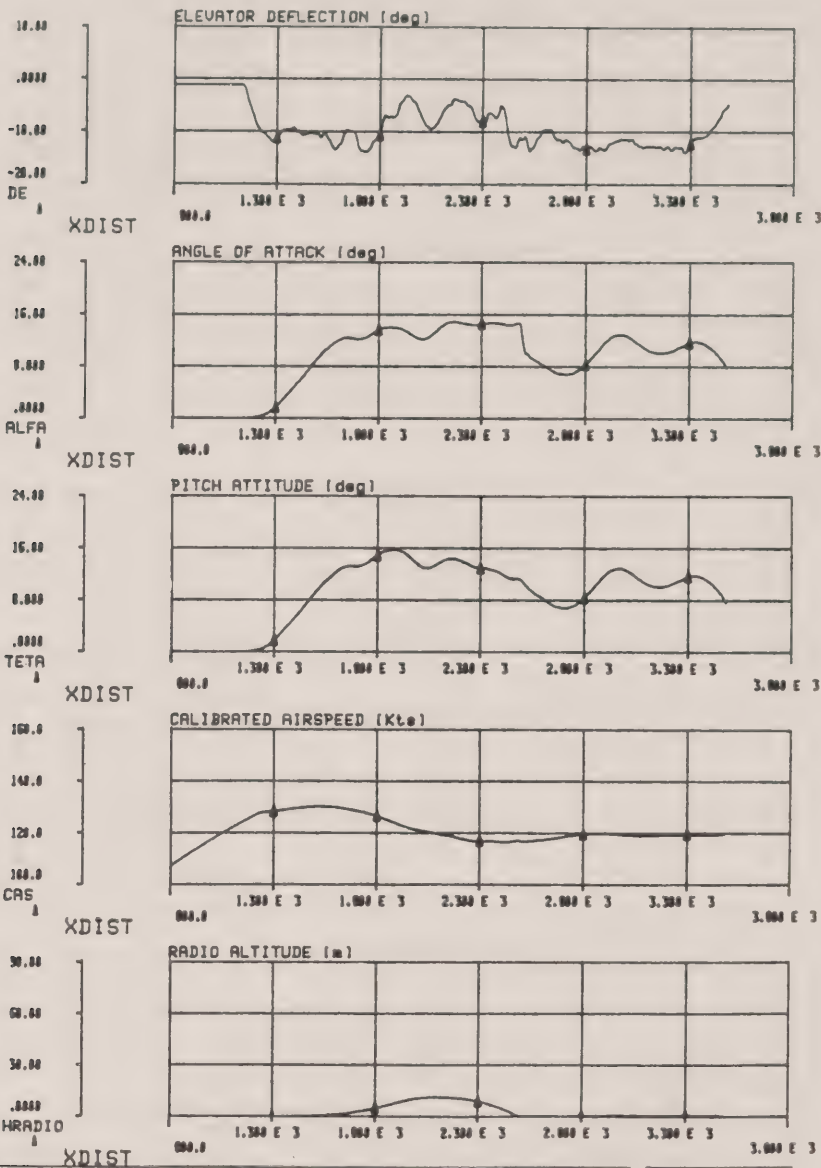| security class	report no..
RESTRICTED	US-28-25

Fokker 100 / TAY620   Condition 19, Ice = 0.25   Slush = 0.15

page 34   Fig 21A

REPORT

Fokker Aircraft B.V.
Amsterdam The Netherlands

	issue date.JUNE 1989 issue no..01
security class RESTRICTED	report no.: VS-28-25

Fokker 100 / TAY620 Condition 19, Ice = 0.25   Slush = 0.15

page 35   Fig 2.17

REPORT

Fokker

Fokker Aircraft B.V.
Amsterdam The Netherlands

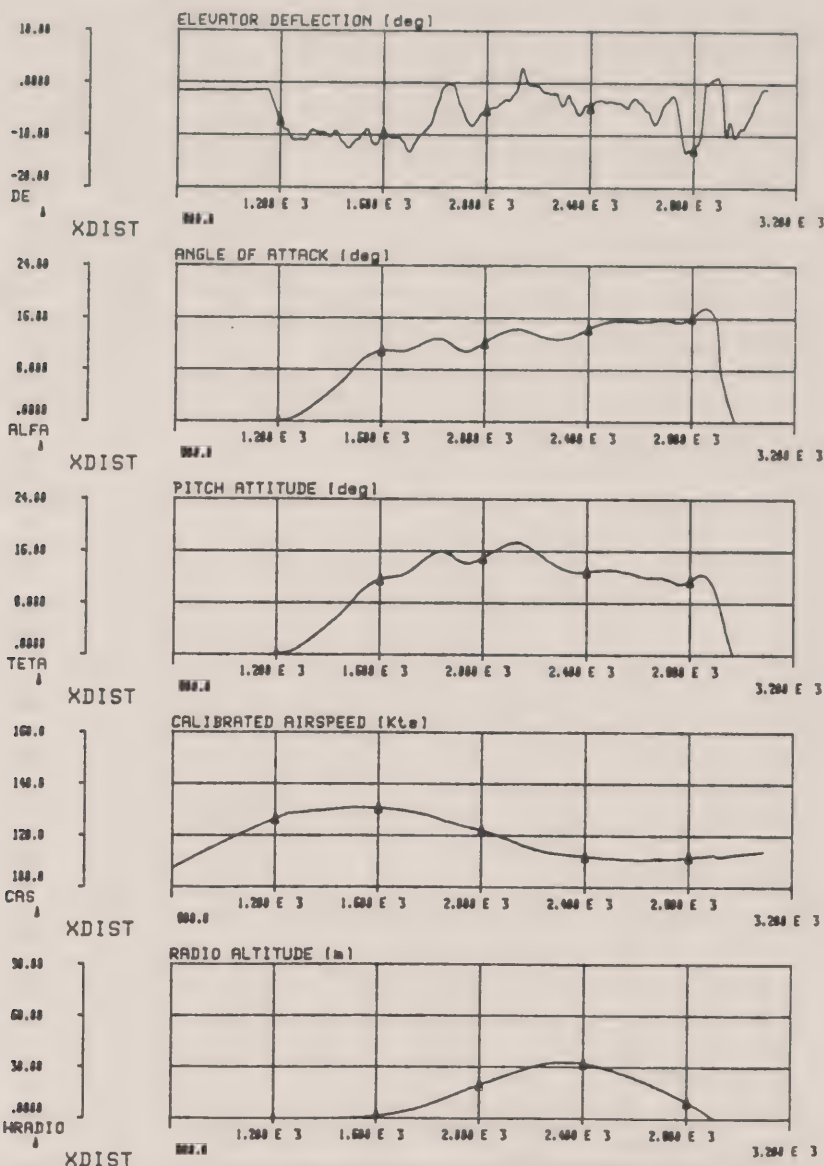|	Issue date:JUNE 1989 Issue no.:01
security class RESTRICTED	report no.: VS-28-25

Fokker 100 / TAY620   Condition 20: Ice = 0.1   Slush = 0.15

page 36

Fig 22.6

REPORT

Fokker Aircraft B.V.

Amsterdam The Netherlands
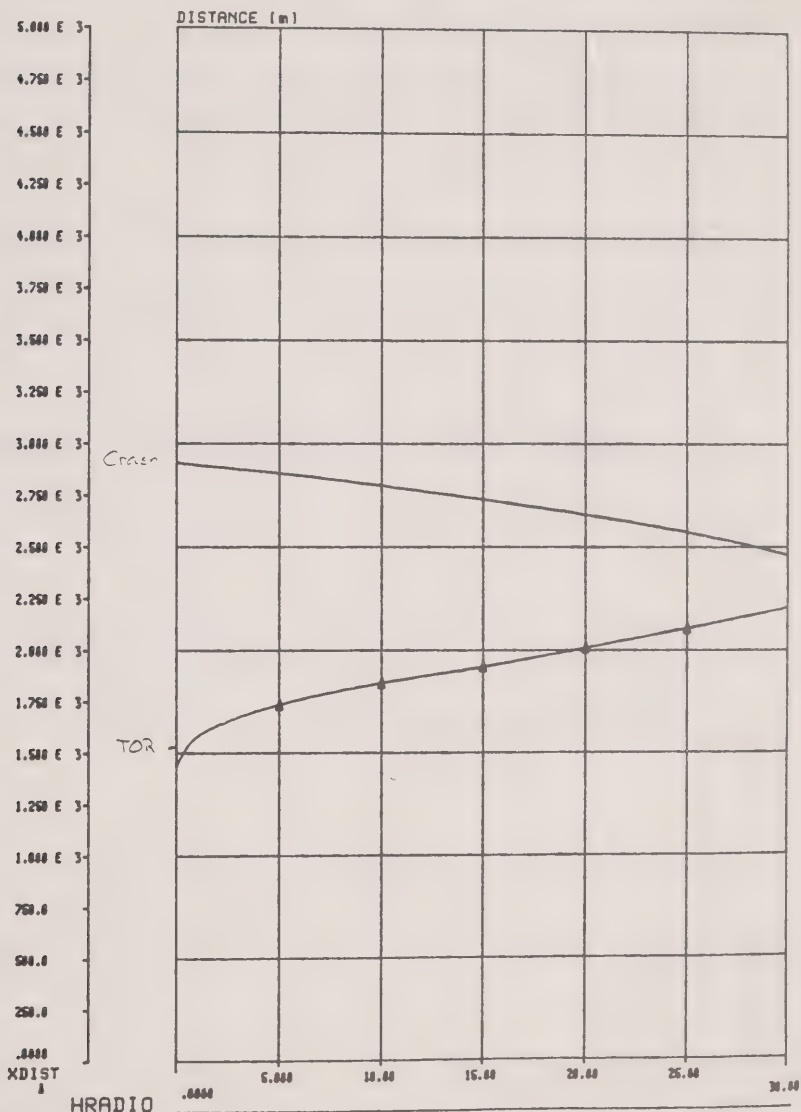
	issue date: JUNE 1989 issue no. :01
security class RESTRICTED	report no. : VS-28-25

Fokker 100 / TAY620 Condition 20, Ice = 0.1   Slush = 0.15

DISTANCE (m)

page 37   Fig 22 B

REPORT
Fokker B.V.
Amsterdam
Holland

security class

RESTRICTED

report no.:

VS-28-25

Ident: 100A4.02 TAY620   File : DMP.SLUSH.1A1   Date : 1- 8-1989
FOKKER 100 / TAY620
ICE=0.0
SLUSH=0.0
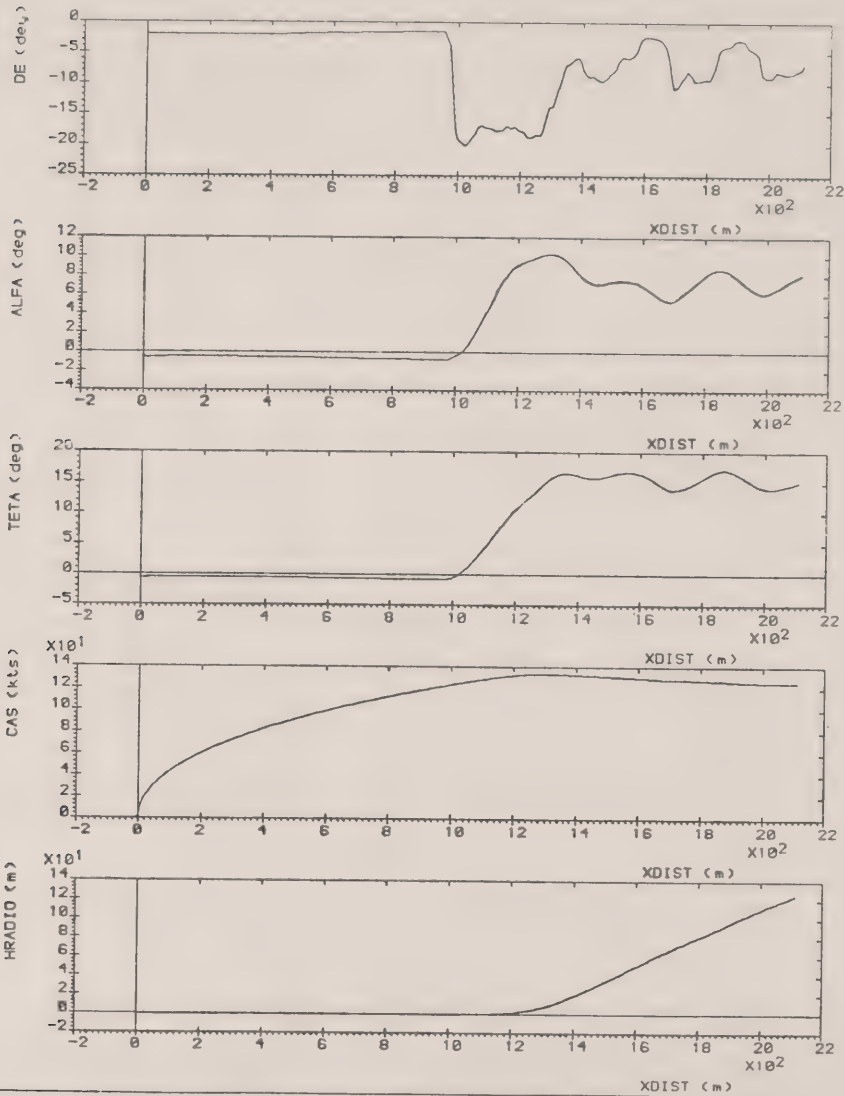
page 38   FIGURE 23

REPORT
Fokker B.V.
Amsterdam
Holland

issue date: AUGUST 1989   issue no.: 2

security class

RESTRICTED

report no.:

VS-28-25

Ident: 100A4.02 TAY620   File : DMP.SLUSH.2A2   Date : 1- 8-1989
FOKKER 100 / TAY620
ICE=.5
SLUSH=0.15

REPORT
Fokker B.V.
Amsterdam
Holland

	issue date: AUGUST 1989	issue no.: 2
security class	report no.:	
RESTRICTED		VS-28-25

Ident: 100A4.02 TAY620   File : DMP.SLUSH.3A1   Date : 1- 8-1989
FOKKER 100 / TAY620
ICE=0.6
SLUSH=0.15
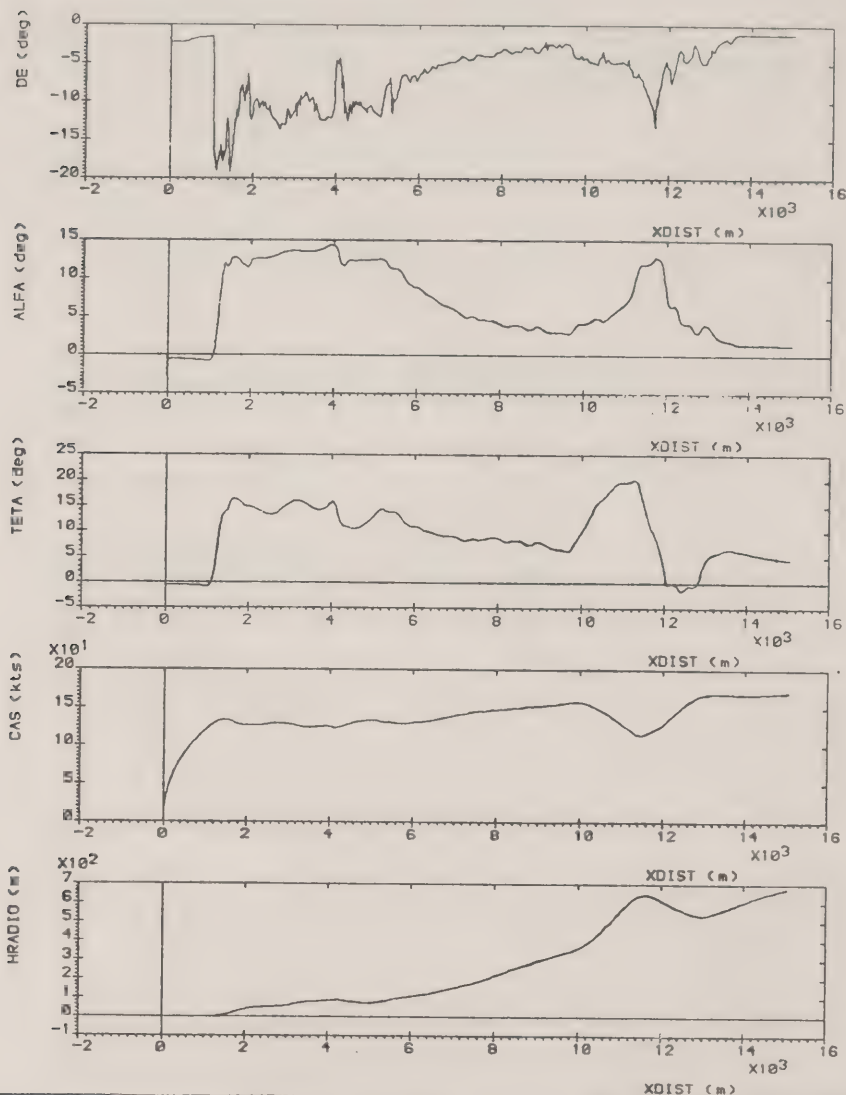
page 40   FIGURE 25

REPORT
Fokker B.V.
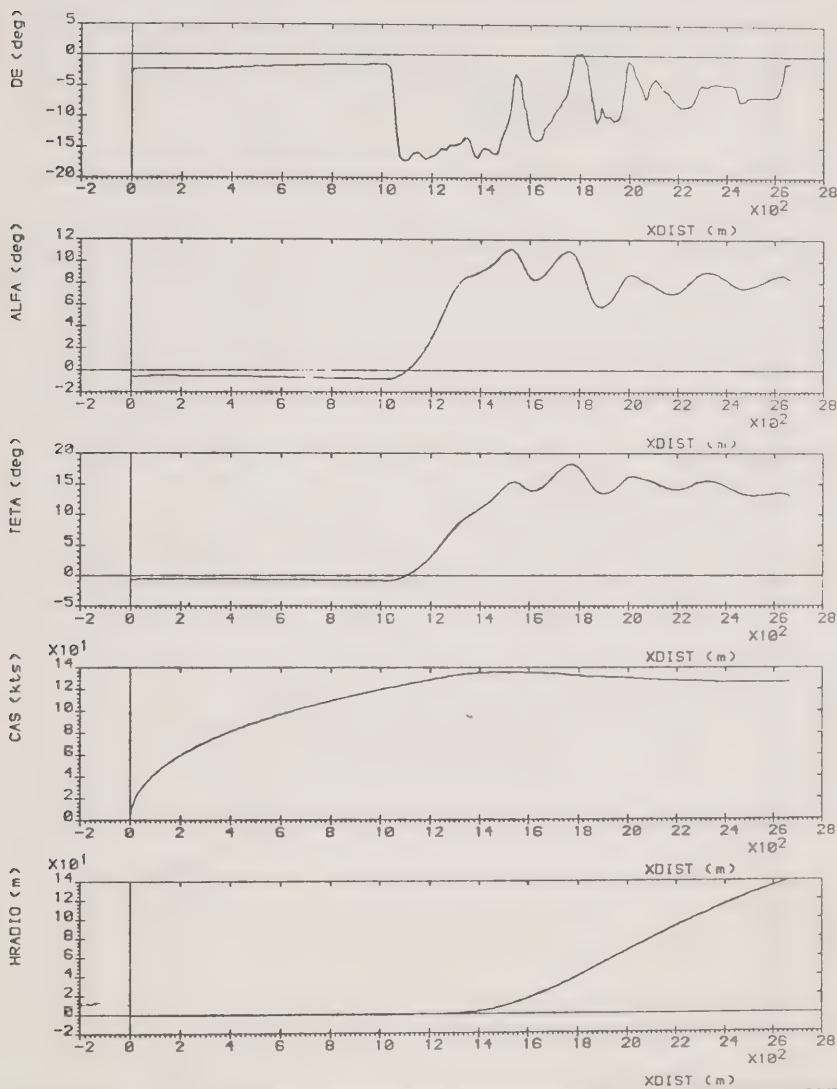Amsterdam
Holland

issue date: AUGUST 1989   issue no.: 2

security class

RESTRICTED

report no.:

VS-28-25

Ident: 100A4.02 TAY620   File : DMP.SLUSH.3A3   Date : 1- 8-1989
FOKKER 100 / TAY620
ICE=0.75
SLUSH=0.15
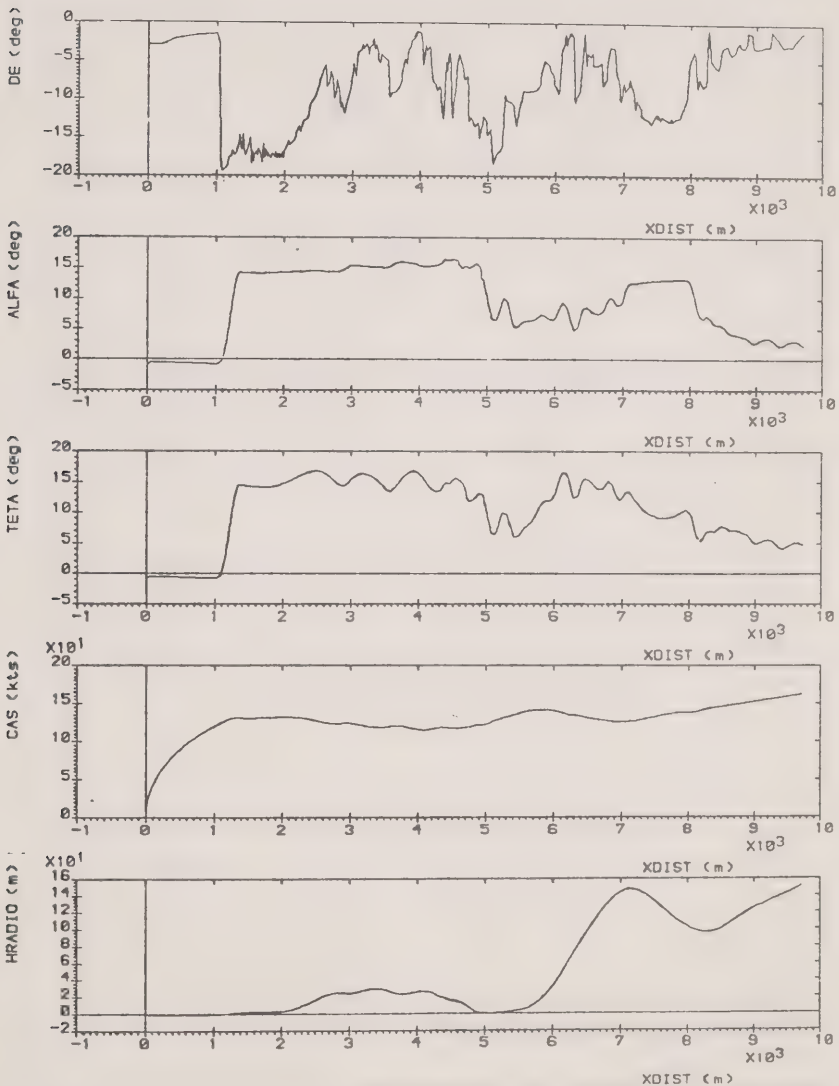
page 42   FIGURE 27

REPORT
Fokker B.V.
Amsterdam
Holland

issue date: AUGUST 1989

security class

RESTRICTED

report no.:

VS-28-25

Ident: 100A4.02 TAY620   File : DMP.SLUSH.3A7   Date : 1- 8-1989
FOKKER 100 / TAY620
ICE=0.8
SLUSH=0.15
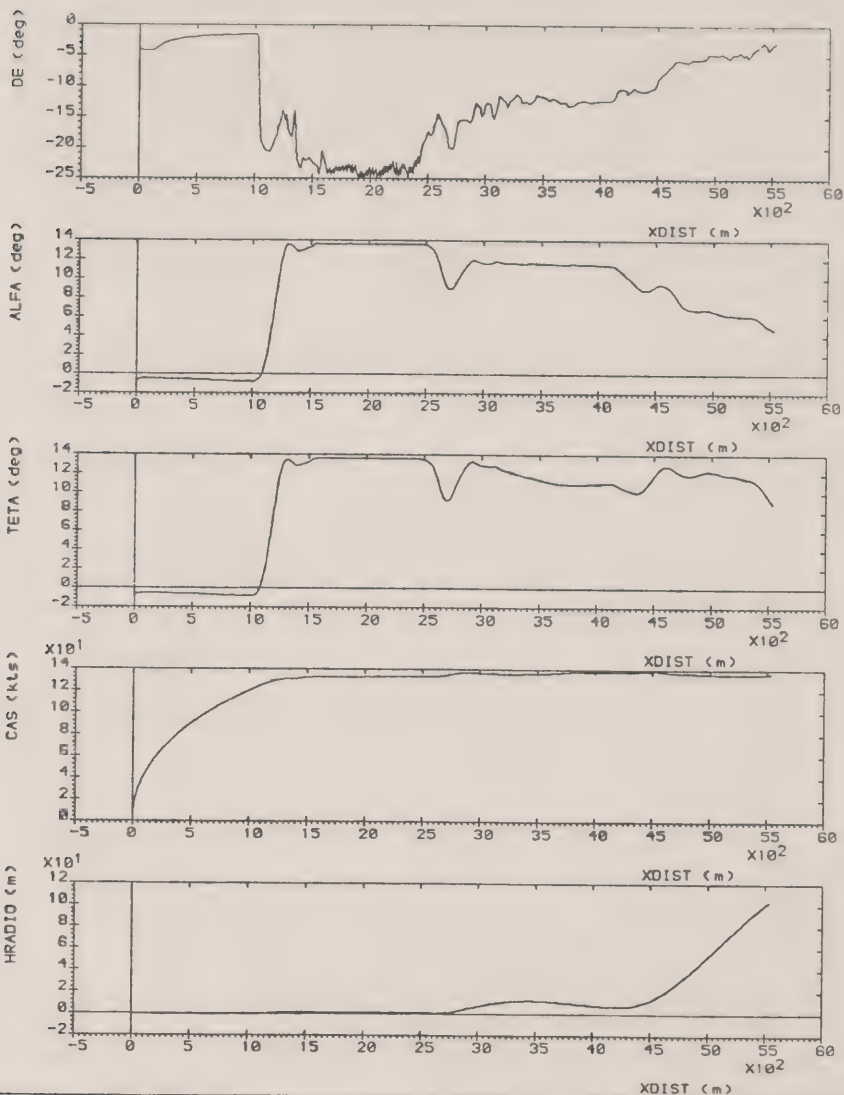
page 43   FIGURE 28

REPORT
Fokker B.V.
Amsterdam
Holland

RESTRICTED

VS-28-25

Ident: 100A4.02 TAY620   File : DMP.SLUSH.3A5   Date : 1- 8-1989
FOKKER 100 / TAY620
ICE=0.9
SLUSH=0.15
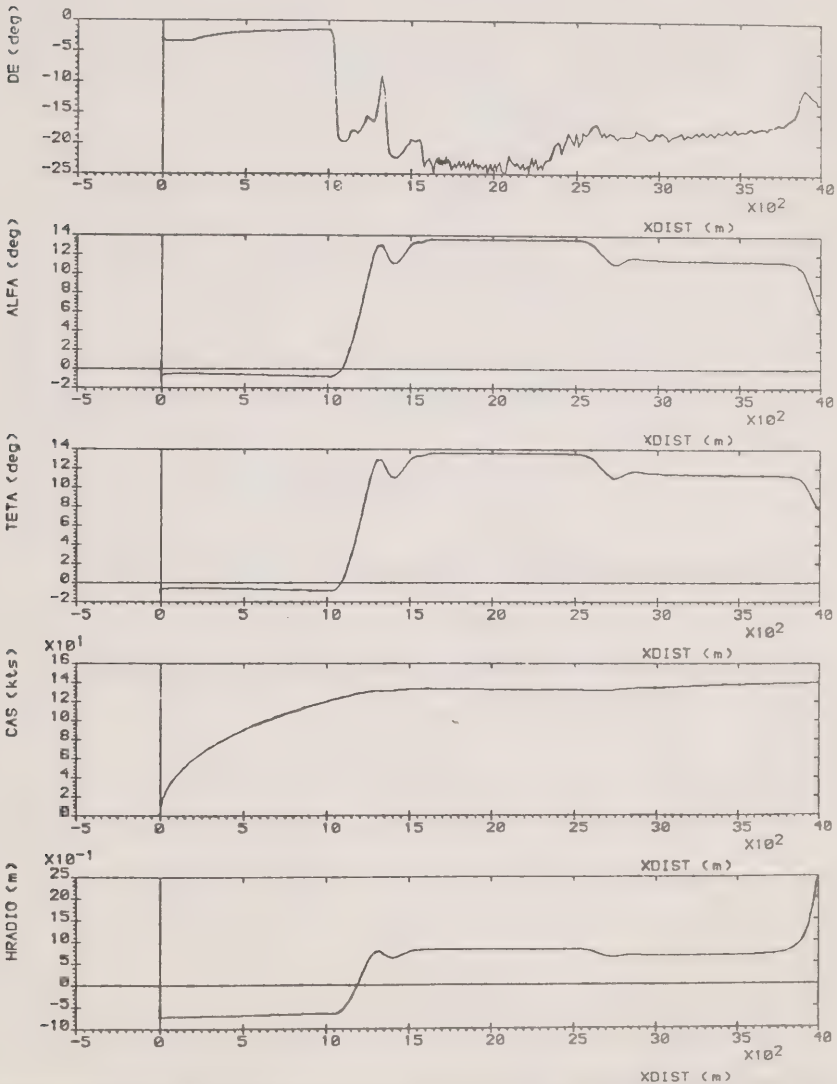
security class	issue date: AUGUST 1989	issue no.: 2
RESTRICTED	report no.:	VS-28-25

Ident: 100A4.02 TAY620   File : DMP.SLUSH.4A2   Date :   1- 8-1989
FOKKER 100 / TAY620
ICE=0.5
SLUSH=0.15
900 KG WEIGHT INCREMENT DUE TO ICE ON AIRCRAFT

REPORT
Fokker B.V.
Amsterdam
Holland

security class	issue date: AUGUST 1989	issue no.: 2
RESTRICTED	report no.:	VS-28-25

Ident: 100A4.02 TAY620   File : DMP.SLUSH.4A3   Date : 1- 8-1989
FOKKER 100 / TAY620
ICE=0.6
SLUSH=0.15
900 KG WEIGHT INCREMENT DUE TO ICE ON AIRCRAFT

page 46 FIGURE 31

REPORT
Fokker B.V.
Amsterdam
Holland

issue date: AUGUST 1989   issue no.: 2

security class   report no.:

RESTRICTED   VS-28-25

Ident: 100A4.02 TAY620   File : DMP.SLUSH.4A4   Date : 1- 8-1989
FOKKER 100 / TAY620
ICE=0.7
SLUSH=0.15
900 KG WEIGHT INCREMENT DUE TO ICE ON AIRCRAFT
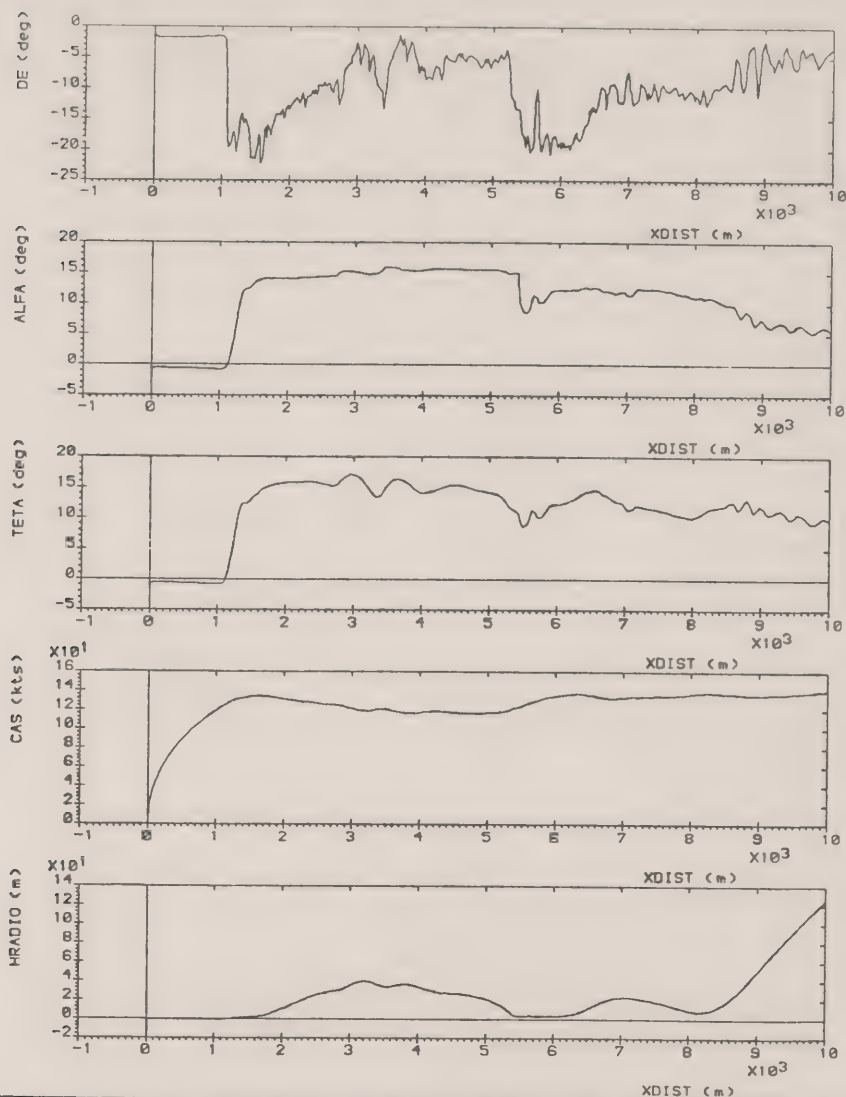
page 47 FIGURE 32

REPORT
Fokker B.V.
Amsterdam
Holland

security class		issue date: AUGUST 1989	issue no.: 2
	RESTRICTED	report no.:	VS-28-25

Ident: 100A4.02 TAY620 File : DMP.SLUSH.4A5   Date : 1- 8-1989
FOKKER 100 / TAY620
ICE=0.75
SLUSH=0.15
900 KG WEIGHT INCREMENT DUE TO ICE ON AIRCRAFT
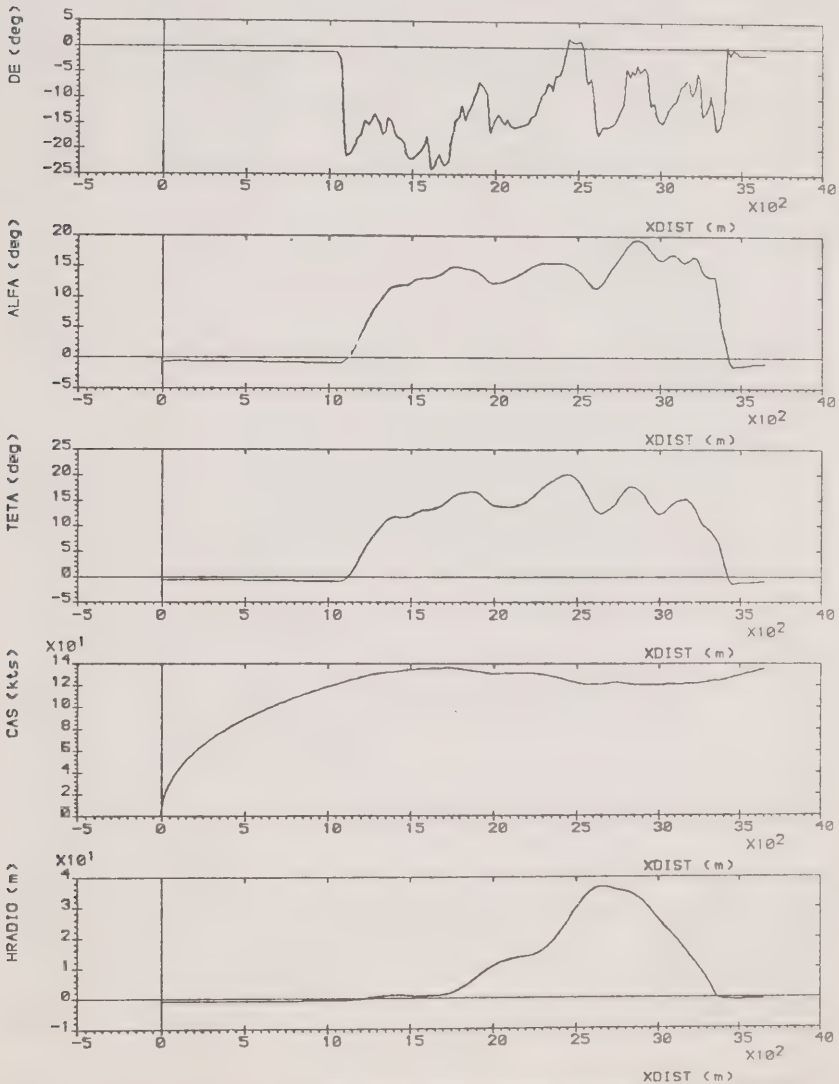
page 48   FIGURE 33

REPORT
Fokker B.V.
Amsterdam
Holland

security class
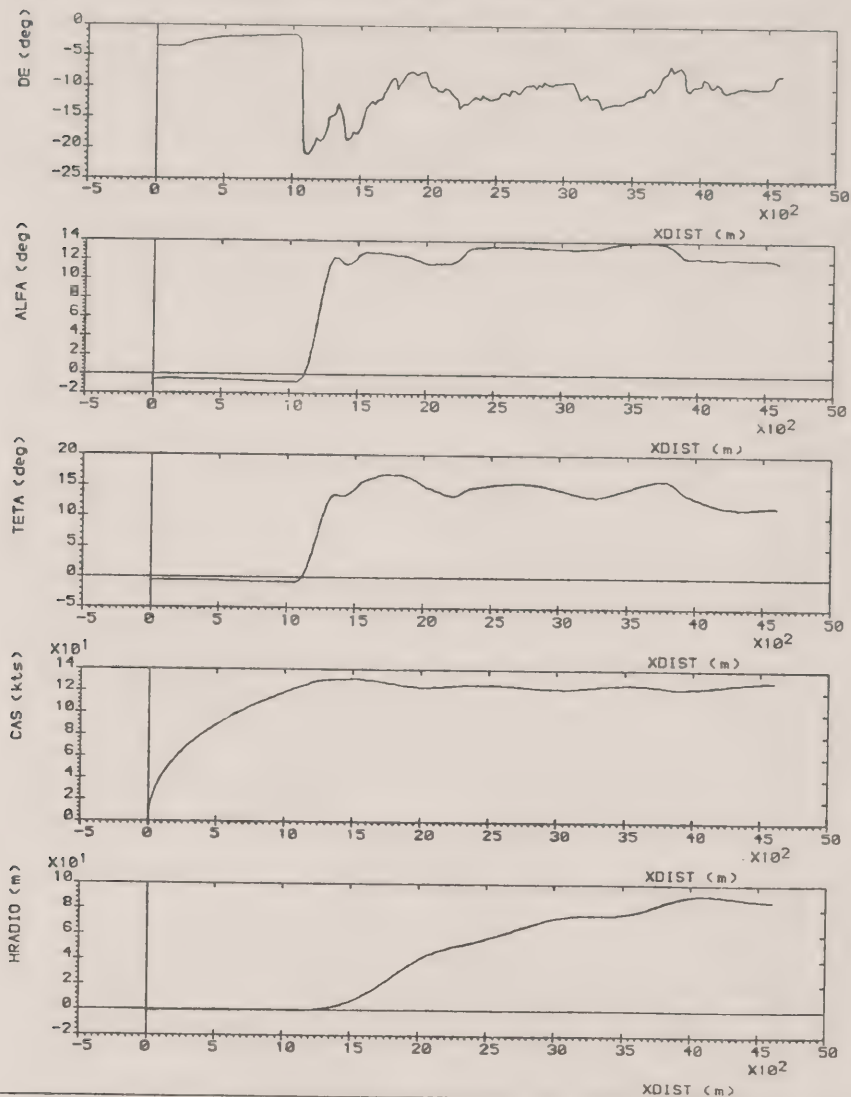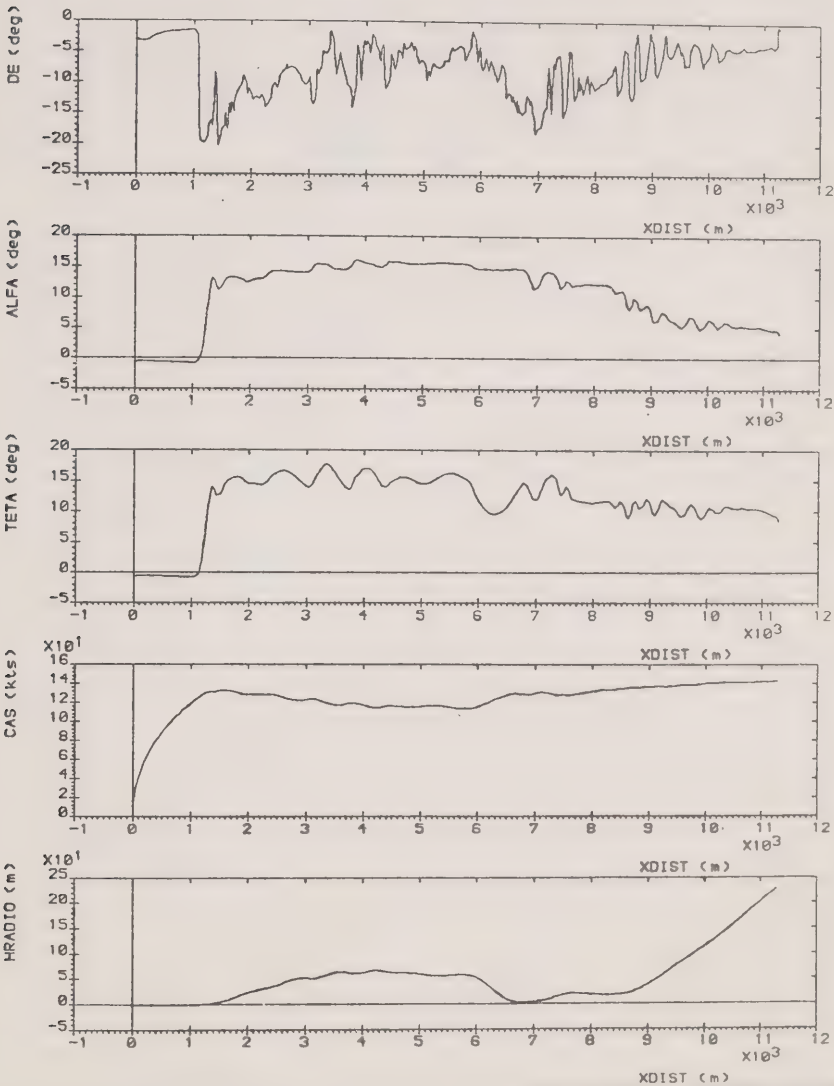
RESTRICTED

report no.:

VS-28-25

Ident: 100A4.02 TAY620   File : DMP.SLUSH.4A6   Date : 1- 8-1989
FOKKER 100 / TAY620
ICE=0.8
SLUSH=0.15
900 KG WEIGHT INCREMENT DUE TO ICE ON AIRCRAFT
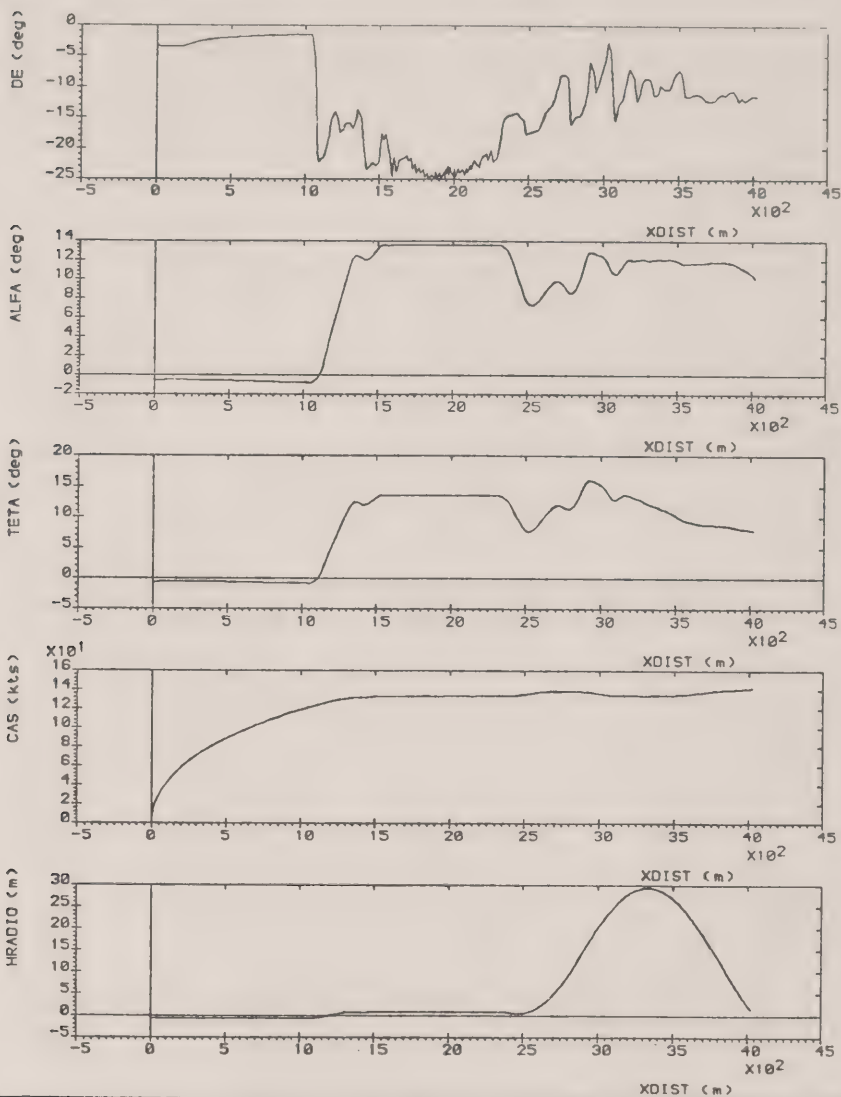
REPORT

security class		issue date June 1989	issue no
	Restricted	report no VS-28-25	

TAKE-OFF WITH ICE

Fokker 100, Flap 18, EPR=1.62, Weight=87000 lbs ISA/SL

○ Take-off run , h=0m, lift off

□ Take-off distance , h=35 ft

Test date June 7th, 1989

NO SLUSH   0.5" SLUSH

Distance [ft]

10000 · 9000 · 8000 · 7000 · 6000 · 5000 · 4000 · 3000

TOD

TOR

nosewheel lift-off

17400

0   50%   100%
Ice on wing

0   50%   100%
Ice on wing

REPORT

TAKE-OFF DISTANCE WITH SLUSH AND ICE

Fokker 100, Flap 18, EPR=1.62, 1500ft/0°C
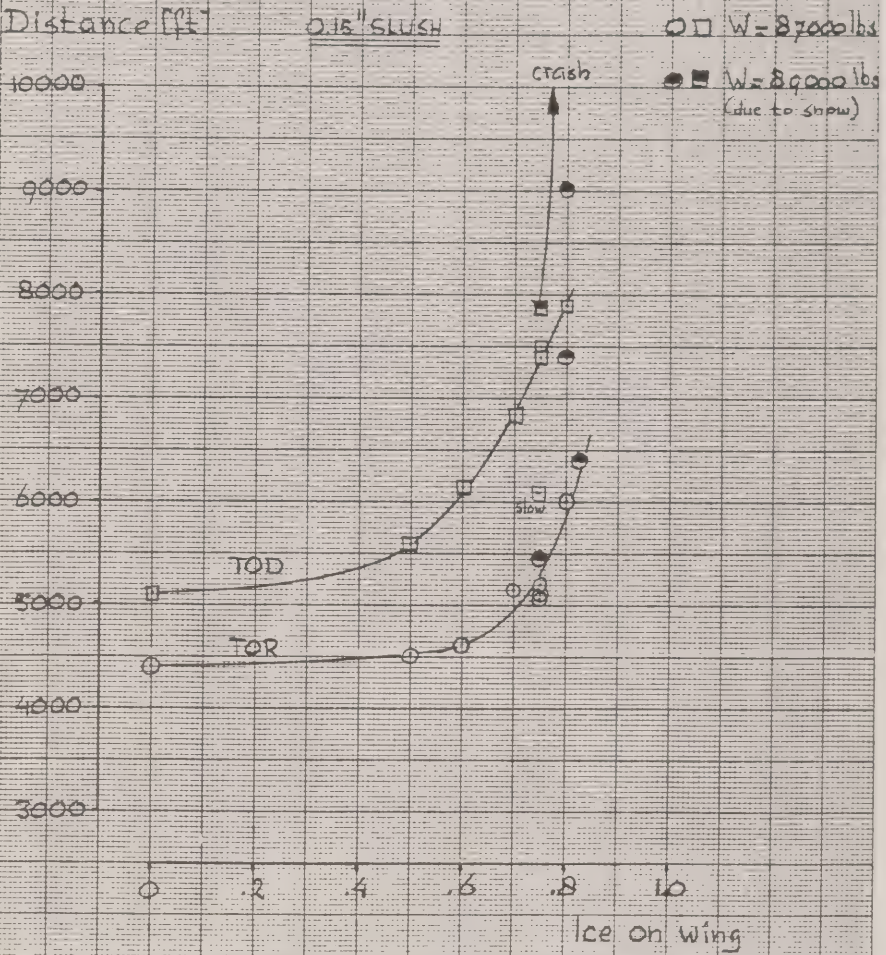
○● Take-Off Run, to lift-off

□■ Take-Off Distance, to h=35 ft

Distance [ft]   0.15" SLUSH   ○□ W=87000 lbs

                                    crash   ●■ W=89000 lbs
                                                     (due to snow)

Figure 36

REPORT

security class	report no
RESTRICTED	VS-28-25

TAKE-OFF DISTANCE WITH SLUSH AND ICE
FOKKER 100, FLAP 25, EPR 1.62, 1500 ft/0°C
○● Take-off Run, to lift-off
☐■ Take-off Distance, to h=35 ft

DISTANCE [FT]

10000

0.15" SLUSH

○☐ W. 83900 lbs

9000   ●■ W=85900 lbs

NO LIFT-OFF

CRASH

8000

7000

6000

5000   TOD

4000   TOR

3000

0   .2   .4   .6   .8   1.0

ICE ON WING
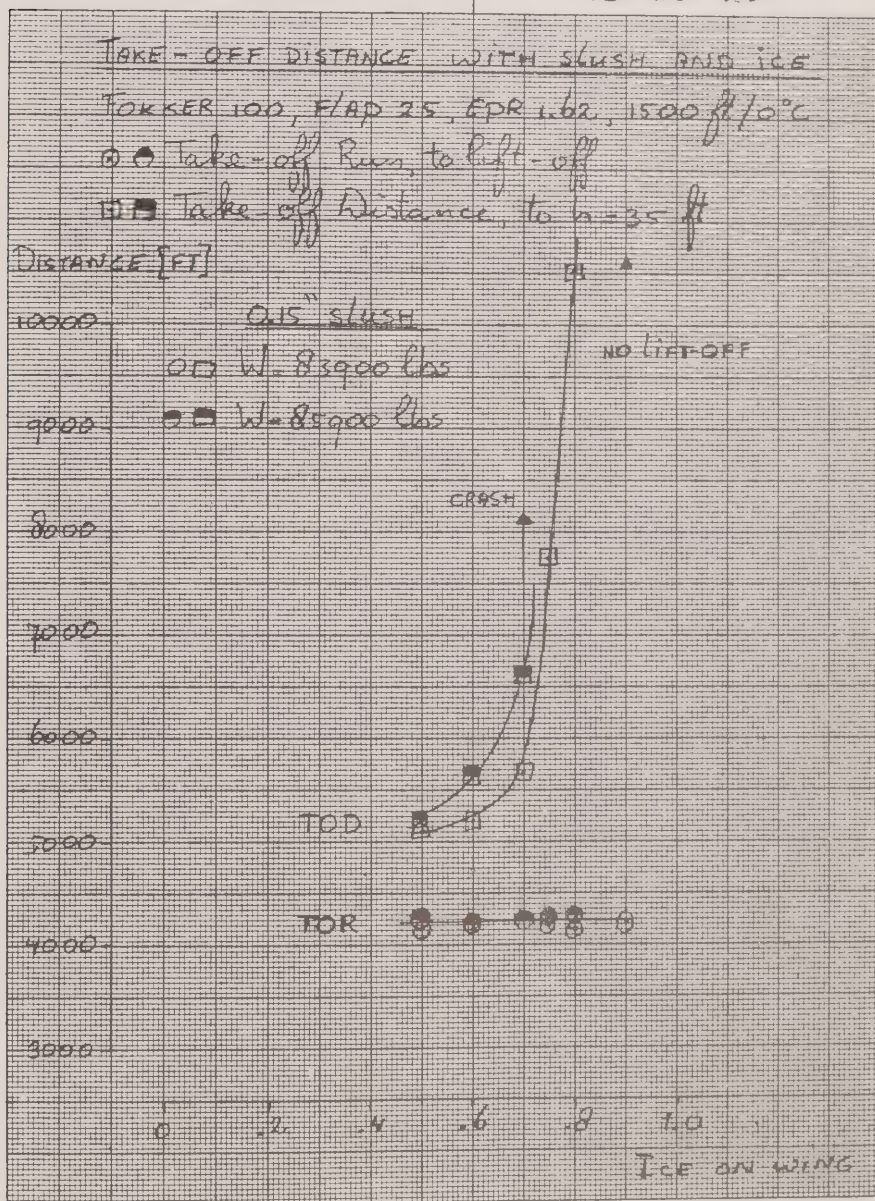
FIGURE 37

Appendix 4

A Report on the Flight Dynamics of the Fokker F-28 Mk 1000 as They Pertain to the Accident at Dryden, Ontario, March 1989

J.M. Morgan
G.A. Wagner
R.H. Wickens

November 22, 1989

Canadä

A REPORT ON THE FLIGHT DYNAMICS OF THE FOKKER F-28 Mk 1000 AS THEY PERTAIN TO THE ACCIDENT AT DRYDEN, ONTARIO, MARCH 1989

Prepared by

J.M. Morgan
Flight Research Laboratory
National Aeronautical Establishment

G.A. Wagner
Air Canada and CALPA

R.H. Wickens
Low Speed Aerodynamics Laboratory
National Aeronautical Establishment

Copy # /2

A REPORT ON THE FLIGHT DYNAMICS OF THE FOKKER F-28 Mᴋ 1000 AS THEY PERTAIN TO THE ACCIDENT AT DRYDEN, ONTARIO, MARCH 1989

Prepared by

J.M.Morgan
Flight Research Laboratory
National Aeronautical Establishment

G.A.Wagner
Air Canada and CALPA

R.H.Wickens
Low Speed Aerodynamics Laboratory
National Aeronautical Establishment

STATEMENT OF OWNERSHIP

F-28 FLIGHT DYNAMICS
TABLE OF CONTENTS

SECTION 1 - GENERAL INTRODUCTION

SECTION 2 - AERODYNAMICS

SECTION 3 - DYNAMIC SIMULATIONS

SECTION 4 - MATHEMATICAL MODELLING

F-28 FLIGHT DYNAMICS
SECTION 1

OVERVIEW AND GENERAL INTRODUCTION

INTRODUCTION

In March 1989 a Fokker F-28 Mk1000, C-FONF, operated by Air Ontario crashed while attempting a take-off at Dryden, Ontario, under adverse weather conditions. The accident investigation is taking the form of a Judicial Enquiry and as such persons not normally a part of the Canadian aviation accident investigative group are assisting or participating in the enquiry. A sub committee of the full fact gathering team has been designated the Performance Sub Committee or the Performance Steering Group and has been charged with investigating the take off performance of the F-28 aircraft and the effects thereon of the environmental conditions existing at the time of the accident. This paper is a distillation of the work of three members of this Steering Group, namely:

J.M.Morgan	National Aeronautical Establishment
G.A.Wagner	Air Canada and CALPA
R.H.Wickens	National Aeronautical Establishment

The three authors represent considerable expertise in a variety of appropriate disciplines. Mr Wickens is a specialist in low speed aerodynamics, Mr Wagner is a practising airline pilot who is also a qualified aeronautical engineer and assistant university professor, while Mr Morgan is a physics graduate and an engineering test pilot with extensive experience in real-time software and mathematical modelling techniques.

DOCUMENT ORGANISATION

The document has been divided up into Sections describing the various aspects of the work conducted, namely:

Section 1. This section is a general introduction and gives a brief overview of information available to the group and the kinds of investigations carried out in support of the enquiry.

Section 2. This section provides in depth background information into the aerodynamics of lift and drag, the effects of surface roughness (contamination) on the performance of an aerofoil and some detailed analysis of the F-28 wing.

Section 3. In Section 3 dynamic man-in-the-loop simulations carried out during a visit to the Fokker plant are described together with tentative conclusion drawn from them.

Section 4. Here analytical mathematical modelling of the F-28 is described in detail and sample trajectories for a F-28 aircraft attempting take off in the presence of flying surface and runway contamination are presented. The results are interpreted and conclusions based on the off-line modelling are discussed.

Section 5. This section deals with validation of the mathematical models described in Section 4.

Section 6. This section completes the document with a brief discussion of the results and offers conclusions as to the engineering reasons for the trajectory observed at the Dryden accident.

OBJECTIVES

The objective of the simulation work was to develop a range of possible flight path scenarios which were similar to that flown by the crew of the F28-MK1000 in the Dryden accident and from that determine a range of conditions which could have caused such a trajectory. The aerodynamic analyses were performed to support the simulation efforts and to provide enhanced background for the accident analysis and investigation.

THE INVESTIGATIVE PROCESS

For some decades now, civil transport aircraft have been required to carry Flight Data Recorders (FDR) and Cockpit Voice Recorders (CVR), devices that record a variety of aircraft state, configuration, power plant and crew activity parameters. These devices are built to withstand high levels of impact and certain exposure to fire while retaining their data in a recoverable fashion. When these recorders are recovered intact and useable after a crash, flight path re-construction is usually possible with a high level of confidence and such re-constructions can be invaluable in determining possible or probable causes of the accident.

Unfortunately the FDR aboard the Dryden aircraft did not survive in a readable state due to an intense post-crash fire. This meant that the group had only the accounts of eye witnesses on which to base any assumptions as to the aircraft's pre-crash behaviour. Luckily there were a comparatively large number of witnesses, including survivors and amongst the latter were several professional pilots, whose recollections have proved very valuable. There was also reasonable agreement among the witness reports as to the trajectory of the aircraft prior to crash, while analysis of tree impacts conducted by personnel of the Canadian Aviation Safety Board (CASB) shed some light on the flight path just prior to the final impact.

GENERAL CONDITIONS OF ACCIDENT

From witness's statements or interviews and the impact swath through the trees, there are some general prima facie conclusions which can be drawn, these are:

The aircraft's wing was, to some extent or other contaminated with snow and or slush at the start of the take-off run, and was at least partially contaminated up to the point of rotation.

The wing trailing-edge flaps were set to 18 degrees at the start of the take-off run and were at or near 25 degrees at the point of impact.

The engines functioned normally throughout the take-off attempt.

The aircraft rotated for the first time rather later than normal, either became briefly airborne or partially so, un-rotated temporarily, re-rotated and became airborne at very low level at or close to the end of the runway. It remained at very low level (failed to climb) until impact.

There is a very high probability that the runway was contaminated with snow or slush at the time of the take off attempt.

ASSUMPTIONS

In this case due to the lack of factual numerical data, the only way to attempt to re-create the flight path was by assuming certain details about the aircraft's mechanical and operational status, and then using a mathematical simulation and varying parameters which were possibly related to the reason the aircraft failed to fly.

The resulting flight paths were then compared with witness reports and other analyses of the aircraft's trajectory. These simulator studies were set up to produce the same forms of numerical and graphical output as would be obtained from a FDR analysis. Simulator studies were conducted both in a real-time dynamic engineering simulator at Fokker in Holland and by the use of mathematical flight path simulations based on aircraft performance data supplied by the manufacturer. The off-line simulations were written and developed by members of the sub-committee on performance.

These studies assume, based on information provided to us by other groups involved in this investigation, that:

o   The aircraft powerplants generated normal thrust throughout the takeoff (although we do consider a single powerplant failure for completeness).

o   There were no structural failures prior to impact.

o   There were no brake failures or seizures, or tire failures which would have extended the ground roll portion of the takeoff or rendered the aircraft incapable of achieving Vus (unstick speed).

o   There were no flight control system failures.

o   There was no interference in the flight control system from any source.

o   The flight crew handled the aircraft with normal handling techniques.

o   There were no system/instrument failures such that the flight crew was unable to fly the aircraft with the precision required for instrument flight. (An example would be failure of pitot heat so that the pilots would not have airspeed information available).

o   There were no adverse wind conditions which would have affected the aircraft's performance.

Based on the above assumptions, these simulations attempt to recreate the flight profile of the aircraft by assuming a range of wing snow/ice contamination levels and runway water/slush/wet snow contamination. These simulations and the results should NOT be interpreted as defining what actually happened to the accident aircraft. Rather, the material presented in this study should be interpreted as follows:

If the aircraft suffered no other operational or technical problems other than wing contamination combined with a certain degree of rolling resistance contamination on the runway, then the results of this simulation are possibly representative of the Dryden accident flight profile. In effect, this simulation and analysis is examining a subset (primarily aerodynamic and handling parameters) of all possible factors which may have been related to this accident.

CONTAMINATED WING TAKE OFFS

There is a long history of aircraft accidents related to flight in icing conditions. Specifically, there have been a number of accidents of aircraft which took off with ice/snow contaminants adhering to the wings and other parts of the aircraft. In these cases, either the aircraft were not de-iced prior to takeoff or the time between de-icing and departure was so long that the aircraft wings were again contaminated at takeoff time.

Additionally, there have been a number of events with F28-1000 aircraft which indicated that this aircraft was no different than others of similar configuration; it is sensitive to ice and snow contaminants on the wing, especially on the first 15% of chord. Experience with the F28 indicated that early flow separation and stalling was a characteristic effect of ice and snow contaminants on the wings. Furthermore, the premature separation on F28 aircraft typically caused wing drop as a result of outer panel flow separation and wing tip stall prior to inboard wing stall. (See Section 2 for details on this characteristic). There were two F28 accidents a number of years ago, one in Turkey and the other in Hanover, Germany, which are similar in a number of characteristics to the Dryden accident.

In the Dryden accident, the witness reports of contaminant on the wings of the aircraft during the takeoff roll, combined with descriptions of the aircraft's flight characteristics during takeoff roll, rotation, liftoff, and the short airborne segment were, in general terms, similar to reports of other ice/snow related accidents. This is true of events involving both the F28 and other aircraft.

These facts, combined with the lack of FDR data, provided the rationale for a requirement to simulate the flight path of the F28-MK1000 while considering significant amounts of wing contaminant and runway contamination. The engine failure case considered in this section was studied <u>not</u> because we had any indication to date that one of the powerplants had failed, but rather for completeness.

GENERAL APPLICABILITY

In this study, great care has been taken to model specifically the performance of the Fokker F-28 in the presence of contamination of both the flying surfaces and the runway. The results obtained, though, should never be interpreted in any way as indicating that this specific aircraft has shortcomings in this respect to any greater or lesser extent than any other aircraft in this class. Such sensitivity to contamination as has been demonstrated in this exercise might reasonably be expected to pertain in any aircraft of this class (ie, swept wing, jet propelled) in far greater measure than is seen in other classes of aeroplane. This is vividly portrayed in Figure 1, taken directly from a Fokker publication [1], which shows the markedly more severe penalties paid for contamination by a jet as opposed to a propeller powered aircraft. Not only does the shallower lift curve slope and

Figure 1 : Jet and Propeller Comparison

reduced C_{Lmax} of the swept wing make the performance more readily degradable, but the jet powered machine does not have the advantage of a relatively large area of its wing being immersed in high velocity air from the propeller slipstream, its only lift producing capability being a result of its motion relative to the air.

F-28 FLIGHT DYNAMICS
SECTION 2

AERODYNAMIC NOTES AND A DISCUSSION
OF THE STALL AND POST STALL BEHAVIOUR

INTRODUCTION

This section of the report on flight dynamics presents a brief survey of the aerodynamic principles which are relevant to the Fokker F-28 transport aircraft, during ground roll and initial climb phase, and to degrees of wing contamination which affect that portion of the flight envelope.

Icing contamination of the lifting and control surfaces is not specifically addressed in this discussion, except in the context of roughness-induced changes to the wing characteristics, including stall and trim changes.

LIFT

The production of lift and drag on a conventional wing is a consequence of the streamline flow around the aerofoil and its smooth departure from the trailing edge. The lift force originates from the circulation and curvature of the flow over the profile and drag is a result of fluid viscosity and span loading.

The flow accelerates over the top and bottom of the aerofoil, especially near the leading edge. The pressures on both surfaces fall below ambient static pressure and the differential between these values, taken over the entire wing surface, results in a net lifting force.

The lift force is the product of flow dynamic pressure, wing area and lift coefficient, it expressed as follows:

$$L = (\tfrac{1}{2}\rho V^2) \times (S) \times (C_L) \tag{1}$$

The lift coefficient, C_L depends on the angle of attack of the wing or aerofoil, where angle of attack is defined as the inclination of the aerofoil chord line to the oncoming flow. A similar expression for drag is:

$$D = (\tfrac{1}{2}\rho V^2) \times (S) \times (C_D) \tag{2}$$

Lift is always at right angles to the direction of flight and drag is directed rearwards along the direction of flight. Figure 1 shows the forces on an aerofoil section in conditions of attached flow and also for separated flow, or stall. For normal attached flow the lift force can be decomposed into two components: a normal force and a force in the plane of the chord line, directed upwind. This latter force is known as leading edge suction and is caused by the curvature and acceleration of the flow around the leading edge. Achieving the full value of leading edge suction is crucial to the efficient operation of the aerofoil. If the value of the leading edge suction is reduced, or lost completely (as may be the case

when the wing is stalled) then the main force on the aerofoil, in addition to friction drag, is the normal force, whose components are a reduced lift and a significant drag component (Figure 1b).

The basic characteristics of an aerofoil can be altered by the use of camber and high lift devices. The effect of camber is to change the relationship between lift coefficient, C_L, and angle of attack (α), see Figure 2. With a cambered aerofoil, C_L has a finite value when α is zero; however, the slope of the lift curve remains unchanged. High lift devices consist of trailing edge flaps, which extend rearwards and downwards and may have complex geometries, and leading edge slats, which extend forwards and downwards and enable the flow at the leading edge to remain attached at higher angles of attack than would otherwise be the case.

The main effect of flaps is to displace the lift curve upwards by an amount which depends on flap angle and geometry (Figure 3a). Maximum C_L is increased but still occurs at an angle of attack similar to that of the unflapped wing. Flap deflection also results in a sizeable drag increment (Figure 3b).

The increment in lift achieved by flap defection results in increased flow acceleration and suction on the nose of the aerofoil. To avoid leading edge separation and to achieve the potential gains in maximum lift, special attention must be paid to the leading edge design. This is done by the use of a generous nose radius (as in the case of the F-28 wing) or by the use of a leading edge slat. Figure 3a shows the effect of the extension of leading edge devices on the lift characteristics of the basic and flapped wing. Maximum C_L is increased significantly and occurs at a greater angle of attack than with the device retracted. Drag also increases as a result of slat extension but not as much as for the extension of flaps.

The pitching moment on the aerofoil is also affected by camber and the deflection of flaps. As angle of attack increases the aerofoil pitching moment is approximately constant until the stall. After the stall the tendency is to pitch nose down. Flap extension produces a further nose down increment in the pitching moment. Pitching moment is expressed as:

$$M = (\tfrac{1}{2}\rho V^2) \times (S) \times (c) \times (C_M) \tag{3}$$

where (c) is the characteristic length, (ie the chord length for an aerofoil) and C_M the pitching moment coefficient.

The foregoing discussion relates to the origins of lift on the wing section, or aerofoil. The lift of the complete wing is more complex, and depends upon the shape of the planform, principally the aspect ratio, (span squared/area). The vortex flow that is a fundamental characteristic of the aerofoil section, extends along the span, and leaves the wing tips in the form of wing tip vortices which stream downwind. Actually, vorticity is shed along the entire wing span in the form of a vortex sheet that subsequently rolls up at the side edges into concentrated free vortices.

For the purpose of analysis the wing can be replaced by a vortex system consisting of a bound vortex travelling with the wing, and free vortices that emanate from the wing tips and stream down wind. A schematic representation of this flow model is shown in Figure (4).

This simple concept has allowed all conventional lifting surfaces to be compared on the same basis; aerodynamic theory shows that aspect ratio is the governing physical parameter that determines lifting performance and induced drag. The slope of the lift curve is linear over the operating range of the wing, and decreases as wing aspect ratio decreases. The upper bound of the relationship is the lift curve slope of the airfoil section, corresponding to an infinite aspect ratio and it is evident from Figure 4b that a high aspect ratio is desirable for efficient flight. Conversely, a disturbance in the distribution of spanwise load, such as that caused by the deflection of trailing edge controls, or a partial stall, corresponds to a lower equivalent aspect ratio, lower lifting effectiveness and higher induced drag as compared to the undisturbed span loading.

The free vortex system behind the wing gives rise to an induced flow, the vertical component of which is termed "downwash". The momentum of this flow is imparted to the undisturbed air per unit time as the wing advances, and is directly related to lift. The energy of the complete downwash field represents the price to be paid for the generation of lift. The downwash flow in the region immediately behind the wing is important for the operation of the tail plane, and the longitudinal stability of the aircraft. Thus if aspect ratio changes, or if a local disturbance occurs on the wing surface, the downwash will be altered, the load on the tail plane will change, and the aircraft trim equilibrium will be disturbed.

DRAG

Drag forces acting on an aircraft consist of two components: pressure drag and friction drag. Pressure drag, which is parallel to the direction of motion, results from the pressure forces acting on the body. Friction drag is the sum of all the tangential forces taken in the same direction, and is the viscous component.

Pressure drag has two components: induced drag, which is dependent upon lift and wing aspect ratio; and wake or form drag, which is dependent upon the shape of the wing section, and the growth of the unseparated boundary layer. Form drag originates from a balance of the pressures over the front and rear portions of the airfoil section, and can be thought of as a buoyancy force directed rearwards.

Form or wake drag is zero if the flow is frictionless, and the external flow closes around the wing (ie. no separation). This is known as D'Alembert's paradox. In a real flow, however, where viscosity consumes the momentum next to the wing surface, the pressure over the rear portion of the airfoil is altered, and therefore no longer balances the forward pressure force. The resulting imbalance is a pressure drag and depends upon the form or profile of the airfoil. If separation, or any other disturbance occurs on the rear portion of the airfoil, this imbalance becomes very large and constitutes a significant increase in drag. Form drag and friction drag, taken together, are called profile drag, and depend on the local cross-section or profile of the wing.

The induced drag of the lifting system arises from the bound and streamwise arrangement of vorticity. In its simplest form, the wing can be thought of as a device which advances into still air, and continuously deflects downwards, a finite mass of air in the wake. This idealization, known as the streamtube concept, suggests that the trailing wake and its circulating flows are contained within a circular tube spanning the wing tips, that contains all of the momentum associated with the production of lift.

Similarly, the work done in producing this deflected streamtube, its internal flows and its downward motion, results in a drag which is dependent upon lift, and is termed induced drag.

A simple formula for total drag is as follows:

$$C_D = C_{D_0} + C_L^2/\pi(Ae) \tag{4}$$

C_{D_0} is the viscous drag coefficient, and (Ae) is the effective aspect ratio. Lift/drag ratio, a measure of wing performance, depends upon effective aspect ratio, and profile drag.

A secondary, but important parameter in the relationship between lift and induced drag, is the distribution of aerodynamic load along the span of the wing. Induced drag is a minimum when the distribution of lift over the span is elliptic in shape and the value of the wing efficiency factor e is 1.0. Any departure from this shape, due to local separation, or deflection of controls, results in a non-optimum load distribution, a value of e less than 1.0, and higher induced drag for the same lift.

SKIN FRICTION AND THE BOUNDARY LAYER

Viscous drag resulting from the frictional force on the wing arises from the loss of momentum of the fluid that has passed over the surface. This phenomenon is confined to a thin layer adjacent to the surface, in which intense shearing takes place. The shearing stress, or frictional force per unit area, is measured by the product of the coefficient of viscosity and the velocity gradient next to the surface. Thus a gas of low viscosity can produce significant frictional drag on a smooth surface. The boundary layer, as this thin region is called, may be composed of either laminar or turbulent flow and its behaviour determines the limits of efficiency and stability of the airflow over the range of operation of the aircraft.

The initial flow in the boundary layer on a smooth surface will be smooth and orderly (ie. laminar), and the velocity increases from zero to its full value across the thin layer of the viscous region. This layer, in which momentum loss occurs, increases in thickness with distance from the leading edge; the frictional force, which depends upon the velocity gradient, diminishes in the same distance. Figure 5 shows, schematically, the main elements of the laminar and turbulent boundary layer.

Viscous drag is the sum of the frictional force over the length of the surface. Thickening of the laminar boundary layer with distance implies a continuous loss of kinetic energy dissipated by viscosity, and at some point separation will occur when the kinetic energy of the flow is sufficiently reduced. This will occur more rapidly if the flow is advancing into an adverse (positive) pressure gradient.

Transition from laminar to turbulent flow in the natural boundary layer is inevitable, and has both beneficial and adverse effects. As is known for the dimpled golf ball, a turbulent flow resists the tendency to separate with a corresponding reduction of form drag. The same observation can be made for the airfoil in which the boundary layer flow is turbulent. The tendency to separate is resisted, and the maximum lift coefficient at which the airfoil will stall is increased. The negative effect is that as far as viscous forces are concerned, the turbulent boundary layer will have a higher skin friction, and hence a higher drag than the laminar layer, even on a smooth surface.

The main criterion which determines whether or not the boundary layer is turbulent is a parameter which expresses the ratio of fluid inertial and friction forces. The parameter is the Reynold's Number[1] and it determines the relationship between the flows on similar bodies, such as the wing boundary layer flow on a full size aircraft, and its scaled-down model counterpart. Reynold's Number also determines, in both cases, when the boundary layer makes the transition from laminar to turbulent flow. Research has shown that for flow on a smooth flat plate, transition to turbulence will occur at a Reynold's number of about one million. This is well below the value for typical transport aircraft on take off, so unless the aircraft wing is designed specifically to have extensive laminar flow, it will be fully turbulent over most of its length, and therefore its flight envelope.

The turbulent boundary layer is characterized by a thick layer of turbulent mixing and dissipation. Embedded below the turbulent region is a thin laminar layer next to the surface, called the laminar sub-layer. It is in this sub-layer where the velocity gradients are high, and the frictional drag originates (Figure 5b). The flow on the airfoil at full scale Reynold's numbers is turbulent except at the nose, near the leading edge attachment point, where the boundary layer is initially laminar. Transition to turbulence occurs within a short distance, however, due to local pressure gradients and the condition of the surface.

The laminar sub-layer over the forward portion of the aerofoil chord has high levels of frictional drag, but its thickness is gradually reduced by the turbulent region adjacent to it, as the flow progresses along the chord. The initial thickness of the sub-layer is important in determining whether or not the surface can be considered aerodynamically "smooth", or "rough". This is especially critical near the nose of the airfoil, where any protuberances or roughness elements will have a serious effect further downstream: further aft on the chord

---

[1] Reynold's Number is defined as:
$$R_e = (velocity)x(chord)/(kinematic\ viscosity)$$

the rising turbulence intrudes into the sub-layer, the surface is always considered "rough", and the energy loss is due mainly to turbulent dissipation.

Because the flow at the trailing edge is theoretically a stagnation point, the external flow must decelerate before coming to rest, resulting in an adverse pressure gradient. If upstream roughness or excessive turbulent dissipation has consumed momentum in the boundary layer, it may separate, and the stall begins. As the wing incidence increases, separation becomes more wide spread until the wing is said to have stalled.

If the surface contamination elements (rivet heads, frost etc.) lie within the laminar sublayer they have virtually no effect on the total resistance. If, however, the roughness elements protrude beyond the laminar sublayer, the result is a noticeable increase in skin friction, and production of more turbulence. An increase of Reynold's number aggravates this problem since the laminar sub-layer becomes thinner at high Reynold's numbers. If the roughness height is large in comparison with the laminar sub-layer, then the frontal drag of these elements determines the average skin friction, and their shape, orientation and distribution become important. The increased turbulence and dissipation in the roughened boundary layer also leads to a premature flow separation and stall for Reynold's numbers above one million. At high Reynold's numbers nearly all of the loss of energy is due to wake formation; the resistance is independent of viscosity, and proportional to the square of the velocity. Figure 5c shows the effect of Reynold's number on drag coefficient in laminar and turbulent flow. If the surface is rough, the curve representing turbulent flow indicates an increase in skin friction drag.

Figure 6a shows the critical roughness size (in terms of percent chord) below which there is no increase in drag on a flat surface. The working range of Reynold's number for the F-28 is also indicated in this Figure. For distributed roughness greater than the critical size, Figure 6b shows the drag increase experienced by both wings and bodies, for a range of Reynold's numbers.

CHARACTERISTICS OF THE STALL OF AEROFOILS

Separation of the turbulent boundary layer is followed by partial or complete detachment of flow over the airfoil, a dramatic decrease in lift, and an increase in drag. The trailing edge no longer completely governs the strength of the circulation and vorticity is shed downwind as a turbulent wake. The chordwise distribution of pressure is greatly altered, and the resulting change in airfoil pitching moment will disturb the aircraft trim conditions. Since the pressure distribution of the stalled airfoil no longer conforms to that of attached flow, form drag will increase. Friction drag is indeterminate over the separated region, but will be active on the lower surface of the airfoil. For the complete wing, induced or vortex drag will be less, since lift is lower.

There are basically three types of aerofoil stall (illustrated in Figure B-1), and the characteristics of each are governed mainly by airfoil geometry and Reynold's number.

Type 1: Trailing Edge Stall

The trailing edge stall is the most common and desirable type of stall for airfoils with thickness/chord ratios 15% and above. At high angles of attack, flow on the upper surface is characterized by a thickening of the turbulent boundary layer, followed by an initial separation at the trailing edge. The separation gradually moves forward, with a corresponding decrease in lift. Maximum lift occurs when the separation reaches mid-chord. The resulting collapse of lift is gradual, drag continues to rise rapidly, and pitching moment becomes less nose down. Flow at the leading edge remains attached, and the leading edge suction force is active to a high angle of attack.

Type II: Leading Edge Stall

As thickness/chord ratio decreases below about 10%, the airfoil experiences an abrupt separation of flow near the leading edge. Separation of the laminar portion of the boundary layer occurs well before maximum lift, and transition to turbulent flow will occur in the separated shear layer. The flow will reattach in the form of a small bubble just aft of the airfoil nose. At moderate angles of attack, the pressure distribution is not seriously altered, and the lift, drag and moment characteristics of the airfoil are not greatly changed.

As angle of attack increases, however, the bubble enlarges and moves aft until reattachment of the turbulent shear layer is no longer possible.The flow then separates over the entire airfoil surface, the leading edge suction collapses, and the pressure distribution along the chord remains nearly constant with low negative values. Lift drops abruptly with no gradual transition; pitching moment becomes significantly less nose down.

Type III: Thin Aerofoil Stall

Separation and stall on very thin sections (<6% t/c) consists mainly of the gradual lengthening and ultimate breakdown of the upper surface short bubble. The breakdown of the bubble with resulting flow separation occurs at moderate angles of attack. The lift curve is characterized by a gradual reduction in lift slope, and a stall which occurs at a low maximum lift coefficient, but with a gradual decline. Pitching moment undergoes a large but gradual negative change. The pressure distribution exhibits negative values, which extend over the length of the bubble, as long as it is attached to the surface. When flow breakdown occurs the long bubble detaches from the trailing edge, and a trailing wake is shed from the leading edge.

In general, modern airfoils do not conform precisely to these three distinct categories of stalling behaviour; rather, combinations of the different stall characteristics may be exhibited, and may be sensitive to minor variations of shape, Reynold's number, leading and trailing edge devices etc. For Reynold's numbers appropriate to the operation of typical transport aircraft, a large nose radius is desirable to delay the breakdown of leading edge suction and to achieve the trailing edge separation (type I) and high maximum lift. Conversely, as Reynold's number diminishes, all airfoils tend to stall from the leading edge (type III). Observations from both wind tunnel and flight test indicate that the aerofoil section of the F-28 wing lies well within the region for TYPE I (Trailing Edge) stalls and, as such, may be considered a conservative design. The reason for this may be attributed mainly to the generous nose radius of the aerofoil.

STALLING CHARACTERISTICS OF ROUGHENED AIRFOILS

The previous remarks regarding airfoil stall relate to flow over a smooth surface. When the airfoil has a roughened surface, transition to turbulence occurs earlier, friction drag increases, and flow separates prematurely from the upper surface.

The effect of distributed roughness on the premature stall of airfoils is shown in Figures 7 and 8 which are from Reference [2]. The roughness was distributed uniformly over part or all of the airfoil, and Reynold's number was varied from about 10^5 to 10^7. Maximum lift coefficient is considerably reduced by roughness for the two airfoils which were tested, and the critical Reynold's number at which this occurs decreases as the magnitude of the roughness increases. The results of Reference [1], for the higher Reynold's numbers, indicate that roughening of the entire wing upper surface results in a loss of maximum lift of as much as 50%. Drag under conditions of premature stall would be due mainly to form drag, and would be high. The size of the distributed roughness in these experiments corresponded to 0.01 in. and 0.004 in. on a wing the size of that of the F-28. Most studies of the effect of roughness on the performance of airfoils deal with the uniform distribution of contamination over the entire upper surface. The importance of preserving smooth attached flow around the nose is important; if the nose contamination is removed, the wing is restored to its original unstalled state. Conversely, the contamination may take the form of a single roughness element, or ridge which extends across the span on the upper surface. The drag of such a protuberance depends upon the degree to which it extends above the sub-layer, and the sharpness of its edges. Maximum lift will be reduced and if the flow over the nose is critical, separation will occur abruptly from the leading edge. Figure 7b shows a comparison of the loss of lift due to uniformly distributed roughness to that due to a single, spanwise ridge extending along the wing upper surface.

STALLING OF COMPLETE WING

Stall characteristics of the complete wing depend upon which portion stalls first, and how the separation spreads along the span. Initial stalling at the wing tip is undesirable since it may induce a violent roll, and a loss of aileron control.

If the boundary layer is encouraged to stall first at the wing root, then the tendency to wing drop is lessened, but the turbulence and low total pressure which results from the separation may result in buffeting of the tailplane and poor quality flow in the engine intakes for fuselage-mounted fan engines. Stall management on wings of current transport aircraft is usually achieved by precipitating the separation at a particular spanwise location. This may be accomplished by the use of various devices at the leading edge, eg; kinks in the leading edge, notches, fences or vortilons. These devices not only result in stall at a particular lift coefficient, but ensure a symmetric stall.

GROUND EFFECT

Ground effect is perceived as a cushioning of the aircraft when landing with a resulting tendency to "float" before touchdown. Ground effect also has a significant effect during take-off, although the physical sensation may not be as obvious.

The phenomenon originates from the interaction of the wing and fuselage with the ground plane and is composed of three different phenomena, which affect both lift and drag. They are usually applied as corrections to design and performance data.

The first effect is due to the volume or displacement of the airplane and the low pressures that will be induced between it and its image. These negative pressures act to suck the aircraft on to the ground, and therefore constitute an effective loss of lift.

The second effect occurs only when the wing is lifting and the resulting interaction results in an increase in lift per unit angle of attack. The sensation experienced on landing is due to this increase of lifting effectiveness. This increase is, in some cases, cancelled or reduced by the displacement effect of the aircraft volume, already described.

The third ground effect results from the interaction of the trailing wake behind the wing with the ground plane. The most important result of this is that the upwash at the wing diminishes, so that the effective angle of attack is lower. This causes a significant reduction of induced drag, thereby lengthening the final flight path before touch down.

The beneficial value of ground effect during take-off is reduced drag and increased lift, however these benefits diminish rapidly as the aircraft climbs. At approximately one wing span above the ground, the ground effect has essentially vanished.

AERODYNAMIC CHARACTERISTICS OF
THE FOKKER F-28, MK. - 1000

FOKKER F-28 MK. - 1000 - SPECIFICATIONS

The Fokker F-28 (Mk.1000) is a twin-turbofan short range airliner. It is a swept, low-wing configuration, with a T-tail, and rear mounted engines. The version of the present

investigation seats 65 passengers, and cruises at a maximum speed of 455 kt at 23000 ft (a Mach number of 0.75).

A full technical specification of the Fokker F-28, (MK.-1000) can be had from Reference [3] and is presented in Appendix A. Some of the geometric, weight and performance parameters relevant to the present investigation are listed as follows. A general arrangement of the aircraft is shown in Appendix A.

TABLE I

Wing Span	77'-4 1/2"
Wing Area	822 ft^2
Aspect Ratio	7.27
Mean Aerodynamic Chord (MAC)	11.5 ft.
Engine Thrust[2]	9850 lb.
Max. take-off weight	65000 lb.
Operating weight empty	35,464 lb.
Max cruise speed (23000')	455 kt.

Rotation speed for the F-28 ranges from 100 to 130 kt. depending on weight and environmental factors.

The flow on the wing changes from a high lift condition at lift off using slotted Fowler flaps, to low transonic flow at cruise. The lift coefficients of the mean chord section based on maximum weight and the above speeds are 1.38 and 0.24 at lift-off and cruise respectively. The maximum lift coefficient for the F-28 wing is about 2.1. The wing is not equipped with leading edge devices (Slats, Kreuger Flaps etc.)

The Reynold's number of the flow at the mean chord ranges from 12 million at sea level (lift off at 130 kt) to 29 million at 23000 ft. (455 kt.). The boundary layer flow is turbulent over the main wing component under normal operating conditions.

AERODYNAMIC DATA FOR THE FOKKER F-28, MK.-1000

Relevant aerodynamic data which was made available by Fokker comes from several sources:

---

[2] Sea Level Static, ICAO Standard Day

1)   Results of a wind tunnel test at the NLR[3] in which the effects of simulated ice contamination of the wing were measured.

2) A description of the aerodynamics of wing stall, including flight experience with the airplane.

3) Computed values of pressure distribution, skin friction and displacement thickness of the boundary layer, for the F-28 airfoil section.

4) An official database from which the F-28 simulator model was assembled.

F-28 WIND TUNNEL TEST DATA

Figure 9 shows the results of wind tunnel tests on a complete model of the Fokker F-28. The test Reynold's number of the Mean Aerodynamic Chord (MAC) was 2.85 million, and the wing flaps were set at 30 degrees. The model angle of attack range was from -2 to +20 degrees. The test was conducted in the NLR wind tunnel and the model was positioned on a mounting which allowed a range of pitch angles to be used.

Data are also shown in which the upper surface of the main wing component is treated uniformly distributed carborundum roughness elements. The wing roughness was intended to simulate ice deposits of 1 and 2 mm thickness full scale, uniformly distributed on the upper wing surface at one element per sq cm. Tests were also done with the first 15% of the wing component cleaned off.   Figure 9 presents C_L and C_M plotted against angle of attack, and also C_L against C_D.

The lift slope in the linear part of the lift curve is 0.100. For angles above about 8 degrees, the lift curve becomes non-linear, due to a thickening and deceleration of the trailing edge boundary layer. Maximum lift occurs at 14 degrees, and has a value of C_L = 2.13. The top of the stall is rounded, but lift falls rapidly to a value of 1.55 as the wing pitches to 16.5 degrees. Lift continues to diminish to a value of C_L = 1.46 at 20 degrees angle of attack.

The wing exhibits a characteristic hysteresis in lift, as the angle of attack reverses. Maximum lift is not achieved, and the data returns to the linear part of the lift curve at an angle of attack of 7.5 degrees and at a lift coefficient of 1.75. Hysteresis is an entirely viscous phenomenon, and is a common occurrence on wings and airfoils. It is associated with flow fluctuations, particulary during reattachment at the stall. Hysteresis does not occur when the wing upper surface is roughened; the maximum lift coefficient under these conditions is 1.6.

---

[3] Nationaal Lucht- en Ruimsevaartlaboratorium, the Dutch National Aerospace Laboratory.

Pitching moment C_M, is nose down relative to the quarter chord of the MAC, for values of lift before and after the stall. There is little hysteresis.

Drag rises slowly with lift until maximum lift is reached, as is shown in the drag polar Figure 9. Drag at C_{LMax} is about triple the drag for small values of lift, and is attributed to induced or vortex drag.

As lift falls, after flow separation, the drag rise is due mainly to form drag from the altered wing pressure distributions. Hysteresis also occurs in drag, since the pressure distribution is also affected by the flow separations. As with the lift curve, roughness reduces the hysteresis effect.

The effect of roughness on the wing upper surface is dramatic. Maximum lift occurs some 7 degrees earlier at an angle of attack of 7.5 degrees, and reaches a value of 1.6. At higher angles lift diminishes to $C_L = 1.4$, and thereafter remains constant.

With roughness applied, pitching moment begins to decrease rapidly beyond 8.5 degrees, and thereafter becomes strongly nose down at maximum lift.

Drag at maximum lift for the roughened wing is less than that for the clean wing, but lift is also less: the drag continues to rise rapidly as lift falls. At angles of attack above 11 degrees, there is a rapid rise in drag, to a value of $C_D = 0.6$, with essentially no change in lift.

With the entire wing upper surface roughened, the levels of turbulence in the boundary layer that is developing on the nose are higher than normal and kinetic energy is being exchanged for pressure at a higher rate than for the clean surface. If the roughness elements are large enough the result is higher local drag and turbulence; the sublayer itself is annihilated by the wake turbulence of the roughness elements. This factor and also the fact that the flow is subjected to a rising pressure aft of the nose suction peak, provide the potential for early boundary layer separation and wing stall.

Conversely, if the wing nose is clean over the first 15% of chord, the boundary layer, and particularly the laminar sublayer, develops naturally and is able to negotiate the adverse pressure gradient on the rear half of the wing successfully. If roughness is present on the rear portion of the wing surface only, the potential for flow separation is modified by a weakening of the adverse pressure gradient and the additional roughness-induced turbulence plays a more active role in resisting the tendency to separation. Friction drag, however, will be higher, due mainly to the drag of the roughness elements themselves.

EFFECT OF ROUGHNESS ON DRAG IN UNSEPARATED FLOW

Roughness elements on a smooth surface will affect skin friction drag and if the local flow is still laminar, roughness will cause an immediate transition to turbulent flow. The resistance formulae of Reference [4] can be used to estimate drag theoretically, resulting

from simulated roughness contamination, assuming separation does not occur. For a chord Reynold's number of 12 million, and a smooth surface of the same length as the F-28 mean chord, the total skin friction drag coefficient is estimated to be 0.0029. When roughened, the drag coefficient rises to 0.0065 and 0.0079 for roughness heights of 1 mm and 2 mm respectively. The wind tunnel results obtained by Fokker indicate that, for angles of attack below the stall, roughness causes a drag rise of about 6% in the complete airframe model compared to the smooth wing configuration.

The wind tunnel data for the F-28 model show very clearly the effects of wing contamination on aerodynamic characteristics. They do not, however, conform precisely to the airplane configuration in the present investigation, since the flap setting on the model was 30 degrees, compared to the 18 to 25 degree settings which the actual aeroplane was thought to have had during the takeoff run. The test Reynold's number was 2.85×10^6, compared with 12×10^6 for the aircraft at take-off. The main effect of these differences will be on maximum lift. The lift curve to C_{LMax} for attached flow for a flap angle of 18 degrees is available from the Fokker data base, and it can be assumed that appropriate Reynold's number corrections have been made. Similar information is available for C_D and C_M beyond stall; the correction process is more uncertain, but it is assumed that the incremental changes in the aerodynamic characteristics due to both stall and contamination can be applied from the wind tunnel data directly to the data base.

STALLING CHARACTERISTICS OF THE F-28 WING

The Fokker F-28 has a wing of aspect ratio 7.27, swept 16 degrees at the quarter-chord line. The leading edge profile has a kink at wing station 4700 (40.7% semi-wing span), and a leading edge fence at station 3784 (32.8% semi-wing span). The mean aerodynamic chord, to which Reynold's numbers are referred, is at wing station 4940 (43.8% of wing semi-span). Investigations by Fokker of the maximum lift, and wing stall aerodynamic characteristics using wind tunnel investigations and flight test, are presented in Reference [5].

An important design objective for the F-28 was the achievement of a high maximum lift coefficient, and satisfactory stall characteristics. The wing sections are characterized by a large nose radius in order to improve maximum lift capabilities. Further improvements were achieved by the use of Fowler flaps, which are single slotted at the 18 degree take off position, and double slotted at higher extensions.

In addition to attaining high values of C_{LMax}, it was desirable to produce airplane stall characteristics that resulted in definite nose down pitching. This avoids large attitude changes, high drag levels and losses in height when the aircraft stalls. The pitching moment curve in Figure 9 for the clean wing attests to the fact that this goal was achieved.

Initial wind tunnel testing of the F-28 prototype was performed on both full and half models at Reynold's number 3 and 5 million respectively. Wing stall was characterized by a rapid spanwise spread of the separation. Initiation of the stall at a particular point along the wing was done using a small leading edge fence. The stall progresses in a wedge-

shaped configuration in both outboard and inboard directions. The outer portions of the wing, and the wing root junction stall last, thus enabling full retention of lateral control, and avoidance of flow distortion into the engine intakes until after maximum lift has been achieved. Flight test observations confirmed the wind tunnel test results with regard to stall progression and maximum lift, but also disclosed an initial, strong buffeting which preceded the fully stalled condition. Figure B-2 shows the main features of the stall patterns and vortex wake of the F-28 wing, inferred from wind tunnel and flight test data.

Observations were also made, during flight test of the F-28, of differences in the stall in free air (at altitude) and in ground effect. It was observed that in free air the stall progresses along the wing in the manner already described, while in ground effect however and with the mainwheels in contact with the surface, it was noted that separation occurred on the inboard wing panels only (Reference [3]): the outer wing panels did not stall. Maximum lift was essentially unchanged, but occurred at an angle of attack some 4 degrees lower than in free air. These observations conform to the results of other research into ground effect (Reference [6]). Similar observations are not available for the effect of ground proximity on the stall characteristics of a roughened wing.

The rate and progression of the stall over the artificially roughened wing surface is not precisely known, although the measured lift and drag coefficients supplied by Fokker indicate a complete breakdown of the flow. Since the entire upper wing upper surface of the wind tunnel model, including the leading edge, was roughened, and recalling the basic research on the effects of roughness on lift (Reference [1]), it is likely that separation occurs simultaneously along the entire span. In this situation, the leading edge fences may be less effective in fixing the initial spanwise location of the stall, and also in ensuring a symmetrical stall across the span. Even when complete stall has not occurred on the outer wing panels, the aileron effectiveness may be adversely affected by roughness. No data were available on this point. Figure B-3 shows a representation of the stall pattern and wake on a contaminated wing.

COMPUTED DATA FOR FOKKER F-28 AIRFOIL

The airfoil section of the Fokker F-28 is a modified NACA 4-digit profile, with a large nose radius. The design cruise Mach number of the Mean Aerodynamic Chord is 0.75, and the dive Mach number is 0.83. Airfoil thickness at the M.A.C. is 14%. The generous nose radius, although a limiting factor in high sub-sonic flight, enables flow around the leading edge to remain attached, and the suction force to reach its full value when trailing edge flaps are used during take-off and landing. The graphs shown in Figure 10 give the top and bottom surface pressures, and boundary layer parameters for a flap angle of 18 degrees, and angles of attack of -2 degrees and 5 degrees. The computation method included viscous effects, and used the code VSWAKE.

The maximum nose suction peak at these angles is about -1.2 for $\alpha = -2$ degrees; and -5.34 at $\alpha = +5$ degrees.   Reynold's number in both cases was 15 million.   The lift coefficients were 0.6515 and 1.5100 respectively, and the moment is nose-down.

Calculations include local values of skin friction C_F and boundary layer displacement thickness δ^*.   The displacement thickness represents the distance by which the outer streamlines have been displaced by viscous retardation of the fluid in the inner streamlines. It is a measure of viscous drag.

AERODYNAMIC DATA BASE

The performance group was supplied with a complete data base of aerodynamic, stability and control information. This data base was originally used by Fokker to construct their F-28 dynamic simulator. It is corrected for the variable effects of Reynold's number, Mach number and altitude; so that the data, when applied to the complete equations of motion, produces the real airplane performance in the simulator. The utility of these data in the context of the present investigation is that it is standardized and credible, and can be used to create a realistic scenario for take off and initial climb.

The data which are of initial interest are lift, drag and moment for the aircraft in free flight and also in ground effect. The data do not go beyond $C_{L_{Max}}$ into the post-stall regime. The effects of wing contamination are presented in the form of incremental changes of lift, and it is believed that these are derived from the single wind tunnel test which has already been described Figure 9 for uniform roughness heights of 1 and 2 mm. Incremental corrections for roughness heights smaller than these values were not available in experimental form, although arbitrary factors could be applied to the data (Figure 14).

The aerodynamic effect of the ground cushion during take off and climb, particularly at high lift coefficients, acts to change the angle of attack necessary to produce a certain lift coefficient.   With flaps extended, below a lift coefficient of about 1.5, ground proximity increases lift; particularly when the trailing edge approaches the ground. This is particularly relevant to swept-wing aircraft, where the tips may come close to the ground during rotation.   An additional phenomenon, which reduces lift and induced drag, arises from a reduction of the wing upwash and induced angle of attack. This is due to the presence of the ground plane, which does not allow vertical velocities.

The F-28 data base also includes the effects of ice accretion on the leading edges of the wings, tailplane and fin, to a thickness of 2 in. Graphs in Figure (12) show the incremental changes in lift, drag and pitching moment which would occur during flight operations in icing conditions.

In the context of the present investigation, these data may not represent precisely the type of uniform contamination which was simulated in the NLR wind tunnel, nor ice that is deposited by freezing rain or snow.

CONCLUSIONS

The following conclusions are based on the various F-28 aerodynamic data which were given by Fokker to the performance group. They do not specifically address or explain the circumstances of the Dryden accident at this time.

The F-28 wing section is designed for a cruise mach number of 0.75, and a high maximum lift coefficient at low speeds. A generous nose radius minimizes the likelihood of separation under high lift conditions and promotes stall from the trailing edge.

Stalling of the basic smooth wing is from the trailing edge. It then spreads outward from the leading edge fence location in a fan-shaped manner toward the tip and wing root regions. These regions separate last, allowing lateral control and engine intake flow to remain effective to high angles of attack.

In ground effect, with the main wheels on the ground, stalling occurs 4 degrees earlier, but only the inner portion of the wing stalls. C_{LMax} is unchanged.

Artificial roughness on the upper surface of the wing of a wind tunnel model caused a premature stall in which boundary layer separation may have occurred all along the leading edge. The roughness corresponded to an element size of about 1 to 2 mm on the full scale F-28 wing while the distribution corresponded to approximately one element per square centimetre on the same wing. With flaps set to 30 degrees on the model the wing stalled at an angle of attack 7 degrees lower than for the clean wing. There was a 33% loss of maximum lift compared to the clean wing.

Research on wing sections at Reynold's numbers ranging from 100,000 to 10,000,000 shows that roughness not only increases drag below the stall but also increases the likelihood of a premature stall, particularly if the nose is roughened. As Reynold's number increases towards the values experienced by the F-28 wing during take-off (greater than 10,000,000) the loss in maximum lift can be as high as 50% compared to a clean surface (Reference [1]).

In some cases the aerofoil is sensitive to the size of the roughness elements; the loss of maximum lift being less for very small roughness heights. Most aerofoil sections, however, respond to roughness of any scale by stalling prematurely and incurring the maximum loss of lift. Removal of roughness on the nose and over the first 15% of chord restores the aerofoil close to its original performance.

LIST OF SYMBOLS

A	Aspect Ratio
b	Wing Span
c	Wing Chord
c (MAC)	Mean Aerodynamic Chord
D	Drag
e	Wing Efficiency Factor
L	Lift
M	Moment
Re	Reynold's Number (Vc/ν)
S	Wing Area
V	Flight Velocity
α	Angle of Attack
ρ	Air Density
ν	Kinematic Viscosity
C_L	Lift Coefficient
C_D	Drag Coefficient
C_M	Moment Coefficient
C_P	Wing Surface Pressure Coefficient
C_F	Boundary Layer Friction Coefficient
δ^*	Boundary Layer Displacement Thickness
SLS	Sea Level Standard Conditions

AERODYNAMIC FORCES ACTING ON A WING SECTION

a) ATTACHED FLOW

b) STALLED FLOW
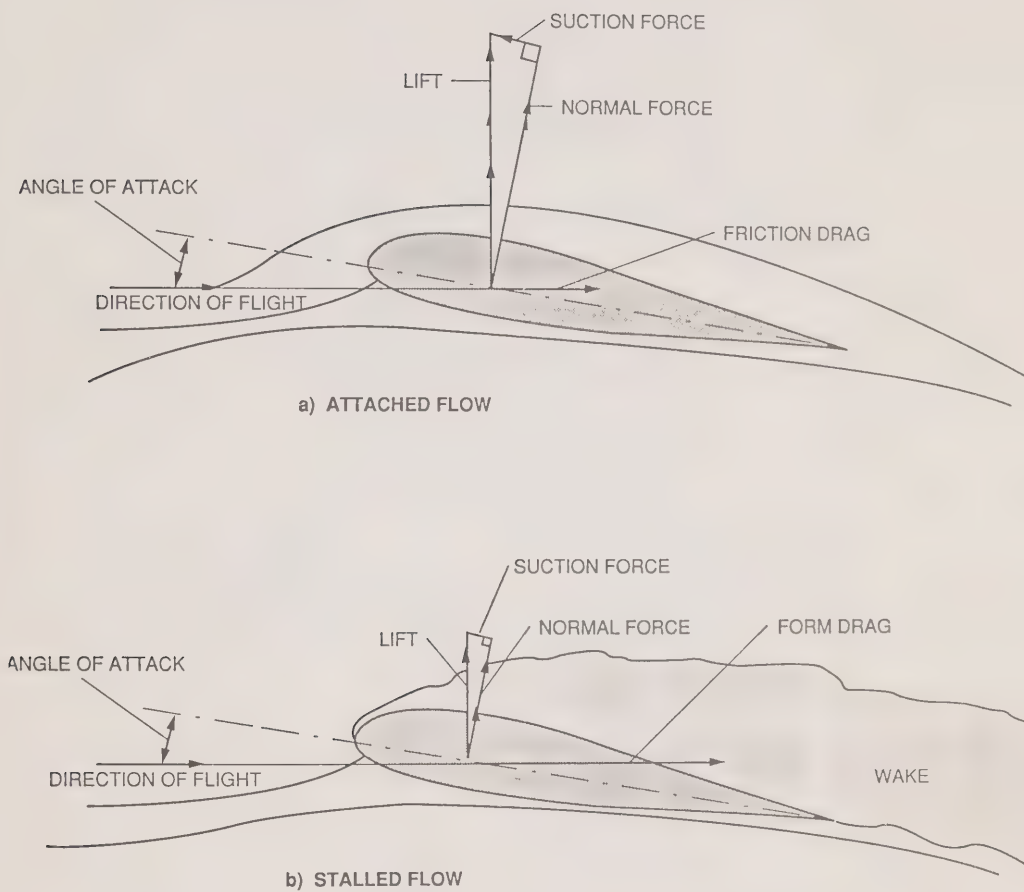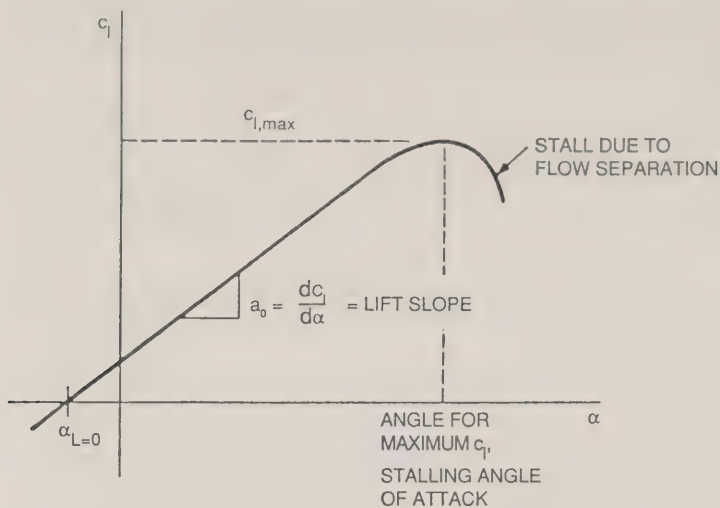
SKETCH OF A TYPICAL LIFT CURVE

(a)
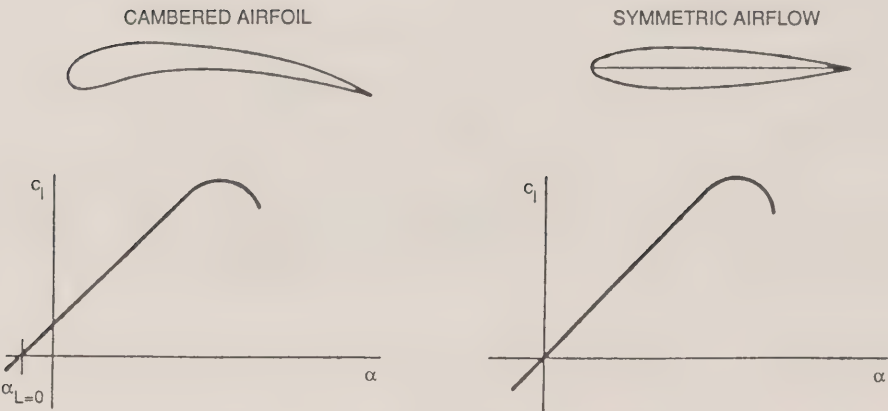
**COMPARISON OF LIFTS CURVES FOR
CAMBERED AND SYMMETRIC AIRFLOWS**

(b)

AIRFOIL LIFT AND DRAG CHARACTERISTICS
WITH HIGH-LIFT DEVICES
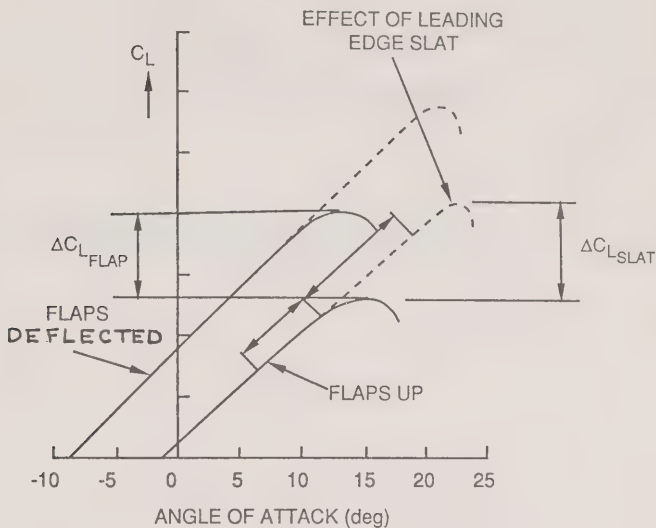
LIFT CURVES WITH AND WITHOUT
HIGH-LIFT DEVICES (REF. 3)
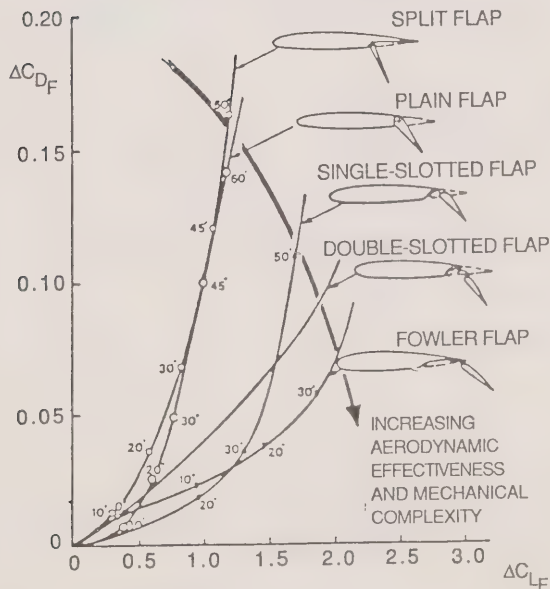
TRENDS IN PERFORMANCE OF
TRAILING-EDGE FLAPS (REF. 3)

TRAILING VORTEX SYSTEM AND LIFT FOR FINITE WINGS

VORTEX

LOW PRESSURE

HIGH PRESSURE

FRONT VIEWING OF WING

(a)

DIRECTION OF FLIGHT

DOWN WASH

WING TIP VORTICES

(b)

**ORIGIN OF WING TIP VORTICES
ON A FINITE WING**

C_L

a_0, LIFT CURVE SLOPE
FOR AN *INFINITE* WING

ANGLE OF ATTACK

(a)

C_L

C_D

C_L

a, LIFT CURVE SLOPE
FOR THE FINITE WING

ANGLE OF ATTACK

(b)

C_L

C_D

**DISTINCTION BETWEEN THE LIFT CURVE SLOPES
FOR INFINITE AND FINITE WINGS**
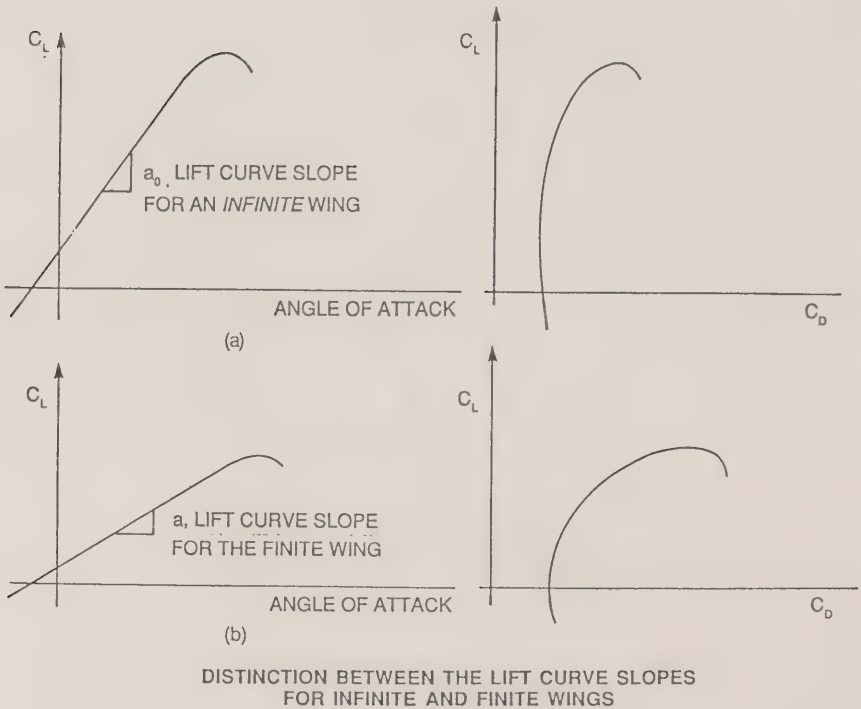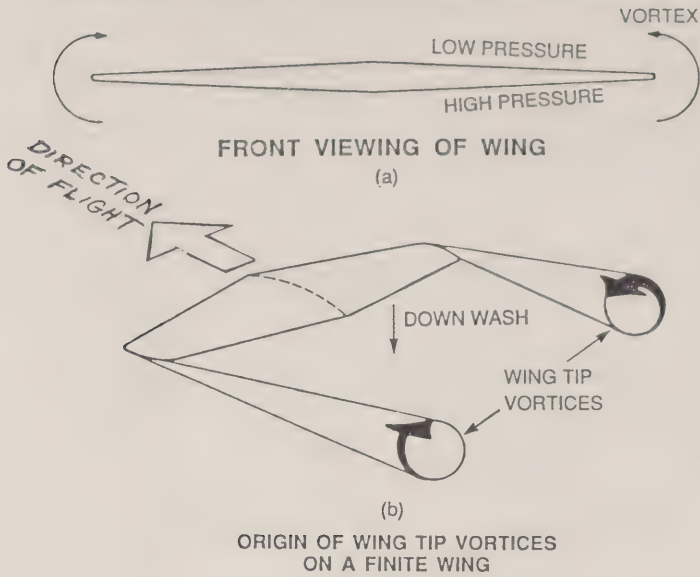
CHARACTERISTICS OF BOUNDARY LAYER FLOW
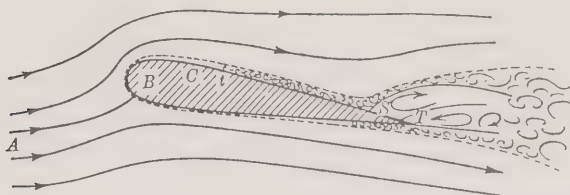
A SKETCH (not to scale) ILLUSTRATING THE NATURE OF THE FLOW OF A UNIFORM
STREAM PAST AN AEROFOIL WHEN SEPARATION OCCURS NEAR THE TRAILING EDGE.
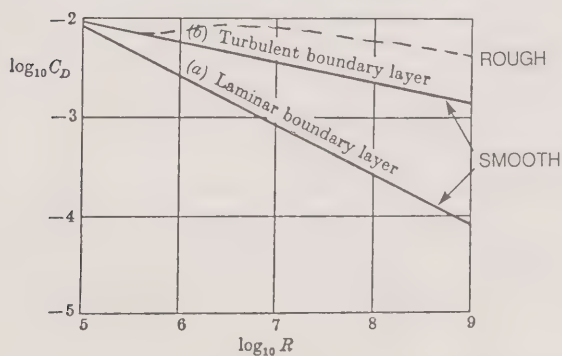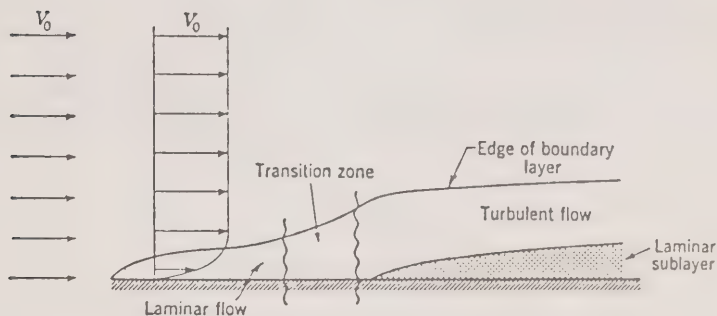
THE SCALE EFFECT ON THE DRAG COEFFICIENT OF A FLAT PLATE IN
A UNIFORM STREAM WITH (a) A LAMINAR AND (b) A TURBULENT BOUNDRY
LAYER OVER THE WHOLE SURFACE.

164 *Appendix 4*

EFFECT OF ROUGHNESS ON DRAG
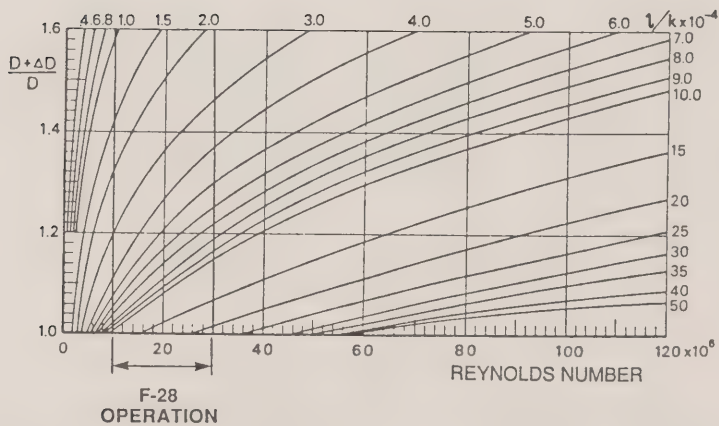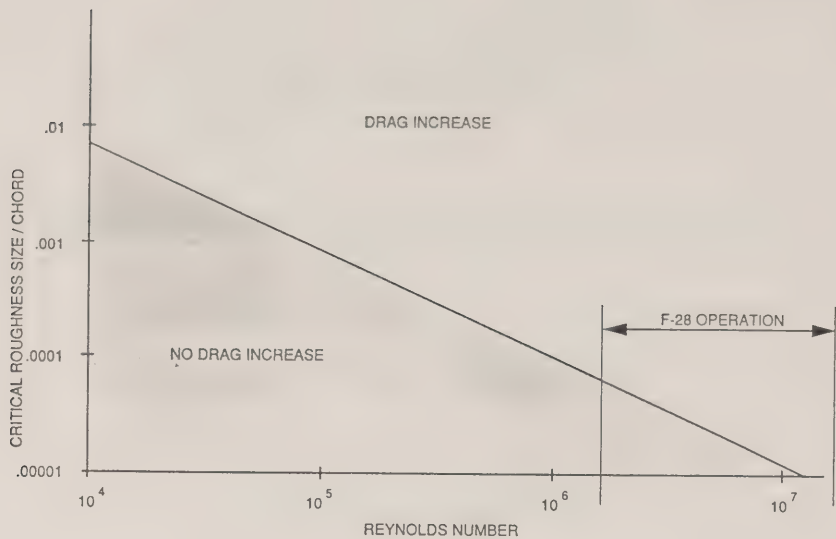
(b) WING OR BODY DRAG DUE TO SURFACE ROUGHNESS (REF 3)

ROUGHNESS EFFECTS ON WING CHARACTERISTICS
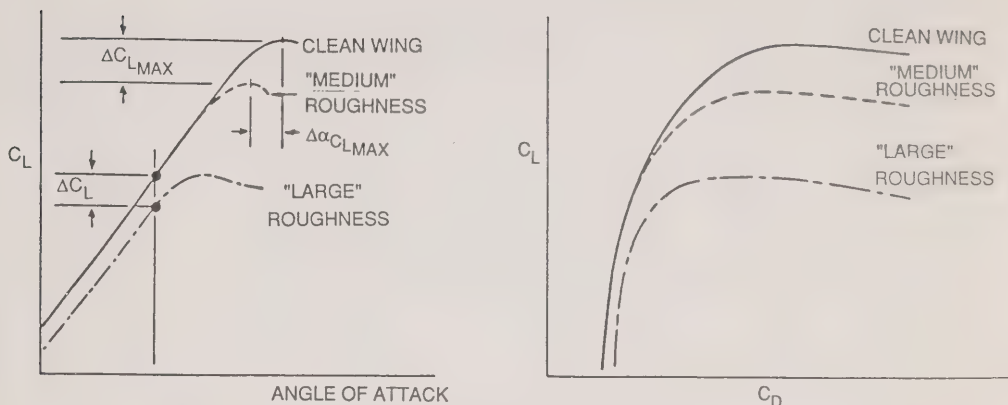
TYPICAL EFFECT OF SURFACE ROUGHNESS AT THE LEADING EDGE ON
AERODYNAMIC CHARACTERISTICS (REF. 12)
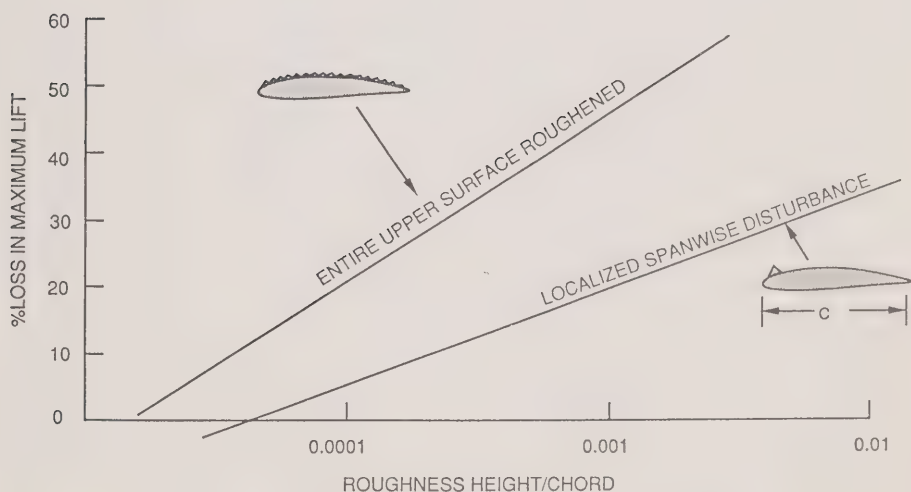
b) EFFECT OF DISTRIBUTED AND ISOLATED ROUGHNESS
ON MAXIMUM LIFT LOSS (REF. 12)

• Hand Finished
◇ Back Half Coated with 0.001" Grains
⊙ Ax Covered with 0.001" Grains

$C_{L_{MAX}}$

R millions

HAND FINISHED AEROFOIL AND AEROFOIL COATED
WITH CARBORUNDUM POWDER

MAXIMUM LIFT ON R.A.F. 34. (8 in. CHORD)

A □ • Chromium plated
B ▷ × Hand finished
C ◁ ◆ 0-0.004" Grains
D ◇ + 0-0.001" Grains
— Increasing Incidence
- - Decreasing Incidence

$C_{L_{MAX}}$

R millions
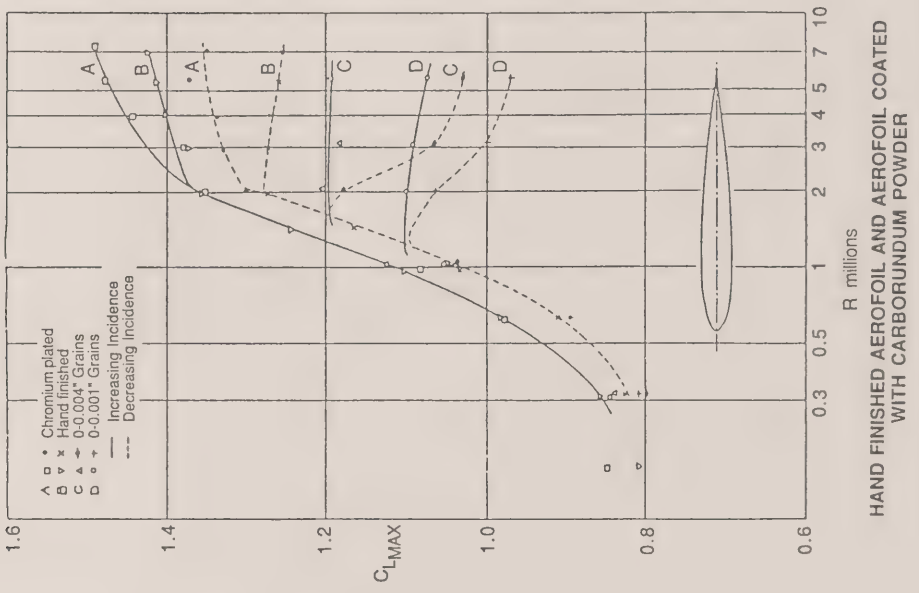
HAND FINISHED AEROFOIL AND AEROFOIL COATED
WITH CARBORUNDUM POWDER

MAXIMUM LIFT ON N.A.C.A. 0012. (8 in. CHORD)

EFFECT OF UNIFORM ROUGHNESS DISTRIBUTION ON THE MAXIMUM LIFT OF WINGS
(REF. 9)

F-28 FLIGHT DYNAMICS   Section 2 - Aerodynamics   Figure 9   Page 31
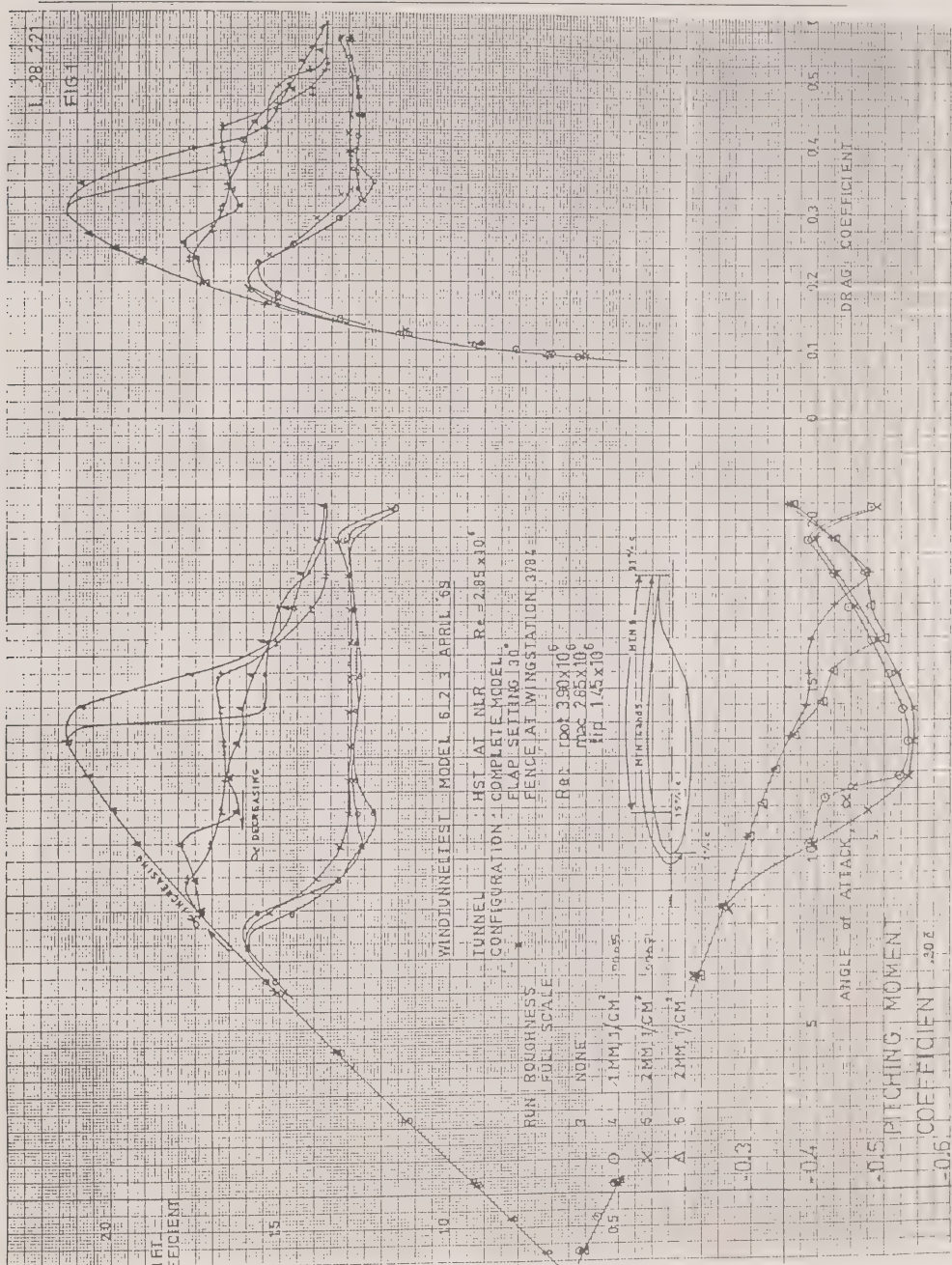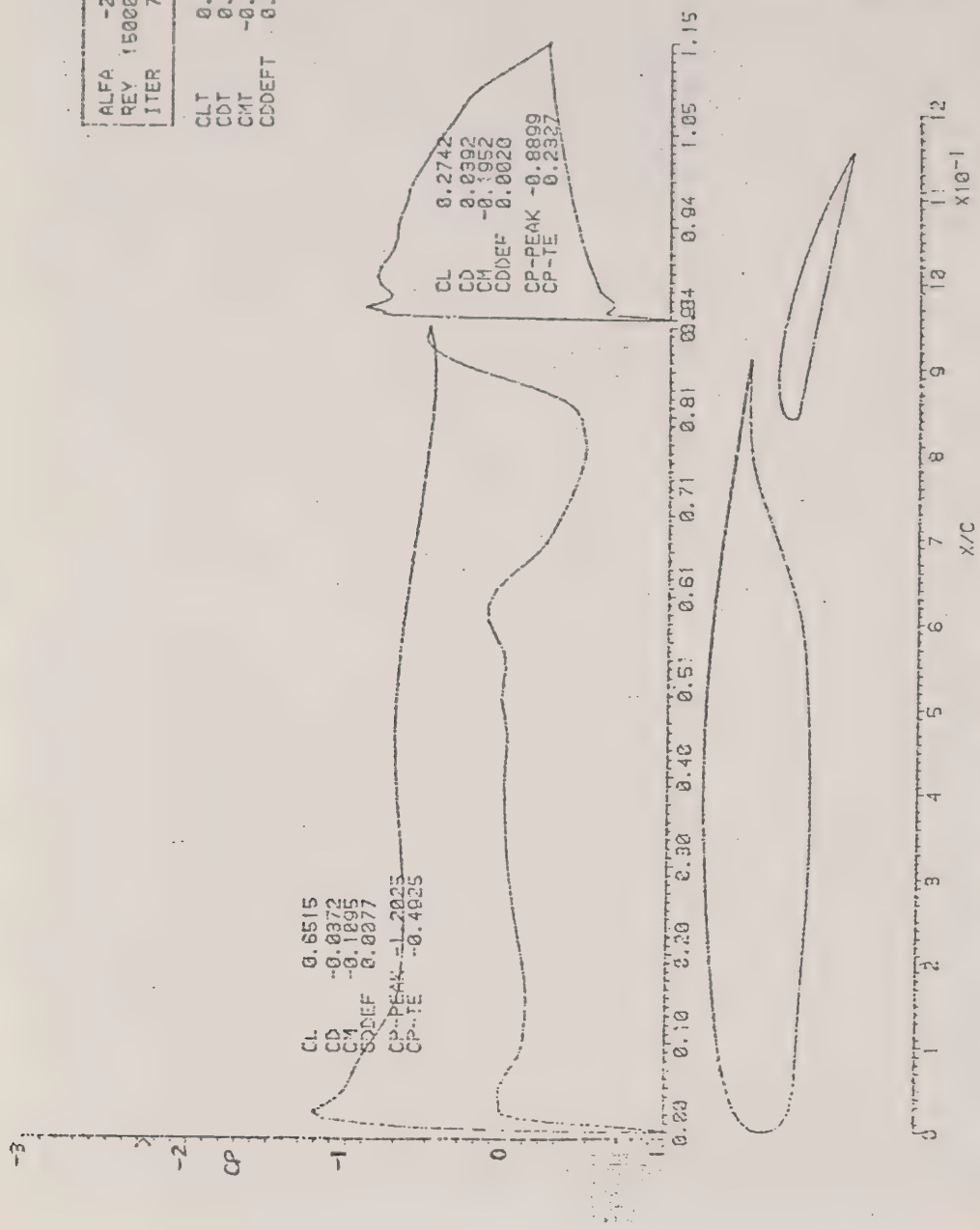
Section 2 FIGURE 10a Theoretical Flow and Pressure Data for
F-28 Aerofoil

VSWAKE CASE 1   FOKKER F28MK1000 (DF 18 DEG)
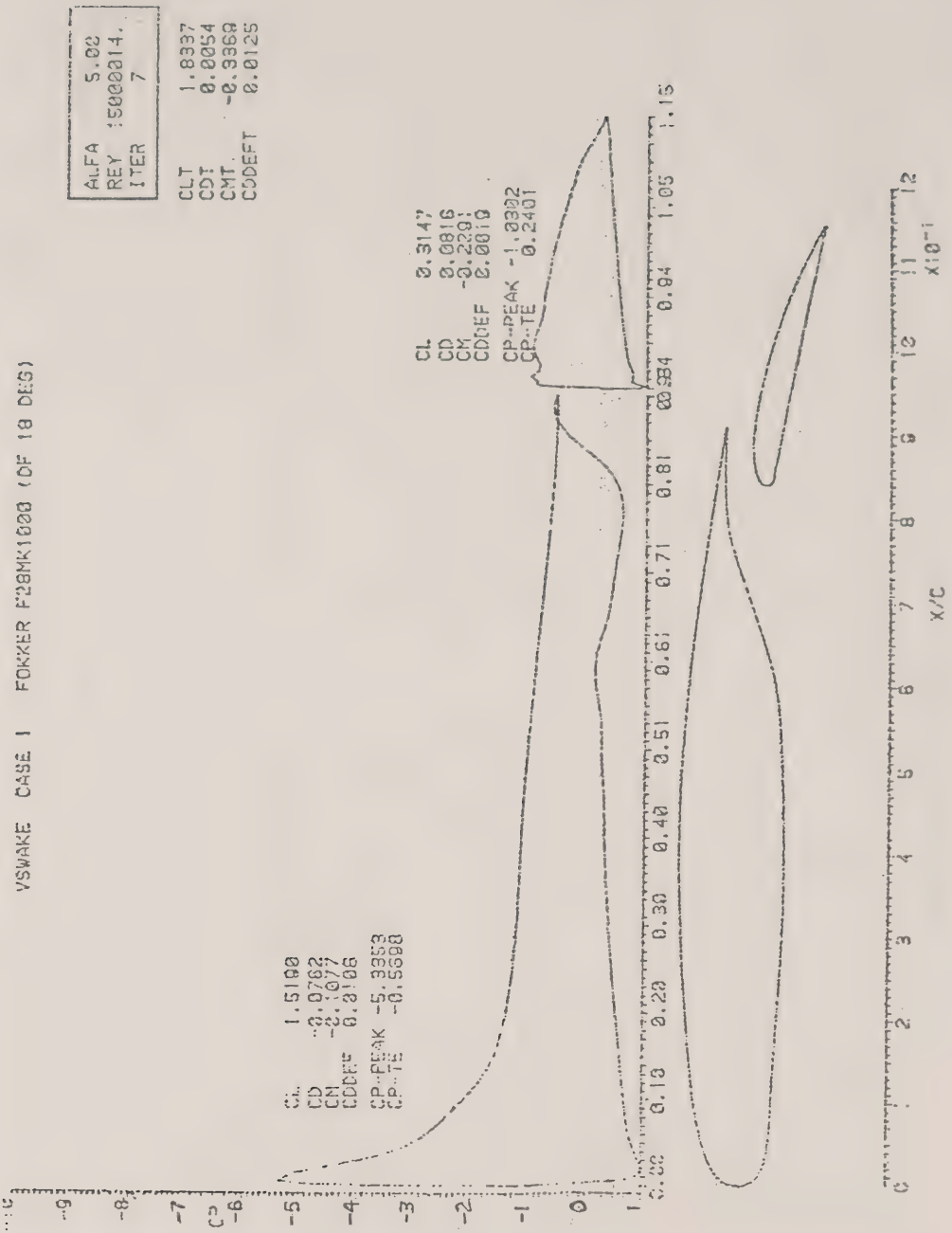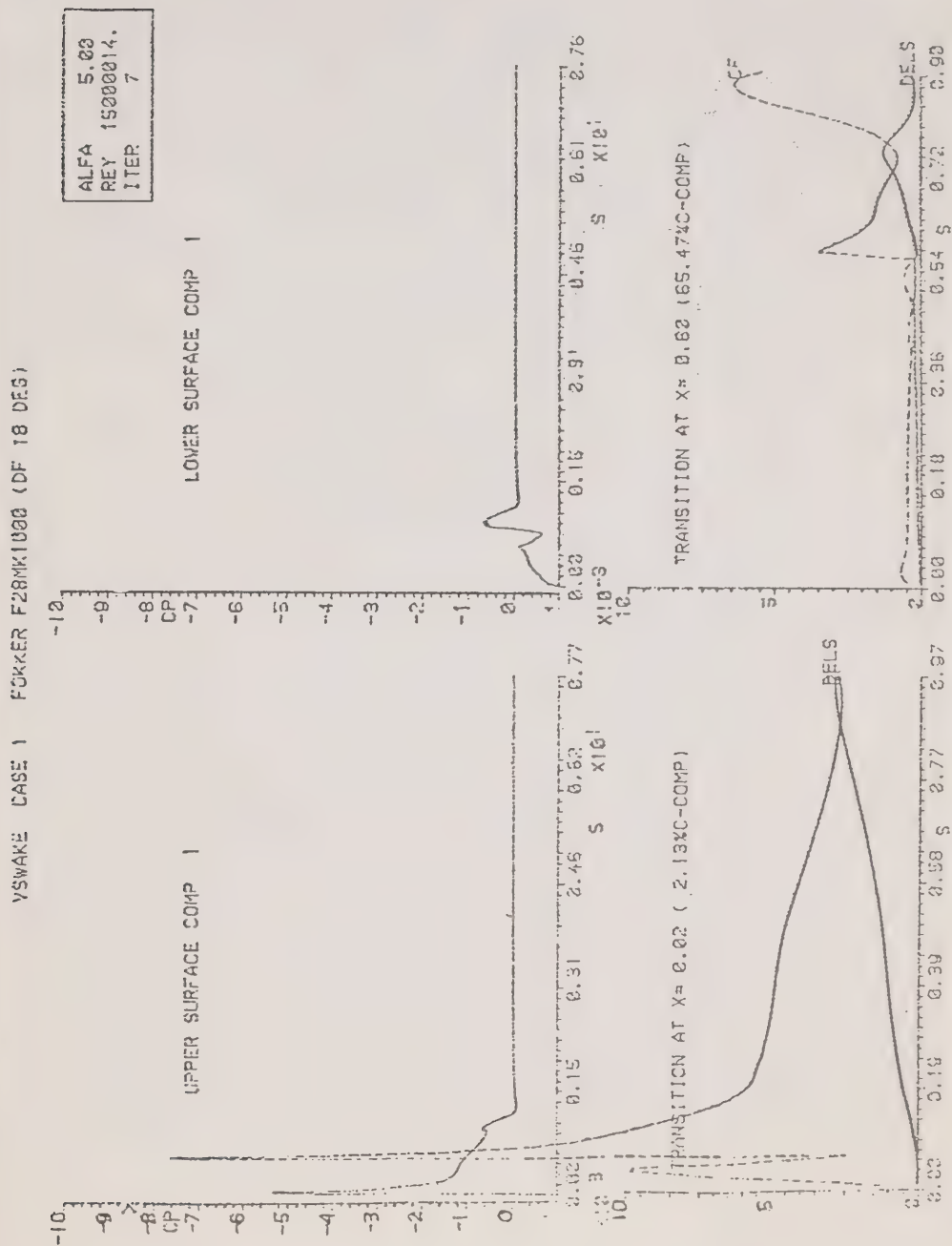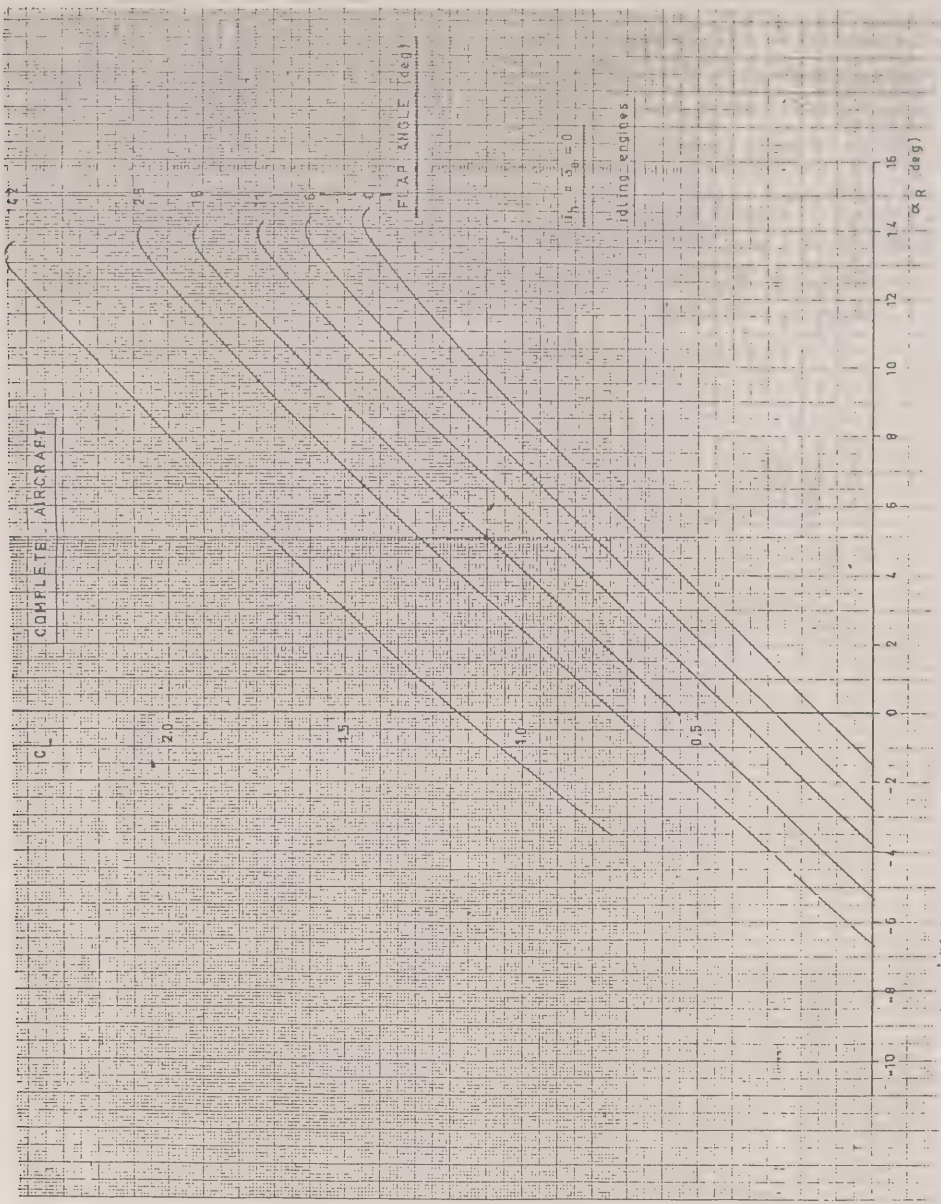
FIGURE 11 F-28 LIFT COEFFICIENT vs ANGLE OF ATTACK (FREE AIR)
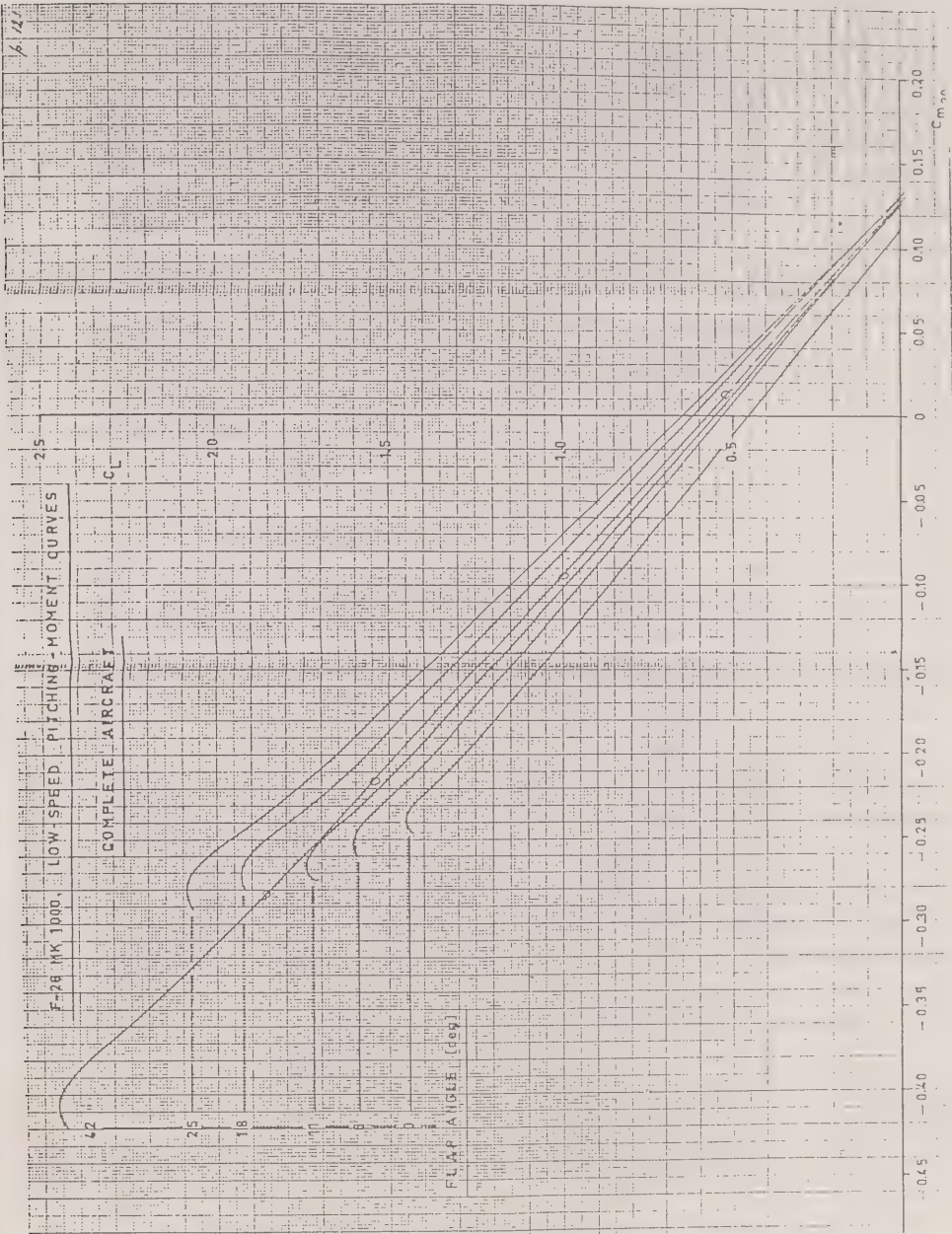
FIGURE 12 F-28 MOMENT COEFFICIENT vs LIFT COEFFICIENT   (FREE AIR)

F-28 FLIGHT DYNAMICS **Section 2 - Aerodynamics** **Page 38**

Fokker **FOKKER-VFW B.V.** RAPPORT NR.+ REPORT NR.

NETHERLANDS AIRCRAFT FACTORIES FOKKER-VFW   L-28-269

BLAD,PAGE _107_

F-28 Mk.1000   Basic low speed drag polars (FREE AIR)

Flap angle   Drag polar
(deg.)

    0   C_D = 0.0195 + 0.0535 C_L^2

    6   C_D = 0.0270 + 0.0515 C_L^2

   11   C_D = 0.0325 + 0.0486 C_L^2

   18   C_D = 0.0405 + 0.0470 C_L^2

   25   C_D = 0.0600 + 0.0470 C_L^2

   42   C_D = 0.1340 + 0.0400 C_L^2

Section 2 FIGURE 13 Low Speed Drag Polars, Free Air

F-28 FLIGHT DYNAMICS Section 2 - Aerodynamics   Figure 14b   Page 40

F-28 FLIGHT DYNAMICS Section 2 - Aerodynamics   Figure 14d   Page 42

FIGURE 15 LIFT COEFFICIENT vs ALPHA – IN GROUND EFFECT

F-28 MK 1000 : CHANGE IN LIFT DUE TO GROUND EFFECT

COMPLETE AIRCRAFT

MAIN GEAR ON GROUND

IDLING ENGINES

$i_h = \delta_e = 0°$

FLAP ANGLE

$\Delta C_{L_{GE}}$

0.30

0.20

25

18

42

11

6

0.10

0

0

0

5

10

α_R (DEG)   15
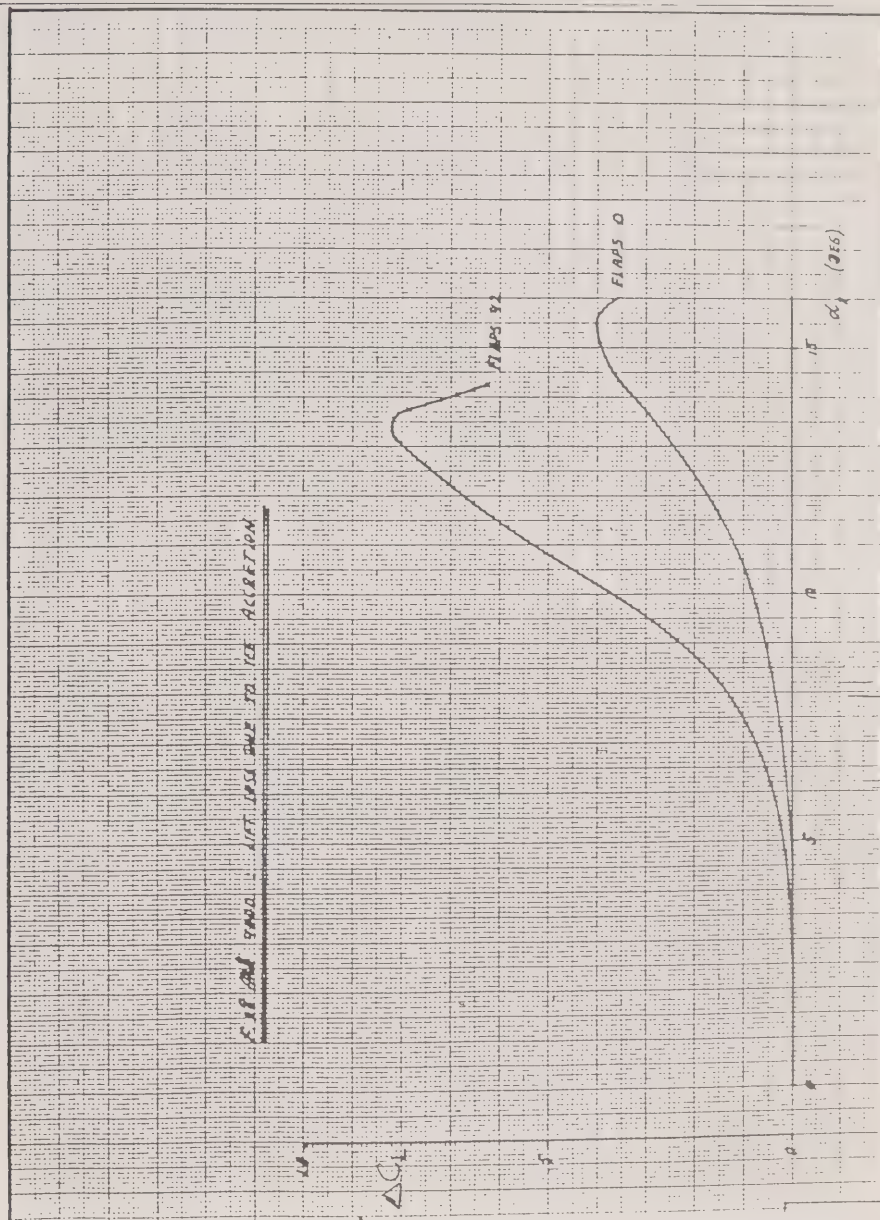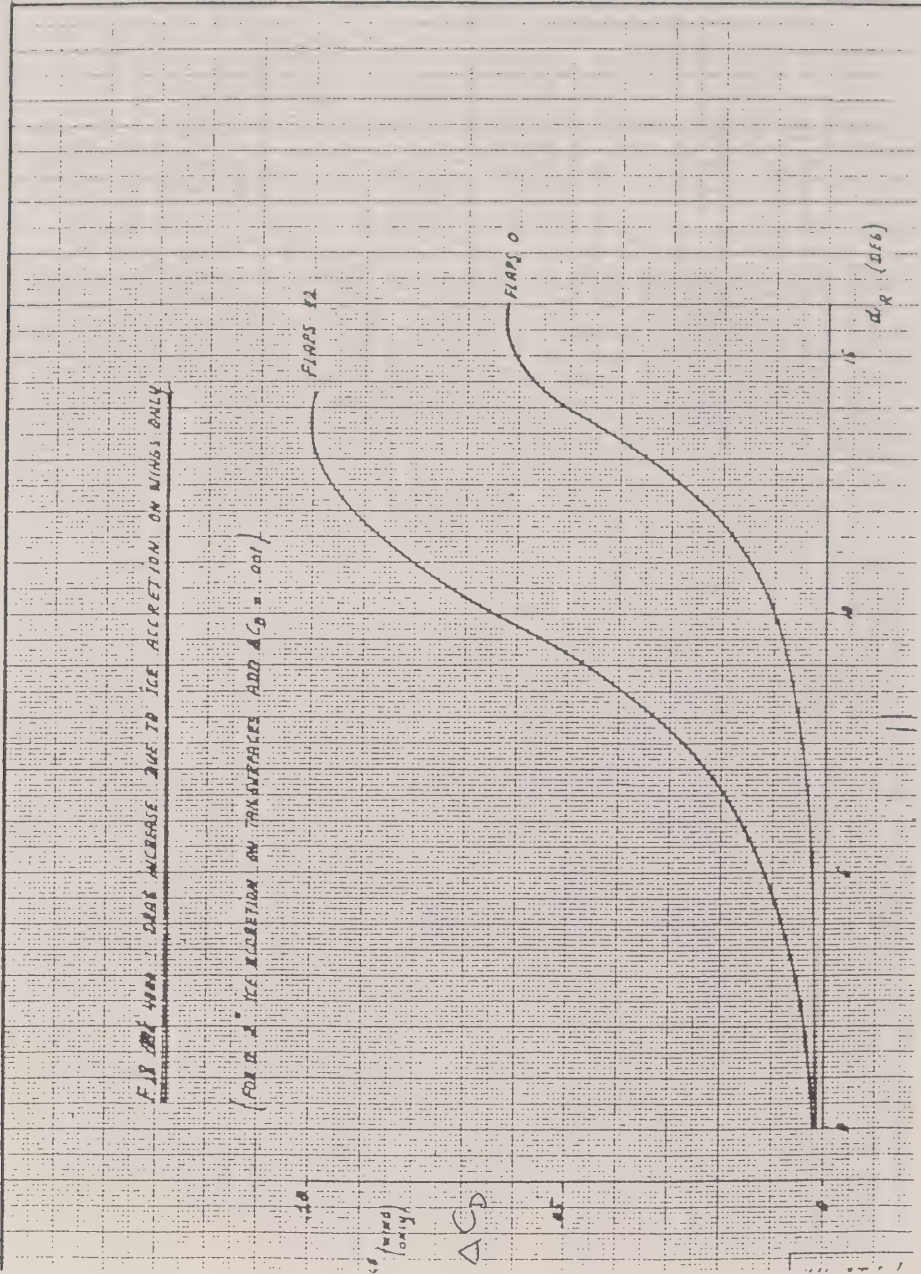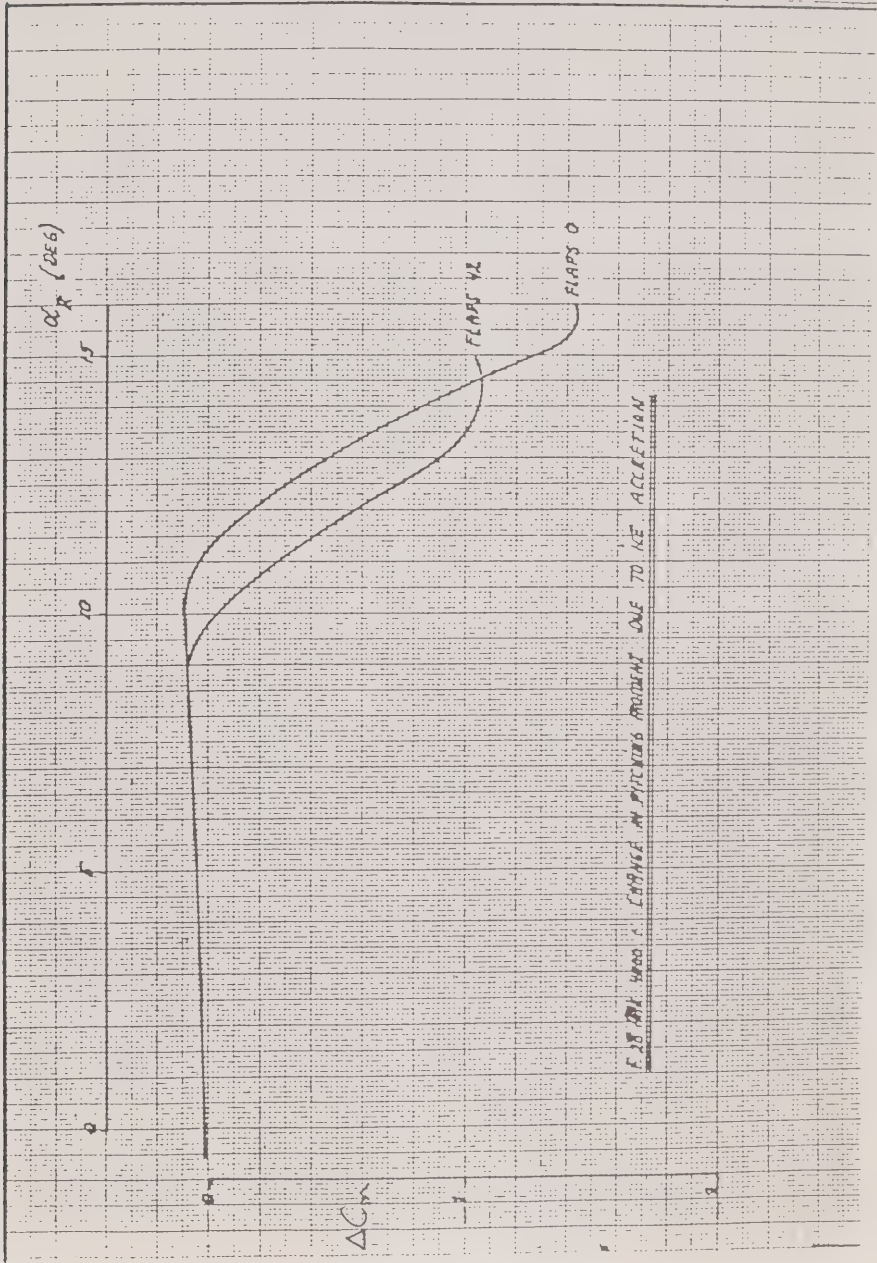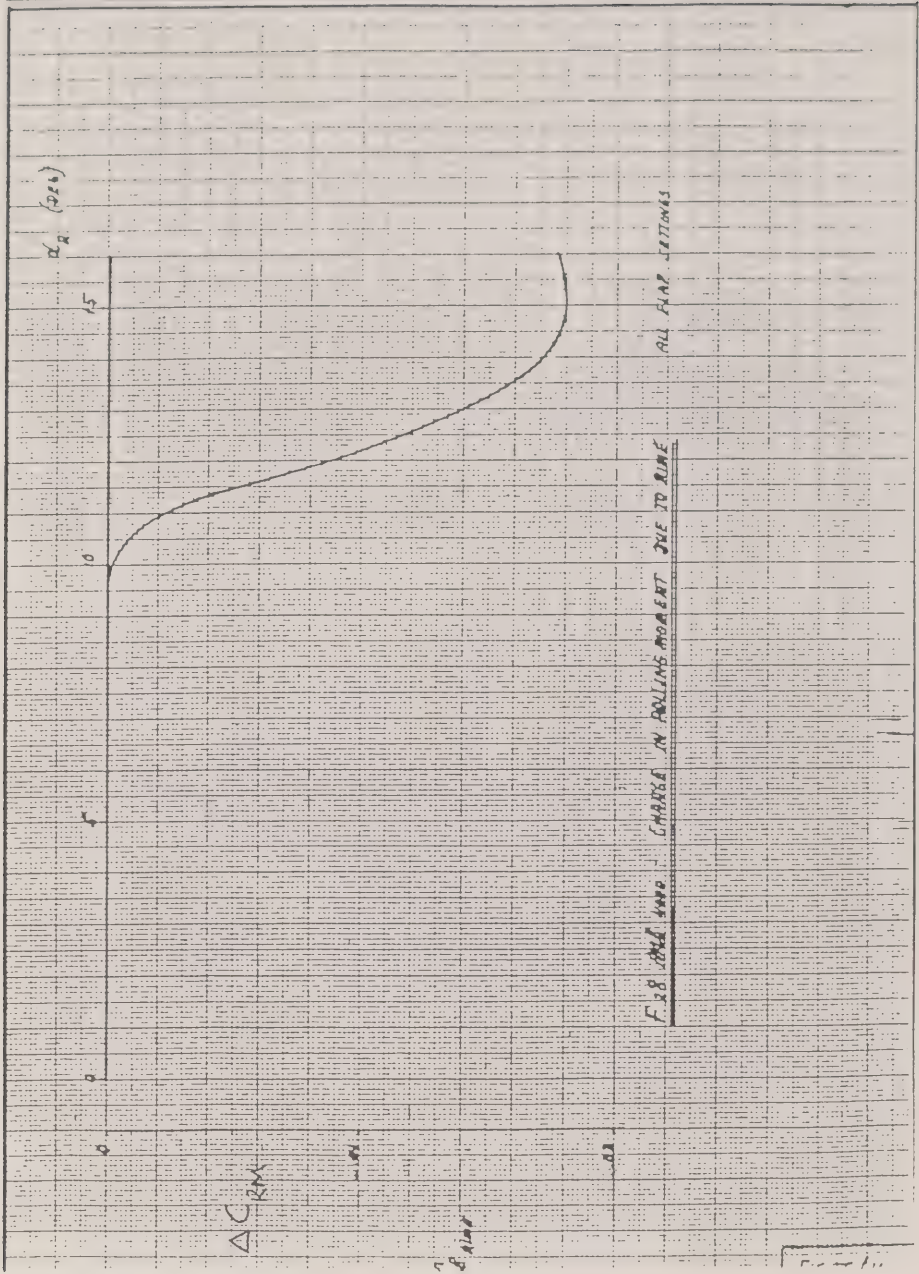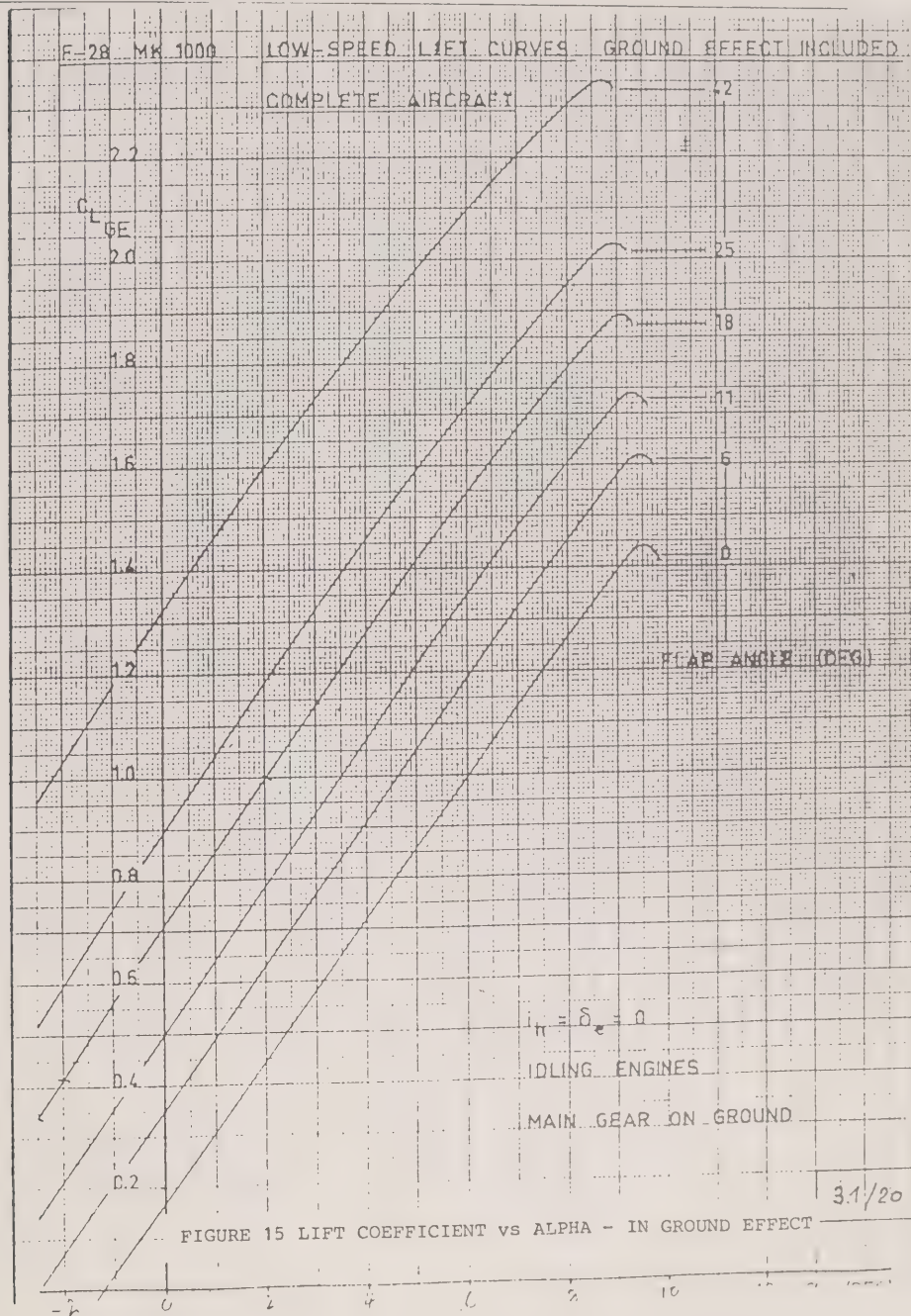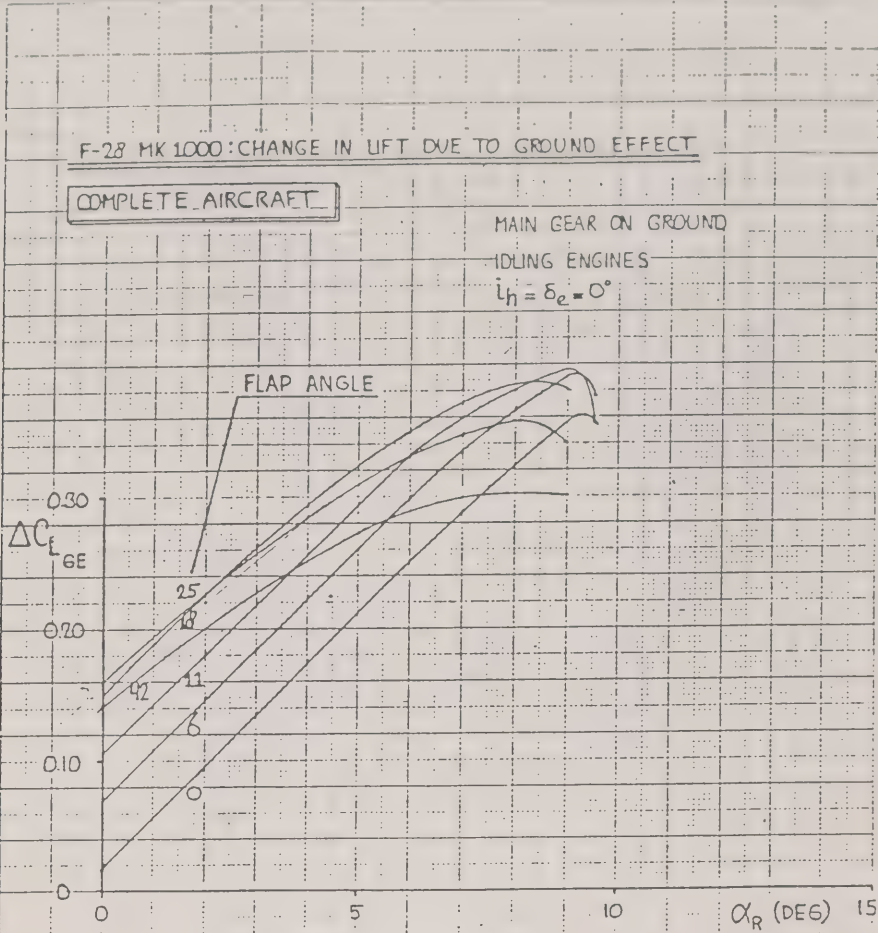
FIGURE 16 CHANGE IN LIFT DUE TO GROUND EFFECT

3.1/20^A

F-28 MK 1000   REDUCTION IN INDUCED DRAG COEFFICIENT
DUE TO GROUND EFFECT AS A FUNCTION OF
UNDERCARRIAGE HEIGHT ABOVE THE GROUND

$$\Delta C_{D_{GE}} = \Delta \beta \cdot C_L^2$$

Average height of
$0.25\bar{c}$ above runway   Vertical distance between $0.25\bar{c}$
(static and groundroll)   and lowest point on f/c
= 7.6 ft   (strut fully extended) at $\alpha_R = 0$
is 2.53 m (8.3 ft).

FIGURE 17 CHANGE IN INDUCED DRAG DUE TO GROUND EFFECT

APPENDIX A TO SECTION 2

TECHNICAL DETAILS OF THE
FOKKER F-28 AIRCRAFT

FIGURE A-1

130   NETHERLANDS: AIRCRAFT—FOKKER-VFW
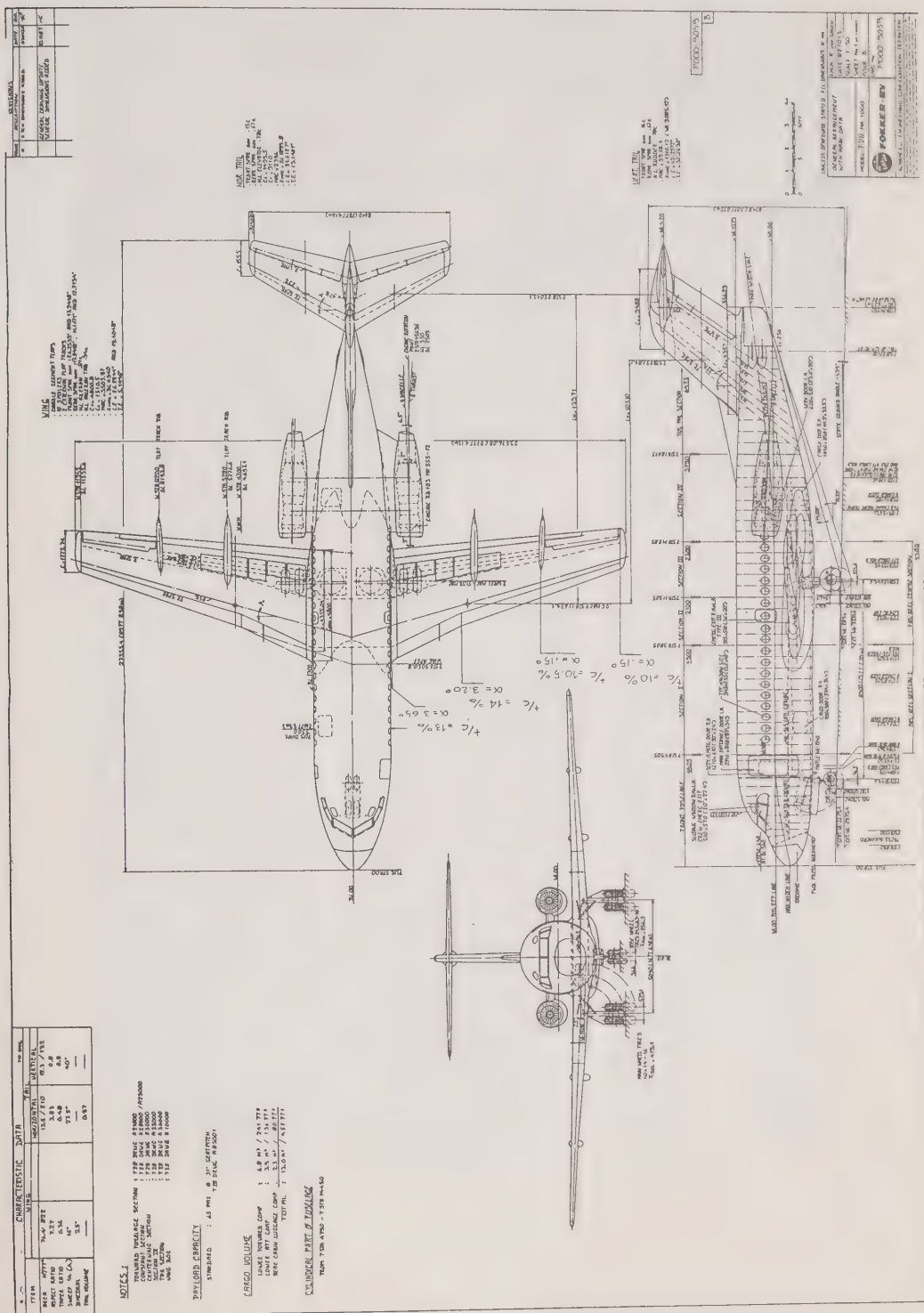
but a basic layout is available. In this, the cabin is divided into three sections: a conference room with six seats, a rest room with settee and divan, and a lounge with four seats. Toilet, galley, wardrobe, baggage space and seat for attendant in forward fuselage. Second toilet and baggage space at rear.

ACCOMMODATION (Mk 400 Combiplane): Principal features of this version are a large cargo loading door forward of the wings on the port side, with the sill at truck-bed height, and a reinforced cargo floor with tiedown rings. Typical layouts include 40 passengers four abreast at 35.5 in (90 cm) seat pitch, plus 218 cu ft (6.17 m³) of cargo space; 28 passengers at same seat pitch plus 583 cu ft (16.65 m³) cargo space; or all-cargo version with 1,727 cu ft (48.9 m³) of cargo space. Alternative layouts for up to 48 passengers.

ACCOMMODATION (Mk 400M): Folding canvas seats, with safety harnesses, along cabin sides for up to 45 paratroops. Toilet and provision for medical supply box or pantry unit at rear. Ambulance version can accommodate 24 USAF-type stretchers, in eight tiers of three, with seats at front and rear for up to nine medical attendants or sitting casualties. All-cargo version fitted with skid strips, tie-down fittings, protection plates and hinged hatracks. Despatch door on each side of fuselage at rear for dropping supplies and personnel.

ACCOMMODATION (Mk 500): Main cabin has standard seating for 52 passengers four abreast at 35.25 in (89.5 cm) seat pitch; alternative layouts enable up to 56 passengers to be carried at 28.5 in (72 cm) pitch.

SYSTEMS: Pressurisation and air-conditioning system utilises two Rootes-type engine-driven blowers. Choke heating and air-to-air heat exchanger; optional bootstrap cooling system. Pressure differential 4.16 lb/sq in (0.29 kg/cm²) in Mk 400, 500 and 600; 5.5 lb/sq in (0.39 kg/cm²) in Mk 200. No hydraulic system. Pneumatic system, pressure 3,400 lb/sq in (239 kg/cm²), for landing gear retraction, nosewheel steering and brakes. Emergency pneumatic circuits for landing gear extension and brakes. Primary 28V electrical system supplied by two 375A 28V DC engine-driven generators. Secondary system supplied via two 115V 400Hz AC constant-frequency inverters. Variable-frequency AC power supply, from 120/208V 15kVA engine-driven alternators, for anti-icing and heating. Two 24V 40Ah nickel-cadmium batteries. 39.4 cu ft (1.12 m³) oxygen system for pilots.

ELECTRONICS AND EQUIPMENT: Standard provisions for VHF and HF transceivers, VHF navigation system (including glideslope), ADF, ILS, marker beacon, dual gyrosyn compass system and intercom system. Provision for weather radar, autopilot etc.

DIMENSIONS, EXTERNAL:

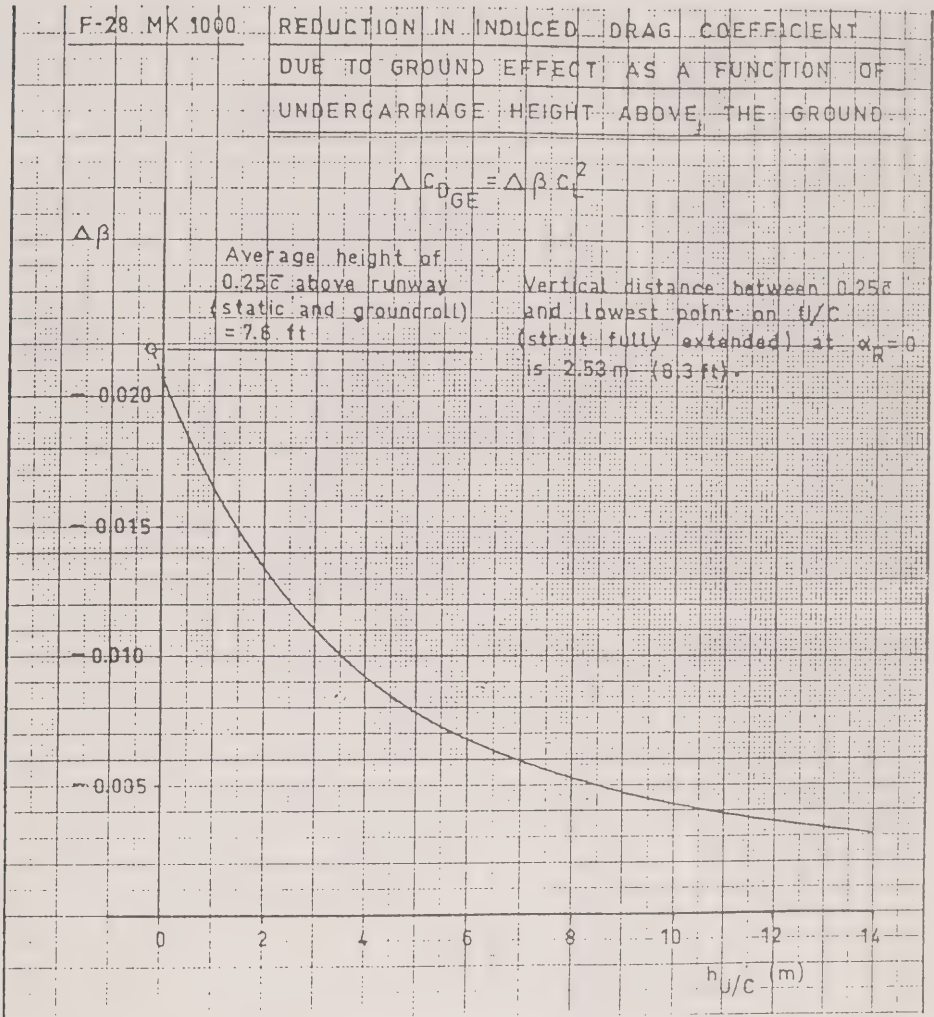|	
Wing span	95 ft 2 in (29.00 m)
Wing chord at root	11 ft 4 in (3.45 m)
Wing chord at tip	4 ft 7 in (1.40 m)
Wing aspect ratio	12
Length overall:	
except Mk 500	77 ft 3¼ in (23.58 m)
Mk 500	82 ft 2½ in (25.06 m)
Fuselage: Max width	8 ft 10¼ in (2.70 m)
Max height	9 ft 1½ in (2.79 m)
Height overall, standard landing gear:	
except Mk 500	27 ft 11 in (8.50 m)
Mk 500	28 ft 7½ in (8.71 m)
Height overall, rough-field landing gear:	
except Mk 500	28 ft 2 in (8.59 m)
Tailplane span	32 ft 0 in (9.75 m)
Wheel track (c/l shock struts)	
	23 ft 7½ in (7.20 m)
Wheelbase:	
except Mk 500	28 ft 8 in (8.74 m)
Mk 500	31 ft 11½ in (9.74 m)
Propeller diameter	11 ft 6 in (3.50 m)
Propeller ground clearance:	
standard landing gear:	
except Mk 500	3 ft 1 in (0.94 m)
Mk 500	3 ft 3 in (0.99 m)
rough-field landing gear:	
except Mk 500	3 ft 4½ in (1.02 m)
Passenger door (aft, port):	
Height	5 ft 5 in (1.65 m)
Width	2 ft 5 in (0.74 m)
Height to sill	4 ft 0 in (1.22 m)
Service/emergency door (aft, stbd):	
Height	3 ft 8 in (1.12 m)
Width	2 ft 5 in (0.74 m)
Height to sill	3 ft 3 in (0.99 m)
Standard cargo door (Mk 200 only):	
Height	3 ft 11 in (1.19 m)
Width	3 ft 5 in (1.04 m)
Height to sill	3 ft 3 in (0.99 m)
Large cargo door (Mks 400, 500 and 600):	
Height	5 ft 10 in (1.78 m)
Width	7 ft 7½ in (2.32 m)
Height to sill:	
except Mk 500	3 ft 3 in (0.99 m)
Mk 500	3 ft 4½ in (1.03 m)
Despatch doors (Mk 400M only, aft, port and stbd, each):	
Height	5 ft 5 in (1.65 m)

Width	3 ft 11 in (1.19 m)
Height to sill	4 ft 0 in (1.22 m)

DIMENSIONS, INTERNAL:
Cabin, excl flight deck:

Length:	
except Mk 500	47 ft 5 in (14.46 m)
Mk 500	52 ft 4 in (15.96 m)
Max width	8 ft 4½ in (2.55 m)
Max height	6 ft 7½ in (2.02 m)
Volume:	
except Mk 500	2,136 cu ft (60.5 m³)
Mk 500	2,360 cu ft (66.8 m³)
Freight hold (fwd) max:	
Mk 200	169 cu ft (4.78 m³)
Mks 400, 500, 600	197 cu ft (5.58 m³)
Freight hold (aft) max:	
all versions	100 cu ft (2.83 m³)

AREAS:

Wings, gross	763.5 sq ft (70.0 m²)
Ailerons (total)	37.80 sq ft (3.51 m²)
Trailing-edge flaps (total)	136.90 sq ft (12.72 m²)
Vertical tail surfaces (total)	153 sq ft (14.20 m²)
Horizontal tail surfaces (total)	
	172 sq ft (16.00 m²)

WEIGHTS AND LOADINGS:

Manufacturer's weight, empty:	
Mk 200, 44 seats	22,436 lb (10,177 kg)
Mk 400, 40 seats	23,290 lb (10,564 kg)
Mk 400M	23,360 lb (10,596 kg)
Mk 500, 52-56 seats	23,578 lb (10,695 kg)
Mk 500M	24,325 lb (11,034 kg)
Mk 600, 44 seats	22,786 lb (10,336 kg)
Operating weight, empty:	
Mk 200, 44 seats	24,612 lb (11,164 kg)
Mk 400, 40 seats	24,875 lb (11,283 kg)
Mk 400M, all-cargo	23,947 lb (10,862 kg)
Mk 400M, medical evacuation	
	24,880 lb (11,286 kg)
Mk 400M, paratrooper	24,336 lb (11,039 kg)
Mk 500, 52-56 seats	25,915 lb (11,755 kg)
Mk 500M, all-cargo	24,912 lb (11,300 kg)
Mk 500M, medical evacuation	
	26,023 lb (11,804 kg)
Mk 500M, paratrooper	25,332 lb (11,491 kg)
Mk 600, 44 seats	24,062 lb (11,323 kg)
Max payload (weight limited):	
Mk 200, 44 seats	12,888 lb (5,846 kg)
Mk 400, 40 seats	12,625 lb (5,727 kg)
Mk 400M, all-cargo	13,553 lb (6,148 kg)
Mk 400M, medical evacuation	
	12,612 lb (5,721 kg)
Mk 400M, paratrooper	13,104 lb (5,971 kg)
Mk 500, 52-56 seats	13,585 lb (6,162 kg)
Mk 500M, all-cargo	14,588 lb (6,617 kg)
Mk 500M, medical evacuation	
	13,477 lb (6,113 kg)
Mk 500M, paratrooper	14,168 lb (6,427 kg)
Mk 600, 44 seats	12,538 lb (5,687 kg)
Max T-O weight:	
all versions	45,000 lb (20,410 kg)
Max landing weight:	
Mks 200, 400, 400M and 500	
	41,000 lb (18,600 kg)
Mks 500 and 500M	42,000 lb (19,050 kg)
Max zero-fuel weight:	
Mks 200, 400, 400M and 500	
	37,500 lb (17,010 kg)
Mks 500 and 500M	39,500 lb (17,900 kg)
Max wing loading:	
all versions	59.7 lb/sq ft (291.5 kg/m²)
Max power loading:	
all versions	10.5 lb/shp (4.76 kg/shp)

PERFORMANCE (at weights indicated):
Normal cruising speed at 20,000 ft (6,100 m) and AUW of 38,000 lb (17,237 kg):

all versions	259 knots (298 mph; 480 km/h)
Rate of climb at S/L, AUW of 40,000 lb (18,143 kg):	
all civil versions	1,480 ft (451 m)/min
both military versions	1,020 ft (494 m)/min
Service ceiling at AUW of 38,000 lb (17,237 kg):	
all civil versions	29,500 ft (8,990 m)
both military versions	30,000 ft (9,145 m)

Service ceiling, one engine out, at AUW of 38,000 lb (17,237 kg):	
all civil versions	11,700 ft (3,565 m)
both military versions	13,300 ft (4,055 m)
Runway LCN at max T-O weight, standard landing gear	16
Required T-O field length (ICAO-PAMC) at AUW of 40,000 lb (18,143 kg), all civil versions:	
S/L, ISA	3,260 ft (991 m)
S/L, ISA + 15°C	3,560 ft (1,085 m)
3,000 ft (914 m), ISA	3,980 ft (1,213 m)
Required T-O field length (military) at AUW of 40,000 lb (18,143 kg), both military versions:	
S/L, ISA	2,310 ft (704 m)
S/L, ISA + 15°C	2,510 ft (765 m)
3,000 ft (914 m), ISA	2,750 ft (838 m)
Required landing field length (ICAO-PAMC) at AUW of 37,500 lb (17,010 kg), all civil versions:	
S/L	3,160 ft (963 m)
3,000 ft (914 m)	3,390 ft (1,033 m)
Required landing field length (military) at AUW of 37,500 lb (17,010 kg), both military versions:	
S/L	1,900 ft (579 m)
3,000 ft (914 m)	2,040 ft (622 m)
Range (ISA, zero wind conditions) with FAR 121.645 reserves for diversion, 30 min hold at 10,000 ft (3,050 m) and 10% flight fuel:	
Mks 200 and 600, 44 passengers	
	1,020 nm (1,197 miles; 1,926 km)
Mk 400, 40 passengers	
	1,025 nm (1,203 miles; 1,935 km)
Mk 500, 52 passengers	
	935 nm (1,082 miles; 1,741 km)
Military transport range (ISA, zero wind conditions) at max T-O weight, reserves for 30 min hold at S/L and 5% initial fuel:	
Mks 400M and 500M, all-cargo, max standard fuel	
	1,195 nm (1,376 miles; 2,213 km)
Mks 400M and 500M, all-cargo, max possible fuel	
	2,370 nm (2,727 miles; 4,389 km)
Military combat radius, conditions as above:	
Mks 400M and 500M, all-cargo, max standard fuel	
	625 nm (719 miles; 1,158 km)
Mks 400M and 500M, all-cargo, max possible fuel	
	1,230 nm (1,416 miles; 2,278 km)
Max endurance at 20,000 ft (6,100 m):	
Mk 400M, max standard fuel	7 hr 23 min
Mk 400M, max possible fuel	12 hr 47 min
Mk 500M, max standard fuel	7 hr 14 min
Mk 500M, max possible fuel	12 hr 26 min

OPERATIONAL NOISE CHARACTERISTICS (FAR Pt 36):

T-O noise level	89 EPNdB
Approach noise level	99 EPNdB
Sideline noise level	92.5 EPNdB

FOKKER-VFW F28 FELLOWSHIP

Announced in April 1962, the F28 Fellowship twin-turbofan short-haul transport was developed in collaboration with other European aircraft manufacturers and with the financial support of the Netherlands government. One half of the Dutch share of the development cost was supplied through the Netherlands Aircraft Development Board, the other half through a loan guaranteed by the government.

Under agreements signed in the Summer of 1964, production is undertaken by Fokker-VFW in association with MBB and VFW-Fokker in Germany and Short Bros and Harland in the UK. Fokker-VFW is responsible for the front fuselage, to a point just aft of the flight deck, the centre fuselage and wing-root fairings. MBB builds the fuselage, from the wing trailing-edge to the rear pressure bulkhead, and the engine nacelles and support stubs. VFW-Fokker is responsible for the rear fuselage and tail unit, and for the cylindrical fuselage s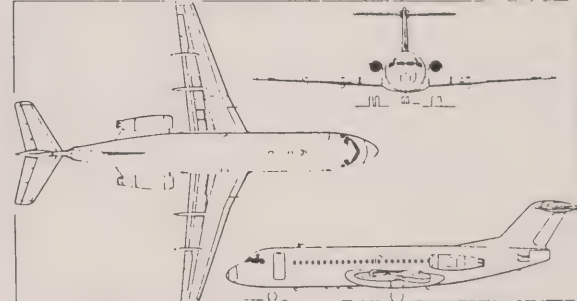ection between the wing leading-edge and flight deck. Shorts are responsible for the wings (including the slatted wings for the Mks 5000 and 6000), and other components, including the main-wheel and nosewheel doors.
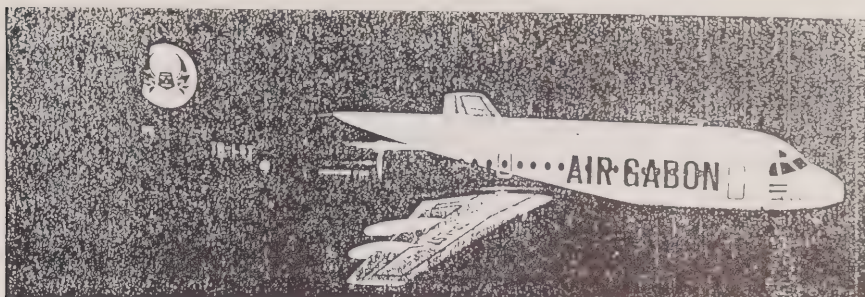
First flight of the first prototype F28 (PH-JHG)

Fokker-VFW F28 Fellowship Mk 6000 twin-turbofan short-range airliner *(Pilot Press)*

Fokker-VFW F28 Fellowship Mk 2000 short-haul transport, in the insignia of Air Gabon

was made on 9 May 1967, and the second prototype, PH-WEV, flew on 3 August 1967. The third F28 (PH-MOL) flew for the first time on 20 October 1967 and was brought up to production standard in the early Summer of 1968.

The Dutch RLD granted a C of A to the F28 on 24 February 1969, and the first delivery (of the fourth aircraft, to LTU) was made on the same day. The aircraft received FAA Type Approval on 24 March 1969 and German certification on 30 March 1969. RLD certification for operation from unpaved runways was granted in mid-1972. The Mk 1000 was granted FAA-approved noise certification on 31 December 1971.

A total of 107 Fellowships (85 Mk 1000, 7 Mk 1000C, 10 Mk 2000 and 5 Mk 4000) had been ordered by 3 June 1975, as follows:

Mk 1000/1000C

Aerolineas Argentinas	3
AeroPeru	3
Air Gabon (1 Mk 1000VIP, 1 Mk 1000C)	2
Air Nauru	2
Ansett Transport Industries (Airlines of NSW and MacRobertson-Miller)	6
Argentine Air Force (Mk 1000C)	5
Argentine government	1
Australian Dept of Transport (Air)	3
Avimeco (Germany)	3
Braathens (Norway)	5
Colombian Air Force	1
Congo (Brazzaville)	1
Enstra (USA)	1
Fairchild Industries	1
Garuda Indonesian Airways	18
Germanair	4
Iberia	3
Itavia (Italy)	3
Ivory Coast (1 Mk 1000, 1 Mk 1000C)	2
Linjeflyg (Sweden)	3
LTU (Germany)	4
Malaysian government	2
Martinair-Holland	1
Netherlands government	2
Nigeria Airways	5
Nigerian government	1
Pelita/Pertamina	2
Peruvian government	1
TILY (Turkey)	5
Togo government	1
Touraine Air Transport	1
Transair (Canada)	2

Mk 2000

Air Gabon	2
Ghana Airways	2
Nigerian Airways	6

Mk 4000

Undisclosed	5

Six versions have been announced, as follows:

Mk 1000. Initial version, in production and service, with seating for up to 65 passengers. First F28 commercial service was flown by Braathens on 28 March 1969. Available optionally, for all-cargo or mixed passenger/cargo operations, with large freight door at front on port side, in which form it is designated **Mk 1000C.**

Mk 2000. Similar to Mk 1000 except for lengthened fuselage, permitting an increase in accommodation for up to 79 passengers in all-tourist layout. F28 first prototype modified to Mk 2000 standard and flown for first time on 28 April 1971. Dutch certification awarded on 30 August 1972. In production and service.

Mk 3000. See Addenda.

Mk 4000. High-density version, announced in early 1975, to seat up to 85 passengers at 29 in (74 cm) pitch. Airframe basically that of Mk 6000, except for omission of leading-edge slats; uprated Spey Mk 555-15H as power plant. Intended for use over stage lengths of about 890 nm (1,025 miles; 1,650 km), using a T-O field length of 5,740 ft (1,750 m). Two additional overwing emergency exits (making a total of four). Design criteria, due to be

finalised by April 1975, include a max T-O weight of 70,990 lb (32,200 kg), max landing weight of 63,935 lb (29,000 kg) and max zero-fuel weight of 57,540 lb (26,100 kg).

Mk 5000. Similar to Mk 1000 except for slatted, long-span wings and improved Spey engines. Available with large cargo door.

Mk 6000. Similar to Mk 2000 except for slatted, long-span wings and improved Spey engines. Prototype, modified from F28 first prototype (previously used for Mk 2000 certification flying) and fitted with modified wings from the second prototype, made its first flight on 27 September 1973. Certification expected by mid-1975.

The following details apply generally to all versions, except where a specific model is indicated:

TYPE: Twin-turbofan short-range airliner.

WINGS: Cantilever low/mid-wing monoplane. Wing section NACA 0000-X 40% series with camber varying along span. Thickness/chord ratio up to 14% on inner wing, 10% at tip. Dihedral 2° 30′. Sweepback at quarter-chord 16°. Single-cell two-spar light alloy torsion-box structure, comprising centre-section, integral with fuselage, and two outer wings. Fail-safe construction. Lower skin made of three planks. Taper-rolled top skin. Forged ribs in centre-section, built-up ribs in outer panels. Double-skin leading-edge with ducts for hot-air de-icing. Irreversible hydraulically-operated ailerons. Emergency manual operation of ailerons, through tabs. Hydraulically-operated Fowler double-slotted flaps over 70% of each half-span with electrical emergency extension. Five-section hydraulically-operated lift dumpers in front of flaps on each wing. Trim tab in each aileron. Mks 5000 and 6000 have extended-span wings with full-span hydraulically-operated leading-edge slats.

FUSELAGE: Circular-section semi-monocoque light alloy fail-safe structure, made up of skin panels with Redux-bonded Z-stringers. Bonded doubler plates at door and window cut-outs. Quickly-detachable sandwich (metal/end grain balsa) floor panels. Hydraulically-operated petal airbrakes form aft end of fuselage.

TAIL UNIT: Cantilever light alloy structure, with hydraulically-actuated variable-incidence T tailplane. Electrical emergency actuation of tailplane. Hydraulically-boosted elevators. Hydraulically-operated rudder with duplicated actuators and emergency manual operation. Honeycomb sandwich skin panels used extensively, in conjunction with multiple spars. Double-skin leading-edges for hot-air de-icing.

LANDING GEAR: Retractable tricycle type of Dowty-Rotol manufacture, with twin wheels on each unit. Hydraulic retraction, nose-wheels forward, main units inward into fuselage. Oleo-pneumatic shock-absorbers. Good-year wheels, tyres and electronically-controlled braking system. Steerable nosewheel. Main-wheel tyres size 39 × 13, 16-ply rating, pressure 100 lb/sq in (7·0 kg/cm²) on Mk 1000, 102 lb/sq in (7·1 kg/cm²) on Mk 2000, 110 lb/sq in (7·7 kg/cm²) on Mks 5000 and 6000. Nosewheel tyres size 24·6 × 8·6, 10-ply rating, pressure 85 lb/sq in (5·98 kg/cm²) on Mk 1000, 78 lb/sq in (5·5 kg/cm²) on Mk 2000, 80 lb/sq in (5·6 kg/cm²) on Mk 5000 and 76 lb/sq in (5·3 kg/cm²) on Mk 6000. Low-pressure tyres optional on all units.

POWER PLANT (Mks 1000 and 2000): Two Rolls-Royce RB.183-2 Spey Mk 555-15 turbofan engines with blade-cooling (each 9,850 lb; 4,468 kg st), mounted in pod on each side of rear fuselage. No water injection or thrust reversers. Thermal anti-icing for air intakes. For Mks 5000 and 6000, a Mk 555-15H version of the Spey engine is under development. This will retain the existing nominal thrust rating of the Mk 555-15, but at ambient temperatures up to

28°C, and will be fitted with a five-chute silencing nozzle. Integral fuel tank in each outer wing panel with total usable capacity of 2,143 Imp gallons (9,740 litres) in Mks 1000/2000; 2,130 Imp gallons (9,682 litres) in Mks 5000/6000. Optional seven bladder-type tank units in wing centre-section with total usable capacity of 726 Imp gallons (3,300 litres). Single refuelling point under starboard wing, near root.

ACCOMMODATION: Crew of two side by side on flight deck, with jump-seat for third crew member. Electrically-heated windscreen. Pantry/baggage space immediately aft of flight deck on starboard side, followed by entrance lobby with hydraulically-operated airstair door on port side, service and emergency door on starboard side, and seat for stewardess. On Mks 1000 and 5000, an optional upward-opening cargo door, to permit all-cargo or all-passenger operation, can be added aft of the passenger airstair door. Additional emergency door on each side of main cabin, over wing. Main cabin layout of Mks 1000/5000 can be varied to accommodate 55, 60 or 65 passengers five abreast at 37, 32/33 or 31 in (94, 81/84 or 79 cm) seat pitch respectively. In Mks 2000/6000, layout can be varied to accommodate 79 passengers at 31 in (79 cm) seat pitch. Aft of cabin are a wardrobe (port), compartment (port) and toilet compartment (starboard). Underfloor cargo compartments fore and aft of wing, with single door on starboard side of forward hold, with one door on rear hold of each version.

SYSTEMS: AiResearch air-conditioning system, using engine bleed air. Max pressure differential 7·45 lb/sq in (0·52 kg/cm²). Two independent hydraulic systems, pressure 3,000 lb/sq in (210 kg/cm²). Primary system for flight controls, landing gear, nosewheel steering and brakes, secondary system for duplication of certain essential flight controls. Flying control hydraulic components supplied by Jarry Hydraulics. All-AC electrical system utilises two 20kVA Westinghouse engine-driven generators to supply three-phase constant-frequency 115/200V 400Hz power. One 20Ah battery for starting APU and for emergency power. AiResearch GTCP 36-4A APU, mounted aft of rear pressure bulkhead, for engine starting, ground air-conditioning and ground electrical power, and to drive a third AC generator for standby use on essential services in flight.

ELECTRONICS AND EQUIPMENT: Standard equipment includes VHF transceivers, VHF navigation system (with glideslope), DME, marker beacon, weather radar, ADF, ATC transponder, dual compass system, interphone and public address systems, Smiths SEP6 autopilot, Collins FD 108 flight director, flight guidance caution system, flight data recorder and voice recorder. Thermal bleed air system for wing leading-edges (slats on Mks 5000/6000), tailplane leading-edge and engine air intakes. Stick pusher system on Mks 5000/6000. Optional equipment to customer's requirements, including equipment for operation in Cat. 2 weather minima.

DIMENSIONS, EXTERNAL:

Wing span:		
1000, 2000	77 ft 4½ in (23·58 m)	
5000, 6000	82 ft 3 in (25·07 m)	
Wing chord at root:		
all versions	15 ft 9 in (4·80 m)	
Wing chord at tip:		
1000, 2000	5 ft 9½ in (1·77 m)	
Wing aspect ratio:		
1000, 2000	7·27	
Length overall:		
1000, 5000	89 ft 10¾ in (27·40 m)	
2000, 6000	97 ft 1¾ in (29·61 m)	
Length of fuselage:		
1000, 5000	80 ft 6½ in (24·55 m)	
2000, 6000	87 ft 9½ in (26·76 m)	

... ., NEW ZEALAND. AIRCRAFT—FOKKER-VFW/AEROSPACE

Fuselage: Max width | 10 ft 10 in (3.30 m)
Height overall | 27 ft 9½ in (8.47 m)
Tailplane span | 28 ft 4½ in (8.64 m)
Wheel track (c/l of shock struts) | 16 ft 6½ in (5.04 m)

Wheelbase:
1000, 5000 | 29 ft 2½ in (8.90 m)
2000, 6000 | 33 ft 11½ in (10.35 m)

Passenger door (fwd, port):
Height | 6 ft 4 in (1.93 m)
Width | 2 ft 10 in (0.86 in)

Service/emergency door (fwd, stbd):
Height | 4 ft 2 in (1.27 m)
Width | 2 ft 0 in (0.61 m)

Emergency exits (centre, each):
Height | 3 ft 0 in (0.91 m)
Width | 1 ft 8 in (0.51 m)

Freight hold doors (each):
Height (fwd, each) | 2 ft 11½ in (0.90 m)
Height (aft) | 2 ft 7½ in (0.80 m)
Width (fwd, each) | 3 ft 1½ in (0.95 m)
Width (aft) | 2 ft 11 in (0.89 m)
Height to sill (fwd, each) | 4 ft 10 in (1.47 m)
Height to sill (aft) | 5 ft 2½ in (1.59 m)

Baggage door (rear, port, optional):
Height | 1 ft 11½ in (0.60 m)
Width | 1 ft 8 in (0.51 m)

Optional cargo door (fwd, port):
Height | 6 ft 1½ in (1.87 m)
Width | 8 ft 2 in (2.49 m)
Height to sill | 7 ft 4½ in (2.24 m)

DIMENSIONS, INTERNAL:
Cabin, excl flight deck:
Length:
1000, 5000 | 43 ft 0 in (13.10 m)
2000, 6000 | 50 ft 3 in (15.31 m)
Max length of seating area:
1000, 5000 | 35 ft 2½ in (10.74 m)
2000, 6000 | 42 ft 6½ in (12.95 m)
Max width | 10 ft 2 in (3.10 m)
Max height | 6 ft 7½ in (2.02 m)
Floor area:
1000, 5000 | 413.3 sq ft (38.4 m²)
2000, 6000 | 482.2 sq ft (44.8 m²)
Volume:
1000, 5000 | 2,525 cu ft (71.5 m³)
2000, 6000 | 2,931 cu ft (83.0 m³)
Freight hold (underfloor, fwd):
1000, 5000 | 245 cu ft (6.90 m³)
2000, 6000 | 308 cu ft (8.70 m³)
Freight hold (underfloor, rear):
1000, 5000 | 135 cu ft (3.80 m³)
2000, 6000 | 169 cu ft (4.80 m³)
Baggage hold (aft of cabin), max | 80 cu ft (2.265 m³)

AREAS:
Wings, gross:
1000, 2000 | 822 sq ft (76.40 m²)
5000, 6000 | 850 sq ft (78.97 m²)
Ailerons (total) | 28.74 sq ft (2.67 m²)
Trailing-edge flaps (total) | 150.7 sq ft (14.00 m²)
Fuselage airbrakes (total) | 38.97 sq ft (3.62 m²)
Fin (incl dorsal fin) | 132.4 sq ft (12.30 m²)
Rudder | 24.76 sq ft (2.30 m²)
Tailplane | 209.9 sq ft (19.50 m²)
Elevators (total) | 41.33 sq ft (3.84 m²)

WEIGHTS AND LOADINGS:
Manufacturer's weight empty:
1000, 65 seats | 31,954 lb (14,492 kg)
1000C | 31,954 lb (14,492 kg)
2000, 65 seats | 32,929 lb (14,936 kg)
5000, 65 seats | 33,504 lb (15,198 kg)
6000, 79 seats | 34,477 lb (15,638 kg)
Operating weight empty:
1000, 65 seats | 35,404 lb (16,084 kg)
1000C | 35,853 lb (16,263 kg)
2000, 79 seats | 36,705 lb (16,650 kg)
5000, 65 seats | 37,014 lb (16,790 kg)
6000, 79 seats | 38,345 lb (17,393 kg)
Max weight-limited payload:
1000 | 19,036 lb (8,030 kg)
1000C | 18,647 lb (8,457 kg)
2000 | 17,705 lb (8,030 kg)
5000 | 17,486 lb (7,930 kg)
6000 | 17,655 lb (8,007 kg)

Max T-O weight:
1000, 2000 | 65,000 lb (29,485 kg)
5000, 6000 | 70,800 lb (32,115 kg)
Max zero-fuel weight:
1000, 2000, 5000 | 54,500 lb (24,720 kg)
6000 | 56,000 lb (25,400 kg)
Max landing weight:
1000, 2000 | 59,000 lb (26,760 kg)
5000, 6000 | 64,000 lb (29,030 kg)
Max wing loading:
1000, 2000 | 79.1 lb/sq ft (386 kg/m²)
5000, 6000 | 83.3 lb/sq ft (406 kg/m²)
Max cabin floor loading:
all passenger versions | 75 lb/sq ft (366 kg/m²)
1000, 5000, with large cargo door | 125 lb/sq ft (610 kg/m²)
Max power loading:
1000, 2000 | 3.3 lb/lb at (3.3 kg/kg st)
5000, 6000 | 3.6 lb/lb at (3.6 kg/kg st)
PERFORMANCE (ISA, except where indicated):
Max never-exceed speed (all versions) | 350 knots (449 mph; 723 km/h) EAS or Mach 0.83
Max permissible operating speed (all versions) | 330 knots (380 mph; 611 km/h) EAS or Mach 0.75
Max cruising speed at 23,000 ft (7,000 m) (all versions) 456 knots (523 mph; 843 km/h) TAS
Econ cruising speed at 30,000 ft (9,150 m), AUW of 59,000 lb (26,760 kg):
1000, 2000 | 362 knots (416 mph; 670 km/h) TAS
5000, 6000 | 366 knots (421 mph; 678 km/h) TAS
Threshold speed at max landing weight:
1000, 2000 | 119 knots (137 mph; 220 km/h) EAS
5000, 6000 | 110 knots (127 mph; 204 km/h) EAS
Max cruising altitude:
all versions | 35,000 ft (10,675 m)
Min ground turning radius:
1000, 5000 | 31 ft 6 in (9.60 m)
2000, 6000 | 35 ft 9 in (10.90 m)
Runway LCN at max T-O weight (hard runway):
1000, standard tyres | 26.5
1000, low-pressure tyres | 22
2000, standard tyres | 27
2000, low-pressure tyres | 22.5
5000, standard tyres | 31
5000, low-pressure tyres | 27
6000, standard tyres | 30
6000, low-pressure tyres | 26
Runway LCN at max T-O weight (flexible runway):
1000, standard tyres | 21
2000, standard tyres | 21.5
5000, standard tyres | 25

5000, low-pressure tyres | 21
6000, standard tyres | 24
6000, low-pressure tyres | 20
FAR T-O field length at max T-O weight (1000, 2000):
S/L | 5,490 ft (1,673 m)
S/L, ISA + 10°C | 5,820 ft (1,774 m)
S/L, ISA + 15°C | 6,160 ft (1,878 m)
2,000 ft (610 m) | 5,970 ft (1,820 m)
3,000 ft (915 m) | 6,320 ft (1,926 m)
FAR T-O field length at max T-O weight (5000, 6000):
S/L | 5,860 ft (1,786 m)
S/L, ISA + 10°C | 6,040 ft (1,843 m)
S/L, ISA + 15°C | 6,168 ft (1,880 m)
2,000 ft (610 m) | 6,120 ft (1,865 m)
3,000 ft (915 m) | 6,530 ft (1,990 m)
FAR landing field length at max landing weight (1000, 2000):
S/L | 3,540 ft (1,079 m)
5,000 ft (1,525 m) | 4,010 ft (1,222 m)
FAR landing field length at max landing weight (5000, 6000):
S/L | 3,120 ft (951 m)
5,000 ft (1,525 m) | 3,527 ft (1,075 m)
Range, high-speed schedule, FAR 121.654 reserves:
1000, 65 passengers | 1,020 nm (1,174 miles; 1,889 km)
2000, 79 passengers | 630 nm (725 miles; 1,167 km)
*5000, 65 passengers | 1,210 nm (1,392 miles; 2,240 km)
6000, 79 passengers | 900 nm (1,036 miles; 1,667 km)
Range, long-range schedule, FAR 121.654 reserves:
1000, 65 passengers | 1,130 nm (1,300 miles; 2,093 km)
2000, 79 passengers | 700 nm (806 mile; 1,296 km)
*5000, 65 passengers | 1,400 nm (1,611 miles; 2,593 km)
6000, 79 passengers | 1,030 nm (1,185 miles; 1,908 km)
*With wing centre-section tanks
OPERATIONAL NOISE CHARACTERISTICS (FAR Pt 36):
T-O noise level:
1000, 2000 | 90 EPNdB
5000, 6000 (estimated) | 88 EPNdB
Approach noise level:
1000 | 101.2 EPNdB
2000 | 101.8 EPNdB
5000, 6000 (estimated) | 97.5 EPNdB
Sideline noise level:
1000, 2000 | 99.5 EPNdB
5000, 6000 (estimated) | 97 EPNdB

Two of three F28 Fellowship Mk 1000 twin-turbofan airliners ordered by Aerolineas Argentinas in early 1975

F-28 FLIGHT DYNAMICS   Section 2 - Aerodynamics   Page 51

Fuselage: Max width 10 ft 10 in (3·30 m)
Height overall 27 ft 9½ in (8·47 m)
Tailplane span 28 ft 4½ in (8·04 m)
Wheel track (c/l of shock struts)
16 ft 6½ in (5·04 m)
Wheelbase:
1000, 5000 29 ft 2½ in (8·90 m)
2000, 6000 33 ft 11½ in (10·35 m)
Passenger door (fwd, port):
Height 6 ft 4 in (1·93 m)
Width 2 ft 10 in (0·86 m)
Service/emergency door (fwd, stbd):
Height 4 ft 2 in (1·27 m)
Width 2 ft 0 in (0·61 m)
Emergency exits (centre, each):
Height 3 ft 0 in (0·91 m)
Width 1 ft 8 in (0·51 m)
Freight hold doors (each):
Height (fwd, each) 2 ft 11½ in (0·90 m)
Height (aft) 2 ft 7½ in (0·80 m)
Width (fwd, each) 3 ft 1½ in (0·95 m)
Width (aft) 2 ft 11 in (0·89 m)
Height to sill (fwd, each) 4 ft 10 in (1·47 m)
Height to sill (aft) 5 ft 2½ in (1·59 m)
Baggage door (rear, port, optional):
Height 1 ft 11½ in (0·60 m)
Width 1 ft 8 in (0·51 m)
Optional cargo door (fwd, port):
Height 6 ft 1½ in (1·87 m)
Width 8 ft 2 in (2·49 m)
Height to sill 7 ft 4½ in (2·24 m)
DIMENSIONS, INTERNAL:
Cabin, excl flight deck:
Length:
1000, 5000 43 ft 0 in (13·10 m)
2000, 6000 50 ft 3 in (15·31 m)
Max length of seating area:
1000, 5000 35 ft 2¾ in (10·74 m)
2000, 6000 42 ft 6½ in (12·05 m)
Max width 10 ft 2 in (3·10 m)
Max height 6 ft 7½ in (2·02 m)
Floor area:
1000, 5000 413·3 sq ft (38·4 m²)
2000, 6000 482·2 sq ft (44·8 m²)
Volume:
1000, 5000 2,525 cu ft (71·5 m³)
2000, 6000 2,931 cu ft (83·0 m³)
Freight hold (underfloor, fwd):
1000, 5000 245 cu ft (6·90 m³)
2000, 6000 308 cu ft (8·70 m³)
Freight hold (underfloor, rear):
1000, 5000 135 cu ft (3·80 m³)
2000, 6000 169 cu ft (4·80 m³)
Baggage hold (aft of cabin), max
80 cu ft (2·265 m³)
AREAS:
Wings, gross:
1000, 2000 822 sq ft (76·40 m²)
5000, 6000 850 sq ft (78·97 m²)
Ailerons (total) 28·74 sq ft (2·67 m²)
Trailing-edge flaps (total) 150·7 sq ft (14·00 m²)
Fuselage airbrakes (total) 38·97 sq ft (3·62 m²)
Fin (incl dorsal fin) 132·4 sq ft (12·30 m²)
Rudder 24·76 sq ft (2·30 m²)
Tailplane 209·9 sq ft (19·50 m²)
Elevators (total) 41·33 sq ft (3·84 m²)
WEIGHTS AND LOADINGS:
Manufacturer's weight empty:
1000, 65 seats 31,954 lb (14,492 kg)
1000C 31,954 lb (14,492 kg)
2000, 79 seats 32,929 lb (14,936 kg)
5000, 65 seats 33,504 lb (15,198 kg)
6000, 79 seats 34,477 lb (15,638 kg)
Operating weight empty:
1000, 65 seats 35,464 lb (16,084 kg)
1000C 35,853 lb (16,263 kg)
2000, 79 seats 36,705 lb (16,690 kg)
5000, 65 seats 37,014 lb (16,790 kg)
6000, 79 seats 38,345 lb (17,393 kg)
Max weight-limited payload:
1000 19,036 lb (8,636 kg)
1000C 18,647 lb (8,457 kg)
2000 17,705 lb (8,030 kg)
5000 17,486 lb (7,930 kg)
6000 17,655 lb (8,007 kg)

Max T-O weight:
1000, 2000 65,000 lb (29,485 kg)
5000, 6000 70,800 lb (32,115 kg)
Max zero-fuel weight:
1000, 2000, 5000 54,500 lb (24,720 kg)
6000 56,000 lb (25,400 kg)
Max landing weight:
1000, 2000 59,000 lb (26,760 kg)
5000, 6000 64,000 lb (29,030 kg)
Max wing loading:
1000, 2000 79·1 lb/sq ft (386 kg/m²)
5000, 6000 83·3 lb/sq ft (406 kg/m²)
Max cabin floor loading:
all passenger versions 75 lb/sq ft (366 kg/m²)
1000, 5000, with large cargo door
125 lb/sq ft (610 kg/m²)
Max power loading:
1000, 2000 3·3 lb/lb at (3·3 kg/kg st)
5000, 6000 3·6 lb/lb at (3·6 kg/kg st)
PERFORMANCE (ISA, except where indicated):
Max never-exceed speed (all versions)
390 knots (449 mph; 723 km/h) EAS
Max permissible operating speed (all versions)
330 knots (380 mph; 611 km/h) EAS
or Mach 0·83
Max cruising speed at 23,000 ft (7,000 m) (all
versions) 455 knots (523 mph; 843 km/h) TAS
Econ cruising speed at 30,000 ft (9,150 m), AUW
of 59,000 lb (26,760 kg):
1000, 2000
362 knots (416 mph; 670 km/h) TAS
5000, 6000
366 knots (421 mph; 678 km/h) TAS
Threshold speed at max landing weight:
1000, 2000
119 knots (137 mph; 220 km/h) EAS
5000, 6000
110 knots (127 mph; 204 km/h) EAS
Max cruising altitude:
all versions 35,000 ft (10,675 m)
Min ground turning radius:
1000, 5000 31 ft 6 in (9·60 m)
2000, 6000 35 ft 9 in (10·90 m)
Runway LCN at max T-O weight (hard run-
way):
1000, standard tyres 26·5
1000, low-pressure tyres 22
2000, standard tyres 27
2000, low-pressure tyres 22·5
5000, standard tyres 31
5000, low-pressure tyres 27
6000, standard tyres 30
6000, low-pressure tyres 26
Runway LCN at max T-O weight (flexible
runway):
1000, standard tyres 21
2000, standard tyres 21·5
5000, standard tyres 25
5000, low-pressure tyres 21
6000, standard tyres 24
6000, low-pressure tyres 20
FAR T-O field length at max T-O weight
(1000, 2000):
S/L 5,490 ft (1,673 m)
S/L, ISA + 10°C 5,820 ft (1,774 m)
S/L, ISA + 15°C 6,160 ft (1,878 m)
2,000 ft (610 m) 5,970 ft (1,820 m)
3,000 ft (915 m) 6,320 ft (1,926 m)
FAR T-O field length at max T-O weight
(5000, 6000):
S/L 5,860 ft (1,786 m)
S/L, ISA + 10°C 6,046 ft (1,843 m)
S/L, ISA + 15°C 6,168 ft (1,880 m)
2,000 ft (610 m) 6,120 ft (1,865 m)
3,000 ft (915 m) 6,530 ft (1,990 m)
FAR landing field length at max landing weight
(1000, 2000):
S/L 3,540 ft (1,079 m)
5,000 ft (1,525 m) 4,010 ft (1,222 m)
FAR landing field length at max landing weight
(5000, 6000):
S/L 3,120 ft (951 m)
5,000 ft (1,525 m) 3,527 ft (1,075 m)

Range, high-speed schedule, FAR 121.654
reserves:
1000, 65 passengers
1,020 nm (1,174 miles; 1,889 km)
2000, 79 passengers
630 nm (725 miles; 1,167 km)
*5000, 65 passengers
1,210 nm (1,392 miles; 2,240 km)
6000, 79 passengers
900 nm (1,036 miles; 1,667 km)
Range, long-range schedule, FAR 121.654
reserves:
1000, 65 passengers
1,130 nm (1,300 miles; 2,093 km)
2000, 79 passengers
700 nm (806 mile ; 1,296 km)
*5000, 65 passengers
1,400 nm (1,611 miles; 2,593 km)
6000, 79 passengers
1,030 nm (1,185 miles; 1,908 km)
*With wing centre-section tanks

OPERATIONAL NOISE CHARACTERISTICS (FAR Pt
36):
T-O noise level:
1000, 2000 90 EPNdB
5000, 6000 (estimated) 88 EPNdB
Approach noise level:
1000 101·2 EPNdB
2000 101·8 EPNdB
5000, 6000 (estimated) 97·5 EPNdB
Sideline noise level:
1000, 2000 99·5 EPNdB
5000, 6000 (estimated) 97 EPNdB

APPENDIX B TO SECTION 2

ILLUSTRATIONS OF STALL TYPES AND
VORTEX FLOW ABOUT A WING

TYPE I - TRAILING EDGE STALL
GRADUAL FLOW BREAKDOWN - HIGH $C_{L_{MAX}}$

TYPE II - LEADING EDGE STALL
ABRUPT FLOW BREAKDOWN - HIGH $C_{L_{MAX}}$

LEADING EDGE
BUBBLE

TYPE III - THIN AIRFOIL STALL
GRADUAL FLOW BREAKDOWN - LOW $C_{L_{MAX}}$

LONG BUBBLE

STALLING CHARACTERISTICS OF AIRFOILS
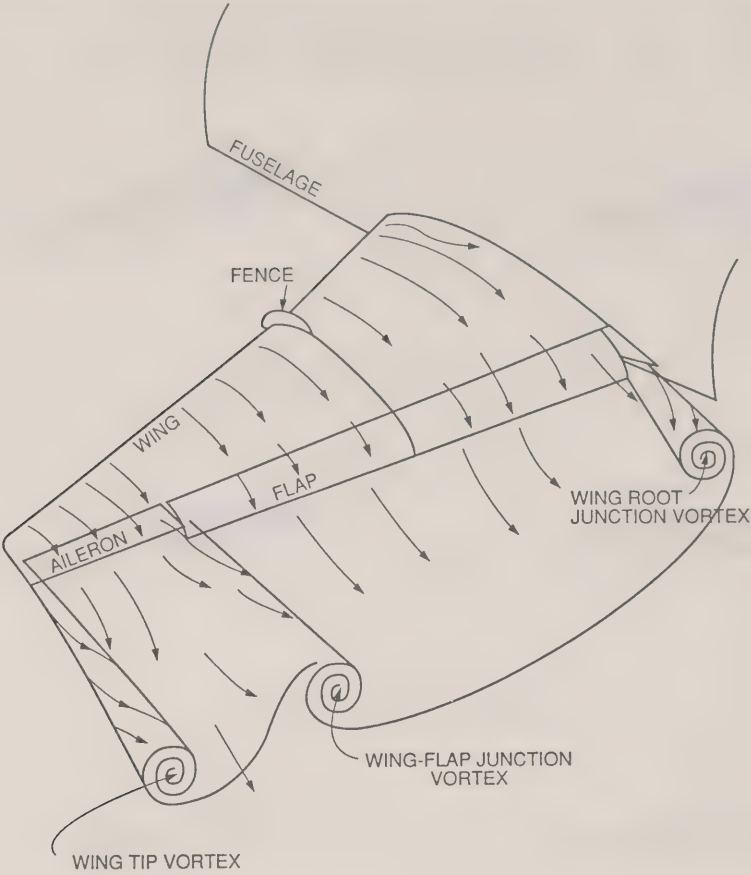
NORMAL FLOW AND WAKE FROM CLEAN WING

REGIONS OF SEPARATED FLOW FROM OUTER WING PANELS AND WING ROOT; CONTAMINATED WING

TURBULENT WAKE

REVERSED FLOW

FUSELAGE

ROUGHNESS

FENCE

ROUGHNESS

WING

REVERSED FLOW

FLAP

AILERON

TURBULENT WAKE

STALL AND TURBULENT WAKE FROM CLEAN WING

TURBULENT WAKE

REVERSED FLOW

FUSELAGE

FENCE

WING

AILERON

FLAP

WING TIP VORTEX
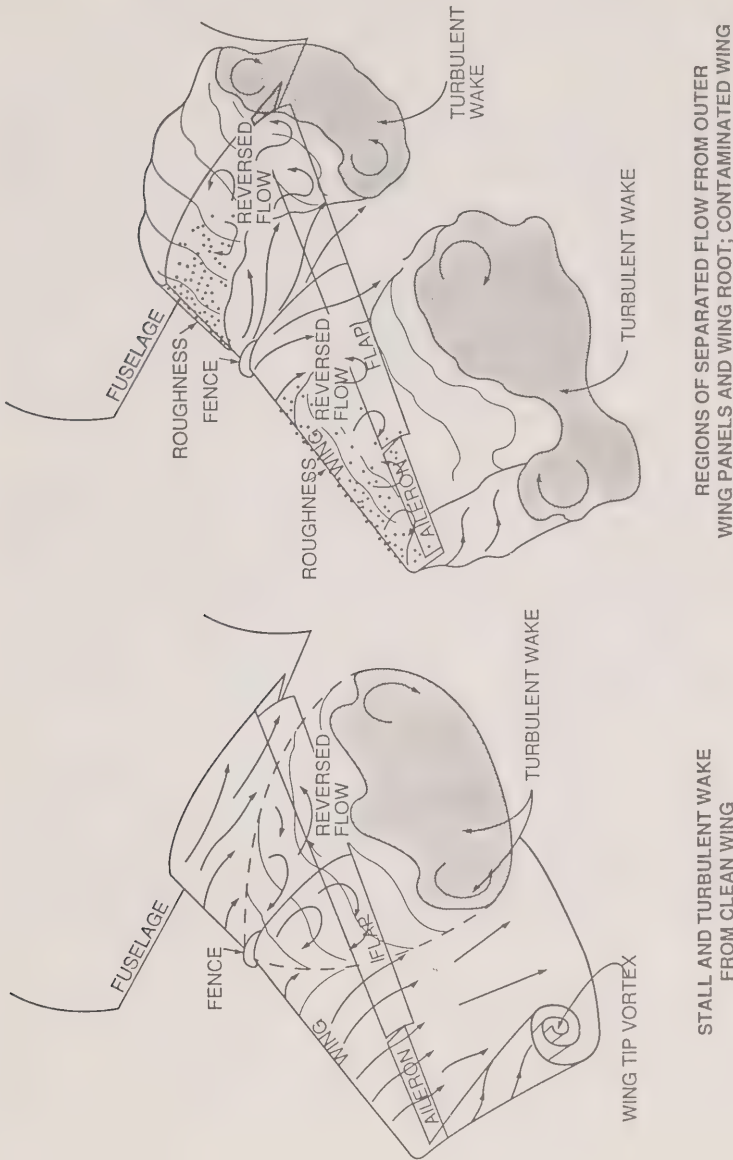
SKETCH OF TYPICAL VORTEX AND TURBULENT WAKE FROM A PARTIALLY-STALLED WING.

F-28 FLIGHT DYNAMICS
SECTION 3
REAL-TIME SIMULATION STUDIES AND ANALYSES

INTRODUCTION

As noted in the introductory section, the destruction of the FDR tape in this accident meant that there were no numerical data on which to base any analysis of the aircraft's trajectory at any point during the attempted take-off: the only guidance available to the investigators was embodied in various witness reports. This meant that simulation, either analytical or real-time, man-in-the-loop, was the only tool available to assist the performance steering group in studying the circumstances of the Dryden accident. Both forms of simulation were used: a visit by the group to the manufacturer's facility in Amsterdam, Netherlands, yielded the opportunity to use the company's engineering dynamic simulator, while extensive mathematical modelling (analytical simulation) was conducted to check and validate the observations made at Fokker Aircraft. This section describes and comments on the results of the dynamic simulations.

DYNAMIC SIMULATION IN THE FOKKER ENGINEERING SIMULATOR

At the time that these dynamic simulations were conducted in the Fokker engineering simulator[4], it was configured as a Fokker F100 aircraft, a somewhat larger derivative of the F-28 with appreciable aerodynamic differences. This aircraft is a new Fokker aircraft and the F28 is no longer produced. Since there was insufficient time to reprogram the engineering simulator with F28 data, it was decided to use the simulator in its existing form, approximating the F28 aircraft by selecting thrust/weight values so that the performance of the machine would be similar to that of the F28. The simulator is a single seat development simulator equipped with a full set of electronic flight instruments at the captain's station, full engine instruments and standard flight controls. It was also equipped with a visual system which provided a night runway scene.

The mathematical model of the F100 used in the engineering simulator included icing performance characteristics for a variety of levels of wing ice. Also, the ground model included the capability to introduce various levels of slush on the runway to provide rolling resistance contamination for the simulation. It was decided to fly the dynamic simulations using a variety of different wing and runway contaminant levels. The data from these simulations were saved and plotted to present pictorially and numerically the flight profiles and changes in the aircraft performance which would be experienced.

---

[4] An engineering simulation is one of great technical detail often used by aircraft designers as a development and research tool.

SIMULATOR APPROXIMATIONS FOR F28-1000 REPRESENTATION

Scaling the Fokker 100 to an F28 MK1000

The objective of the dynamic simulation was to obtain flight profiles which would have been achieved by an F28 MK1000 for various sets of conditions. To accomplish this task, it was necessary to choose a number of parameters carefully.

A weight was selected for the F100 so that the stall speeds and other reference speeds (V_1, V_R and V_2) were the same as those of a F-28 at 63,500 lb weight. This would provide for the same rotation and V_2 speeds and allow for take off roll comparisons to be made for dry and contaminated runways with the thrust level appropriately selected. Also, use of the same speeds resulted in achieving roughly the same wing Reynold's number (a non dimensional ratio of dynamic to viscous forces used in aerodynamics) at rotation. This would ensure that the aerodynamic characteristics of the wing would simulate as closely as possible to those of the F28 in the same conditions.

With the weight so selected, it was necessary to select a thrust level less than full takeoff thrust for the F100 so that the thrust to weight (T/W) ratio was equivalent to that of the accident F28. The T/W ratios were matched for zero velocity. Fokker engineers indicated that thrust decay with speed of the F100 engine was similar to that of the F-28 engine. Thus, the acceleration of the dynamic model should have been similar to the F28.

The aerodynamic drag profiles of the aircraft were similar enough that it was felt that the data the dynamic simulation would provide would be representative since:

    o   Aerodynamic drag did not become a significant factor until roughly 80 knots during the takeoff roll.

    o   The exact characteristics of the icing contaminant being modelled were unknown but adjustment to the contaminant level would compensate for minor differences in the drag profiles.

An obvious concern was the use of the F100 wing in icing studies where wing profile was critical to the results. The Fokker F-100 wing has the same wing box section as the F-28 wing, however, the aerofoil section forward of the front spar has been redesigned. The wing planform has been changed and the wing tips extended and redesigned. The trailing edge flaps have a different camber to change the wing load distribution.

Although differences in wing section characteristics may have some effects as regards this study, the magnitude and nature of the effects due to severe ice/frost contaminant does not seem to be strongly dependent on the wing section in this class of jet transport aircraft. (See Section 1 - Aerodynamics)

The centre of gravity position of the F100 was set at 30% MAC to give the F100 the same rotation response to control as the F28 at 22%, the setting for the Dryden takeoff.

The F28 involved in the Dryden accident took off at a weight of approximately 63,500 lb plus the accumulated weight of the snow/ice. The aircraft had a static takeoff thrust level of 19,700 lb. total, assuming that the engines were functioning normally. The T/W ratio equalled 0.30 at this full takeoff thrust. The F100 in the simulation had a weight of 87,000 lb and a thrust level of 26,100 lb was selected so that the T/W ratio also equalled 0.30. The F100 weight was selected so that the stall speeds for clean wings were the same in both cases, 107 kt. In both cases, flap settings of 18 degrees were used.

Baseline Conditions

The baseline conditions for the dynamic simulation were established with clean wings and a dry runway. Takeoffs were accomplished in these conditions and the rotation point checked against witness reports of the accident to validate, roughly, the modelling of the F28.

The baseline simulation results correlated well, in general terms, with the F28 characteristics. In addition, these baseline runs gave the simulation pilot time to develop a feel for the simulator so that consistent rotation and handling techniques could be applied to all takeoffs.

Slush Modelling

The slush model depth was varied to determine the level of slush contaminant required to extend the takeoff roll to the distance reported by the witnesses.

Slush depth was varied from 0 to 0.45 inches in small steps. The additional takeoff distance was noted in each case and a slush depth of 0.15 inches selected as a baseline value for the simulation. This slush depth resulted in an increase in takeoff distance of approximately 500 feet, that is, of the same order as the excess take-off run reported by witnesses to the Dryden accident. It should be noted, however, that there is an additional component of extended takeoff roll which results from the icing contaminant on the wings requiring rotation to a higher pitch attitude prior to liftoff. This factor was considered later in the simulation.

Wing Contaminant Modelling

The wing contaminant was modeled by using the Fokker rough ice/snow simulation for the entire wing. The contaminant factor could be varied between 0 and 1.0. It should be carefully noted, however, that this factor is not equivalent to contaminant depth although it is so labelled on the plots provided by Fokker. The reason is that wing contaminants with different characteristics will result in very different performance of the wing at the same depth. In other words, a very thin layer of a very rough contaminant can result in a far greater performance loss than a thick layer of very smooth contaminant which follows the

wing contour. It is sufficiently important a point that despite repetition it must be restated that *the FORM and POSITION of a wing contaminant is much more important than its thickness in considering wing performance.*

Hence, a better description of the contaminant factor would be to say that at levels above approximately 0.8, the aircraft would not fly off the runway at the speeds and in the conditions of the test. As a result, we worked with a variety of contaminant levels in the range of 0.5 to 0.80 which resulted in flight profiles which matched, in general terms, the accident profile.

The runs which most closely matched the profile described by witnesses at Dryden were achieved with a slush depth of 0.15 inches and a contaminant level of about 0.8.

Fokker's description of the wing ice simulation is quoted from page 3 of Warrink[7].

> *Ice on the wing is simulated as a change in lift-, drag- and pitching moment coefficient. The magnitude of it has been determined in the wind tunnel, in which one inch thick horn shaped ice on the leading edge was simulated. From tests with different ice shapes and from literature it is known that these effects are also valid for rime ice or frozen slush in the leading edge region. Through calculations in which static equilibrium conditions are determined the effect of 1 inch ice (in ground-effect) on lift, flight path angle and elevator deflection has been assessed. See figures 1, 2 and 3. In the simulation the effect of ice on the wing could be varied linearly between 0 and 1.0.*

Engine Failure On Take-off

A few take offs were flown during which an engine was failed just after rotation. Regardless of the contaminant level on the aircraft, directional control was not a problem. However, the contaminant level at which the aircraft was still able to liftoff and climb was significantly reduced. Successful takeoffs were accomplished at a contaminant factor of less than 0.5, and that level provided for minimal performance. It should be noted that the relationship between contaminant *level* and contaminant *thickness* is highly nonlinear, so that this should not be interpreted as meaning that the aircraft is able to carry half the contaminant load with an engine failure.

However, it was clear that the reduced thrust at rotation severely reduced the available performance margin and thus limited the aircraft's capability to carry any contaminant through a successful takeoff.

DYNAMIC SIMULATION HANDLING TECHNIQUES

Overview

A fundamental assumption made during the simulation exercise was that the pilots of the accident aircraft would have believed that their aircraft was flyable and would, therefore, have employed normal handling techniques. Therefore, for 'Dryden' simulations no special procedures or techniques were allowed which would have provided a better flight profile due to the simulator pilots' a priori knowledge of the external conditions being applied. Ad hoc experiments with off nominal techniques left no doubt that handling technique greatly affects the resulting flight profile in the presence of contamination. This observation was later confirmed by the off-line numerical modelling.

Handling technique in the context of this exercise includes the following:

o   Selection of rotation speed. A pilot who applied a speed increment above V_r prior to rotation would have a higher probability of a successful takeoff. The converse is also true.

o   Use of a lower rotation rate. A pilot who used a slower rotation rate would also have a higher probability of a successful takeoff.

o   Use of a partial rotation. A pilot who rotated the aircraft to the usual liftoff attitude and held it there rather than rotating further would also have a higher probability of a successful takeoff.

It is important to note that the above comments should not be interpreted as recommend-ations for aircraft handling in adverse conditions. The reason is that there are many other trade-off factors which are balanced out in any takeoff which these techniques may degrade. The only parameter being examined in this case is the specific question of whether, for the selected conditions at the planned speeds, this aircraft would fly.

The dynamic simulations were all flown by Mr. Wagner, a current B767 first officer with Air Canada, to preserve consistency in the handling of the simulation. The simulator flying was monitored by Mr. Morgan, an engineering test pilot with National Aeronautical Establishment. Techniques for flight control handling during different phases of the simulation were reviewed by the two pilots during the exercise to attempt to ensure that reasonable procedures were used at all times.

Flying Techniques and Methods

Each takeoff run was started from the threshold of the runway at zero velocity with the thrust already at planned takeoff power. The brakes were released and the takeoff roll commenced. No wind was simulated because in the Dryden accident, the wind was effectively calm.

The aircraft was accelerated to rotation speed with a very slight push force on the control wheel to ensure positive nosewheel steering. As rotation speed was reached, the rotation was initiated by use of nominal wheel pull force to achieve a rotation rate of approximately 3 degrees per second. The rotation attitude was limited to 18 degrees, somewhat higher than that for the F28, but appropriate for the Fokker 100 aircraft.

After the aircraft became airborne, the aircraft was accelerated to the reference V_2 speed plus a speed increment, depending on the configuration and conditions for the test run. The run was terminated at an altitude of about 400 feet above airport altitude or when the aircraft impacted with the ground during unsuccessful takeoff runs. Some takeoffs were also terminated after extended flight just above the terrain in ground effect where a successful climb-out could not be achieved.

All the data from each run were recorded by the simulation computer.

Flying Techniques During Contaminated Runway Takeoffs

For the contaminated runway takeoffs, normal control wheel inputs were used except for a few runs where the nose was raised about 2 to 3 degrees at about 80 knots to get the nosewheel out of the slush. This is a procedure specified in the F28 manual and was flown to determine what effect use of the technique could have had on the takeoff in this case.

The data from the runs were analyzed and it was found that raising the nosewheel to reduce slush drag had a measurable, but rather small effect, on takeoff distance. The difference was on the order of 100 feet.

Flying Techniques During Contaminated Wing Takeoffs

For contaminated wing takeoffs, normal control wheel rotation forces were used, even though the rotation rate that resulted was somewhat slower than with the clean wing model. This is because the contaminant had the effect of
increasing the nose down pitching moment of the wing therefore there was less excess nose up moment from the elevator to cause rotation.

As the contaminant levels were increased, numerous takeoff runs were flown where the stick shaker[5] actuated immediately on or just after liftoff. This was due to the significantly greater angles of attack achieved in these cases. It was judged that normal pilot technique would be to attempt to reduce the angle of attack to stop the stick shaker and nose down control wheel inputs were made accordingly. However, an attempt was made to maintain

---

[5] A 'stick shaker' is a warning device which vibrates the pilot's control column if the wing reaches a pre-determined angle of attack. Under normal operations this device warns against impending stall, and its onset is generally used to indicate the prudent limit of useable lift.

an aircraft attitude right at the edge of stick shaker activation. This is because it is believed that most pilots, in view of current training with respect to wind shear escape manoeuvres and ground school training, would expect to achieve close to maximum available lift at the point of stick shaker activation.

It should be noted that in cases of significant wing contamination, the wing can be well beyond the stalling angle of attack by the time the stick shaker activates. In essence, the stick shaker is responding to the normally expected maximum angle of attack of the clean wing. The stall warning system is not actually measuring stall and flow separation from the wing. Rather, it infers the onset of stall from the known performance of the wing and is programmed to activate at a fixed geometric angle of attack based on that knowledge.

Thus, the pilot flew many contaminated airfoil simulations in or near stick shaker. The simulation pilot worked hard to try to keep the aircraft at the edge of stick shaker and that is the reason that there is noticeable pitch oscillation on the recordings from those runs.

Flying Techniques During Engine Out Takeoffs

Normal pitch handling of the aircraft was used for the engine out takeoffs. In these cases, an engine was failed just at Vr and appropriate rudder inputs made by the pilot to ensure that the aircraft continued to track straight. Small roll inputs were required to correct any incipient rolling tendency in the aircraft due to any remaining yaw from the engine failure. The climb-out characteristics of the aircraft were conventional with the engine failure, except that, as described, only a limited wing contaminant load could be carried in these cases.

Summary of Dynamic Simulation Experience

The Dynamic Simulation data is presented in Fokker Report VS-28-25, Order Number 22192. This report summarizes the work done in the Fokker simulator between June 7th and June 8th, 1989.

The effect of varying runway slush depth was primarily reflected in increased takeoff run. There were some additional effects seen related to the ability of the aircraft to accelerate after rotation with the wing significantly contaminated. However, the slush effect was limited in its effect, in general terms, to increasing the takeoff run.

The effect of the wing contamination was to degrade the performance of the wing, the degree of degradation being a nonlinear function of the contaminant level.

A few principal effects were noted in this simulation.

1. As the wing contaminant level increased from zero, the aircraft's performance immediately reflected the fact by a reduction in climb performance.

2. At moderate levels of contaminant, the aircraft experienced stick shaker shortly after unstick and the profile after that point was related to the simulation pilot attempting to keep the aircraft right at the edge of stick shaker, 13 degrees angle of attack. It should be pointed out that for the contaminated wing, that angle of attack was already post stall in most of those cases. Climbing out of ground effect became impossible in many instances.

3. At critical levels of wing contaminant between 0.75 and 0.825, the aircraft was able to unstick and sometimes fly. However, as the aircraft climbed out of ground effect, the performance loss resulted in the aircraft descending, touching down again or crashing off the end of the runway.

4. In summary, as the contaminant level increased, the liftoff pitch attitude and airspeed (not rotation airspeed) had to be increased to provide adequate lift to unstick. Also, since increasing levels of contaminant decreased the stalling angle of attack, liftoff occurred closer and then beyond the true stalling angle of attack. Eventually, liftoff was occurring post stall (contaminated wing) or the aircraft stalled shortly after liftoff as it climbed out of ground effect. Successful flight with the wing contaminated at levels between 0.7 and 0.825 was effectively impossible using normal techniques. The profiles resulting from flight at these contaminant levels were, in general terms, close to the profile which is representative of the Dryden accident. (See figures 17 to 19 in the Fokker Report)

5. In cases where an engine was failed, the aircraft was not flyable with even moderate levels of contaminant. The drag increase due to the contaminant is so great that the thrust of only one powerplant is inadequate to carry even these moderate ice levels. The reason is that the high angles of attack required to generate adequate lift with the contaminated wing produces much higher drag levels. Post stall drag also is extremely high. The only way to get the aircraft to fly with the contaminant is to have enough thrust to accelerate to a high enough speed. However, the thrust level with one engine is inadequate to provide that acceleration.

F-28 FLIGHT DYNAMICS
SECTION 4

OFF-LINE MODELLING
INTRODUCTION

Subsequent to a visit to the manufacturer of the aircraft and man-in-the-loop ground based simulations carried out there (Section 2), off line modelling of the F-28 during take off was performed to examine both the normal take-off performance and the effects of runway and flying surface contamination. The purpose of the numerical simulations was to confirm observations made at the Fokker Establishment using a modified engineering simulation of the Fokker 100, a similar but not identical vehicle. This report outlines the methods used, approximations and extrapolations made and provides appropriate samples of the model output. Two models were developed simultaneously by Wagner in Montreal and Morgan in Ottawa. Their outputs were periodically checked one against the other and where differences were found the source was isolated and either corrected or, if conceptual or algorithmic, modified after consultation.

A secondary, but important, purpose of this section is to provide accountability for the theoretical engineering used in modelling the F-28 take-off. To that extent, the language used is, at times, quite technical and there is an extensive use of descriptive mathematics. For this, the author apologises to the lay reader, but it was felt to be imperative that the work which led to the conclusions presented here should be available for scrutiny by his peers.

DATA SOURCES

Three primary and two secondary data sources were used in building the off-line simulation. Aerodynamic and performance data were taken from the F-28 simulation data base provided by Fokker Aircraft[8] and from an internal Fokker wind tunnel study of the F-28 lift and drag characteristics when the flying surfaces were contaminated with artificial roughness. For cognitive pilot modelling through the rotation and immediately post lift-off, flight data were extracted from time histories of 21 previous take-offs flown in the actual aircraft involved in the Dryden accident (C-FONF), which were provided by the Engineering Branch of the CASB. Runway contamination was modelled using information published by NASA[9] and the Royal Aeronautical Establishment (UK)[10].

SITUATION OVERVIEW

Fokker F-28 C-FONF crashed into a treed area some 750 or so meters from the end of the runway at Dryden immediately after a take-off attempt. The aircraft struck trees at a height about one meter above the runway height at the lift-off end and subsequently cut a swath through the trees for a further 240 meters before coming to rest. The flight data recorder (FDR) suffered fire damage to the extent that no data were recoverable and eye witness reports are the only available source of information regarding the trajectory of the aircraft during the take-off run and prior to the crash. There was a general trend in the witness reports suggesting that the aircraft's wings were at least partially contaminated with slush or ice during the take-off attempt and there is additional information suggesting that the runway was to some extent or other contaminated with slush or wet snow at the time

of the accident. The general tenor of the witness reports, together with the absence of ground markingsground markings between the runway end and the first point of impact suggests a sequence of events approximately thus:

> The aircraft, in an 18 degree flap configuration, commenced its take-off run from a normal position on the runway, achieved rotation speed somewhat further down than was normal and commenced a rotation. During the initial rotation the machine either became briefly airborne, or simply extended the oleos, and then settled back onto the runway, reducing its body angle somewhat. A second rotation very close to the end of the runway resulted in the aircraft becoming airborne but maintaining a very low altitude until striking the trees. Subsequent technical investigation has shown that at some time during the take-off attempt the wing flaps were extended from 18 to 25 degrees and that at the time of impact the undercarriage was in transit (neither fully down nor fully up).

The above general concept has, for modelling purposes been termed the 'Dryden Scenario'.

SCOPE OF MODELLING

Since it is clear that the aircraft did not gain significant altitude, the modelling task was greatly simplified. The change of flap setting was accounted for after the first rotation, while the change on overall drag coefficient due to in-transit undercarriage was so small that it was ignored. The take-off was treated as a three phase task, ground run, rotation and post lift-off, these being defined as follows:

a: **Ground Run.** This was taken to be the phase from the start of the take-off, with the aircraft stationary at the end of the runway to the point at which the pilot commenced rotation into the pre-planned take-off attitude. Pilot intervention at this stage is not significant: with aircraft of this class it usually consists of maintaining a continuous forward pressure on the control column to ensure good nosewheel contact with the runway and hence good directional control by use of nosewheel steering.

b: **Rotation.** This phase covers the time from the end of the ground run during which the aircraft is rotated in pitch with the object of permitting the wing to generate sufficient lift to raise the aircraft from the surface so that it becomes completely airborne. While the technique may vary somewhat between aircraft types, it is usual to rotate to a pre-set attitude and at a given rate, the aircraft generally becoming airborne as or shortly after the target attitude is achieved. Here pilot technique becomes of significance if the best performance of the wing is to be realised. The pitch rate used and the precision with which the target attitude is achieved can both influence the realisation of the optimum performance of the wing.

c: **Post Lift-Off.** This phase is here taken to mean the time between the aircraft becoming completely airborne from rotation to its either climbing out of ground-effect or settling back to the surface as the case may be. In developing the numerical model it became apparent that pilot technique was a vital ingredient during this phase of flight.

The aircraft has been continuously modelled through these three phases, however the rudimentary pilot cognitive model changes in reaction to the phase condition.

PILOT MODELLING AND AIRCRAFT DYNAMICS

Early experience during model development indicated that the results of the simulations were likely to be critically dependent on pilot technique, which supported observations made during the dynamic simulations. It was also thought desirable to explore alternate pilot control strategies in the case of badly contaminated flying surfaces. To these ends a rudimentary pilot cognitive model was built. That is, no attempt was made to model pilot compensatory or physiological characteristics, but provision was made for a variety of pilot behaviours, each resulting in a commanded pitch rate for the aircraft. The output from this section of the simulation was fed to a simple first order low-pass filter with a break point set at 1.5 radians/sec, roughly representative of the expected pitching response of an aircraft of this class at typical take-off speeds.

Pilot behaviour was modelled during two of the take-off phases, the rotation and the immediate post lift-off regime, as described below.

ROTATION

For the rotation, four representative behaviours were considered, these being:

a. **Normal.** A study of the time histories of 21 take-offs provided by the CASB indicated that the 'normal' or customary take-off rotation consisted of a fairly rapid rotation to about 10 degrees of pitch attitude, followed a short time later (about 1.5 seconds or so) by a further rotation to between 13 and 15 degrees of pitch. The latter increment in pitch attitude appears to be 'open loop' in nature as on a significant number of the take-offs recorded it was accompanied by a slight transient reduction in airspeed. This procedure was taken as the initial model. The take-off data available showed a mean pitch rate during the first stage of rotation of 3.81 deg/sec with a standard deviation of 0.76 deg/sec, the maximum value noted was 5.1 deg/sec and the minimum 2.9. The mean value was used in the model as a commanded pitch rate limit.

b. **Slow Rotation.** The structure of the rotation manoeuvre here is exactly the same as that described in paragraph a., with the exception that the limit on commanded pitch rate was set to 1.9 deg/sec, a half of the nominal value.

c. **Over-rotation.** This strategy was based on a consideration of typical pilot response when the aircraft unexpectedly fails to become airborne after the normal rotation to 10 degrees of pitch attitude. After a slight delay (1.5 seconds) the aircraft is further rotated in pitch to 12.0 degrees. Under normal circumstances, that is with an uncontaminated aircraft such a failure to fly at the normal attitude might be experienced if, say, the weight of the vehicle had been underestimated or an error had developed in the airspeed measuring system. In this case an increment in attitude *could* cause sufficient lift to be developed to achieve lift-off. In the case of the uncontaminated F28 the wing would still be operating below the maximum C_L and the drag penalty for the additional rotation would be small.

d. **The 'Dryden' Scenario.** Eye witness reports generally agree that the aircraft at Dryden was rotated twice, though whether or not it became temporarily airborne after the first rotation is uncertain. A significant number of the passenger witnesses remarked on a final power surge shortly before the machine became airborne close to the end of the runway. A basic scenario which answers to the preponderance of the witness reports was described on pages 1 and 2. For modelling purposes this was treated as a dynamic sequence with the aircraft being pitched nose down after the initial rotation either at a fixed rate or to an arbitrary attitude. The further flap extension to 25 degrees was modelled assuming that the crew selected the extension after having failed to become fully airborne at the first rotation: the extension was modelled at 1 degree per second with a linear interpolation of both lift and drag between the 18 degree and 25 degree conditions. While this set of motions meets the described aircraft motions and is, to an experienced pilot, a plausible set of pilot actions under these circumstances, *it can not be too strongly emphasised that this is conjecture, based, in the absence of factual knowledge, on an informed but judgemental interpretation of witness descriptions.*

POST LIFT-OFF

Following lift-off, three piloting options are provided, these being:

a. **Increment Pitch Attitude.** This mode was derived from a study of the time-histories of take-offs previously performed in the actual crash aircraft which suggest that an increase in pitch attitude immediately after lift-off is usual. Whether or not this is an habitual procedure or whether the pilot is at that time attempting to track airspeed is uncertain. For the majority of samples the airspeed is stagnant during this manoeuvre, but there were several cases where an airspeed loss was noted during the secondary rotation. The increment in pitch attitude by 3 degrees is again based on a survey of the data mentioned above. This procedure follows closely the approved procedure contained in the Fokker flight manual for the F-28.

b. **Constant Airspeed.** This is akin to a frequently used procedure for aircraft of this class, wherein the pilot, during initial climb, attempts to maintain the speed at which he broke ground plus a certain increment, the 10 knots used in the model being typical.
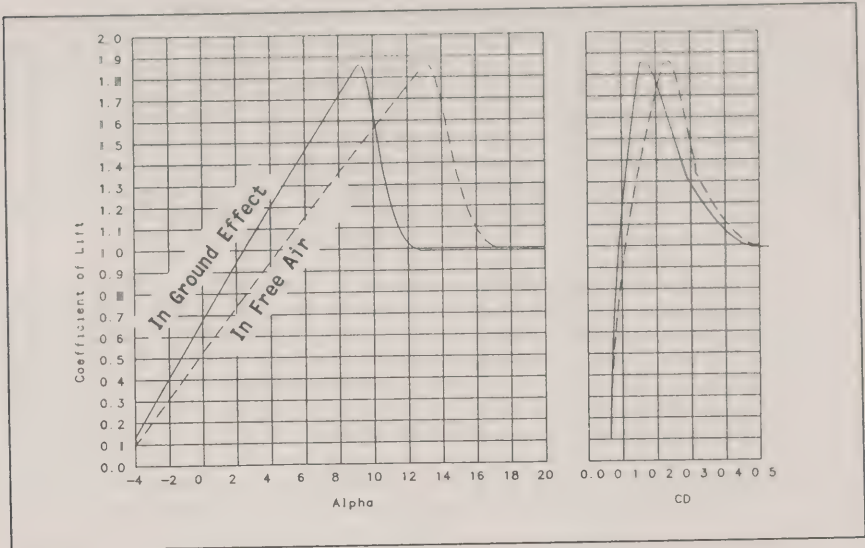
Figure 2: C_L and C_D for Clean Wing

c. Constant Angle of Attack. While not in the normal piloting repertoire, since the required information is not generally available in the cockpit, this probably represents the most efficient way of establishing an initial climb. It was included for performance limit comparisons only and is not intended to represent real pilot behaviour.

AERODYNAMIC MODELLING

Since, by its very nature, this investigation had to concentrate on stall and post-stall behaviour of the aircraft, great care was taken to achieve good modelling of the aircraft's characteristics in this region. Additionally it was necessary to model ground effect with some precision and to derive an intelligent estimate of the effects on both lift and drag of a wing contaminant. The model was developed using data from both Reference 1 and the Fokker wind-tunnel experiments. The procedure used in determining the clean wing characteristics in and out of ground effect was first to use curve fitting techniques to obtain the C_L/α curve for the 18 flap wing out of ground effect (OGE) and then to enter this curve using not the reference angle of attack, but an effective angle of attack based on the aircraft's height and a ground effect interpolation curve provided in Reference 1. The curve for angles lower than 13 degrees was taken directly from Reference 1, while the extended range was derived by interpolation from the wind tunnel data, maintaining the
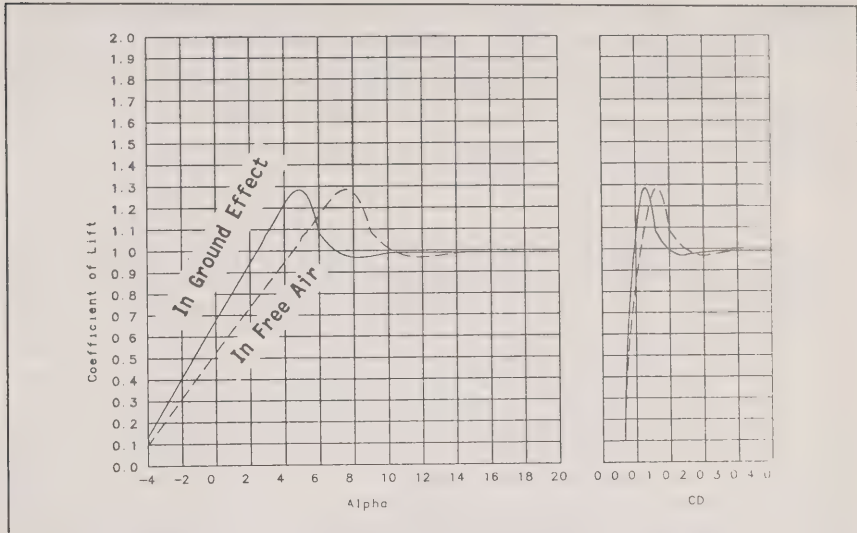
Figure 3: C_L and C_D for Contaminated Wing

form of the curve while reducing its magnitude to that anticipated for the 18 flap case. The resulting curves for the uncontaminated wing are shown in Figure 1. In modelling flap extensions to 25 a simple increment, again based on the data in Reference 1 was used.

The contaminated wing curve was derived from three sources, the clean wing curve for very low angles of attack, a plot of lift loss due to rime ice as given in Reference 1 and the wind tunnel data, using the same techniques as described above. The final curves used are at Figure 2. While this may appear to be a rather sparse data set on which to model a regime critical to the study, it has the merit of being fact based and applying specifically to the F-28 wing. Additionally, there is ample theoretical support for the form of the curves used and even their magnitude, particularly following Jones and Williams[11] and Cebeci[12]. Additional information derived from both wind tunnel and flight test was obtained from Zierten and Hill[13], although the research reported here referred to aircraft with leading edge high lift devices, the general trend and the specific references to stick shaker activation were of use.

Drag

An initial examination of the available F28 data indicated that drag would be critical to these simulations. Provided the wing is producing a reasonable value of C_L even when contaminated, then if the aircraft accelerates to a sufficiently high speed it will fly. If, however, the drag becomes so great that there is insufficient engine thrust to accelerate the aircraft after rotation, then such an event becomes impossible. For the take-off to be

successful it is also necessary for the aircraft to accelerate when airborne to compensate for the reduction in C_L at a given angle of attack as the machine climbs out of ground effect. Drag curve estimates were again derived from a combination of data from the Fokker data base and the company's wind tunnel data. The effects of wing contamination came from the same sources. Figures 1 and 2 also show the drag polar plots used in the simulation and their relationship to C_L and α.

Degree of Wing Contamination

Since it is impossible to determine the exact form of the wing contamination present during the Dryden accident, it is taken that the wing is either contaminated beyond the critical condition or not.   The evidence for this type of binary approach to critical contamination is strong. It was implied by Jones[14] 53 years ago and is amply supported by Abbott and Von Doenhoff[15] and Hoerner[16]. However, to permit gradations of contamination, it may be considered that part of the wing was contaminated and part was not. There is some witness support for this approach. This being accepted, the contamin-ation coefficient used in the simulations simply interpolates the lifting capability of the wing on a proportional basis between the clean and contaminated conditions. This approach leads to a C_L/α curve with two distinct peaks for intermediate contamination conditions, which may or may not occur in reality but does indicate a reduced performance capability commensurate with that described by Wolters[17] and the previously cited works of Cebici and Zierten and Hill: this is considered to provide an adequate and realistic representation of performance degradation due to wing contamination.

Engine Failure

The Wagner model accounts for possible engine failure during the take off attempt, this is done for the sake of completeness, *not because there is any suspicion that the power plants behaved abnormally during this accident*. While there is a general agreement in the witness reports that there was a power increase shortly before the final lift off, very few suggest that a power reduction occurred during the take off. The professional pilot who was seated adjacent to the engine intakes did not report any power reduction. Engine failure was modelled by reducing the thrust instantly to approximately half of nominal, while adding the drag term corresponding to the ram drag of the failed engine and the required deflection of the rudder to maintain directional control.

MODEL RUN MATRIX

Once the modelling had been completed and validated (Section 5), a matrix of cases to be run was determined empirically. For all cases, the baseline configuration was a weight of 63,500 lb, full rated thrust, 18 degrees of flap and a V_r of 122.5 kt. The nominal rotation was an initial pitch rate of 3 deg/sec towards a target attitude of 10 degrees followed by a further rotation at 1 deg/sec to 13 degrees of pitch attitude after unstick, ie, following the preferred Fokker procedure. Thereafter, three parameters were varied as being of prime interest in this study, the depth of slush, the proportion of wing contamin-ation and the selection of V_r. These runs were completed using both the nominal rotation

technique described above and the 'Dryden Scenario' described at length earlier. Nominal (3 deg/sec) and a reduced (2 deg/sec) rotation rates were used for the initial rotation. The full set of conditions tested was:

a. Slush Depth. 0, 0.1, 0.2, 0.3 and 0.4 inches.

b. Contaminant Ratio. 0 and 50 to 100 % in steps of 1%. When this resolution produced ambiguous results boundaries were defined by making special runs at finer resolution

c. Rotate Speeds. 117.5, 122.5 (nominal) and 127.5 kt.

d. Rotation Rates. 3 and 2 degrees/second.

PRESENTATION OF RESULTS

Initial plots, Figures 4 to 6 are presented to clarify some of the effects of flying surface and runway contamination described earlier. Figure 4 shows the effect of runway slush and wing contamination on the take-off distances to both rotation and lift-off. It can be seen that while the presence of slush changes the distance required to reach V_r significantly, wing contamination has very little effect, almost all the traces for distance to rotation overlay each other. This is definitely not so for the distance to lift off. As the level of wing contamination increases, the distance penalty to unstick increases quite rapidly due to the marked increase in drag produced by the contaminated wing at high angles of attack. This characteristic represents a situation in which the full extent of performance loss may not be apparent until the aircraft is rotated; prior to this the reduction in acceleration is little more than could be attributed to a slush layer. Figure 5 is presented to indicate the reasons for this effect. It shows that as contamination level increases, even in the absence of slush, the distance the aircraft has to travel between V_r and the unstick point increases only slowly until a dramatic 'knee' is reached (numerically at just over 0.6 contamination ratio). This is coincident with the aircraft being at or beyond C_{Lmax} for the contaminated wing at its rotation angle of 10 degrees and having to generate the necessary lift by increasing speed rather than C_L. The low acceleration rates available once the drag rise caused by wing contamination has been encountered mean that excessive distance has to be consumed for this to occur. A secondary effect can be seen in the same figure by examining the trace of Theta (body angle). At first moderate increases for Theta at lift off are enough to compensate for the loss of C_L due to contamination, but a point is reached, at about 0.58 contamination ratio, when the rate of increase in theta steepens noticeably. This is related to the reduced lifting capability of the wing as indicated earlier in Figure 2.

The next two plots in this section represent the crux of this investigation. They show that it is possible to define two boundary conditions in terms of combinations of slush depth and contamination factor which can both lead to catastrophic results of attempted take-offs. A *boundary condition* here means a continuous relationship between level of

contamination and runway slush depth which represents the dividing line between a successful take-off or not, as illustrated in Figure 3. In both Figures 6 and 7, several boundaries are shown for varying conditions of V_r and rotation rate, these should be individually interpreted according to Figure 3.

Figure 3: A Boundary Condition Plot

Figure 6 indicates a boundaries for a condition in which the aircraft will simply fail, in the distance available, to leave the ground and will run off the end of the runway. It also shows that any reduction in the rotation speed will have an adverse effect on the available performance. At somewhat lesser levels of both factors, another boundary was found to exist, defining a condition wherein the aircraft would at first leave the runway, but fail to climb out of ground effect and settle back to the surface (Figure 7). This boundary existed for all conditions of rotation speed and rotation rate tested, and is annotated to indicate the effects of varying the various aircraft handling parameters on the placement of the boundary. When this condition was met it was possible, by making subtle changes in the assumed pilot control strategy after the initial lift off (eg, rate of pitch, response to stick shaker) to cause the model to fly for considerable distances at very low altitudes, but it was not possible to make it fly except by assuming extremes in pilot behaviour.
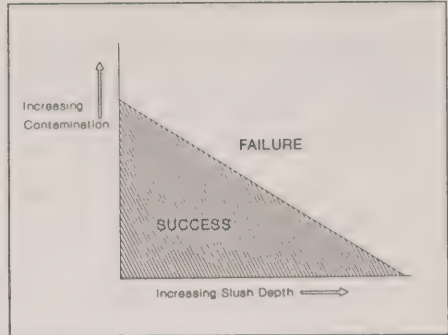
The final sets of Figures provided with this section are intended to illustrate the effects and observations made earlier in the text. Figure 8, a,b and c shows the overall effects of increasing contamination factor in a gross way. The rotation speed here was 122.5 kt and slush depth 0.25 in. At 65% contamination the aircraft flies away normally, at 68% the machine sinks following the initial lift off, due both to the loss of lift with height and the pilot's reaction to stick shaker, but then climb away. Note that the scale of the height trace is such that at 6500 feet (500 feet beyond the end of the runway) the aircraft is still only at 10 feet. In 7c, contamination now being set at 69% the aircraft returns to the runway and subsequently runs off the end. The series in Figure 9 a,b and c shows that fine graduation of the contaminant level creates subtle differences in the aircraft responses. This set of plots refers to a much shallower slush layer (0.1 in) and an incremented rotation speed of 127.5 kt. Figure 9a indicates that at 82.3% contamination the aircraft flies away despite two bursts of stick shaker, while by the time contamination is at 82.4% the machine never exceeds about 5 ft, eventually returning to the surface some 1100 feet beyond the end of the runway. When there is 0.1% additional contamination the result is a short hop and an over-run. Finally, Figure 10 a and b demonstrate the remarkable sensitivity to assumed pilot behaviour noted earlier. The only difference in these two runs is that the angle to

which the aircraft is un-rotated following the initial hop is two degrees lower in 9b than 9a, the latter strategy resulting in a second lift-off and climb out and this at a very high level of contamination.

The implication of the results presented here, especially the two sets of boundary conditions, is that there exist a combination of values of slush depth and wing contamination which can cause aircraft trajectories of the type described by witnesses to the Dryden accident.

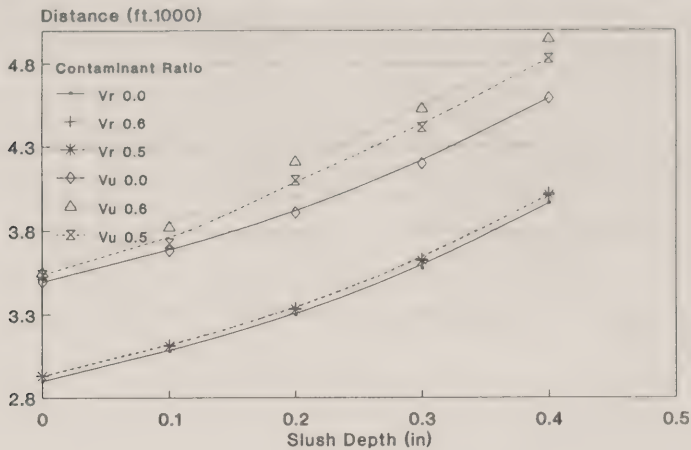Figure 4 Effect of Contamination and Slush on the
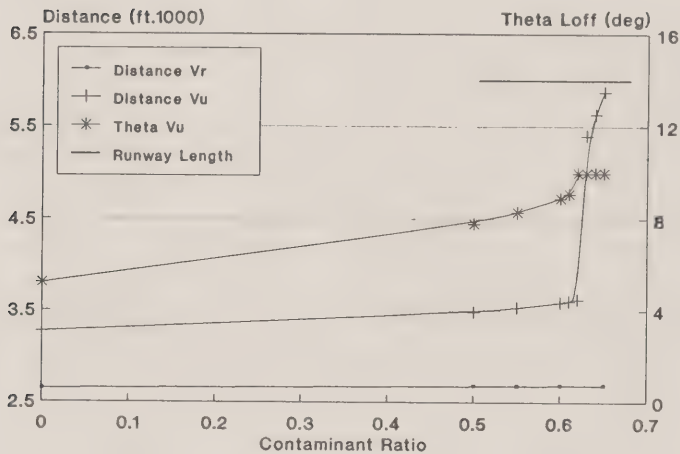Distance Required to Reach V_r and V_u

Figure 5 Effect of Wing Contamination on Distance Required
To Reach V_r and V_u Illustrating the 'Knee' Effect at Limiting
Body Angle
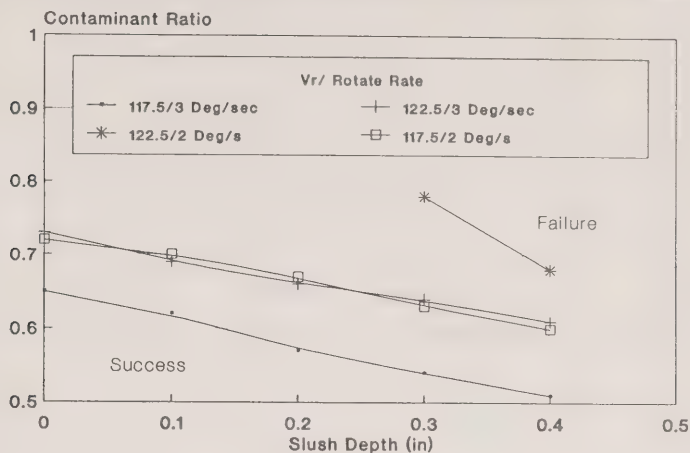
Figure 6   Various Boundary Plots at Different Values of V_r and Rotation Rate for Overrun Case
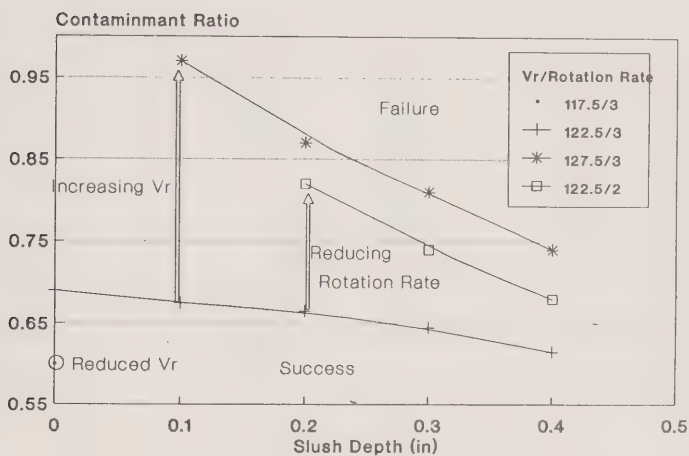
Figure 7 Various Boundary Plots for the 'Bounce' Case

F-28 FLIGHT DYNAMICS   Section 4 - Mathematical Modelling   Page 78

Lift
Margin

Thrust
Margin

Alpha   10

Theta   10

Speed   150

Height   10.0

Stick Shaker
Coarse Height

0   1000   2000   3000   4000   5000   6000   7000   80

Distance (ft)

F-28 Take Off Simulation   Weight 64227   Slush depth (in) 0.25 Contamination (%) 65.0
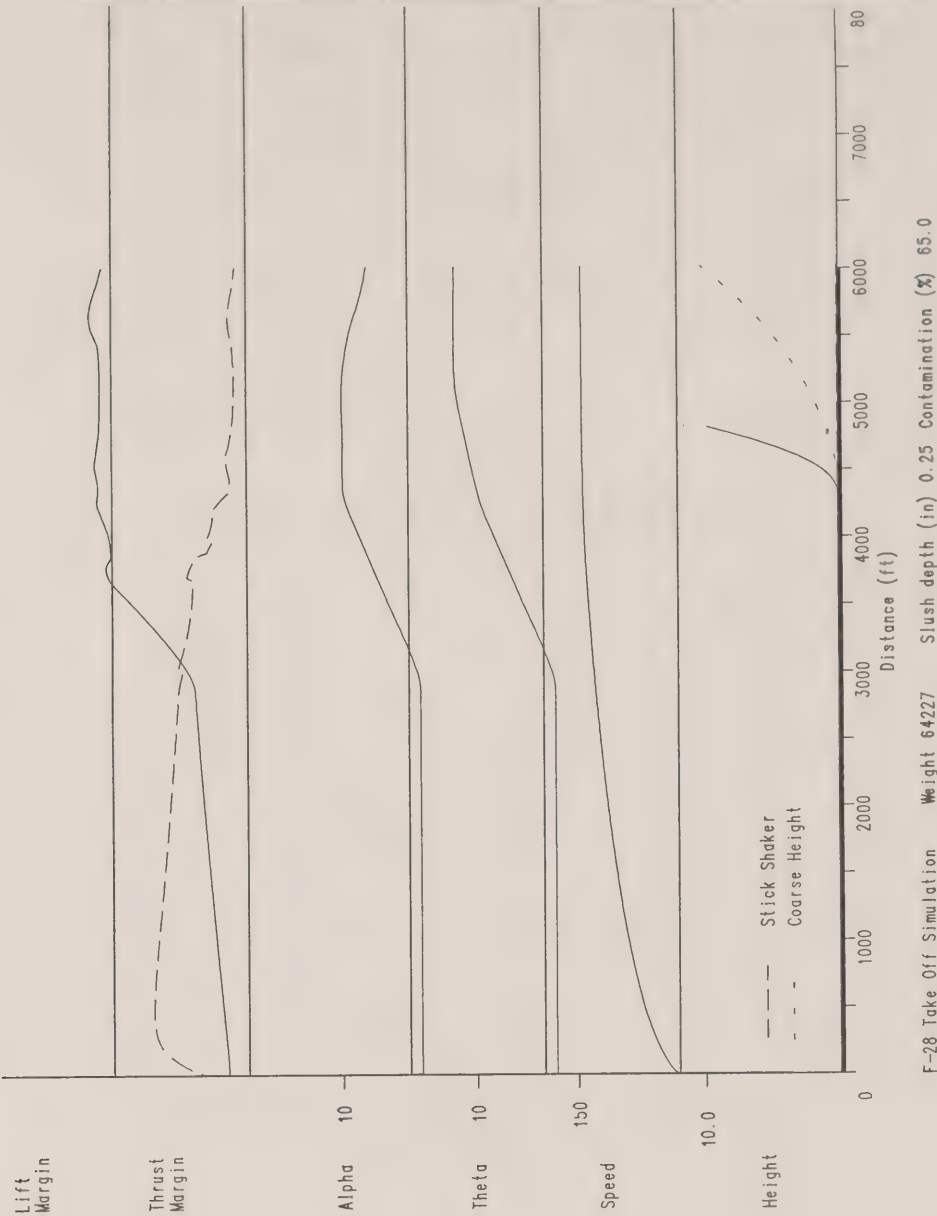
Figure 8a Successful Take-Off

F-28 Take Off Simulation   Weight 64260   Slush depth (in) 0.25   Contamination (%) 68.0
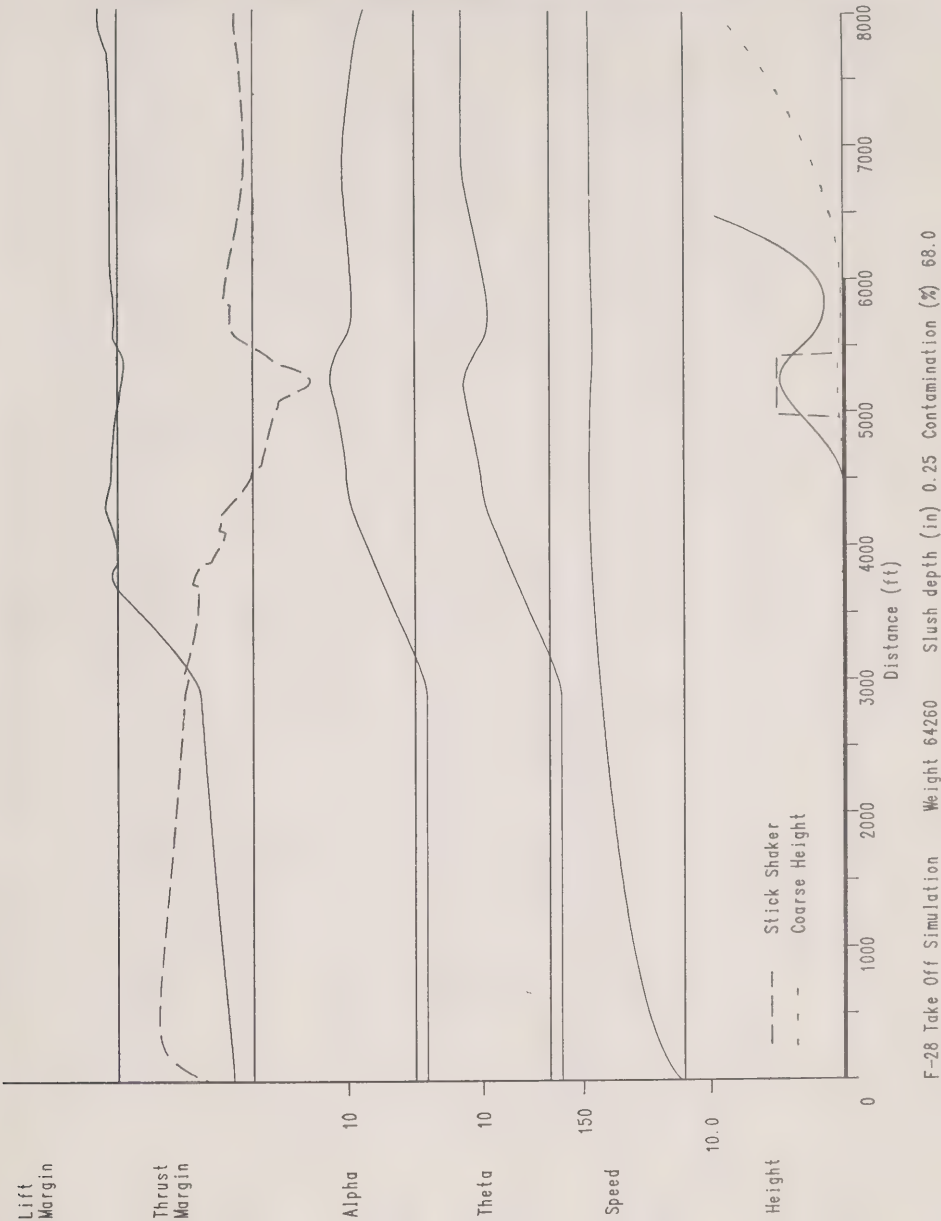
Figure 8b Marginal Take-Off

F-28 Take Off Simulation   Weight 64271   Slush depth (in) 0.25   Contamination (%) 69.0
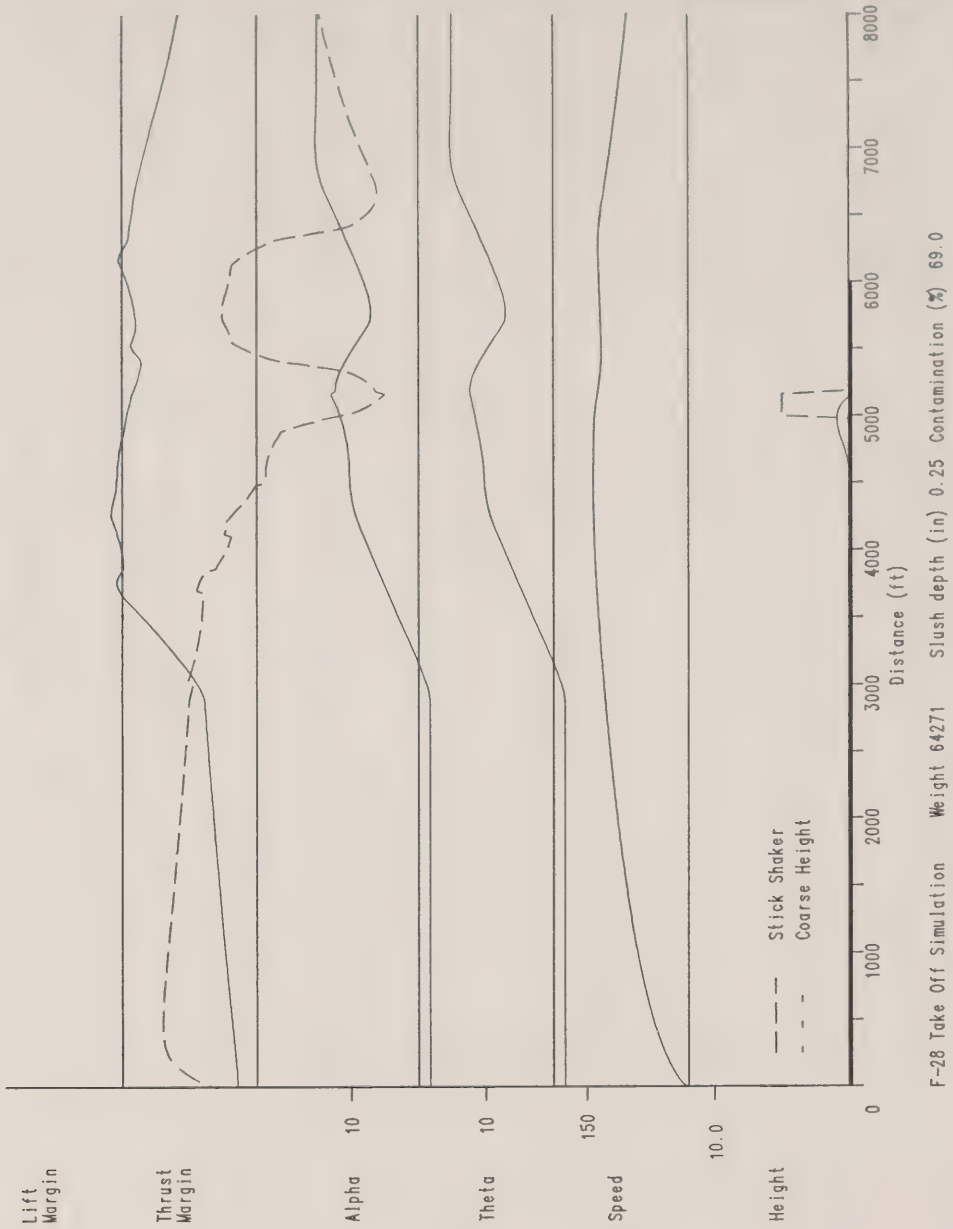
Figure 8c Unsuccessful Take-Off
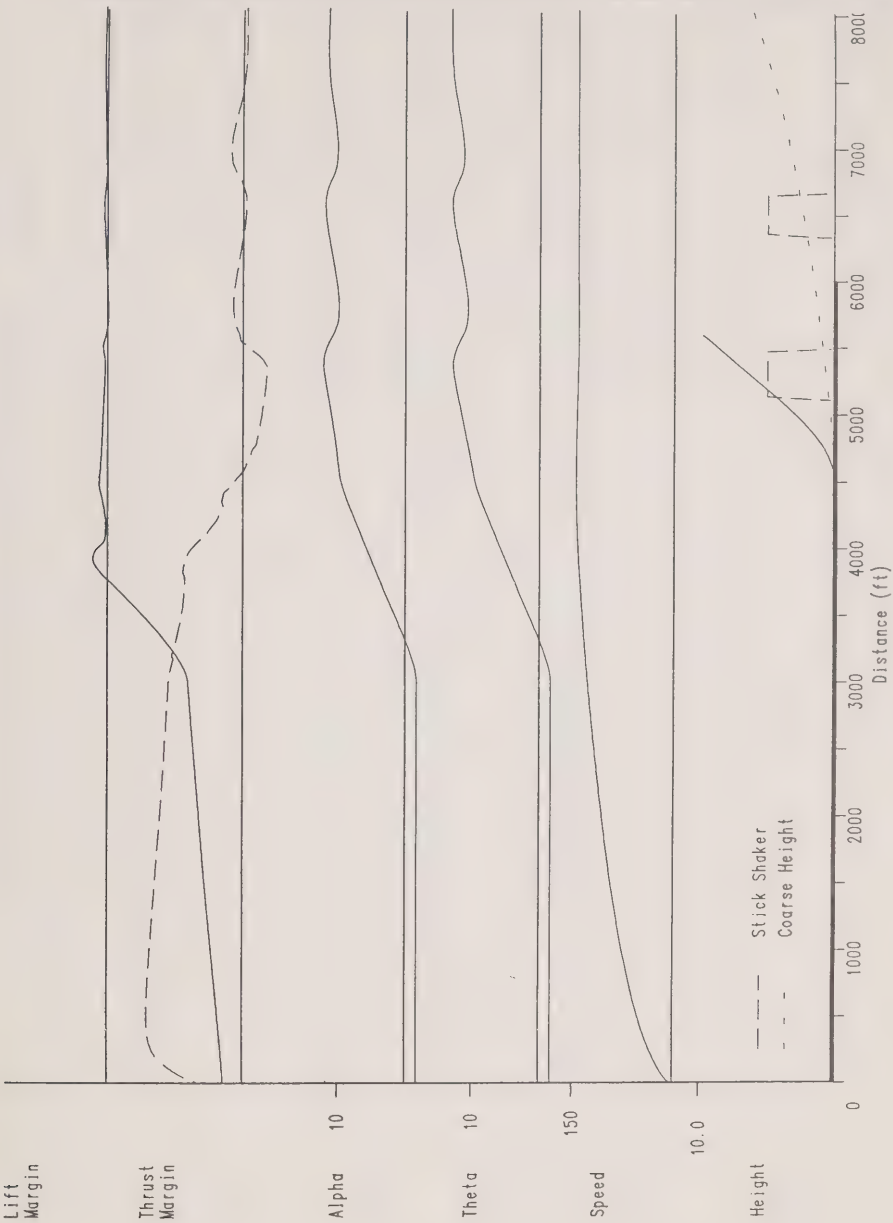
F-28 Take Off Simulation   Weight 64420   Slush depth (in) 0.10 Contamination (%) 82.3

Figure 9a Successful Take-Off at 82.3% Contamination
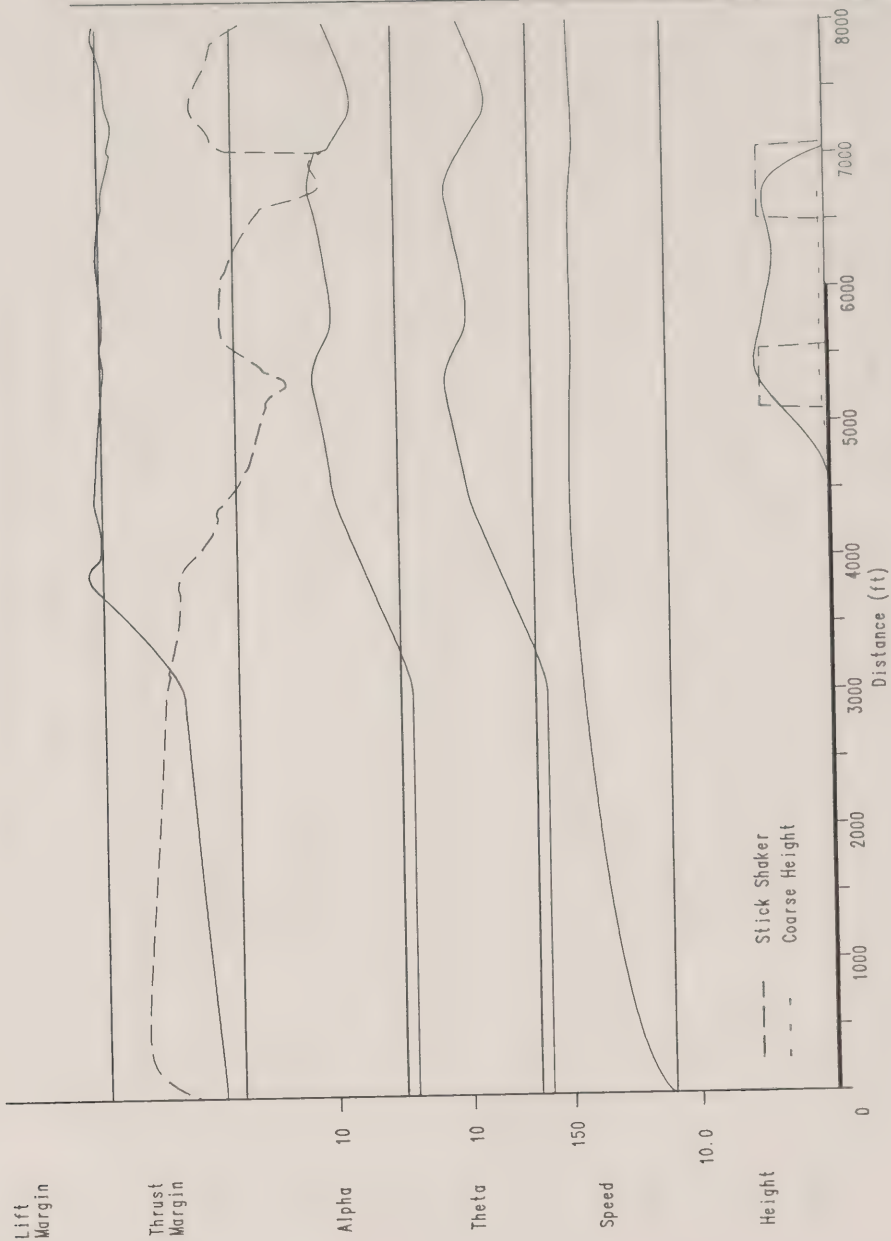
F-28 Take Off Simulation   Weight 64421   Slush depth (in) 0.10 Contamination (%) 82.4

Figure 9b Unsuccessful Take-Off at 82.4 % Contamination, Identical Technique
The Aircraft Flew over 2400 feet before Crash
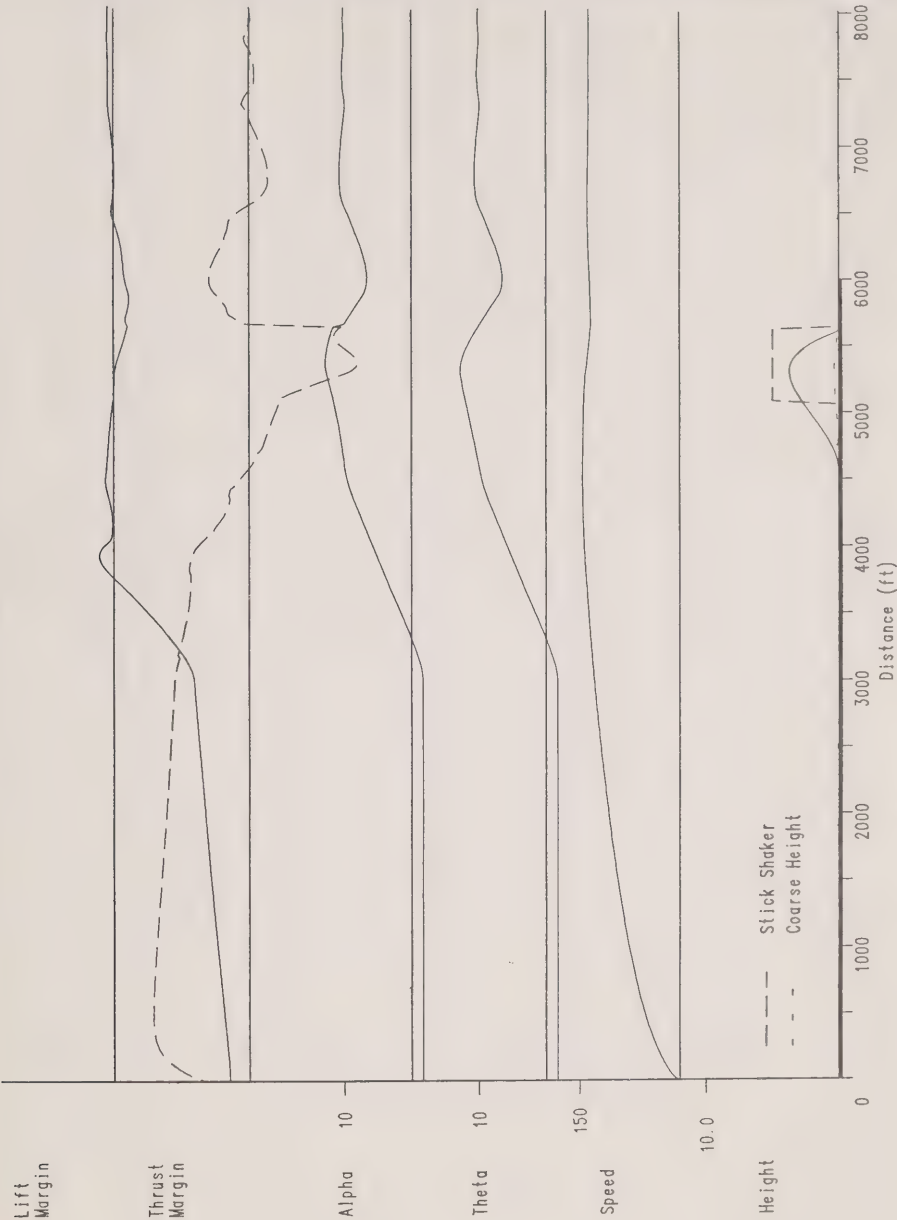
F-28 Take Off Simulation   Weight 64422   Slush depth (in) 0.10 Contamination (%) 82.5

Figure 9c At 82.5% Contamination the Take-Off Becomes a Short Hop and Runway Overrun

Figure 10a Second Lift-Off Following Hop

F-28 Take Off Simulation   Weight 64584   Slush depth (in) 0.10 Contamination (%) 97.0

Distance (ft)

Lift Margin

Thrust Margin

Alpha

Theta

Speed

Height

Stick Shaker
Coarse Height

Lift
Margin

Thrust
Margin

Alpha

Theta

Speed

Height

Stick Shaker
Coarse Height
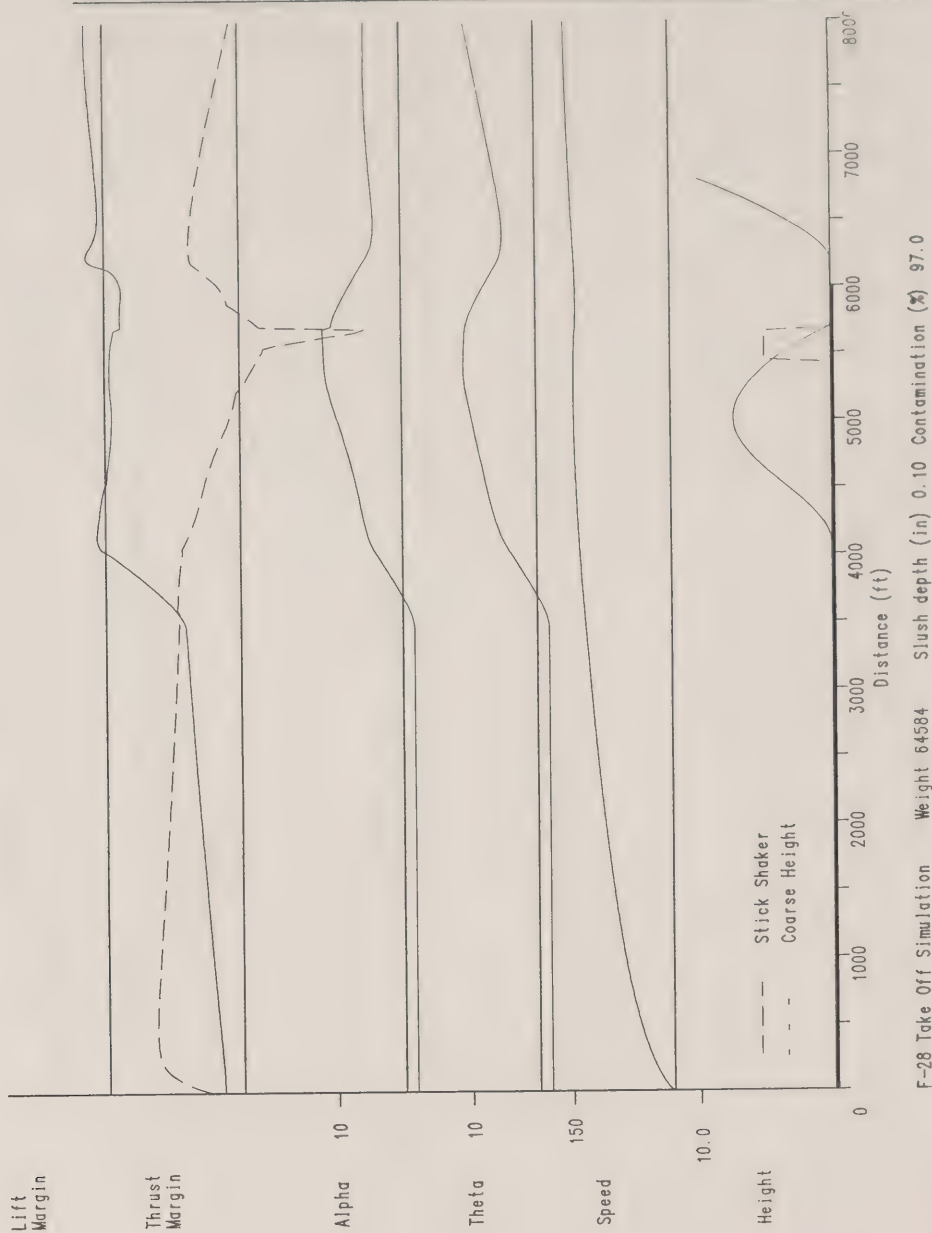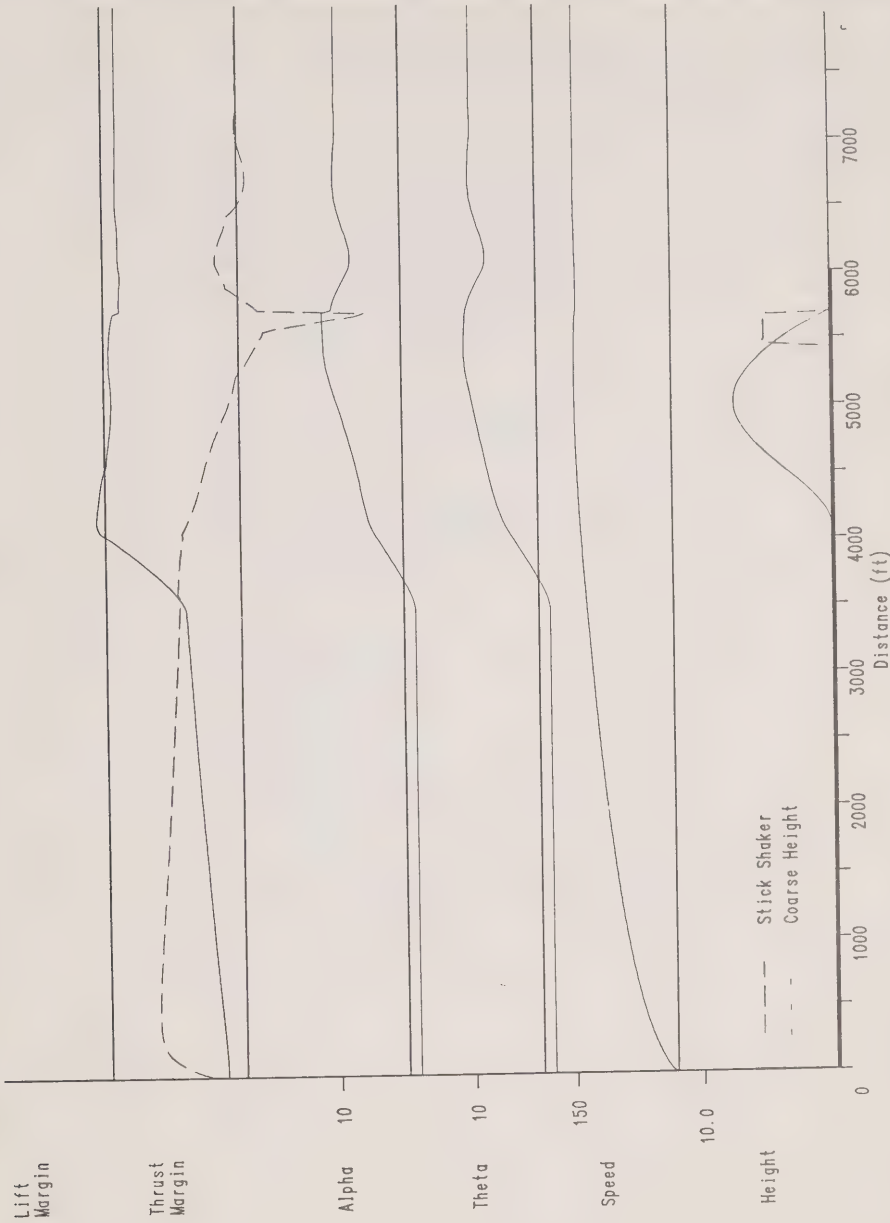
F-28 Take Off Simulation   Weight 64584   Slush depth (in) 0.10   Contamination (%) 97.0

Figure 10b Slight Change in Technique Causes Overrun

APPENDIX A TO SECTION 4
NUMERICAL MODEL STATEMENTS

SYMBOL TABLE

C_L	Coefficient of Lift, complete aircraft, flap 18
C_{Lc}	As above for fully contaminated wing
C_{Lw}	Effective C_L sample wing with contaminant
C_D	Coefficient of drag uncontaminated wing
δC_D	Increment in C_D due to wing contamination
C_{Dw}	Effective C_D for sample wing with contaminant
c	Wing contamination factor (0 to 1.0)
d	Depth of runway contaminant (in)
D	Drag (lb force)
e	The Naperian constant
h	height (feet)
K_{ge}	Ground effect interpolation parameter
L	Lift (lb force)
m	mass (lb)
q_a	dynamic pressure of atmosphere ($\frac{1}{2}\rho V^2$ psf)
q_s	dynamic pressure of slush (psf)
q	body pitch rate (deg/sec)
s	the Laplace operator
t	time
t_0	reference time
T	Engine thrust (lb force)
u	velocity along body axis X
V	total velocity (ft/sec)
V_r	Planned rotation speed
W	Weight (lb force)
δW	Weight increase due to contaminant
w	velocity along body axis Z
w	width of wheel tyre
α	angle of attack (referenced to fuselage) degrees
λ	flight path angle (degrees)
δ	static depression of tires
ϵ	error
Θ	pitch attitude (degrees)
ρ	Air density

Subscripts

a	aerodynamic
b	body
c	commanded
e	effective

n	iteration cycle
max	maximum value
main	pertaining to mainwheel
nose	pertaining to nosewheel
ref	reference value at moment of lift-off
s	slush
T	true
tot	total
0	reference value (in context)

ADJUST WEIGHT FOR CONTAMINANT

(This assumes an even coating of contaminant of specific gravity 0.85 covering the contaminated proportion of all horizontal surfaces to a depth of 0.3 in. Contaminant on the fuselage is not considered.)

$$\delta W \quad = \quad 1117c$$

$$W \quad = \quad W + \delta W$$

AERODYNAMIC COEFFICIENTS

Obtain C_L and C_D for pertaining conditions

Note: C_L and C_D are   computed by curve fitting from data provided in the Fokker simulation data base for the 18 degrees of flap Out of Ground Effect (OGE) case.   The curves for In Ground Effect are computed by calculating an α_e (alpha effective) based on the displacement of C_{Lmax} in and out of ground effect and noting that C_{L0} for the F28 is at - 5.3 degrees, α_e is a function of the ground effect interpolation parameter thus:

$$K_{ge} \quad = \quad e^{-0.11h} \qquad \text{(Approximation of Fokker parameter)}$$

$$\alpha_e \quad = \quad (\alpha + 5.3)(1 + 0.27K_{ge}) - 5.3 \quad | \quad \alpha_e \leq 19.9 \text{ (arbitrary limit)}$$

Compute C_L

   1.1 $\alpha_e < 13.0$

$$C_L \quad = \quad 0.52508 + 0.10672\alpha_e - 0.0003387\alpha_e{}^2$$

   1.2 $13.0 \leq \alpha_e < 15.0$

$$C_L \quad = \quad -235.18 + 50.024\alpha_e - 3.4957\alpha_e{}^2 + 0.08097\alpha_e{}^3$$

   1.3 $\alpha_e \geq 15.0$

$$C_L \quad = \quad 60.6598 - 9.7969\alpha_e + 0.53588\alpha_e{}^2 - 0.0097648\alpha_e{}^3$$

   1.4 $\alpha_e > 17.5$

$$C_L \quad = \quad 0.99$$

For the fully contaminated wing, a parameter C_{Lc} is computed thus:

2.1 $\alpha_e < 5.0$

$$C_{Lc} \quad = \quad C_L$$

2.2 $5.0 \leq \alpha_e < 9.0$

$$C_{Lc} \quad = \quad 3.8156 - 1.5516\alpha_e + 0.27697\alpha_e^2$$

2.3 $9.0 \leq \alpha_e < 15.0$

$$C_{Lc} \quad = \quad 5.5399 - 1.0486\alpha_e + 0.079142\alpha_e^2 - 0.0019817\alpha_e^3$$

2.4 $\alpha_e \geq 15.0$

$$CLc \quad = \quad 0.99$$

Combining these two coefficients:

$$C_{Lw} \quad = \quad C_L - c(C_L - C_{Lc})$$

To evaluated C_{Dw} the procedure to compute C_D is:

3.1 $\alpha_e \leq 13.0$

$$C_D \quad = \quad 0.0405 + 0.0235 + (0.04760 - 0.2K_{ge})C_{Lw}^2$$

3.2 $13.0 < \alpha_e \leq 14.9$

$$C_D \quad = \quad 0.46097 - 0.072393\alpha_e + 0.0042269\alpha_e^2$$

3.3 $\alpha_e > 14.9$

$$C_D \quad = \quad -3.5630 + 0.42198\alpha_e - 0.01086\alpha_e^2$$

For the contaminated wing a value for δC_D is computed by table look-up and linear interpolation and the value

$$C_{Dw} \quad = \quad C_D + c\delta C_D$$

is evaluated

FLUID DYNAMIC FORCES

$$L \quad = \quad C_{Lw}q_a S$$

$$D_a \quad = \quad C_{Dw}q_a S$$

$$D_W \quad = \quad 0.2(L - W)$$

if $h > 0.0$ $D_W = 0.0$

Compute Slush Drag

$$D_S \quad = \quad C_{DS}q_s d f(w)$$

$$f(w) \quad = \quad 2w\sqrt{[(\delta + d)/w - ((\delta + d)/w)^2]}$$

$$\delta nose \quad = \quad 2.1(W - L)/W$$

$$\delta_{main} \quad = \quad 2.4(W - L)/W$$

$$D_{Stot} \quad = \quad 4D_{Smain} + 2D_{Snose}$$

if $\Theta > \Theta_0 + 1$

$$D_{Stot} \quad = \quad 4D_{Smain}$$

Total drag

$$D_{tot} \quad = \quad D_a + D_W + D_S$$

Engine Thrust

$$T \quad = \quad 19592. - 17.75(V_T/1.69)$$

PILOT MODELLING

GROUND RUN

$$q_b \quad = \quad q_c = 0.0$$

$$\Theta_0 \quad = \quad -2.0$$

ROTATION (Commences when $V_T > V_r$)

Normal

$$\Theta_c \quad = \quad 10.0$$

$$\epsilon_\Theta \quad = \quad \Theta_c - \Theta$$

$$q_c \quad = \quad \epsilon_\Theta \mid 3.81 \geq q_c$$

Slow

$$q_c \quad = \quad \epsilon_\Theta \mid 1.9 \geq q_c$$

Overrotate

if $(\Theta \geq 10.0).(q_c = 0.0)\ t_0 = t$

rotate as normal

if $(t - t_0) \geq 1.5\ \ \Theta_c = 12.0$

POST UNSTICK

if $(h_n > 0.0).(h_{n-1} = 0.0)$

$$\alpha_{ref} \quad = \quad \alpha$$

$$V_{ref} \quad = \quad V_T$$

Constant alpha

$$\epsilon_\Theta \quad = \quad \alpha_{ref} - \alpha$$

$$q_c \quad = \quad \epsilon_\Theta$$

Normal (increment Theta)

$$\Theta_c \quad = \quad 13.0$$

$$q_c \quad = \quad \Theta_c - \Theta$$

Constant Speed

$$\epsilon_\Theta \quad = \quad V_T - V_{ref}$$

$$q_c = 0.5\epsilon_\Theta$$

RESPONSE TO STICK SHAKER

The stick shaker response assumes a 0.8 second delay in reaction to onset (assuming 0.5 second recognition time and 0.3 seconds neuromuscular delay) but only 0.4 seconds delay to termination, assuming a 0.1 second recognition delay for an alerted pilot.

if $\alpha \geq$ 11.4 ssk TRUE

if $(ssk_n = TRUE).(ssk_{n-9} = TRUE)$ q_c = -2.0

if $(ssk_{n-5} = FALSE)$ $q_c = q_c$

ALL CASES (The aircraft is not permitted to decelerate without pilot intervention)

if $(V_{i(n)} < V_{i(n-1)}) \cdot (q_c > 0.0)$ q_c = -0.5

ROTATIONAL EQUATIONS

$$\frac{q_b}{q_c} = \frac{1.5}{(s + 1.5)}$$

$$\Theta = \int q_b dt + \Theta_0$$

$$\lambda = Tan^{-1}(\hbar/\dot{x})$$

$$\alpha = \Theta - \lambda$$

KINEMATIC EQUATIONS IN BODY AXES

$$m = W/32.18$$

$$\dot{u} = (T + LSin(\alpha) - DCos(\alpha) - WSin(\Theta))/m - qw$$

$$\dot{w} = (LCos(\alpha) + Dsin(\alpha) - WCos(\Theta))/m + qu$$

$$u = \int \dot{u} dt$$

$$w = \int \dot{w} dt$$

$$V_T = \sqrt{(u^2 + w^2)}$$

$$\dot{x} = uCos(\Theta) + wSin(\Theta)$$

$$d = \int \dot{x} dt$$

$$\dot{z} = wCos(\Theta) - uSin(\Theta)$$

$$\dot{h} = -\dot{z}$$

$$h = \int \dot{h}\,dt$$

Note: in all cases

$$\int x\,dt \text{ is approximated as } \Sigma(x_{(n-1)} + x_{(n)})/2 \; \delta t$$

where $\delta t = 0.1$ secs

F-28 FLIGHT DYNAMICS
SECTION 5

FOKKER F-28 MODELLING VALIDATION

INTRODUCTION

As a part of the investigation into the accident involving Fokker F-28 C-FONF at Dryden airport, an off-line computer model was constructed to investigate the effects of aircraft and runway contaminants on the take-off performance of this aircraft. The model was based on a simulation data base provided by the manufacturer. At the same time, actual Flight Data Recorder (FDR) records were available covering some 21 take-offs of this specific aircraft during the month of February 1989 (the accident occurred in March).

Since the FDR was destroyed in the crash and there are, therefore no numerical data available concerning the aircraft's trajectory prior to impact, it was felt to be of prime importance that the model used in the investigation be validated as rigorously as possible. To this end, the existing FDR records were analysed and compared with the model outputs for the same sets of conditions. Generally there was very close agreement once one minor adjustment to the model had been made; this will be described in detail in a following section.

FLIGHT DATA RECORDER DATA

To use the existing FDR data to validate the simulation, it was first necessary to confirm the internal consistency of the FDR records and then to develop a sense of their quality or accuracy. Four of the FDR parameters were of prime interest in determining the runway performance of the aircraft, these being:

Indicated Airspeed (IAS) [kt]
Thrust [%]
Pitch Attitude (Θ)[deg]
Longitudinal Acceleration (A_x) ['g' units]

For each take-off, the aircraft weight, airport elevation, ambient temperature and prevailing wind were known.

The Relationships

The relationships among the above parameters can be quite complex if the aircraft is permitted to enjoy all of its degrees of freedom so to simplify the analytical processes only the take-off ground roll up to, but not including rotation, was used in this exercise. This effectively constrains the aircraft in the pitch, roll and yaw rotational freedoms and permits simpler linear

comparisons to be used in testing for mutual consistency. In this condition, the relationships may be expressed thus:

$$\dot{x} = (A_x - Sin(\Theta))g \tag{1}$$

$$V = \int \dot{x} \, dt \tag{2}$$

$$V_i = V\sqrt{\sigma} + V_w \tag{3}$$

$$V = (V_i - V_w)/\sqrt{\sigma} \tag{4}$$

$$\dot{x} = T_{net}/Weight \tag{5}$$

$$T_{net} = Thrust - Drag \tag{6}$$

Where $\dot{x}$ is the acceleration along the runway, 'g' the acceleration due to gravity, V_i the equivalent airspeed (closely related to, but not identical with IAS), V is true inertial speed relative to the earth, V_w the component of wind along the aircraft's longitudinal axis, positive for a headwind, σ the relative density of the atmosphere and T_{net} the net thrust. These equations offer sufficient redundancy to permit a recursive approach towards validation to be effective. It is accepted that Equation (1) is an approximation, and should read, in its full form

$$\dot{x}/g = (A_x - Sin(\Theta)) \cdot Cos(\Theta) - (A_z + Cos(\Theta)Cos(\Phi)) \cdot Sin(\Theta)$$

(where A_z is the body axis vertical acceleration and Φ the angle of bank) the restricted range of Θ while on the runway (from -2 to .5 degrees) makes the second term so small, and $Cos(\Theta)$ so close to unity that the approximation is justified in the interests of simplicity.

Interpreting FDR Records

The most difficult of the FDR parameters with which to deal was the one named Thrust, which was expressed as a percentage, but for which we had no a priori relationship to the thrust being developed by the engines. Since during normal take-offs the thrust was applied slowly (up to 10 seconds at times) it was critical not only to understand the relationship between the recorded parameter and actual thrust, but also to make the model capable of accepting the same schedules of thrust application as the aircraft for each take-off. It was also noted that the Thrust parameter reached different maximum values for each take-off.

To obtain a relationship between the Thrust parameter and actual thrust, an assumption was made that each take-off was performed using normal take-off thrust, ie, 19,500 lb force. The FDR print-outs were examined for maximum values of acceleration

(using Eqn (1) to compute $\ddot{x}$) the value of V_i at this point was estimated by the use of Equations (2) and (3) and the total aircraft drag estimated from

$$\text{Drag} = C_d qS + (\text{Weight} - \text{Lift})\mu$$

Where C_d, the coefficient of drag, was derived from the Fokker data base, (q) was the dynamic pressure at V_i, (S) the reference wing area and μ the assumed coefficient of rolling friction for the aircraft. This permitted the use of Equations (5) and (6) to estimate a value for thrust at that point. The value of V_i was also used to calculate the thrust decrement due to speed (approximately 17 lb per knot) which was applied to the model thrust output at the same point. Since the point of maximum acceleration was always met at very low speeds, such that the aerodynamic drag was always low (of the order of 150 lb, compared to normal engine thrust of 19500 lb), the sensitivity of this procedure to errors in the aerodynamic model is very weak. Differences between the values for thrust developed from the FDR data and the model could therefore be assumed to be dominated by other factors, off-nominal engine performance in the aircraft, erroneous estimations of μ, discrepancies in the recorded values of A_x or Θ or an incorrect initial assumption that full rated power was being used. In fact, agreement was generally quite close, and a minor adjustment to μ from .02 to .022[6] was sufficient to produce agreement within reasonable scatter.

Having gained some measure of confidence in the FDR recordings by this method, the same technique was now used to compute actual thrust from the start of throttle advance to maximum Thrust parameter value for a selection of take-offs chosen from the full set. The selection criterion was that a time-history of airspeed (once the IAS sensor had become fully functional) should show as little wind effect as possible, thereby reducing errors in the application of Equations (3) and (4) due to indeterminate variations in V_w. The resulting data showed a remarkably good linear correlation between thrust and the Thrust parameter, regression analysis yielding the relationship:

$$T = T_{max}(-.55464 + 1.56045 T_{irel})$$

Where T_{max} is the full rated thrust and T_{irel} is the ratio between the value of the recorded Thrust parameter and its maximum value for that specific take-off. This value for thrust (T) was used for the remaining validations.

Speed Profile Comparisons

Since the whole object of the modelling exercise was to examine the effects of contamination on both the take-off run and post lift-off behaviour of the F-28, it was felt that the final stage of validation of the model should be a full comparison of the speed

---

[6] The literature on rolling friction was very sparse, giving such generalities as "μ can vary from .02 on a runway or deck to .05 on a well kept grass field", so this adjustment is by no means excessive.

profiles between the FDR data and the model. However, prior to this a final check on the modelling was made by comparing model indicated airspeed with that of the FDR for a variety of weights and ambient wind conditions. Two short segment plots, Figures 1 and 2, show the FDR IAS, and integrations of the corrected FDR longitudinal acceleration and the model output of IAS. It can be seen from these that a very close match has been achieved, and it should be noted that the model on which this is based did not vary in any way from the data provided by the manufacturer, while model thrust was based on the standard engine model. The extremely close agreement noted provides adequate confidence to complete the final comparisons.

Figures 3,4,5 and 6 show the full airspeed correlations between FDR IAS, FDR accelerations integrated and model output. It can be seen that the airspeed trace displays considerable non-linearity below 100 kt, but that in all cases there is a terminal confluence of all three parameters. Figure 6 is of considerable interest. This take-off case was reported to have taken place in zero wind, yet the curves did not overlay but, as can be seen from Figures 6,10 and 15, both the speed, thrust and acceleration traces diverged as time increased. This indicated an error in some function of speed rather than in the thrust estimation. The assumption of a rolling take off for this case produced curves which overlay very closely as can be seen in Figures 6 (diamond symbol),11 and 15(Filled square symbol). The rolling take-off assumption is analytically attractive since it has exactly the desired effect of removing the speed dependent divergence between FDR and model, since it serves simply to displace the inertial velocity to time curve without changing its form, while it changes the slope of the V^2 to time relationship, as illustrated in Figure 16.

Acceleration and Thrust Comparisons

Figures 12 to 15 for acceleration and 7 to 11 for thrust estimates also show agreements which are probably as close as can be reasonably hoped for using data of this kind.

SUMMARY

The plots provided with this document are sufficient to indicate that very close agreement between the recorded performance of C-FONF and the math model has been achieved. This being so, the author has very high confidence that the model outputs will fairly and accurately represent the basic behaviour of the subject aircraft in its normal state.
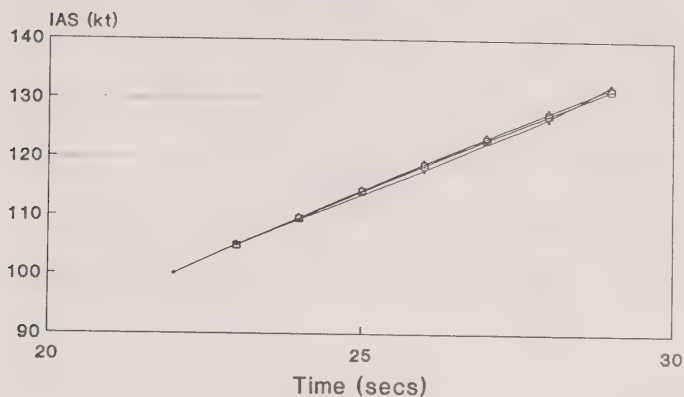
TO #12, IAS + 1/s(Ax)
zero net wind

Figure 1 Airspeed, FDR Ax and Model Correlation

TO #13 IAS + 1/s(Ax)
net wind 2 kt (Tail)
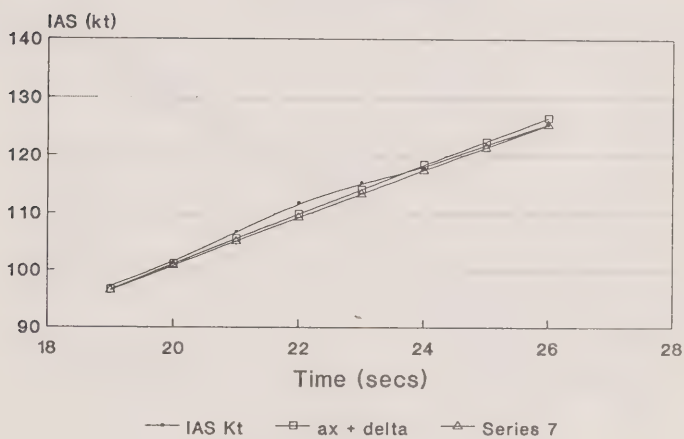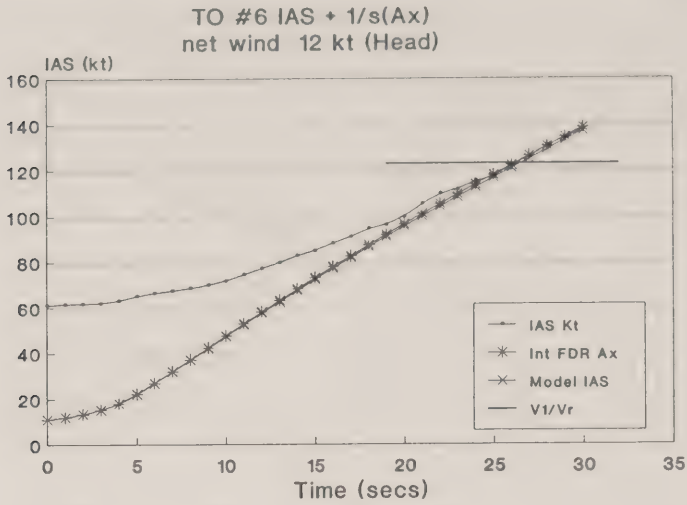

Figure 2 Airspeed, FDR Ax and Model Correlation

234 *Appendix 4*

TO #6 IAS + 1/s(Ax)
net wind 12 kt (Head)

Figure 3 FDR and Model Comparison, Speeds

TO #8, IAS + 1/s(Ax)
Net wind -3

Figure 4 FDR and Model Comparisons, Speeds

TO #12, IAS + 1/s(Ax)
zero net wind

IAS (kt)

Legend:
- IAS Kt
- Int FDR Ax
- Model IAS
- V1/Vr

Time (secs)

Figure 5 FDR and Model Comparisons, Speeds

TO #13 IAS Analysis
net wind zero

IAS (kt)

Legend:
- IAS Kt
- FDR Int Ax
- Int ax model
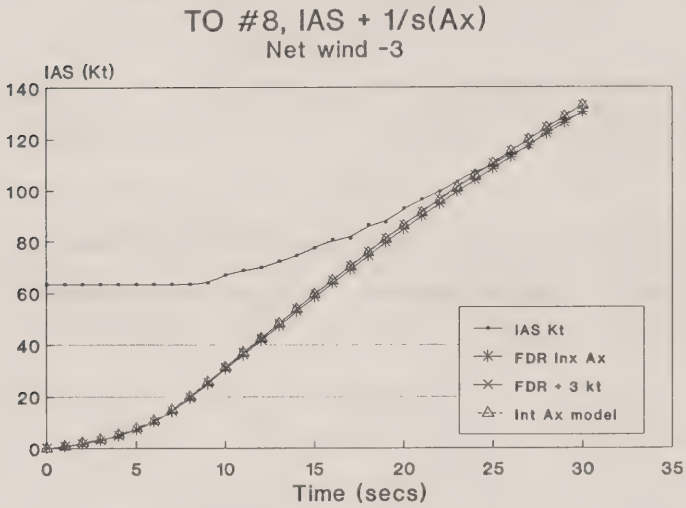- Model + 12kt
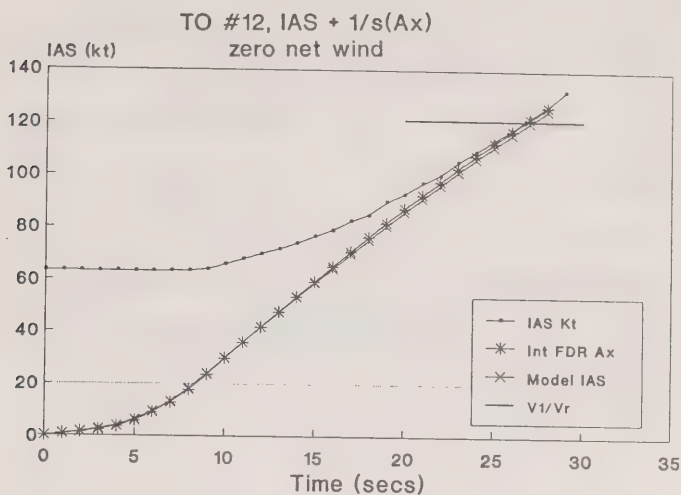- V1/Vr

Time (secs)
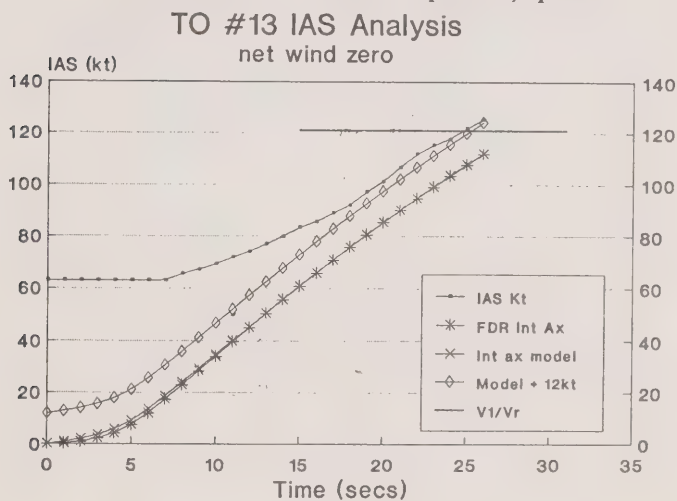
Figure 6 FDR and Model Comparisons, Speeds
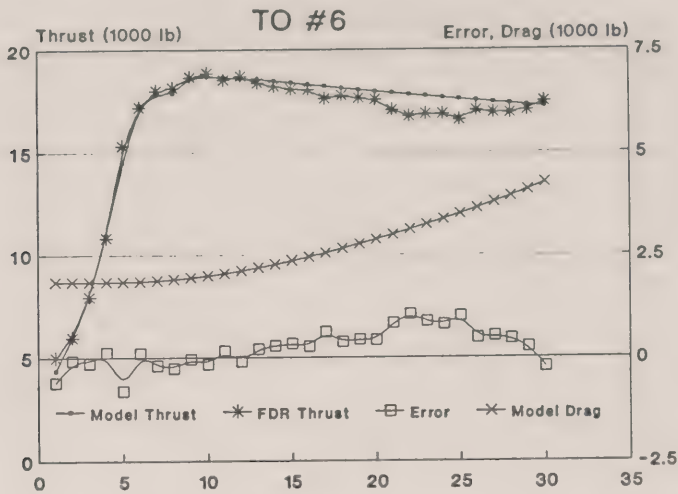
Figure 7 FDR and Model Comparisons, Thrust
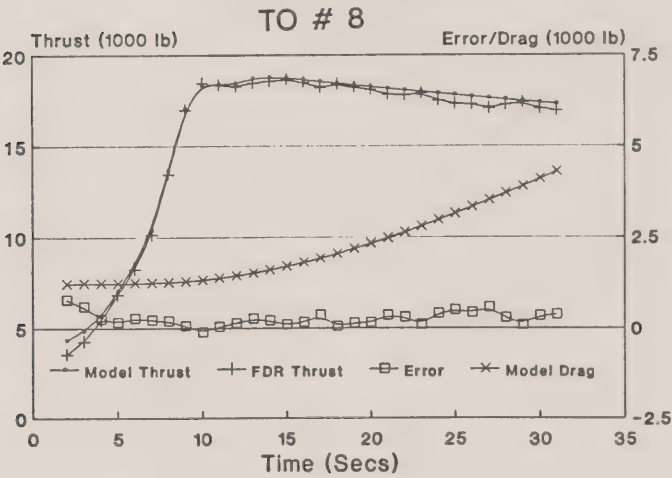
Figure 8 FDR and Model Comparisons, Thrust
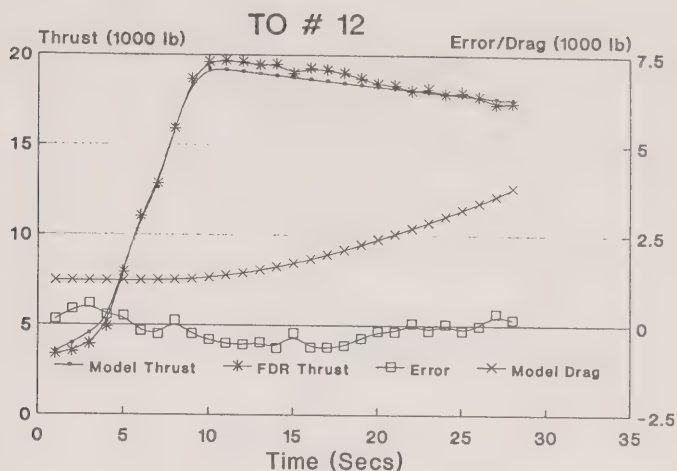
Figure 9 FDR and Model Comparisons, Thrust
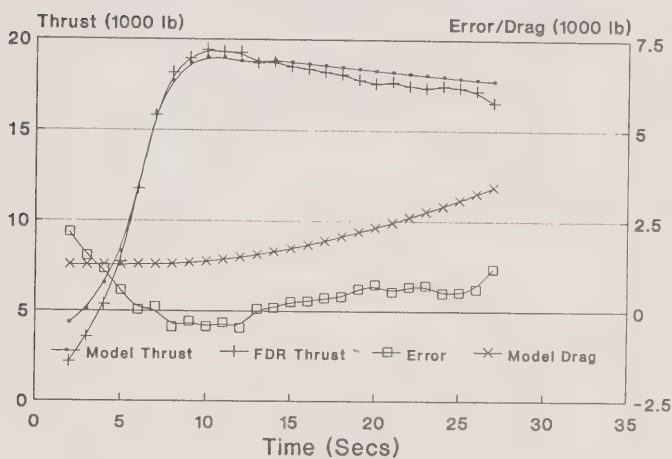
Figure 10 FDR and Model Thrusts, TO #13, Standing Start

Figure 11 FDR and Model Thrusts, TO #13, Rolling Start

Figure 12 FDR and Model Comparisons, Acceleration

Figure 13 FDR and Model Comparisons, Acceleration
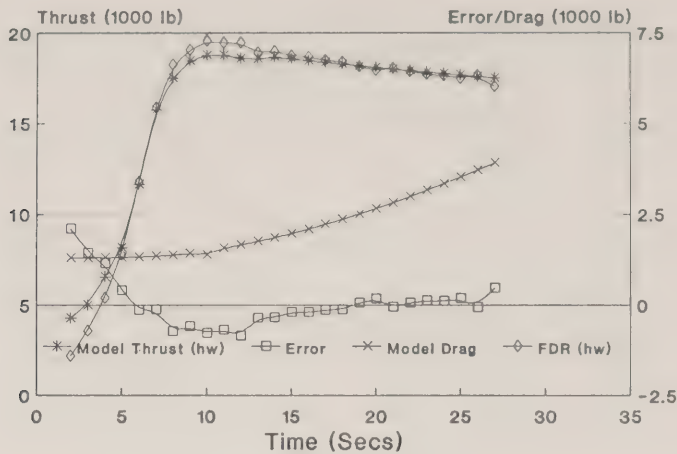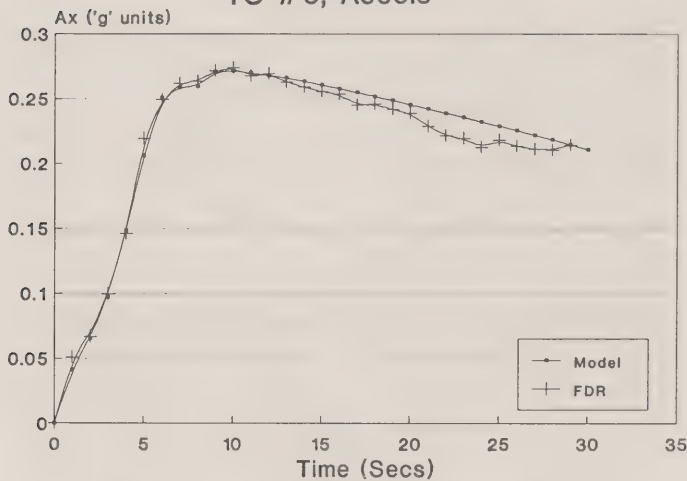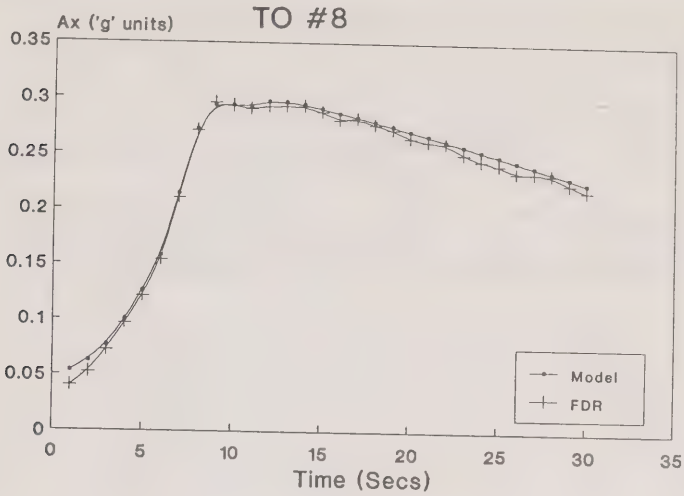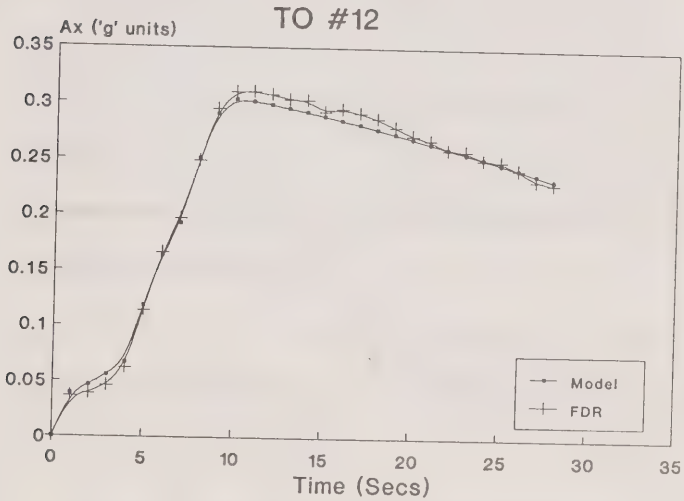

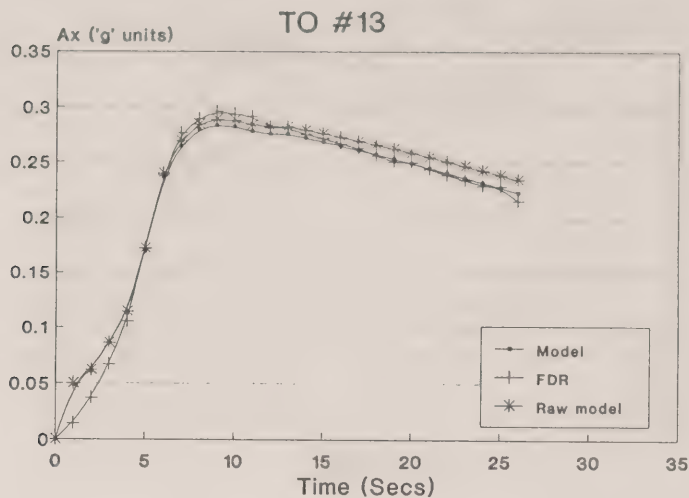**Figure 14 FDR and Model Comparisons, Acceleration**

**Figure 15 FDR and Model Comparisons, Acceleration
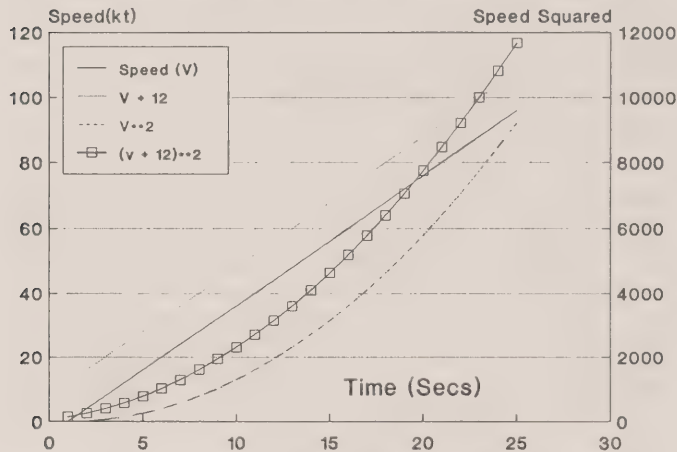Showing Raw Model and Model with Assumed Rolling Start**

Figure 16 Effects of Rolling Take-off

F-28 FLIGHT DYNAMICS
SECTION 6

DISCUSSION AND CONCLUSIONS

DYNAMIC SIMULATIONS

The dynamic simulations demonstrated that the increased takeoff roll and short airborne segment could have been the result of the conditions tested in these simulations.

An increase in takeoff run on the order of 500 to 700 feet will result from slush accumulation on the takeoff runway on the order of 0.15 inches for the F28-1000 aircraft in those conditions, combined with the additional time to rotate the aircraft to the higher required liftoff attitude.

The airborne segment is more difficult to clearly define because there is a lack of a clearly defined flight path, nor do we have any knowledge of the pilot's control strategies as he attempted to complete the take-off. However, witness reports indicate that airborne segment was limited in absolute altitude to less than one wingspan, suggesting that the aircraft never climbed out of ground effect. The horizontal trajectory is defined by tree cut and wreckage location information after the first tree strike. Based on those data, simulations with moderate wing contaminant factors resulted in airborne segments which, in general terms, matched the witnesses' descriptions of the Dryden trajectory.

It is probably of significance that in those runs during which moderate to high levels of wing contamination were represented, stick shaker activation was a constant feature. The onset of this warning will usually trigger a highly trained response on the part of the pilot, who has been taught to use this indication as a means of achieving close to the maximum lifting performance of his wing when so needed. With the wing performance degraded by roughness this device can be misleading if used in an attempt to optimise lift since at stick shaker activation the wing may already be past the maximum C_L achievable in the presence of the contaminant. It should also be noted that the use of stick shaker triggering as an indication of maximum lifting capability must be essentially a *short term* procedure, even with the clean wing this operating point is well removed from the optimum lift/drag ratio for the aircraft and is not, therefore, a suitable operating condition for sustained climb. However, a pilot generally[7] has no other indication available to him and it is only to be expected that he would respond as trained.

NUMERICAL SIMULATIONS

The numerical simulations described in detail in Section 4 supported very strongly the observations made in the Fokker simulator. This indicates that the behaviour of that simulation may be taken, with some confidence, to represent closely the behaviour to be expected of an F-28 aircraft in actual flight.

---

[7] Note, however, that unlike the majority of current transport aircraft, the Fokker F-28 is equipped with an angle of attack indicator

Additionally, the off-line modelling complemented the dynamic simulations in that it permitted the investigators to examine a wide range of conditions in a very clinical manner and in a relatively short time. In particular it permitted the definition of two critical boundary conditions for contaminated take-off attempts, either of which would result in a catastrophic occurrence. Specifically, the region between the boundaries represents an entire range of slush and wing contamination conditions which could give rise to a trajectory of the kind described by witnesses to the Dryden accident.

A general observation based on the results of the numerical simulations is that the higher the rotation speed and the slower the rotation rate, the greater was the probability that the take off attempt would be successful. This is exactly what would be expected from an engineering evaluation of the effects of contamination on the aircraft's characteristics. Advice given in the F-28 handbook supports this observation.

GENERAL DISCUSSION

This statement immediately above raises two issues pertinent to this accident and worthy of comment here inasmuch as they bear on the act of attempting a take-off under the conditions pertaining at the time. It is not in the least likely that the average airline pilot would have sufficient theoretical knowledge to be able to assess in detail the effect on his aircraft's performance of these forms of contamination. Indeed, it is not possible to make such an assessment on the spur of the moment while already in the cockpit. The second issue concerns the pilot's awareness of his aircraft's external state under these kinds of conditions. Again, in some ways this is a function of the size and shape of aircraft of this class. By and large direct observation of the flying surfaces by the crew is either very difficult or impossible, once strapped in for take-off. In the F-28 approximately 50% of the wing can be viewed obliquely from the cockpit window with special effort, while by opening the window and leaning out the entire wing can be viewed. The automatic ice detection systems that presently exist are designed to detect and warn against the accretion of ice in flight rather than that due to the exposure of the aircraft to precipitation or frost formation while on the ground: the effects of the two types of airframe icing are quite different.

OTHER FACTORS

Wing Leading Edge Paint Deterioration

There have been reports that the wing leading edge of the F28 involved in this accident had a significant degree of paint cracking and deterioration. The paint thickness on the aircraft leading edge was measured at 0.016 inches, consisting of 3 or 4 layers of paint. This issue was brought up with Fokker's aerodynamics group who indicated that while the cracked paint certainly did not enhance performance, its effect on the maximum lift coefficient and stalling angle of attack was not judged to be significant.

There is a question of whether the deteriorated leading edge paint condition could have contributed to the degree that any contaminant would adhere to the wing. To date, there is no clear answer to that.

CONCLUSIONS

It is difficult when writing a report of this nature to be adequately mindful of the semantics or etymology of the words used. This is often the case when persons working in a specific discipline assign to a common word a precise or special meaning more limiting than that which applies in the vernacular. We have several times used the word 'cause' and phrases such as 'the cause of the accident'. It must be remembered that we use that word in a very technical sense to indicate a sequence of events which would or could give rise to a flightpath similar to the one reported at Dryden. The 'cause' to which we refer means a set of physical or engineering conditions which have a direct and predictable result (that is, we are describing a causal relationship). These are not of themselves the cause of the accident in the general sense, simply the result of a pilot attempting to take-off in a significantly contaminated aircraft.

It must be remembered that the conclusions of this subgroup report present possible causes of the flight path for the Dryden accident. It is critically important to remember that the assumptions listed in the beginning of this report must be clearly borne in mind in the final analysis of this accident. This report treats only the aerodynamics and aircraft handling aspects of this accident and assumes that there were NO other factors which could have been the related to the accident. There is no doubt that major failures of aircraft systems or other factors not mentioned in this report and not considered in this simulation could also have resulted in the accident flight profile, alone or in conjunction with the known wing contaminant.

With these caveats in mind, we are prepared to state:

1. The witness reported flight paths and "Dryden Scenario" which was based on those reports is physically possible from an engineering viewpoint.

2. The aerodynamic performance of the F28 in the Dryden accident was definitely degraded by the wing contamination which was reported by the witnesses on board the aircraft. This conclusion is based on knowledge of the sensitivity of aircraft lifting surfaces to contaminant and our analysis of the degree of contamination of the wings described by the witnesses. The work done by Fokker in their wind tunnel, general knowledge of aircraft aerodynamics and analyses of other accidents with F28's and similar aircraft clearly support the conclusion that the contaminants on the wings degraded the lifting capability and increased the drag on the accident aircraft.

3. The increased ground distance to the reported liftoff point could have been due to the following factors, individually or in combination:

   a) Small slush accumulations on the runway

   b) Selection of higher than normal rotation speed

4. An additional contributing factor to the increased ground distance to liftoff was the higher speed and/or pitch attitude required for liftoff as a result of wing

contaminant. This would have   increased the takeoff run to the liftoff point, irrespective of any other factor. This was due to the additional time required to reach the required speed and/or to rotate the aircraft to the higher liftoff attitude. At the liftoff speed for the F28 in the Dryden case on the order of 130 knots, each additional second during rotation increased the ground run by approximately 200 feet.

5. The deteriorated condition of the paint on the wing leading edge probably did not affect the aerodynamic characteristics of the aircraft directly. However, the effect of the deteriorated paint on the adherence characteristics of contaminants at the leading edge is unknown, but could potentially have been a minor factor in the amount of contaminant that remained on the wing.

6. Simulation and analytical work done by this group has defined a range of conditions in terms of wing and runway contaminant levels which, alone, could have resulted in the accident profile.

7. Without FDR data, CVR data, the pilots themselves, and a mathematical description of the wing and runway contaminant levels, it can NOT be conclusively stated that wing or runway contamination alone caused the aircraft to crash.

REFERENCES

1. Wolters, S.R., <u>Watch it in Winter</u>, Operation and Maintenance of Fokker Aircraft, NO 3, Feb 1984

2. Jones, R., and Williams, D.H., <u>The Effect of Surface Roughness on the Characteriestics of the Aerofoils NACA 0012 and RAF 34.</u> NPL(UK) Reports and Memoranda No 1708, Feb 1936

3. Jane's All the World's Aircraft, 1975-76, p. 144

4. Schlichting, <u>Boundary Layer Theory</u> Pergamon Press, 1955

5. Schuringa, Tj., <u>Aerodynamics of the Wing Stall of the Fokker F-28.</u> AGARD CP-102, #20

6. Torenbeek, E., <u>Synthesis of Subsonic Airplane Design</u> Delft University Press

7. Warrink B.J., <u>Simulation Report vs-28-25</u>, Fokker Aircraft, June 1989, Order 22192

8. Anon   F28 Simulation Data Base, Master File

9. Walter B. Horne et al. <u>Studies of the Retarding Force Developed on an Aircraft Tire Rolling in Slush or Water.</u> NASA TN D-552, September 1960

10. Slatter N.V. and Maltby R.L.,<u>The Measurement of the Effects of Slush and Water on Aircraft During Take-Off.</u> RAE R&M 3604, 1969.

11. loq. cit.

12. Cebeci, T., <u>Effects of Environmentally Imposed Roughness on Airfoil [sic] Performance</u>, Paper delivered at the Von Karman Institute for Fluid Dynamics, February 1987.

13. Zierten, T.A. and Hill E.G.,<u>Effects of Wing Simulated Ground Frost on Airplane Performance.</u> von Karman Institute Lecture Series on "Influence of Environmental Factors on Aircraft Perfromance", 1987.

14. loq. cit.

15. Abbott Ira H. and Von Doenhoff Albert E. <u>The Theory of Wing Sections</u> Dover Publications Inc. New York 1959, Ch 7, 7.5c pp157 et seq

16. Hoerner Dr-Ing S.F. Fluid-Dynamic Drag Published by the Author, 1965 Library of Congress No 64-19666 Ch 5.1

17. loq. cit.

Appendix 5

Wind Tunnel Investigation of a Wing-Propeller Model Performance Degradation due to Distributed Upper-Surface Roughness and Leading Edge Shape Modification

R.H. Wickens
V.D. Nguyen

WIND TUNNEL INVESTIGATION OF A WING-PROPELLER MODEL PERFORMANCE DEGRADATION DUE TO DISTRIBUTED UPPER-SURFACE ROUGHNESS AND LEADING EDGE SHAPE MODIFICATION

R.H. Wickens and V.D. Nguyen
Applied Aerodynamics Laboratory
Institute for Aerospace Research
National Research Council Canada
Ottawa, Canada   K1A 0R6

April 1991

SUMMARY

A wind tunnel investigation has assessed the effects of distributed upper surface roughness, and leading edge ice formation on a powered wing propeller model.

In the unpowered state, it was found that roughness reduces the lift slope, and maximum lift by 30 to 50 percent, depending upon particle size and Reynolds number. The leading edge region is especially sensitive to these disturbances, however removal of the roughness over a small portion of the nose restored the wing to close to its original performance.

The application of power to the wing, with an increase of slipstream dynamic pressure increases the lift slope and maximum lift; however this benefit is lost if the wing is roughened. Subtraction of the propeller reactions indicated that the slipstream interaction accounted for half the lift increase, and also resulted in reduced drag for the clean surface. This drag reduction was removed when the wing was roughened, indicating that the degradation of wing performance due to roughening is relatively greater when a slipstream is present, compared to the unpowered wing.

Leading edge ice accretion causes similar large losses in lift and increases of form drag although a comparison of the two types of contamination showed that leading edge ice produces a smaller reduction of lift slope prior to flow separation. In both types of contamination, Reynolds number is important, and emphasizes the necessity of testing under near full-scale conditions.

List of Symbols

C_L lift coefficient $\dfrac{L}{\frac{1}{2}\rho V^2 S_w}$

C_D Drag coefficient $\dfrac{D}{\frac{1}{2}\rho V^2 S_w}$

C_m moment coefficient $\dfrac{M}{\frac{1}{2}\rho V^2 S_w c}$

c wing chord

S_w wing area

C_{Tp} propeller thrust coefficient $\dfrac{T_p}{\rho N^2 D^4}$

C_{Np} propeller normal force coefficient $\dfrac{N_p}{\rho N^2 D^4}$

C_{mp} propeller pitching moment coefficient $\dfrac{M_p}{\rho N^2 D^5}$

C_c wing chord force coefficient $\dfrac{C_c}{\frac{1}{2}\rho V^2 S_w}$

C_{Do} parasite drag coefficient (unpowered)

C_{L_s}, C_{D_s}, C_{m_s} wing coefficients with the propeller reactions removed

C_s leading edge suction coefficient

D propeller diameter

N propeller rotation speed (RPS)

2

J   propeller advance ratio $\dfrac{V}{ND}$

k   roughness particle size

INTRODUCTION

Recent flying accidents resulting from adverse weather conditions in the form of freezing rain or snow, have focussed attention on the degradation of aerodynamic surfaces. One of the most recent accidents, involving a Fokker F-28, mk 1000 jet aircraft, and the subject of a Commission of Inquiry in Canada, dealt specifically with the degradation of such surfaces due to ice and snow contaminants on the wings. The information contained in this paper stems in part from the investigation conducted for the Commission of Inquiry into the Air Ontario Crash at Dryden, Ontario, March 10, 1989. (Ref. 10) Investigations of the effects of uniform roughness on airfoils shows clearly that stalling is premature, loss of maximum lift can be as high as 50%, (depending on Reynolds Number) and form drag reaches very high levels at angles of attack below normal clean wing stall.

The effect of upper surface roughness on complete aircraft configurations is less well known; however there is a long history of aircraft accidents related to flight in icing conditions, and several recent accidents, including the Air Ontario F-28 accident, involving swept-wing jet aircraft have highlighted the problem. In these situations it was observed that early flow separation and stalling was a characteristic result of ice and snow contaminants on the wing. Flow breakdown was accompanied not only by a loss of lift and an increase of drag, but also wing-dropping as a result of outer panel flow separation and wing tip stall prior to inboard wing stall. Experimental data on simulated upper surface contamination on a swept-wing model of a typical jet-commuter aircraft have confirmed what was suspected from flight experience, and have also demonstrated that large changes of trim will occur on the full-scale aircraft.

Figure (1a) from ref. (1) shows, for various two-dimensional airfoil configurations, losses in maximum lift and reductions the angle of attack for maximum lift that result from simulated hoar frost contamination. Large increases of drag also occur, and are attributed to form drag after separation and stall. Early wind tunnel tests on the effects of upper surface roughness on maximum lift of airfoils is also reported in reference (2), for conventional airfoils. This data shows that the loss of maximum lift is critically dependent on Reynolds Number, and also roughness particle size. For example at Reynolds Number greater than 10 million (typical for takeoff) the loss in maximum lift approaches 50% of the clean airfoil value. In comparison, at the

3

Reynolds number values typical of low speed wind tunnel testing the loss of maximum lift is much lower, thus highlighting the dangers of assessing wing contamination effects at other than full-scale conditions. There is little or no corresponding data for modern, supercritical airfoil shapes.

Wing drag also increases as a result of surface roughness. This is due to an increase in skin friction in unseparated flow, but mainly from increases in form drag after premature separation has occurred. If the roughness elements protrude above the laminar sublayer of the turbulent boundary layer in attached flow, the result is an increase of skin friction and the production of more turbulence. Increasing the Reynolds Number aggravates this effect and increases the probability of separation particularly around the nose, since the sub-layer will be thinner. This would presumably explain the higher losses in maximum lift incurred at high Reynolds number.

If the roughness height is large in comparison to the laminar sub-layer (as would be the case for freezing rain or ice accretion) then the frontal drag of these elements determines the average tangential force, and their shape, orientation and distribution become important, and increased turbulence and dissipation in the thickened boundary layer will lead to premature flow separation and stall.

Propeller-driven aircraft, where the slipstream passes over the wing surface, are thought to be less sensitive to the effects of upper surface contamination compared to the typical swept-wing configuration. This is due in part to the effects of sweep, that reduce the wing lift-slope, compared to a straight wing; and the effects of slipstream interaction, that augment span loading locally, increase wing lift slope, and also delay flow separation at high angles of attack. Thus the rotation angle on takeoff of a straight wing propeller-driven aircraft is likely to be less than that for an equivalent swept wing aircraft, with no slipstream interaction, and the likelihood of a premature stall may not arise.

Notwithstanding this apparent beneficial comparison, the propeller-driven aircraft may still experience significant losses of lift and large increases of drag if premature flow separation occurs when the wing upper surface is contaminated. Figure 1b from Ref. (1) for the Fokker F-27 turboprop transport wind tunnel model indicates however, that smaller losses in maximum lift may be expected from a contaminated wing, compared with the airfoil test results of Figure (1a). The corresponding reduction in critical angle of attack is also small and in some cases positive, and was attributed to a significant change in the wing-slipstream stall pattern. The extent to which the slipstream may remain attached to the wing surface is unknown but its influence may affect the overall stall pattern even when roughened by ice.

4

In view of the unknown nature of the complex interactions of wing boundary layer, propeller slipstream and distributed roughness, and the lack of experimental data, it was decided to use the half-wing propeller model of reference (3) to obtain some preliminary data on the effects of upper surface roughness in a slipstream and also the effects of typical in-flight ice accretion shapes on the leading edge. The utility of the data to aircraft design or performance estimation will be limited; the model configuration is not typical of current propeller transport configurations, and the test Reynolds Number was low (Re = 1.3 million).

MODEL

The general arrangement of the rectangular, unswept half-wing model is shown in figure 2. The wing, having a NACA 4415 airfoil section, was untwisted and was equipped with a 30 percent chord plain flap extending along the semi-span. The aspect ratio was 4.85. A nacelle containing a 20 hp water-cooled induction motor was underslung on the wing approximately one chord length above the floor. The four-bladed propeller was located 70% chord in front on the leading edge and was equipped with an adjustable pitch-setting mechanism. The two foot diameter propeller was the same model used in the investigations reported in references (3) and (4). In these reports full aerodynamic characteristics of the isolated propeller and also the interference effects of this wing model are reported. The relevant geometry of the propeller is listed as follows:

<u>Propeller</u>

Diameter	2.0 ft.
No. of blades	4
Solidity	0.127
Blade section at 0.75R	65 Series (design Cl = 0.7)

The complete model installation Figure, (2a), (2b), was mounted on the wind tunnel balance at the 30% chord location. The propeller motor was supported in a slender nacelle but did not have a separate thrust or normal force balance in this experiment. The wind tunnel balance thus measured the combined effects of wing and propeller reactions.

EXPERIMENTAL PROCEDURE

The wing was pitched through an angle of attack range from 6 to 26 degrees. A complete stall and flow breakdown was not achieved with this model due probably to the effects of the low aspect ratio, Reynolds number and the half-model configuration. Maximum lift was achieved however, and this was used as a basis of comparison for the effects of roughness. Model lift, drag and pitching moment were measured on the wind tunnel balance. Pitching moment was taken about the 30% chord location. The

5

measured forces include the propeller reaction comprised of thrust, normal force and pitching moment. The test Reynolds Number was 1.3 million (2.3 million for the unpowered wing only).

Propeller static thrust was measured on the wind tunnel balance under wind-off conditions. At the desired test conditions thrust was varied by adjusting the blade pitch settings to a value that corresponded approximately to the take off thrust coefficient of a typical turbo-prop aircraft. Under wind-on conditions at a dynamic pressure of 25 psf, and a propeller rotational speed of 3000 rpm, this thrust coefficient C_{Tp} was estimated from the data of ref. (5) to have a value of 0.115. Propeller thrust and normal force change with incidence, and the variation of these quantities, used in other section of this report, were also determined from the data of Ref. (5).

SIMULATED ROUGHNESS

Roughness, in the form of a uniform distribution of carborundum grit was applied over various portions of the chord. Three grades of standard grit were used: 150(.0041"), 80(.0083"), 46(.0165"). These correspond approximately to average roughness heights of .03", .06", and .11" respectively on a full-scale wing of 10 ft. chord. The roughness height/chord ratios for this test were 0.000227, .000461 and .000916 respectively. In addition a heavy grade (50 grit) of commercial sandpaper was applied to the wing surface. The roughness height and concentration of this application was considered to be significantly greater than the standard grit particles applied manually to the wing surface.

The roughness was applied initially to the upper surface from the leading edge stagnation region to the flap hinge line. Since only the forward portion of the chord was found to be sensitive however, most of the investigation was performed with only the first 25-30% of the chord roughened and the results presented in this report are for 30% coverage. The density of application was not varied or determined precisely.

In addition to distributed roughness application, shapes representing rime and glaze ice accretions were applied to the wing leading edge. The shapes were similar to those of ref. (6) and are shown in Figure (2c).

PRESENTATION OF RESULTS

Unpowered Wing

The unpowered wing data presents the effects of various grit sizes (46, 80, 150) deposited on the upper surface, and also a heavy grade of sandpaper attached to the upper surface. The amount of coverage along the chord corresponded to about 30%. Tests were also done at a higher Reynolds number (2.3 million), for the unpowered wing only.

6

Figure 3 shows the behaviour of Cl, Cd, and Cm for the unpowered wing in the clean and contaminated states for standard grit sizes at the test Reynolds number of 1.3 million, and for heavy sandpaper at Re = 2.3 million. The main effect of wing contamination is a reduction of lift slope and maximum lift by amounts that range between 20 - 25% for a Reynolds number of 1.3×10^6, and larger losses for the higher Reynolds number. The angle of attack for maximum lift (clean) was 20 degrees; this was reduced to about 15 degrees with contamination on the upper surface.

Drag is also increased at angles of attack below stall, and large increases of form drag occur when the flow separates. In general these losses, particularly at maximum lift, increase with particle size, with the highest loss occurring where sandpaper was applied to the wing (Fig. 3a). All reductions of lift increase with increasing Reynolds number as Reference (2) points out, and this is also the case in this test. The effect of roughness on pitching moment was small at angles of attack below stall; there appears to be a slight nose-up shift of the Cm versus α curve, and its magnitude increases slightly with grit size. The application of rough sandpaper at the high reynolds number increases this nose-up shift slightly.

The most significant parameters appear to be roughness size and Reynolds number, however it was observed that when a small portion (15%) of the leading edge was cleaned off, wing lift and drag was restored to close to its clean performance, however moment was not fully restored.

Powered Wing

With the blades installed and set to the angle for take-off thrust, the propeller was operated wind-on at an advance ratio of 1.4. This was much higher than a typical takeoff advance ratio, however it was the only way a high thrust coefficient could be achieved due to current and temperature limitations of the motor. As mentioned before propeller forces were not measured separately, however both thrust and normal force were inferred from the isolated propeller data of references (3) and (5) for further analysis of these results.

Figure (4) shows the effects of propeller thrust on lift, drag and pitching moment on the unpowered clean wing at a Reynolds number of 1.3 million. A higher Reynolds number test condition was not possible in the powered tests due to limitations of the motor. The application of power with the resulting slipstream interaction results in an increase of both the lift slope and the maximum lift by about 25%, and stalling angle is increased by about 4 degrees. The drag polar is shifted by an amount that corresponds to the thrust force plus a leading edge thrust on the wing due to increased suction. The drag equivalent of the estimated propeller thrust has a value of about 0.085, which, when subtracted from the total wing force at zero lift, apparently produces

7

a negative drag or thrust on the wing. This effect, known as the "Squire Effect", has been alluded to before (Ref. 7), and is attributed to the effects of flow rotation in the slipstream.

The pitching moment shown in figure (4c) exhibits an increased nose-up tendency due to the effects of the propeller and slipstream flow. The slope of the pitching moment curve vs α is increased with the application of power and beyond maximum lift there is a large nose-down shift of the pitching moment. The large change in moment is attributed mainly to the propeller normal force acting about the wing centre of rotation (Figure 2).

Effects of Roughness - Powered Wing

With roughness applied to the wing upper surface there appears to be a loss of lift slope and maximum lift of about 25 to 35% depending upon roughness element size. (Figure (5)). In effect, the benefits of powered lift, resulting from slipstream interaction, is lost. Drag also increases as the flow separates prematurely, and there also is an increase in the parasite drag at zero lift due to roughness, and increased dynamic pressure in the slipstream. The effect of roughness on wing pitching moment is small at angles of attack below stall, ($\alpha < 10°$) but the moment becomes more nose down as roughness size increases.

The application of the heavy sandpaper roughness further deteriorated the wing performance under power at the Reynolds number of 1.3 million. Maximum lift decreased slightly, as did the lift slope; although the stall was not sharply defined. Drag also increased near zero lift but the pitching moment did not change significantly, although the tendency continued to be nose-down.

A comparison was made between the powered and unpowered wing drag polars to show the relative effects of roughness with and without power (Figure 6). It is clear from these graphs that roughness, especially when it reaches the heavy proportions of sandpaper coverage, has a much more adverse effect on drag of the powered wing than for the unpowered wing in uniform flow. The lift curves exhibit about the same degree of degradation of performance between powered and unpowered configurations. The pitching moment change appears to be smaller when the wing is powered and is accompanied by an increase in slope (Cm vs alpha) and a small displacement in the nose up direction.

In order to simulate the scrubbing action of the slipstream, a portion of the roughness was removed at the propeller location. This resulted in a modest improvement of performance.

8

Wing-slipstream characteristics

In order to separate the propeller from the total wing forces, and to compare unpowered wing characteristics with those with the wing immersed in a slipstream, the isolated propeller data were estimated from Reference (5) and (Figure 7) and were removed from the wind tunnel balance data as follows:

$$C_{L_s} = C_L - \left(2/J^2\right)\left(D^2/S_w\right)\left[C_{T_p} \sin \alpha + C_{N_p} \cos \alpha\right] \tag{1}$$

$$C_{D_s} = C_D - \left(2/J^2\right)\left(D^2/S_w\right)\left[C_{T_p} \cos \alpha - C_{N_p} \sin \alpha\right] \tag{2}$$

$$C_{M_s} = C_M - \left(2/J^2\right)\left(D^2/S_w\right)\left[C_{N_p}\left(\frac{\overline{x}}{c}\right) + C_{T_p}\left(\frac{\overline{y}}{c}\right) + C_{M_p}\left(\frac{D}{c}\right)\right] \tag{3}$$

No attempt was made to correct the propeller data for the blockage and upwash effects of the wing; however the comments of Ref (8) and the experimental data of Ref (4) suggest that these interactions may be small.

The powered clean wing characteristics with the propeller reactions removed are shown in Figure (8). The lift curve lies between the powered and unpowered curves, suggesting that the slipstream interaction contributes about half of the powered lift increment to maximum lift, and lift-slope.

The drag polar (Figure 8) indicates significantly less drag due to the effects of the slipstream flow, particularly at low values of C_L (< 0.4), and near zero lift the wing actually produces a thrust. This has been attributed to the effects of slipstream rotation (Ref. 7), with the wing acting as a flow straightener. This result should probably be taken with caution, however, since no direct measurement of propeller thrust or normal force was available.

There appears to be a nose-down change in pitching moment when propeller forces are removed, since neither thrust or normal force are contributing (Figure 8c). The slipstream interaction evidently produces a lesser slope of the Cm vs α curve, and more nose-down moment, compared with the unpowered wing. A partial explanation of this change is given in Reference 4, and is attributed to changes in chordwise pressure distribution over the region of the wing covered by the slipstream.

Slipstream Interaction - Roughness

The loss of performance due to distributed roughness, for the wing-slipstream interaction, appears to be somewhat larger than that for the unpowered wing in steady uniform flow. This may be due to the high thrust coefficient of this test, and the resulting

9

augmentation of local pressures on the wing. Figure (9) shows lift ,drag and moment for the unpowered wing and for the wing immersed in a slipstream. Also shown is a shaded boundary that indicates the changes in drag due to increasing roughness in each case. The shaded areas in both graphs represent the maximum loss incurred by distributed roughness of varying grit size, including the heavy sand paper application. The negative drag generated on the wing near zero lift (Figure 9b) is all but removed by the action of the contamination on the nose and upper surface of the wing. In contrast the unpowered wing incurs a slightly lower drag loss due to roughness. At a lift coefficient Cls of about .36, the net drag is zero on the clean powered wing. For values of lift greater than this, drag rises rapidly, and eventually exceeds that of the unpowered wing since thrust is now no longer contributing a force in the streamwise direction and lift is reduced by the amount of the propeller normal force contribution. The effect of increasing roughness in both cases increases drag, particularly before stall.

The propeller contribution to pitching moment is mostly unstable (i.e. nose up). Therefore, removal of the propeller forces makes Cm more negative, and decreases the slope of the Cm vs α curve. The changes to pitching moment are relatively smaller when roughness is applied to the wing (Figure 9) compared to the clean condition. The slipstream interaction on the clean wing results in a slightly more stable pitching moment curve (Cms vs α) compared with the unpowered wing. The application of roughness causes, in both cases, a loss of stability in the pitching moment curves.

Leading edge ice accretion

In addition to uniform roughness on the wing upper surface, tests were also made with modifications to the leading edge that represented rime and glaze ice accretion (Figure 2). The data shown in Figure (10) for the unpowered wing show that such gross changes to the leading edge profile cause losses of maximum lift in the 30 to 50 percent range. Reynolds number is important and a further reduction of maximum lift of 15 to 20% will occur when reynolds number is increased to 2.3 million. Similar significant changes to pitching moment also arise from these leading edge shapes, particularly at high Reynolds numbers.

With the application of power, lift slope and maximum lift are increased but the wing performance is well below normal and the drag polars indicate high drag levels at all lift coefficients. Figure (11) shows a comparison between uniform contamination and leading edge accretion of heavy rime ice, for the drag polars and pitching moments of the ice-contaminated wing for the powered configuration. Leading edge ice results in less reduction of lift slope before stall, but a larger lift loss after stall.

Figure (11d) shows the effect of a slipstream interaction on the wing lift and drag for a medium and heavy leading edge rime accretion. As with distributed roughness,

leading edge ice contamination effectively removes the benefits of slipstream flow rotation.

Chord force and leading edge suction

The effective performance of an airfoil or wing depends on the production of negative pressures along the leading edge, and a leading edge suction force that ensures that the aerodynamic force becomes normal to the relative wind. The determination of the chord force coefficient C_c and the leading edge suction coefficient C_s indicate the degree to which lifting efficiency can be achieved.

C_c and C_s can be determined from experimental data as follows:

$$C_c = C_D \cos \alpha - C_L \sin \alpha \tag{4}$$

and for small angles

$$C_s = C_{D_o} - C_c \tag{5}$$

C_c and C_D can also be determined from the parabolic drag polar relationship (Ref. 9). Figure 12a shows the relationship between unpowered wing drag C_D and chord force C_c, and the effects of distributed roughness on both parameters, for the unpowered wing. It appears that roughness has a relatively larger effect on drag than on chord force.

Corresponding values of leading edge suction coefficient for the unpowered wing also show the effects of contamination. Below stall C_s is not greatly diminished by contamination around the nose, but drops suddenly beyond maximum lift.

Figure (12c) shows chord force vs. lift coefficient for the powered wing with leading edge ice and roughness, and with the propeller forces removed. The accretion of ice tends to lower the leading edge force at low values of C_{L_s}, but distributed roughness appears to have a more serious effect at higher lift coefficients.

CONCLUSIONS

1) The main effect of distributed upper surface roughness on an unpowered wing is to reduce lift slope and maximum lift by as much as 30 to 50 percent, depending upon roughness size, Reynolds number, and to a lesser extent, coverage.

2) The magnitude of the loss of maximum lift increases with roughness size, and also with Reynolds number and testing of roughened wings should be done at as high a Reynolds number as possible.

11

3) Roughness increases the parasite drag at zero lift and also results in a premature stall with resulting large increases of form drag.

4) The leading edge region is especially sensitive to distributed roughness regardless of particle size; there is a significant increase in drag and corresponding decrease of leading edge suction at angles of attack below stall. Conversely, removal of the roughness over a small portion of the nose restores the wing to almost clean performance.

5) If the wing is powered and clean, the slipstream interaction increases lift slope and maximum lift by 25 percent, for thrust coefficients appropriate to the take-off condition. If roughness is applied, maximum lift decreases by more than 25%, thus producing a lifting performance somewhat below the unpowered wing in the clean state. This may have significance in the event of an engine failure; the contaminated wing will suffer a further loss in maximum lift in the unpowered state.

6) An attempt was made to isolate the slipstream interaction on the wing by subtracting estimated propeller forces. When comparing the performance of the powered and unpowered wings, it was noted that roughness produced slightly higher losses on the wing immersed in the slipstream.

7) Loss of lift due to an accretion of rime or glaze ice on the leading edge of the wing may reach as high as 50 percent even when the wing is powered, and is sensitive to Reynolds number. Loss of maximum lift is greater for heavy rime ice than for heavy distributed roughness.

LIST OF REFERENCES

1. Wing Tips - Fokker product support division, #14, December 1989.

2. Jones, R., Williams, D.H. - The effect of Surface Roughness on the Characteristics of Airfoils. RAE R&M 1708, Feb. 1936.

3. Nishimura, Y. - An Experimental Investigation by Force and Surface Pressure Measurements on a Wing Immersed in a Propeller Slipstream. Part I: Force and Moment Measurements. NRC-CR-501, March 1968.

4. Nishimura, Y. - Surface Pressure Measurements Part II, NRC LR-525, June 1969.

5. Wickens, R.H. - Aerodynamic Force and Moment Characteristics of a Four-Bladed Propeller Yawed through 120 Degrees. NRC-LR-454. May 1966.
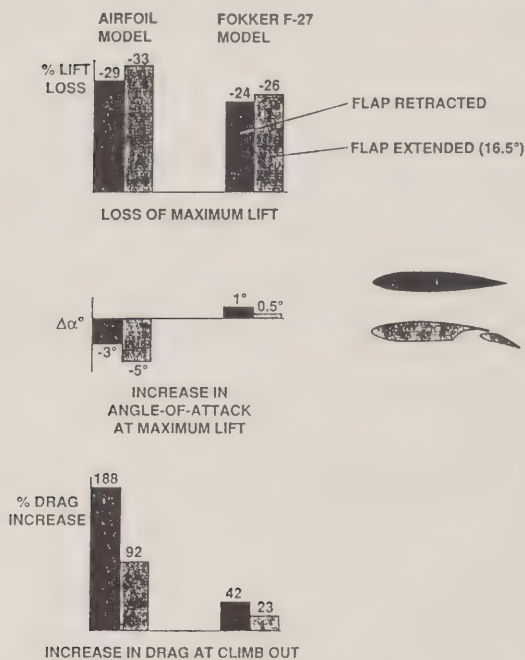
12

6.   Olson, W., Shaw, R., Newton, J. - The Shapes and the Resulting Drag Increase for a NACA 0012 Airfoil, NASA   TM 83556, 1984.

7.   Squire, H.B., Chester, W. - Calculation of the Effect of Slipstream on Lift and Drag. ARC R&M 2368, 1950.

8.   Durand, Vol II. Aerodynamic Theory.

9.   Schlichting, H., Truckenbrodt, E. - Aerodynamics of the Airplane - McGraw-Hill 1979.

10. Morgan, J.M., Wagner, G.A., Wickens, R.H. - A Report of the Flight Dynamics of the Fokker F-28 mk 1000 as they pertain to the accident at Dryden, Ontario, March 1989. NRC/NAE misc. 64

13
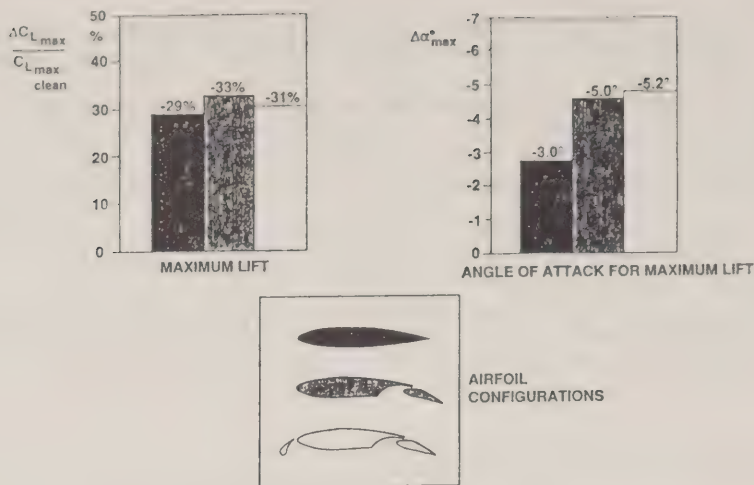
WING-ROUGHNESS-INDUCED LOSS OF MAXIMUM LIFT AND REDUCTION
IN ANGLE OF ATTACK FOR MAXIMUM LIFT (REF. 1)

FIGURE 1

COMPARISON OF LIFT LOSS AND DRAG RISE FOR AIRFOIL
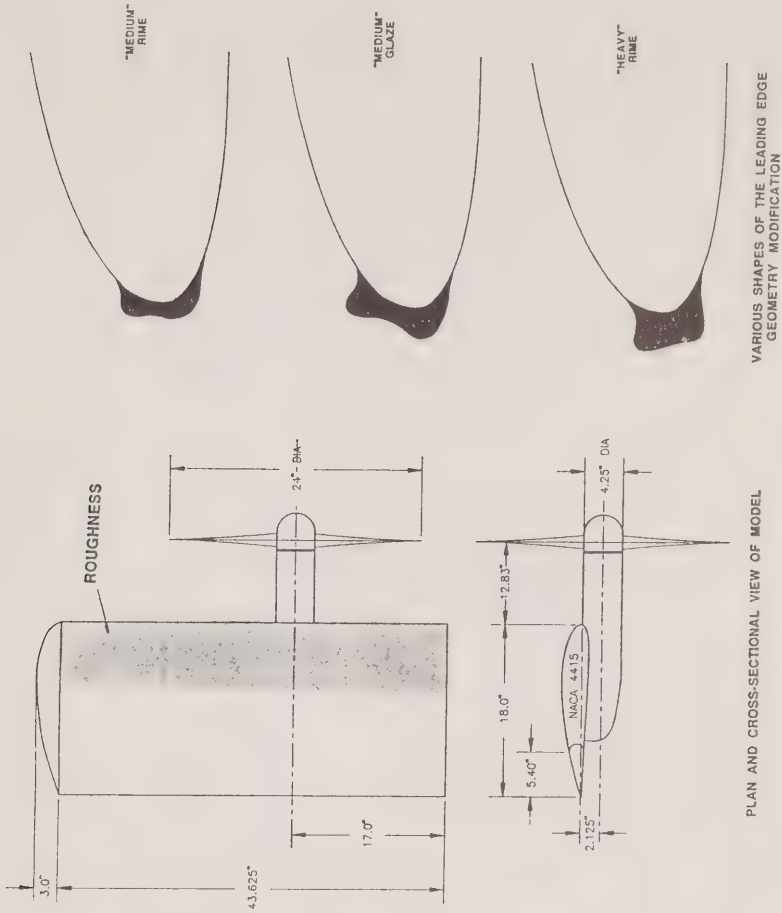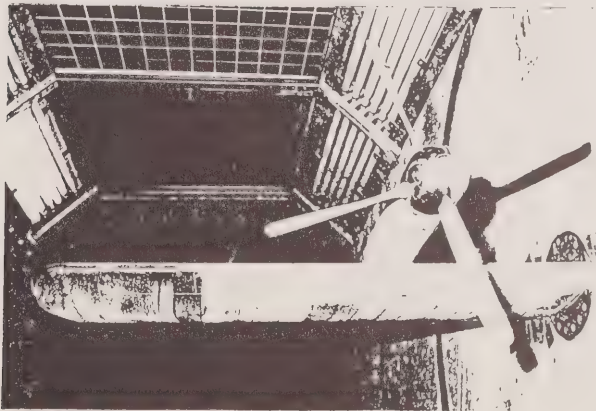AND PROPELLER-SLIPSTREAM MODELS

14

"MEDIUM" RIME

"MEDIUM" GLAZE

"HEAVY" RIME

VARIOUS SHAPES OF THE LEADING EDGE GEOMETRY MODIFICATION

ROUGHNESS

24" — DIA

4.25" DIA

12.83"

18.0"

NACA 4415

5.40"

2.125"

17.0"

3.0"

43.625"

PLAN AND CROSS-SECTIONAL VIEW OF MODEL

FIGURE 2

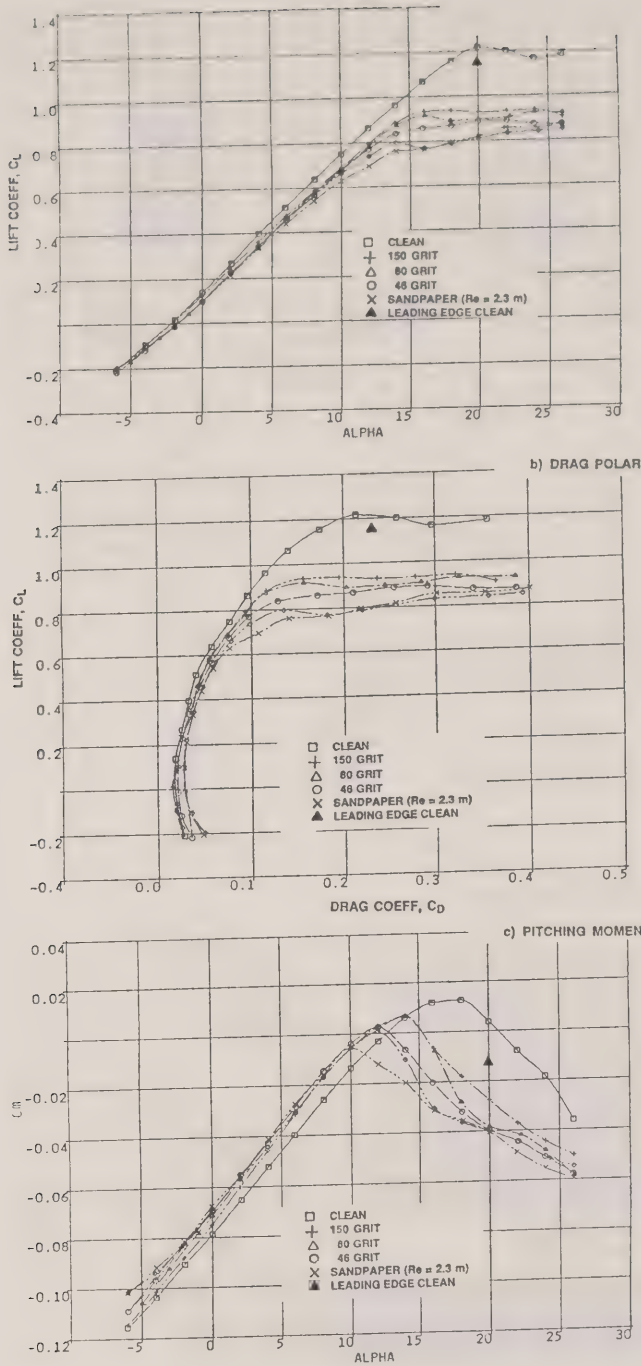WING-PROPELLER MODEL WITH DISTRIBUTED ROUGHNESS

15

FIGURE 3

b) DRAG POLAR

c) PITCHING MOMENT

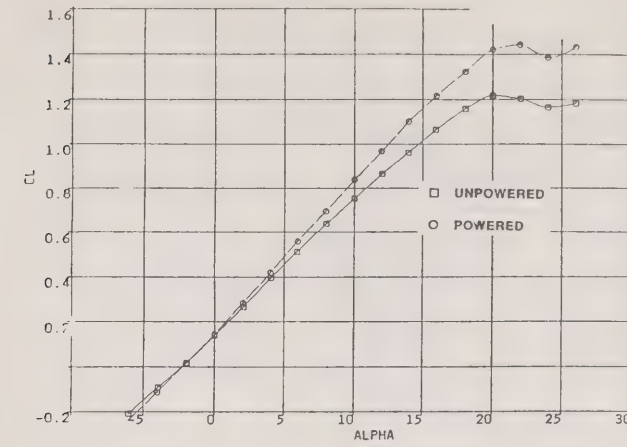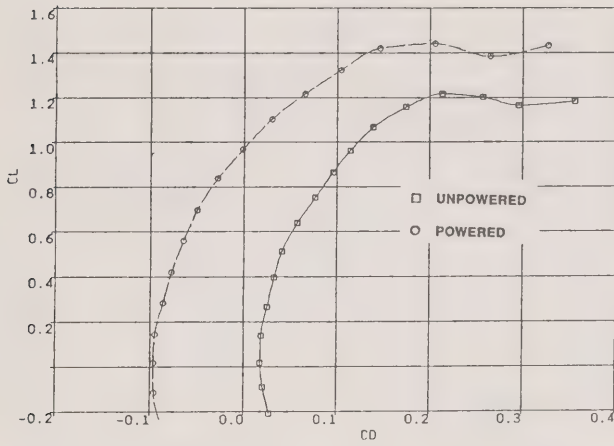EFFECTS OF UNIFORM ROUGHNESS ON UNPOWERED
WING PERFORMANCE, Re = 1.3 m, 30% COVERAGE
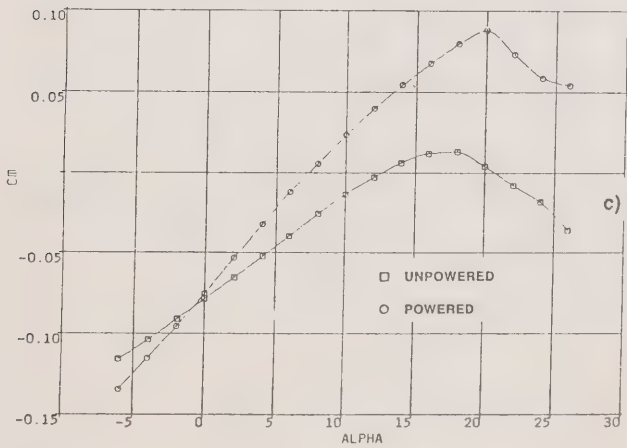
FIGURE 4

a) LIFT

b) DRAG

c) PITCHING MOMENT

COMPARISON OF POWERED AND UNPOWERED CLEAN WING PERFORMANCE $C_{T_p} = 0.115$, Re = 1.3 m

17
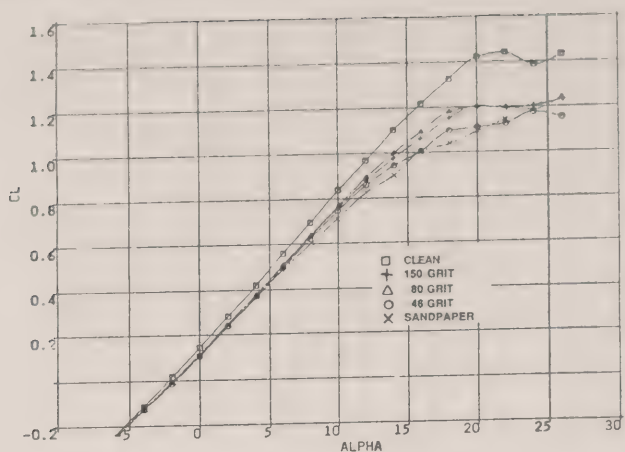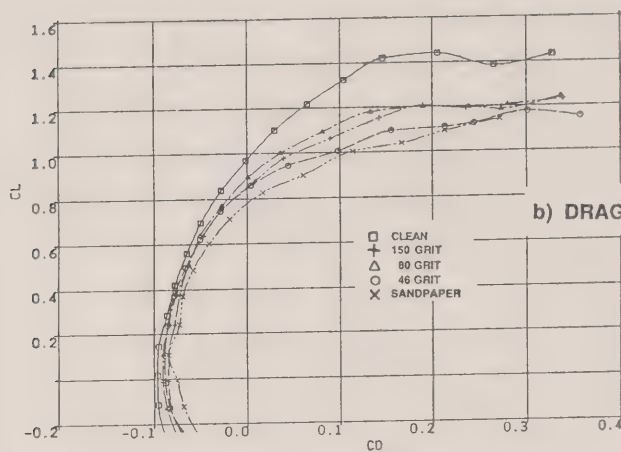
FIGURE 5

a) LIFT

b) DRAG POLAR
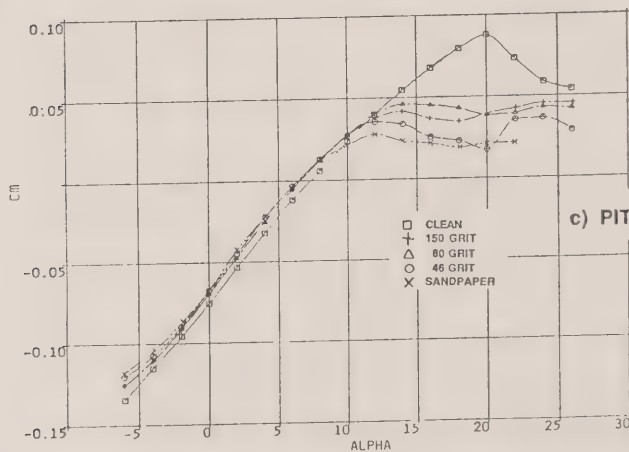
c) PITCHING MOMENT

EFFECT OF UNIFORM ROUGHNESS ON POWERED WING PERFORMANCE, $C_{T_p} = 0.115$, Re = 1.3 m
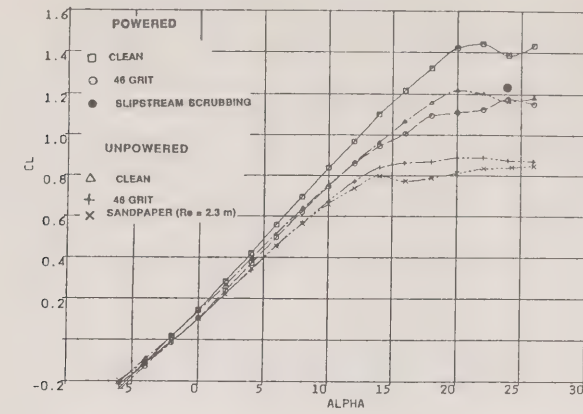
FIGURE 6

a) LIFT
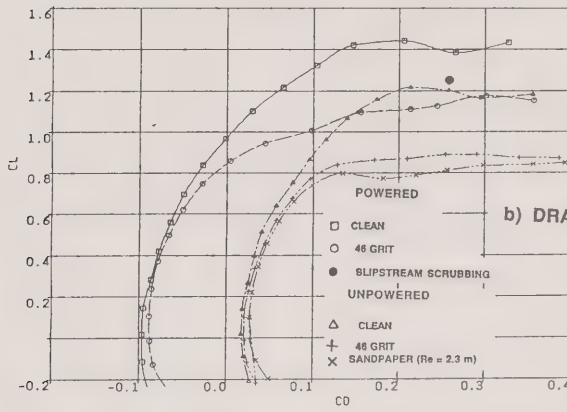
b) DRAG POLAR
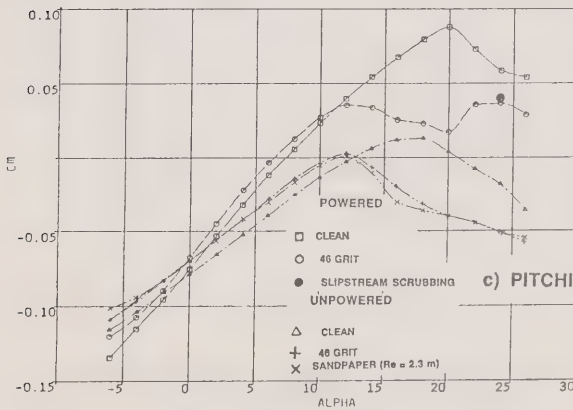
c) PITCHING MOMENT

COMPARISON OF EFFECTS OF UNIFORM ROUGHNESS ON POWERED AND UNPOWERED WING, 46 GRIT, 30% COVERAGE, $C_{Tp} = 0.115$, Re = 1.3×10^6

19

PROPELLER THRUST, NORMAL FORCE AND PITCHING MOMENT
(REF)

FIGURE 7

ANGLE OF ATTACK-DEG.
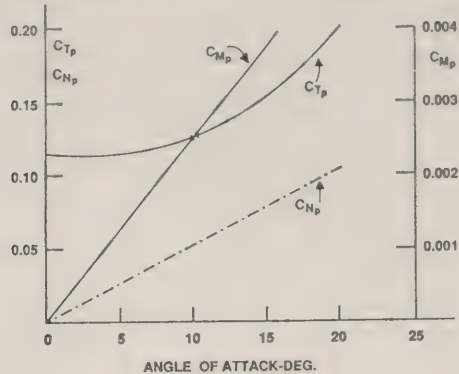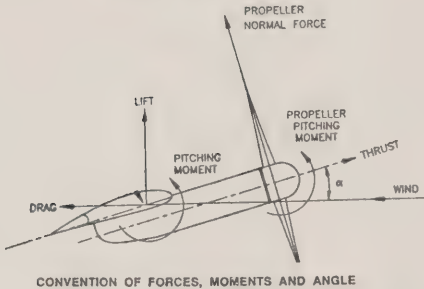
CONVENTION OF FORCES, MOMENTS AND ANGLE
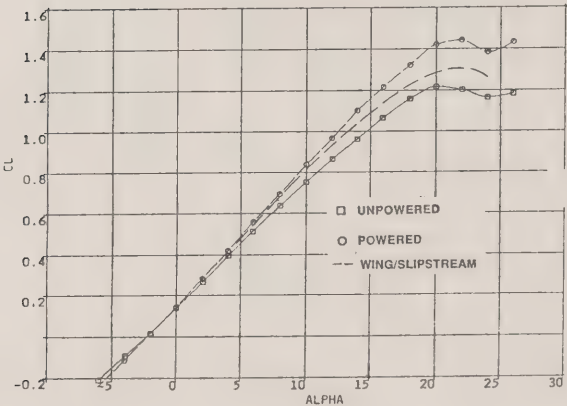
FIGURE 8

a) LIFT

REMOVAL OF PROPELLER REACTIONS FROM THE CLEAN,
POWERED WING, C_{T_p} = 0.115, Re = 1.3 m
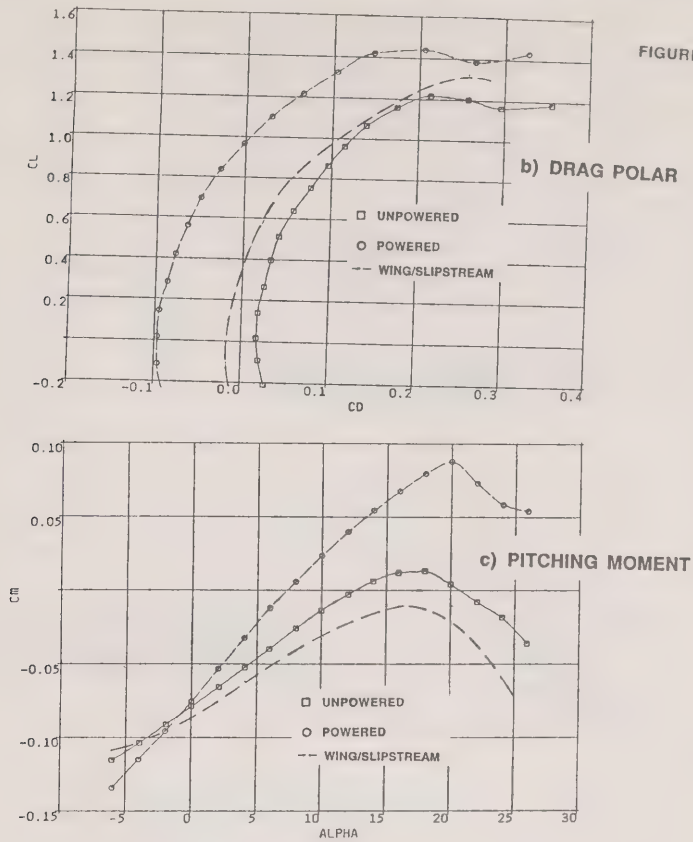
20

FIGURE 8

b) DRAG POLAR

c) PITCHING MOMENT

REMOVAL OF PROPELLER REACTIONS FROM THE CLEAN, POWERED WING, C_{T_p} = 0.115, Re = 1.3 m
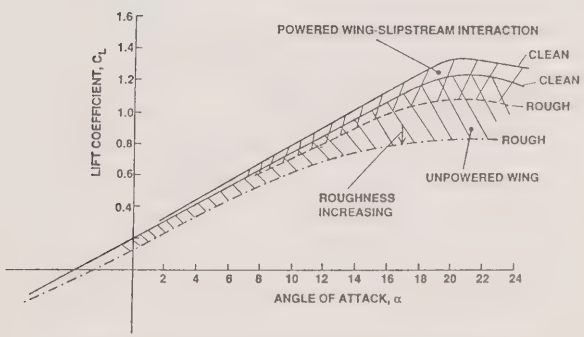
FIGURE 9

COMPARISON OF LIFT LOSS DUE TO DISTRIBUTED ROUGHNESS, OF AN UNPOWERED WING, AND A POWERED WING WITH PROPELLER REACTIONS REMOVED. C_{T_p} = 0.115, Re = 1.3 x 10^6

21
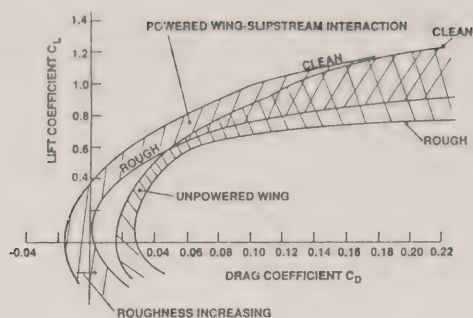
FIGURE 9

COMPARISON OF DRAG LOSSES DUE TO DISTRIBUTED
ROUGHNESS, OF AN UNPOWERED WING AND A POWERED
WING WITH PROPELLER REACTIONS REMOVED.
$C_{T_p} = 0.115$, Re $= 1.3 \times 10^6$
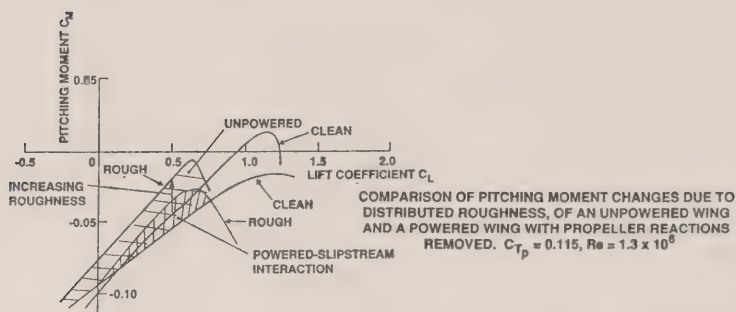
COMPARISON OF PITCHING MOMENT CHANGES DUE TO
DISTRIBUTED ROUGHNESS, OF AN UNPOWERED WING
AND A POWERED WING WITH PROPELLER REACTIONS
REMOVED. $C_{T_p} = 0.115$, Re $= 1.3 \times 10^6$
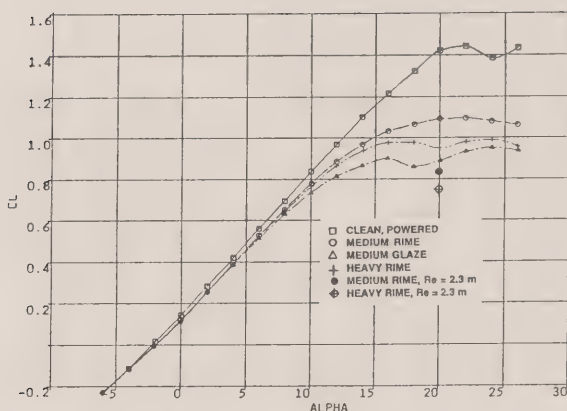
FIGURE 10

a) LIFT

EFFECT OF LEADING EDGE ICE ON POWERED WING PERFORMANCE,
$C_{T_p} = 0.115$, Re $= 1.3$ m

22
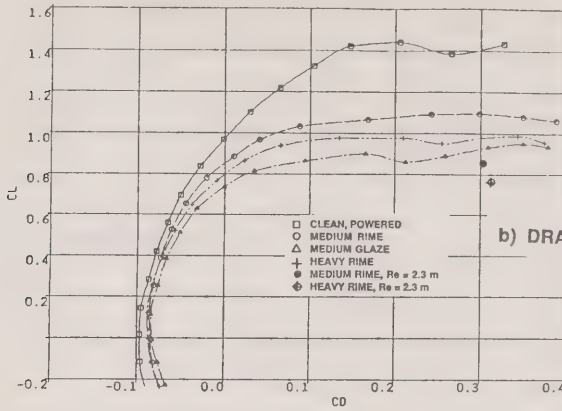
FIGURE 10

b) DRAG POLAR

c) PITCHING MOMENT

EFFECT OF LEADING EDGE ICE ON POWERED WING PERFORMANCE, C_{T_p} = 0.115, Re = 1.3 m
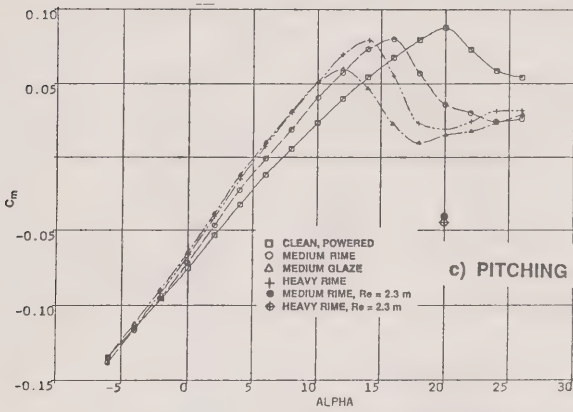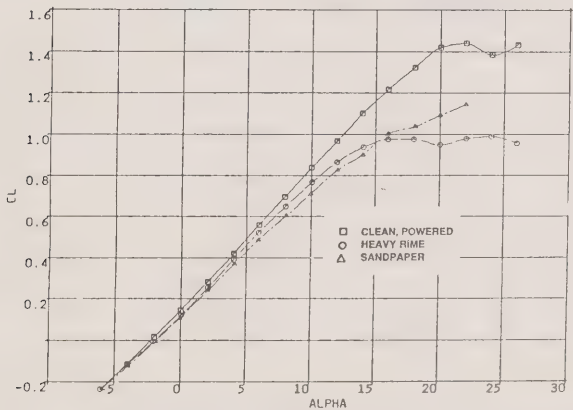
FIGURE 11

a) LIFT

COMPARISON OF LEADING EDGE ICE AND UNIFORM ROUGHNESS, C_{T_p} = 0.115, Re = 1.3 m

23

FIGURE 11

b) DRAG POLAR

c) PITCHING MOMENT

COMPARISON OF LEADING EDGE ICE AND UNIFORM ROUGHNESS, $C_{T_p} = 0.115$, Re = 1.3 m

DRAG POLAR
COMPARISON OF DISTRIBUTED ROUGHNESS (50 GRIT SANDPAPER) AND LEADING EDGE ICE FOR POWERED WING-SLIPSTREAM INTERACTION (PROPELLER REACTIONS REMOVED) $C_{T_p} = 0.115$, Re = 1.3×10^6

24
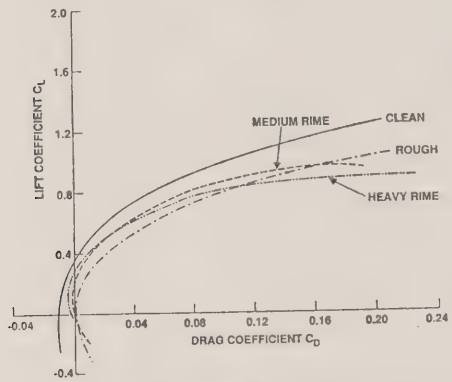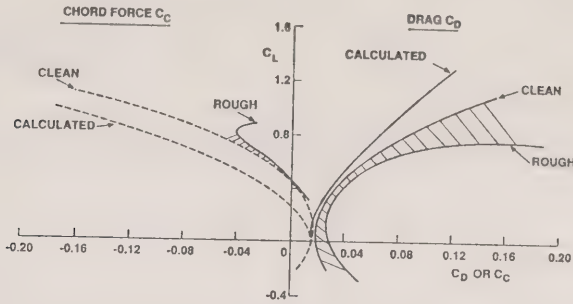
COMPARISON OF DRAG AND CHORD FORCE FOR CLEAN AND ROUGHENED
UNPOWERED WING (50 GRIT SANDPAPER)
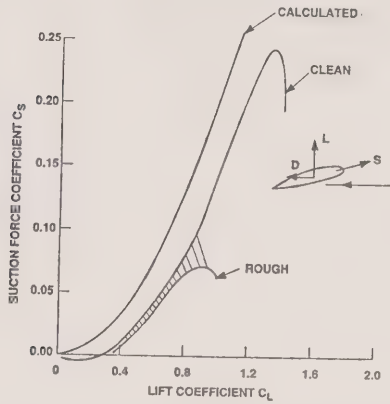
LEADING EDGE SUCTION FORCE COEFFICIENT
FOR CLEAN AND ROUGHENED UNPOWERED WING
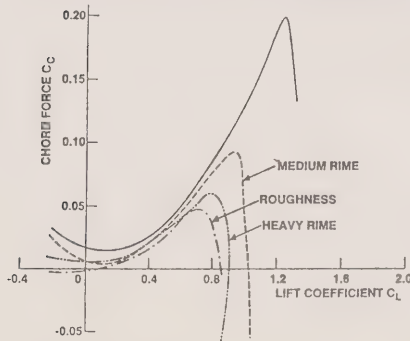
CHORD FORCE vs LIFT COEFFICIENT
COMPARISON AND LEADING EDGE ICE FOR POWERED
WING-SLIPSTREAM INTERACTION (PROPELLER
REACTIONS REMOVED) $C_{T_p} = 0.115$, Re = 1.3 x 10^6

25

Appendix 6

Freezing Precipitation on Lifting Surfaces

Myron M. Oleskiw, Ph.D.

April 23, 1990
Updated September 1991

National Research
Council Canada

Institute for
Mechanical Engineering

Cold Regions Engineering

Conseil national
de recherches Canada

Institut de
génie mécanique

Ingénerie des régions froides

NRC CNRC

Freezing Precipitation on Lifting Surfaces

M. M. Oleskiw

Canadä

FREEZING PRECIPITATION ON LIFTING SURFACES

PRÉCIPITATION GLAÇANTE SUR LES SURFACES PORTANTES

M. M. Oleskiw, Ph.D.

IME-CRE-TR-003

ABSTRACT

As a part of its investigation, the Commission of Inquiry into the Air Ontario Crash at Dryden, Ontario asked the National Research Council to estimate the quantity and form of the precipitation adhering to the Fokker F-28's wings during its ill-fated take-off attempt.

Since precipitation measurements at Dryden were not taken sufficiently frequently to determine the quantity of precipitation which fell during the aircraft's stopover at Dryden, an empirical formula, utilizing the visibility recorded by the weather observer and by a transmissometer, was used to provide an estimate of 1.38 mm of snowfall.

A thermodynamic analysis of the influence of the take-off roll upon the precipitation layer on the wings indicated that no significant change occurred during this interval. However, the wing tank fuel temperature during the final stopover was calculated to be below 0°C. Therefore, heat removed from the lower part of the precipitation layer could have caused it to freeze. As a result, when the upper snow layer was blown away during the take-off roll, it likely left behind, on the wing, a very rough ice layer with potentially serious effects on the aircraft's aerodynamic performance.

RÉSUMÉ

La Commission d'enquête sur l'écrasement d'un avion d'Air Ontario à Dryden (Ontario) a demandé au Conseil national de recherches Canada d'estimer la quantité et la forme de précipitation qui a adhérée aux ailes du Fokker F-28 au moment de sa malheureuse tentative de décollage.

Puisque les mesures de précipitation à Dryden n'ont pas été prises assez fréquemment pour déterminer la quantité de neige qui a tombée durant l'escale de l'avion à Dryden, une formule empirique, utilisant la visibilité notée par l'observateur météorologique et par un transmissomètre, a été employée pour donner une estimation de 1.38 mm de la chute de neige.

Une analyse thermodynamique de l'influence du roulement au décollage sur la couche de précipitation sur les ailes a indiqué qu'il n'y avait pas eu de changement considérable pendant cet intervalle. Toutefois, la température du carburant dans les réservoirs des ailes de l'avion durant l'escale finale était moins de 0°C. Par conséquent, la chaleur transmise de la plus base partie de la couche de précipitation aurait pu geler celle-ci. À cause de ça, quand la plus haute couche de neige s'est envolée durant le roulement au décollage, elle a probablement laissé une couche de givre très rugueuse sur les ailes, avec des effets possiblement sérieux sur le fonctionnement aérodynamique de l'avion.

IME-CRE-TR-003

CONTENTS

CONTENTS (Cont'd)

LIST OF TABLES

CONTENTS (Cont'd)

LIST OF SYMBOLS

Symbol		Units
a	Constant	K^3
a_∞	Speed of sound in the freestream flow	$m \cdot s^{-1}$
C	Mean aerodynamic chord of the wing	m
C_p	Pressure coefficient	
c_p	Specific heat at constant pressure	$J \cdot K^{-1} \cdot kg^{-1}$
C_s	Mass concentration of the snowflakes in the air	$kg \cdot m^{-3}$
D	Cylinder diameter	m
$e_{0°C}$	Saturation vapour pressure over the precipitation layer's surface	kPa
e_a	Saturation vapour pressure just outside the boundary layer	kPa
h	Convective heat transfer coefficient	$W \cdot m^{-2} \cdot K^{-1}$
h_C	Local convective heat transfer coefficient over a wing	$W \cdot m^{-2} \cdot K^{-1}$
h_D	Local convective heat transfer coefficient over a cylinder	$W \cdot m^{-2} \cdot K^{-1}$
I	Mass flux of accreting snowflakes	$kg \cdot m^{-2} \cdot s^{-1}$
k	Constant	
k_a	Thermal conductivity of air	$W \cdot m^{-1} \cdot K^{-1}$
k_f	Thermal conductivity of wing tank fuel	$W \cdot m^{-1} \cdot K^{-1}$
k_m	Fraction of precipitation layer in liquid form	$W \cdot m^{-1} \cdot K^{-1}$
k_p	Thermal conductivity of the precipitation layer	$W \cdot m^{-1} \cdot K^{-1}$
k_s	Thermal conductivity of aluminum	$W \cdot m^{-1} \cdot K^{-1}$
L_e	Latent heat of evaporation at 0°C	$J \cdot kg^{-1}$
L_f	Latent heat of fusion	$J \cdot kg^{-1}$
m_1	Mass of liquid 1	kg
m_2	Mass of liquid 2	kg
Nu_C	Wing Nusselt number	
Nu_D	Cylinder Nusselt number	
p_a	Local air pressure just outside the boundary layer	kPa
p_∞	Static pressure	kPa
q_a	Heat flux to cool the precipitation layer to the freezing point	$W \cdot m^{-2}$
q_c	Heat flux due to convection	$W \cdot m^{-2}$
q_e	Heat flux due to evaporation or sublimation	$W \cdot m^{-2}$
q_f	Heat flux to freeze the unfrozen portion of the precipitation layer	$W \cdot m^{-2}$
q_i	Heat flux due to conduction into the wing of the aircraft	$W \cdot m^{-2}$
q_k	Heat flux from kinetic energy of the impinging snowflakes	$W \cdot m^{-2}$
q_m	Heat flux from freezing the partially-melted impinging snowflakes	$W \cdot m^{-2}$
q_s	Heat flux from short and long-wave radiation	$W \cdot m^{-2}$
q_v	Heat flux from frictional heating of the air in the boundary layer	$W \cdot m^{-2}$
R	Precipitation rate	mm/h

CONTENTS (Cont'd)

Symbol		**Units**
r	Recovery factor for viscous heating	
Re_C	Wing Reynold's number	
Re_D	Cylinder Reynold's number	
T	Thickness of accumulated snow layer	m
T_f	Thickness of a given volume of wing fuel	m
T_p	Thickness of precipitation layer	mm
T_s	Thickness of the aluminum skin of the aircraft wing	m
t_a	Local air temperature just outside the boundary layer	°C
t_f	Temperature of wing tank fuel	°C
t_{fi}	Fuel temperature before flight	°C
t_{fc}	Fuel temperature after flight at altitude of duration τ	°C
t_m	Temperature of mixture of liquids 1 and 2	K
t_p	Temperature of the precipitation layer	°C
t_T	Total air temperature at altitude	°C
t_w	Wet-bulb temperature	°C
t_1	Temperature of liquid 1	K
t_2	Temperature of liquid 2	K
V	Visibility	km
V_a	Local air velocity	$m \cdot s^{-1}$
V_∞	Aircraft airspeed	$m \cdot s^{-1}$
β	Local collision efficiency	
ν_∞	Kinematic air viscosity	$m^2 \cdot s^{-1}$
ρ_s	Snow density	$kg \cdot m^{-3}$
ρ_∞	Freestream air density	$kg \cdot m^{-3}$
σ	Stefan-Boltzmann constant	$W \cdot m^{-2} \cdot K^{-4}$
τ	Time to freeze snow layer	s
τ_a	Duration of flight at altitude	s

FREEZING PRECIPITATION ON LIFTING SURFACES

1.0 INTRODUCTION

In a letter dated 1989 June 20, Mr. D. J. Langdon of the Canadian Aviation Safety Board (now the Transportation Safety Board of Canada, CTSB) wrote to the Low Temperature Laboratory (now Cold Regions Engineering) of the National Research Council (NRC) requesting assistance in the investigation of the 1989 March 10 accident to Fokker F-28 Mk1000, registration C-FONF, at Dryden, Ontario. Witness testimony to that point had indicated that snow had been seen to fall on the wings of the aircraft during its station-stop at Dryden, and some witnesses had reported that the snow had appeared to turn to ice during the take-off roll.

Mr. Langdon (acting on behalf of Mr. J. Jackson, an advisor to the Inquiry) requested that the following analyses be performed:
- an estimation of the weight of snow per unit area which could have collected on the aircraft prior to take-off;
- a determination of whether or not wet snow crystals could have stuck to the leading edge of the wing during take-off; and
- a determination of whether or not snow on the surface of the wing could have turned to ice (as reported by witnesses) through the mechanisms of adiabatic and evaporative cooling of the airflow over the wing.

This report addresses these requests in the three sections which follow. Section 2 attempts to estimate the amount of snow which would have accumulated on the aircraft during its station-stop at Dryden. Section 3 presents an analysis of adiabatic and evaporative cooling of the wing and its effects on the precipitation extant and impinging on the wing during the take-off roll. Finally, Section 4 discusses the possibility of the wing surface being cooled by the fuel in the wing tanks, and what effect that might have had on the precipitation.

2.0 QUANTITY OF PRECIPITATION ACCUMULATED

2.1 Precipitation Recorded on the Surface Weather Record

With respect to estimating total precipitation accumulation on the upper surfaces of the Fokker F-28 aircraft during its station-stop at Dryden, the aircraft movements of interest are: the time of arrival from Thunder Bay (17:40 UTC); and the time of take-off from Dryden (18:10 UTC). During this time period, the weather details of interest at the Dryden Airport, as observed and reported on the Atmospheric Environment Service (AES) Surface Weather Record, are noted in Table 1. Column 1 shows the recorded

Table 1. Weather at Dryden, Ontario on 1989 March 10

TIME (UTC)	DRY BULB TEMP. (˚C)	DEW POINT TEMP. (˚C)	WEATHER	VISIBILITY (mi)	SNOWFALL RATE WATER EQUIVALENT (mm/h)
17:00	1.0	-4.0	very light snow grains	14	0
17:07			light snow grains	14·	0 to 2.5
17:23			-	14	0
17:42			light snow	14	0 to 2.5
17:48			light snow	2.5	0 to 2.5
18:00	0.7	-3.0	light snow	2.5	0 to 2.5
18:06			moderate snow	0.375	2.6 to 7.5
18:11			light snow	0.75	0 to 2.5
18:12	0.3	-2.1	light snow	0.75	0 to 2.5

time of the observation. Columns 2 and 3 respectively give the dry bulb and dew point temperatures as measured by the observer. Column 4 records the type of weather, including the type of precipitation and its rate of accumulation. The visibility indicated in Column 5 was obtained by determining the most distant object visible to the observer. The water equivalent of the snowfall rate (quantity of water which would be measured if the snow was melted) is presented in Column 6. This rate is derived from the precipitation rate in Column 4 by the definitions presented in the AES Manual of Observations (MANOBS).

The ranges of snowfall rate indicated in Table 1 are not sufficiently precise to allow a reasonable estimate of the amount of snowfall during the F-28's station-stop. Fortunately, precipitation accumulation may also be estimated from visibility data. Two sources of visibility data from the Dryden Airport are available for analysis: the meteorological observer's data as given in Table 1; and recordings from a Transport Canada transmissometer.

2.2 Relating Precipitation Rate to Visibility

Stallabrass (1987) performed a series of experiments relating snowfall concentration with visibility, and snowfall concentration with precipitation rate. The correlation coefficient

for the best-fit line relating the former two quantities for all types of snow crystals was 94.3%. Stallabrass stated that the correlation between the latter two quantities was expected to be poorer based on earlier predictions by other researchers. This was believed to be a function of the considerable variability in terminal fall velocity of the ice crystals and snowflakes, depending upon, for example, whether or not the crystals and flakes were heavily rimed or partially melted. This variability would tend to affect the rate of precipitation more than the mass concentration in the air. Despite these difficulties, Stallabrass suggested that based upon his measurements, precipitation rate R (mm/h water equivalent) could be estimated from visibility V (km) by the relationship

$$V = 0.919 R^{-0.64} \qquad (1)$$

with a correlation coefficient of 0.91. Inverting this relationship with V in miles gives

$$R = 0.417 V^{-1.56} ; \qquad (2)$$

and with V in feet gives

$$R = 2.68 \times 10^5 V^{-1.56}. \qquad (3)$$

Based upon Stallabrass's observations, the extreme values of the precipitation rate measured for a given visibility were approximately between 1/3 to 3 times those predicted by the best-fit line.

Given this degree of variability in the precipitation rate versus visibility relationship, an attempt has been made to compare two predictions of total precipitation accumulation at Dryden versus the recorded precipitation accumulation. Two sources of visibility data have been used: the Surface Weather Record; and transmissometer data. The actual precipitation accumulation has been assumed to be that noted by the meteorological observer during the 6 hour interval between 18:00 UTC on March 10 and 00:00 UTC on March 11. Unfortunately, no optional measurement of precipitation accumulation was noted between the measurements at these two mandatory times.

2.3 Precipitation Inferred from Surface Weather Record Visibility

Table 2 displays the estimation of total water-equivalent snowfall accumulation at Dryden between March 10 18:00 UTC and March 11 00:00 UTC as derived from the visibility data recorded on the AES Surface Weather Record. Column 1 indicates the time at which an interval begins with approximately constant visibility. Column 2 gives the length of the time interval, while Column 3 shows the visibility. The precipitation rate derived from Column 3 using Eq. 2 is given in Column 4. The accumulation of snowfall in each time interval (Column 2 multiplied by Column 4) is displayed in Column 5. The total interval length (3.8 h) is not equal to 6 h because no snow was observed to fall

Table 2. Integration of precipitation rate based upon the meteorological observer's visibility estimates for the period between March 10 18:00 UTC and March 11 00:00 UTC.

BEGINNING OF TIME INTERVAL (UTC)	INTERVAL LENGTH (h)	VISIBILITY (mi)	WATER EQUIVALENT SNOWFALL RATE (mm/h)	WATER EQUIVALENT SNOWFALL OVER TIME INTERVAL (mm)
18:00	0.10	2.5	0.10	0.01
18:06	0.08	0.375	1.93	0.15
18:11	0.52	0.75	0.65	0.34
18:42	0.30	2.5	0.10	0.03
19:00	0.35	3.0	0.08	0.03
19:21	0.65	5.0	0.03	0.02
20:52	0.13	4.0	0.05	0.01
21:00	0.12	2.5	0.10	0.01
21:07	0.30	1.5	0.22	0.07
21:25	0.37	1.0	0.42	0.16
21:47	0.30	0.5	1.23	0.37
22:05	0.33	0.75	0.65	0.21
22:25	0.25	1.0	0.42	0.11
TOTALS:	3.80			1.52

during some of the 6 h interval. The total accumulated water-equivalent snowfall is predicted as 1.52 mm. This is significantly less than the total accumulated water-equivalent snowfall recorded on the Surface Weather Record of 6.0 mm. This discrepancy will be discussed in more detail below.

2.4 Precipitation Inferred from Transmissometer Data

Table 3 presents data recorded by and interpreted from the Transport Canada transmissometer which was located near the runway on which C-FONF landed and departed on March 10. The strip-chart recorded by this device has been analysed by Mr.

Table 3. Integration of precipitation rate based upon the Transport Canada Transmissometer's visibility estimates for the 6 h period between March 10 18:00 UTC and March 11 00:00 UTC.

BEGINNING OF TIME INTERVAL (UTC)	INTERVAL LENGTH (h)	TRANSMIS-SIVITY (%)		VISIBILITY (ft)		WATER EQUIVALENT SNOWFALL RATE (mm/h)		WATER EQUIVALENT SNOWFALL OVER TIME INTERVAL (mm)	
		RAW	CORR.	RAW	CORR.	RAW	CORR.	RAW	CORR.
18:00	0.08	76	70	2600	2050	1.26	1.83	0.10	0.15
18:05	0.08	74	68	2400	1900	1.43	2.06	0.11	0.16
18:10	0.08	82	76	3700	2600	0.73	1.26	0.06	0.10
18:15	0.08	87	81	5000	3500	0.45	0.79	0.04	0.06
18:20	0.08	83	77	4000	2800	0.64	1.12	0.05	0.09
18:25	0.08	85	79	4500	3000	0.54	1.01	0.04	0.08
18:30	0.92	90	84	6000	4200	0.34	0.60	0.31	0.55
19:25	0.58	91	85	6000	4200	0.34	0.60	0.20	0.35
20:55	0.08	85	79	4500	3000	0.54	1.01	0.04	0.08
21:00	0.08	78	72	2900	2200	1.06	1.64	0.08	0.13
21:05	0.08	82	76	3700	2600	0.73	1.26	0.06	0.10
21:10	0.17	83	77	4000	2800	0.64	1.12	0.11	0.19
21:20	0.08	78	72	2900	2200	1.06	1.64	0.08	0.13
21:25	0.33	54	48	2600	2050	1.26	1.83	0.42	0.60
21:45	0.08	58	52	1400	1100	3.31	4.83	0.26	0.39
21:50	0.08	54	48	1250	1050	3.95	5.19	0.32	0.42
21:55	0.08	61	55	1450	1300	3.14	3.72	0.25	0.30
22:00	0.08	67	61	1850	1500	2.14	2.97	0.17	0.24
22:05	0.08	68	62	1900	1550	2.06	2.83	0.16	0.23
22:10	0.17	83	77	4000	2800	0.64	1.12	0.11	0.19
22:20	0.33	88	82	5500	3700	0.39	0.73	0.13	0.24
TOTALS:	3.70							3.10	4.78

B. Sheppard, Senior Instrument Meteorologist, Data Acquisition Systems Branch, Atmospheric Environment Service, Environment Canada. His interpretation of these data has been provided to the Inquiry in the form of a report. Mr. Sheppard has noted that at certain intervals, the transmissometer turns off its transmitting light for a short time to determine the amount of background skylight received. Two such intervals were recorded during the period of interest, and both show values of about 6%. One possible interpretation of this result, as indicated by Mr. Sheppard, is that all values taken from the transmissometer strip-chart should be reduced by 6%.

Column 1 of Table 3 indicates the time at which an interval, with approximately constant visibility (as interpreted from the sensor's strip-chart), begins. Column 2 gives the length of this time interval. Column 3 shows a representative value of transmissivity for the interval as interpreted from the strip-chart. Column 4's transmissivity has been obtained from Column 3's "raw" value by applying the 6% "correction" discussed above. Columns 5 and 6 display the visibility values obtained from Columns 3 and 4. Columns 7 and 8 give the water-equivalent snowfall rate derived from Column 5 and 6 using Eq. 3. Finally, Columns 9 and 10 exhibit the accumulated water-equivalent snowfall obtained by multiplying Column 2 by Columns 7 and 8, respectively.

The total interval length at the bottom of Column 2 of Table 3 is, to within the resolution of the interpretation of the strip-chart, the same as for the comparable quantity in Table 2. The total accumulated water-equivalent snowfall values displayed at the bottoms of Columns 9 and 10 are significantly higher than the 1.52 mm of Table 2. The "corrected" value is 80% of the 6.0 mm measured over the interval by the meteorological observer. However, in comparing the "corrected" visibility values in Table 3 with those made by the meteorological observer, it is evident that the subtraction of 6% from all "raw" transmissivity values to obtain the "corrected" ones has resulted in "corrected" visibility values which are significantly lower than those noted by the observer. A case in point is the time period surrounding 19:15, where the observer recorded a visibility value of 3 mi (15,840 ft) as compared to the "corrected" value of 4200 ft. Evidently, while this correction may be appropriate for lower values of tranmissivity, it should not be equally applied to "raw" values near the upper limit of transmissivity (in the range of 87 to 100%). Even the "raw" value of transmissivity at this time indicates a lower value of visibility (6000 ft) than noted by the observer. This may be attributed to the values of transmissivity between 18:30 and 20:00 UTC (90 or 91%) which should actually be interpreted as greater than 6000 ft. The maximum water-equivalent snowfall rate derived from the observer's visibility estimates during this period is 0.10 mm/h. If the transmissometer's values are reduced from 0.34 mm/h, then the accumulated water-equivalent snowfall over this 1.5 h period would be reduced from 0.51 mm to 0.15 mm. That would reduce the accumulated water-equivalent snowfall for the 6 h period from 3.10 mm to 2.74 mm.

The net result of this analysis is to indicate that if the observer's accumulated water-equivalent snowfall is to be "calibrated" to achieve 6.0 mm over the 6 h period, then the

value of 1.52 mm from Table 2 must be multiplied by a factor of 3.95. If the transmissometer's "raw" accumulated water-equivalent snowfall (corrected for those periods when the transmissivity is 87 to 100%) is compared to the observed amount, the multiplicative "calibration" factor is 2.19.

2.5 Estimating Precipitation During C-FONF's Station Stop at Dryden

Returning to the period of C-FONF's station-stop at Dryden, Table 4 contains data from both of these methods for this time period. Columns 1 and 2 once again indicate the

Table 4. Integration of precipitation rate during the station-stop of C-FONF at Dryden on 1990 March 10.

BEGINNING OF TIME INTERVAL (UTC)	INTERVAL LENGTH (h)	TRANSMIS- SOMETER READING (%)	VISIBILITY (ft)		WATER EQUIVALENT SNOWFALL RATE (mm/h)		WATER EQUIVALENT SNOWFALL OVER TIME INTERVAL (mm)	
			TRANS.	OBS.	TRANS.	OBS.	TRANS.	OBS.
17:40	0.083	93	73920	73920	0.01	0.01	0.00	0.00
17:45	0.083	91	73920	73920	0.01	0.01	0.00	0.00
17:50	0.083	91	13200	13200	0.10	0.10	0.01	0.01
17:55	0.083	92	13200	13200	0.10	0.10	0.01	0.01
18:00	0.033	86	4700	13200	0.50	0.10	0.02	0.00
18:02	0.033	76	2600	13200	1.26	0.10	0.04	0.00
18:04	0.033	68	1900	13200	2.05	0.10	0.07	0.00
18:06	0.033	74	2400	1980	1.43	1.93	0.05	0.06
18:08	0.033	79	3000	1980	1.01	1.93	0.03	0.06
TOTALS:	0.50						0.23	0.14

beginning of the time interval and the length of the time interval respectively. The transmissometer reading is displayed in Column 3. Columns 4 and 5 exhibit a representative visibility for the interval. Column 4's data are derived from Column 3 with a correction to the observer's values when the transmissometer reading is between 87 and 100%. The data in Column 5 are converted from the values taken from the

Surface Weather Record. Columns 6 and 7 give the water-equivalent snowfall rate as derived from Columns 4 and 5. Finally, Columns 8 and 9 tabulate the accumulated water-equivalent snowfall obtained from Columns 2, 6 and 7.

Totals over the 0.5 h time interval of the accumulated water-equivalent snowfall derived from the transmissometer and the observer's notes are 0.23 mm and 0.14 mm respectively. Multiplying these two values by their corresponding "calibration" factors (as determined above), produces best estimates of water-equivalent snowfall accumulation, while the aircraft was on the ground, of 0.50 mm and 0.55 mm. These accumulations are equivalent to a mass per unit area of 0.5 and 0.55 kg m^{-2}.

In order to determine the likely thickness of this layer of precipitation, we need to know its density. Estimating an appropriate value for the precipitation layer density when it has been formed through the accumulation of wet snow is rather difficult since it can vary depending upon the conditions of snowflake formation and also upon the heat balance within the layer itself. A simplification adopted by Makkonen (1989), which will be accepted here as well, is to utilize a statistical mean value for the snow density (ρ_s) of 400 kg·m^{-3}. The higher of the two estimates of water-equivalent snowfall accumulation then gives a best value for the thickness of the precipitation layer of $T_p = 1.38$ mm of snow. Because of the inherent uncertainty involved in estimating snow density and precipitation rate from visibility (especially when the crystals and snowflakes are wet), the level of confidence to attribute to this value is difficult to assess.

3.0 FREEZING OF THE ACCUMULATED PRECIPITATION

3.1 Thermodynamic Influences upon the Accumulated Precipitation Layer

The state (frozen/liquid) of the precipitation which had accumulated on the wings of Fokker F-28 C-FONF by the end of its station-stop and during the aircraft's take-off roll at Dryden on 1989 March 10 can be estimated through an analysis of the thermodynamic influences upon this precipitation layer.

While the aircraft was parked near the terminal building, the precipitation layer would have been influenced by: the temperature and humidity of the surrounding air; the ambient wind speed; the quantity and temperature of continuing precipitation; the solar and long-wave radiation; and the conduction of heat in to or out of the aircraft wing. These influences could have allowed the layer to begin freezing, depending upon their relative values. Acting differentially upon the layer itself, would have been variations in the conductivity to the wing, depending upon the underlying structure of the wing and variations of its temperature. As the aircraft taxied to the runway and then began its take-off roll, the importance of the ventillation by the airflow over the wing would have increased.

In order to completely evaluate the relative contributions of these factors, an extensive numerical modelling effort of the differential equations involved would be necessary. However, because of the inherent uncertainty in estimating several of the factors, and as a result of the comparatively slow variation of the most important ones, the problem can be simplified somewhat. This section will deal with the heat balance during the aircraft take-off roll, while Section 4 will estimate net heating or cooling of the precipitation layer while the aircraft was stopped or taxiing.

3.2 Terms in the Heat Balance Equation

Following (in part) the lead of Makkonen (1984), a steady-state heat balance equation may be formulated for the processes influencing the precipitation layer:

$$q_a + q_f + q_v + q_k + q_m + q_s = q_c + q_e + q_i \; , \qquad (4)$$

with the heat fluxes (heat per unit area and time: $J \cdot m^{-2} \cdot s^{-1}$) defined as:

q_a the heat which must be released to cool the precipitation layer from the air temperature to the freezing point;

q_f the heat which must be released to freeze the unfrozen portion of the precipitation layer;

q_v the frictional heating of the air in the boundary layer;

q_k the kinetic energy converted to heat during the impact of the impinging snowflakes;

q_m the heat released in freezing the partially-melted impinging snowflakes;

q_s the heat added by short and long-wave radiation;

q_c the heat removed by convection;

q_e the heat removed by evaporation (from a wet surface) or sublimation (from frozen surface); and

q_i the heat conducted into the wing of the aircraft.

The terms on the left hand side of Eq. 4 are sources of heat which must be dissipated if the precipitation layer is to freeze completely. The terms on the right hand side are potential heat sinks.

If all of the terms in Eq. 4 except for q_f are evaluated for a given set of conditions and a location on the wing's surface, and Eq. 4 is rearranged to solve for q_f, then the value for q_f may be substituted into Eq. 5 to determine the time τ (s) required for the accumulated snow layer of thickness T (m) to freeze:

$$\tau = \frac{L_f \rho_s k_m T}{q_f} \tag{5}$$

where L_f is the latent heat of fusion (freezing of water = 3.34×10^5 J·kg^{-1}), ρ_s is the density of the precipitation layer, and k_m is the fraction of the precipitation layer which is in liquid form.

Incorporating a suitable value for the fraction of the precipitation layer which is liquid upon its formation can be a difficult task. Makkonen (1989) was able to derive a criterion to determine whether or not snowflakes would be partially melted as they fall. For the flakes to begin to melt during their fall, the wet-bulb temperature (t_w) must be greater than 0°C. The Surface Weather Record provided by AES indicates that t_w was near -0.7°C during the station-stop of C-FONF at Dryden. This suggests that the snowflakes should not have been melting during their fall through the layer of the atmosphere nearest the ground. To better estimate the state of the snowflakes upon impact, it would be necessary to have a temperature and dew-point sounding at Dryden from which to estimate the wet-bulb temperature aloft. However, an atmospheric sounding is not taken at Dryden on a regular basis. Since the estimated sounding provided by AES was derived from actual soundings at rather distant locations (the nearest available), it contains a uncertain amount of error. Witness testimony has indicated that the snow which fell during the station-stop was in the form of large wet flakes. Since the formation of such large flakes is greatly enhanced by partial melting of the ice crystals which accumulate to form the flakes, we must assume that the snowflakes were indeed partially melted upon impact. For the purposes of this section, a value for the water fraction of the falling snow of $k_m = 0.1$ has been utilized in the calculations which follow. Section 4 will present further discussion upon the fraction of the precipitation which was melted at impact with the wings and upon the effect of this estimate on the final results.

The above discussion of the thermodynamic influences upon falling snowflakes reveals an interesting and possibly surprising fact. The snowflakes may remain completely frozen because of the convective and evaporative cooling they experience even if the air temperature is above 0°C, provided that the dew-point temperature is sufficiently low (ie. the air is sufficiently dry) that the wet-bulb temperature remains below 0°C. Using the conditions at Dryden on 1989 March 10 1800 Z as an example, the flakes could remain completely frozen at an air temperature as high as about +1.3°C. In any case, unless the snowflakes were completely melted during their fall through a very warm layer of air, they would remain at 0°C. As a result, we shall assume that the precipitation layer formed by the snow on the aircraft wings was initially at the freezing temperature, and thus that no heat would be required to cool this layer to the freezing point (ie. $q_a = 0$).

The frictional heating of the air in the boundary layer will be given by:

$$q_v = \frac{h r V_a^2}{2 c_p}$$ (6)

where h is the convective heat transfer coefficient (see below), r is the recovery factor for viscous heating (either 0.85 for a laminar boundary layer, or 0.90 for a turbulent boundary layer), V_a is the local air velocity (m·s⁻¹) just outside the boundary layer at a given location on the wing, and c_p is the specific heat of air at constant pressure (1004 J·K⁻¹·kg⁻¹).

The local air velocity V_a at some point on the wing can be estimated in the following way. First, the local air pressure just outside the boundary layer (p_a) is obtained from a rearrangement of the following definition of the pressure coefficient (see, for example, Houghton and Brock, 1970):

$$C_p = \frac{p_a - p_\infty}{\frac{1}{2} \rho_\infty V_\infty^2}$$ (7)

where V_∞ is the airspeed (m·s⁻¹) of the aircraft and p_∞ is the static pressure and ρ_∞ is the air density at a distance away from the wing. A value of 1.24 kg·m⁻³ has been used for ρ_∞. Appropriate values of C_p for the F-28 wing were obtained from Fokker. Next, the speed of sound (a_∞) in the freestream flow is calculated from: .

$$a_\infty = \sqrt{\frac{1.4 p_\infty}{\rho_\infty}} .$$ (8)

Finally, the local air velocity V_a can be determined from:

$$V_a = \sqrt{5 a_\infty^2 \left[1 - \left(\frac{p_a}{p_\infty} \right)^{1/3.5} \right] + V_\infty^2} .$$ (9)

The kinetic energy of the snowflakes transferred to heat as the snowflakes collide with the wing's surface is:

$$q_k = \frac{I V_\infty^2}{2}$$ (10)

where I is the mass flux ($kg \cdot m^{-2} \cdot s^{-1}$) of the accreting snowflakes. The mass flux of the accreting snowflakes, in turn, is given by:

$$I = \beta C_s V_\infty$$ (11)

where β is the local collection efficiency of the wing for snowflakes and C_s is the mass concentration of the snowflakes in the air ($kg \cdot m^{-3}$).

The heat released in freezing the melted fraction k_m (estimated to be 0.1) of the impinging snowflakes may be calculated from:

$$q_m = I k_m L_f .$$ (12)

The heat added by long-wave radiation can be approximated by:

$$q_s = \sigma a (t_\infty - t_{0°C})$$ (13)

where σ is the Stefan-Boltzmann constant (3.24×10^{-9} $J \cdot m^{-2} \cdot K^{-4} \cdot s^{-1}$), $a = 8.1 \times 10^7$ K^3 and t_∞ is the air temperature in the freestream flow. Eq. 10 has been obtained by linearizing the equation for the difference in the long-wave radiation emitted by the precipitation surface and the snowflake-laden air. The effect of short-wave (solar) radiation on the wing's surface during the take-off roll is difficult to estimate because of the uncertainty of the quantity of radiation which would have been able to penetrate the precipitation falling at that time. As a result, it will be assumed that the precipitation was sufficiently heavy that little solar heating occurred at this time.

The heat removed by convection to the airflow passing over the wing is:

$$q_c = h (0°C - t_a)$$ (14)

where t_a, the local air temperature just outside the boundary layer at a given location on the wing, is obtained from:

$$t_a = t_\infty \left(\frac{p_a}{p_\infty} \right)^{2/7}$$ (15)

The heat removed by evaporation to the drier air flowing over the wing is:

$$q_e = \frac{h k L_e}{c_p p_a}(e_{0°C} - e_a) \tag{16}$$

where $k = 0.62$, L_e is the latent heat of evaporation at 0°C (2.50×10^6 J·kg^{-1}) and $e_{0°C}$ and e_a are the saturation vapour pressures over the precipitation layer's surface and the air just outside the boundary layer respectively.

If it is assumed for the moment that there is no conduction of heat into the wing of the aircraft (ie. $q_i = 0$), then Eq. 4 can now be evaluated locally at various points along the surface of the wing where the various terms may have differing relative values. In order to determine the variation of these terms during the take-off roll of the aircraft, three representative airspeeds (10, 30 and 50 m·s^{-1}) have been chosen to cover the interval of 0 to 130 kt (the airspeed interval during the take-off roll). The points which have been chosen along the wing's upper surface are at about 3% chord and at about 25% chord. The first point is intended to be representative of the portion of the wing where the pressure coefficient has its greatest negative value (at an angle of attack of -2°, during the take-off roll), whereas the second is typical of the upper wing surface in contact with the fuel cell inside the wing.

Returning for a moment to define the convective heat transfer coefficient (mentioned earlier):

$$h_C = \frac{k_a \text{Nu}_C}{C} \tag{17}$$

where k_a is the thermal conductivity of air (2.41×10^{-2} J·m^{-1}·s^{-1}·K^{-1}), C is the mean aerodynamic chord of the wing (3.5 m), and Nu$_C$ is the wing Nusselt number which in turn is related to Re$_C$, the wing Reynold's number. This latter quantity is defined by:

$$\text{Re}_C = \frac{V_\infty C}{v_\infty} \tag{18}$$

where v_∞ is the kinematic air viscosity. A representative value of 1.34×10^{-5} m^2·s^{-1} has been used.

Following Pais et al. (1988), the local Nusselt number on a smooth NACA 0012 airfoil (which shall be used to approximate the characteristics of the Fokker F-28 wing) over a Reynold's number range of $7.6 \times 10^5 \le \text{Re}_C \le 2.0 \times 10^6$ can be approximated by

$$2.4 \leq \frac{Nu_C}{\sqrt{Re_C}} \leq 4.2 \tag{19}$$

over the first 5% of the airfoil surface at an angle of attack of 0°, and by

$$2.2 \leq \frac{Nu_C}{\sqrt{Re_C}} \leq 3.4 \tag{20}$$

near the 17% point (which will be assumed to be representative near the 25% point as well).

The wing Reynold's numbers for the three representative airspeeds chosen earlier (10, 30 and 50 m·s⁻¹) are 2.61×10^6, 7.84×10^6 and 1.31×10^7 respectively. Since the latter two Reynold's numbers do not fall within the range of application of Eqns. 19 or 20, another attempt has been made to estimate the appropriate values over the first 5% of the airfoil. For the purposes of estimating the local convective heat transfer coefficient, the forward several percent of the wing's surface may be represented approximately by the front half of a cylinder with diameter $D = 0.25$ m. The local convective heat transfer coefficient over the cylinder is then:

$$h_D = \frac{k_a Nu_D}{D} \tag{21}$$

with the cylinder Nusselt number Nu_D related to the cylinder Reynold's number, in turn given by:

$$Re_D = \frac{V_\infty D}{\nu_\infty} . \tag{22}$$

The values of the cylinder Reynold's numbers for the three airspeeds are $Re_D = 1.86 \times 10^5$, 5.60×10^5, and 9.36×10^5 respectively. Žukauskas and Žiugžda (1985) give the following relationships between cylinder Reynold's numbers and cylinder Nusselt number for flow over the appropriate portions of a smooth cylinder:

$$0.6 \leq \frac{Nu_D}{\sqrt{Re_D}} \leq 1.0 \tag{23}$$

for $Re_D = 1.86 \times 10^5$, and

$$1.05 \leq \frac{\mathrm{Nu_D}}{\sqrt{\mathrm{Re_D}}} \leq 1.4 \tag{24}$$

for $\mathrm{Re_D} = 7.7 \times 10^5$. The values for flow over a rough cylinder tend to be at least 2 to 3 times higher.

Two other quantities require calculation before Eq. 4 can be evaluated. The mass concentration of the snowflakes in the air C_s may be estimated from the visibility data of Section 2. During the time of take-off, the visibility was estimated to be 3000 ft by the transmissometer and 1980 ft by the AES observer. Using a mean value of about 2500 ft, and the relationship between visibility and mass concentration given by Stallabrass (1987):

$$C_s = 0.286 \, V^{-1.286} \tag{25}$$

for C_s in g·m^{-3} and V in km, we obtain a value for the mass concentration of $C_s = 4.06 \times 10^{-4}$ kg·m^{-3}.

The other quantity requiring estimation is the local collision efficiency of the wing for snowflakes, β. Very little information is available regarding the collision efficiency of snowflakes with objects such as wings. However, King (1985) has been able to demonstrate that snowflake trajectories in the vicinity of the disturbed airflow around an aircraft wing or fuselage may be approximated by the trajectories of appropriately-sized droplets. It appears that the relationship between the droplet and snowflake sizes is related to their terminal velocity in air. Noting that the largest snowflakes in a study by Mellor and Mellor (1988) tended to have terminal velocities in the vicinity of 1.3 m·s^{-1}, and that water droplets of diameter 300 µm fall at about that same speed, the numerical model described in Oleskiw (1982) was used to calculate the trajectories of such droplets in the vicinity of a NACA 0012 airfoil under conditions equivalent to those during the take-off roll of C-FONF. These simulations indicated that for an airfoil of 3.5 m chord, in an airflow at a temperature of 0°C and a pressure of 97.1 kPa, the collision efficiencies at 10, 30 and 50 m·s^{-1} would be 25%, 31% and 32% respectively at a position about 0.03 C (ie. at a distance of about 3% of the chord length rearward from the nose. Further, it was determined that the droplets (and thus, by inference, the snowflakes) would not impact any further back along the wing than 0.19 C. Thus, the collision efficiency at 0.25 C would be 0%.

3.3 Evaluating the Heat Balance Equation

The derived values of the various terms in Eqns. 4 and 5 for each of the three airspeeds and each of the two positions along the wing surface are displayed in Table 5. Column 1 indexes the rows by Case Number. Columns 2 and 3 indicate the airspeed (V_∞) and the

Table 5.   Derivation of the time required to freeze the layer of precipitation on the wings of C-FONF at various speeds during the takeoff roll and at two positions along the wing's surface.

CASE	CASE PARAMS. V_∞ ($m \cdot s^{-1}$)	X/C	CONVECT. HEAT TRANSFER COEFF. h ($W \cdot m^{-2} \cdot K^{-1}$)	SNOW MASS FLUX I ($kg \cdot m^{-2} \cdot s^{-1}$)	PROPERTIES OF AIRFLOW JUST OUTSIDE BOUNDARY LAYER p_a (kPa)	V_a ($m \cdot s^{-1}$)	t_a (°C)	CONTRIBUTING HEAT FLUX TERMS q_c ($W \cdot m^{-2}$)	q_e ($W \cdot m^{-2}$)	$- q_v$ ($W \cdot m^{-2}$)	$- q_k$ ($W \cdot m^{-2}$)	$- q_m$ ($W \cdot m^{-2}$)	$- q_s$ ($W \cdot m^{-2}$)	NET HEAT FLUX q_f ($W \cdot m^{-2}$)	TIME TO TOTALLY FREEZE PRECIP. LAYER τ (s)
1	10	0.03	35	1.02×10^{-3}	96.97	18.9	0.27	-9.45	52.7	-5.3	-0.1	-33.9	-0.1	3.85	4800
2	30	0.03	88	3.78×10^{-3}	96.46	44.5	-0.14	12.3	133.2	-73.9	-1.7	-126.3	-0.1	-56.50	-
3	50	0.03	114	6.50×10^{-3}	95.27	74.3	-1.11	126.2	174.8	-282.1	-8.1	-217.1	-0.1	-206.40	-
4	10	0.25	30	0	97.09	13.1	0.37	-11.1	45.2	-2.2	0	0	-0.1	31.80	574
5	30	0.25	52	0	96.74	39.1	0.09	-4.4	78.9	-35.7	0	0	-0.1	38.70	471
6	50	0.25	67	0	96.05	65.3	-0.48	32.1	101.9	-128.4	0	0	-0.1	5.50	316
7	67	0.03	132	6.80×10^{-3}	83.21	167.9	-11.4	1499.1	230.8	-1661.7	-15.3	-227.1	-0.1	-174.30	-

fractional distance along the chord from the nose, respectively. Column 4 shows the convective heat transfer coefficient from Eq. 17 (h_c) or Eq. 21 (h_D). Column 5 indicates the mass flux of accreting snowflakes (I), while Columns 6, 7 and 8 indicate the air pressure, air velocity and air temperature just outside the boundary layer (p_a, V_a and t_a respectively). The terms q_c, q_e, $-q_v$, $-q_k$, $-q_m$ and $-q_s$ (which contribute to the net heat flux) are given in Columns 9 through 14. Column 15 shows the net heat flux (q_f) obtained from the sum of Columns 9 through 14 while Column 16 indicates the time (τ) required to freeze the water fraction of the precipitation layer.

Beginning with Case 1 (10 m·s⁻¹ and $X/C = 0.03$), the convective heat transfer coefficients predicted from Eqns. 17 and 21 are $h_c = 36.7$ W·m⁻²·K⁻¹ and $h_D = 33.3$ W·m⁻²·K⁻¹ respectively. The good agreement between these values appears to validate the approach of using a cylinder to approximate the leading edge of the wing for the purposes of obtaining appropriate convective heat transfer coefficients. Since the air temperature outside the boundary layer remains above freezing (0.27°C), the convective heat transfer (q_c) is negative. While there is significant cooling by evaporation (q_e), it is offset to a large extent by the sum of the frictional heating of the boundary layer (q_v) and the heat released by the freezing of the incoming partially-melted snowflakes (q_m). Both the kinetic energy released by the impacting snowflakes (q_k) and the heat added by long-wave radiation (q_s) make very small contributions to the overall heat balance. The net result (q_f) is an extremely slow rate of cooling at this point on the airfoil.

Case 2 (30 m·s⁻¹ and $X/C = 0.03$) shows that the local air temperature would be reduced below freezing, thus creating some convective cooling (q_c). The evaporative cooling (q_e) is also increased, but almost exactly offset by the heat released by the freezing of the incoming snowflakes (q_m). The other significant heat source is the frictional heating of the boundary layer. The net result in this case is thus a consistent rate of heating at the precipitation layer.

In Case 3 (50 m·s⁻¹ and $X/C = 0.03$), the air temperature outside the boundary layer has cooled adiabatically to -1.11°C, significantly increasing the convective cooling (q_c). The greater airspeed has also increased the evaporative cooling (q_e) from Case 2. The much greater heat load imposed by the frictional heating (q_v) of the boundary layer and by the influx of partially-melted snowflakes (q_m), however, results in a large overall heat gain. The temperature of the precipitation layer at this speed is predicted to increase with time.

Moving to a point on the wing further back from the leading edge (Case 4, 10 m·s⁻¹ and $X/C = 0.25$), there is no mass flux of accreting snowflakes because the flakes do not impinge upon the airfoil this far back from the leading edge. As a result, there is no kinetic energy converted to heat (q_k) or heat released from freezing (q_m) of the snowflakes. Because of the relatively low airspeed at this point (13.1 m·s⁻¹ versus the freestream value of 10.0 m·s⁻¹), the temperature just outside the boundary layer remains above freezing (0.37°C), and thus the convective heat transfer (q_c) is negative. Other

contributions to the heat transfer equation are small, and thus the net cooling (q_f) is small but positive. The time required to freeze the layer, however, remains very long.

Case 5 (30 m·s^{-1} and $X/C = 0.25$) is very similar in net effect to Case 4. The evaporative cooling (q_e) and frictional heating (q_v) of the boundary layer are greater than in the previous case, but the convective heat transfer (q_c) remains negative because of the air temperature outside the boundary layer which remains just above freezing. Again, the time required to freeze the layer at this airspeed is very long.

With the higher speeds of Case 6 (50 m·s^{-1} and $X/C = 0.25$), the air temperature just outside the boundary layer once again goes negative (-0.48°C), and thus some convective cooling (q_c) takes place. This cooling plus the evaporative cooling (q_e) are almost exactly offset by the frictional energy (q_v) added to the boundary layer. The net effect (q_f) is almost no heating or cooling of the precipitation layer.

Finally, in order to determine if conditions on the wing would change significantly when the aircraft rotated at an airspeed of about 130 kt, another set of calculations (Case 7) was made using the pressure coefficient distribution provided by Fokker for an angle of attack of $\alpha = 5°$ (67 m·s^{-1} and $X/C = 0.03$). The high airspeed near the point of minimum aerodynamic pressure (167.9 m·s^{-1} as compared to the freestream value of 67 m·s^{-1}) led to significant cooling of the airflow just outside the boundary layer (to -11.4°C) and thus to a high convective heat transfer (q_c). However this high value was more than offset by an even higher heat input from the frictional heating (q_v) of the boundary layer. The high evaporative cooling (q_e) was almost exactly matched by the heat released by the freezing of the melted fraction of the incoming snowflakes (q_m). As a result, the net effect (q_f) was a continued heating of the precipitation layer under these conditions.

The calculations of this section have demonstrated that under the assumptions that have been adopted, it does not appear that sufficient cooling would have been available during the take-off run of the Fokker F-28 at Dryden to have had any significant impact upon the state of the precipitation layer accumulated on the upper surface of the wing. In general, the adiabatic cooling of the air just outside of the boundary layer plus the evaporative cooling caused by less than saturated air are more or less offset by the frictional heating of the boundary layer in combination with the heat required to freeze the partially-melted snowflakes impacting on the wing.

Only two potentially significant heat transfers have been omitted from this analysis. Any solar radiation which might have penetrated the cloud layer and precipitation would have contributed still more heating to the accumulated precipitation. Conduction of heat into the wing, on the other hand, could have contributed to the cooling of the layer, and thus will be investigated in the next section.

4.0 CONDUCTION OF HEAT INTO THE WING FUEL TANKS

In order to estimate the effect of heat conduction into the wing of the aircraft from the layer of precipitation which accumulated during the station-stop of C-FONF at Dryden, it is necessary to realize that the wing of the Fokker F-28 contains integral fuel tanks which wet the wing skin for most of the length of the wings. These tanks are situated between wing spars located at about 12% and 56% of the wing chord back from the wing's leading edge. For the purposes of calculating heat transfers in to and out of the precipitation layer, it is thus essential to be able to determine the temperature of the fuel in the wing tanks both before and after the refuelling at Dryden. The temperature of fuel before refuelling would have been influenced primarily by: the temperature of the fuel stored in the tanks during the previous night; the temperature of the fuel which was loaded into the aircraft at various refuelling stops that morning; and by the cooling of the fuel during flight at altitudes where the outside air temperature was significantly cooler than near the ground. The temperature of the fuel after refuelling would have also been influenced by the temperature of the fuel added during refuelling at Dryden. We shall begin this section by estimating the wing tank fuel temperatures during the station-stop at Dryden.

4.1 Estimating Wing Tank Fuel Temperatures During C-FONF's Stop at Dryden

During 1989 April 5 and 6, Mr. Garry Cooke of the TSBC Winnipeg office undertook a set of measurements in Dryden at the direction of Mr. Dave Rohrer of the Inquiry staff. These measurements are reproduced in Table 6.

Column 1 of Table 6 shows the date and time of the measured outside air temperatures. The fuel tender temperatures are displayed in Columns 2 and 3 respectively. The variation of outside air temperature over the approximately 24 h period of the measurements shows the typical diurnal variation which would be expected. The data of Column 3 indicate that the fuel tender temperature also exhibits a diurnal variation, but of lesser magnitude than that of the outside air temperature. Additionally, the diurnal cycle of the fuel temperature appears to be delayed by perhaps two hours. Both these effects are expected because of the relatively poor conductivity of the fuel, and the fact that the temperature of this volume of fuel is being changed primarily by conduction through the skin of the fuel tank as well as by convection in the fuel and in the outside air. From these data, it may be generalized that under outside air temperature variations similar to those measured during this experiment, the tank temperature in the early morning (when the outside air temperature is near its minimum) would likely be about 2°C warmer than ambient, whereas several hours later in the morning, it would likely be 2 to 3°C colder than ambient. An important assumption in these estimates is that there would be no significant solar radiation at this time of day to cause additional heating of the tank. Since, according to information provided by Mr. Dave Rohrer, the fuel at Winnipeg and Thunder Bay is also stored in above-ground tanks, we shall assume that the above relationship between outside air temperature and fuel temperature can be

Table 6. Outside air and fuel tender temperatures at Dryden, Ontario on 1989 April 5 and April 6.

DATE AND TIME	OUTSIDE AIR TEMPERATURE	FUEL TENDER TEMPERATURE
(CST)	(°C)	(°C)
April 5 16:00	7.5	3.2
April 5 19:00	2.0	2.2
April 5 22:00	-2.0	0.0
April 6 06:15	-8.0	-5.0
April 6 09:15	-3.0	-3.5
April 6 12:15	1.5	-1.5
April 6 15:15	3.0	0.5

applied for the fuel loaded from those facilities as well.

The next step is to estimate the rate of cooling of the fuel in the Fokker F-28's wing fuel tanks during flight at altitude. Three sources of information on this subject have been consulted to aid in this determination.

Walker (1952) displays the fuel temperature in the wings of a de Havilland Comet measured during a flight at near 450 mph at an ambient air temperature of about -60°C. The fuel temperature begins at near 15°C, and decreases initially, upon ascent to altitude, at a rate of about $20°C \cdot h^{-1}$.

Mr. G.L. Borst of Propulsion Engineering, Renton Division, Boeing Commercial Airplanes has provided similar curves of the variation with time of the main wing tank fuel temperature during the flight of a Boeing 757-200 aircraft. Utilizing a temperature difference between initial tank temperature and outside air temperature during flight of about 50°C, leads to an estimate of the initial rate of change of fuel temperature of near $15°C \cdot h^{-1}$.

Mr. R. Jellema, Manager Fleet Airworthiness, Engineering Department, Fokker Aircraft has stated that the limited F-28 fuel cooling records available indicate a maximum cooling rate of the fuel in the wing tanks of about $15°C \cdot h^{-1}$. He has also provided the following relationship using the total air temperature at altitude (t_T) and the initial fuel temperature before flight (t_{f_i}) to predict the fuel temperature (t_{f_τ}) during flight at altitude of duration τ_a:

$$t_{f\tau} = t_T + (t_{fi} - t_T) e^{-\tau_c/2} \ . \tag{26}$$

For an initial temperature difference $(t_{fi} - t_T)$ of 50°C, the fuel temperature predicted by this equation drops by about 25°C during the first hour. Since this equation appears to give results similar to the others reported above, it will be utilized to predict the cooling of the fuel within the wing tanks of the Fokker F-28.

During an experiment performed by Mr. Dave Rohrer and Mr. Ron Coleman of the TSBC on 1989 April 14, the temperatures of various parameters relating to the fuel tank temperatures of the Fokker F-28 were measured at several station-stops (Dryden, YHD; Thunder Bay, YQT; and Sault Ste. Marie, YAM) during a flight from Winnipeg (YWG) to Toronto (YYZ). In order to verify the utility of Eq. 26 for the prediction of fuel temperatures as a result of flight at altitude, the data from this experiment are presented in Table 7.

Column 1 of Table 7 indicates the location and relative time of the measurements which follow. Columns 2 and 3 show the duration and temperature of flight segments at cruise altitude. Columns 4 and 5 display the quantity and temperature of the fuel uploaded into the aircraft at a given station-stop (if applicable). Column 6 gives the quantity of fuel in the F-28's wing fuel tanks just prior to take-off or upon landing. Column 7 exhibits the fuel temperature measured by draining a small amount of fuel from the wing drain valve nearest the fuselage of the aircraft. Column 8 indicates the fuel temperature predicted through the use of Eq. 26 for flight segments, and the "law of mixtures" (Eq. 27) after refuelling. If two liquids of mass m_1 and m_2 and initial absolute temperatures t_1 and t_2 (K) respectively, are well mixed together, then the absolute temperature (K) of the resulting mixture is given by:

$$t_m = \frac{(t_1 m_1 + t_2 m_2)}{m_1 + m_2} \ . \tag{27}$$

Column 9 of Table 7 shows the temperature of the fuel in the tanks deduced from the temperature measured on the wing's lower surface nearest the fuselage. These data have been displayed because it seems significant that the temperatures measured at this location are consistently colder than the measured fuel temperature in Column 7. This may indicate that the fuel temperature displayed in Column 7 is not really representative of the fuel in the tanks. This particular location was chosen because the interior of the wing's skin is always in contact with the fuel in the wing tank at this location. It should also respond rapidly to changes in fuel temperature as a result of refuelling. A "correction" of up to 2°C was applied to the measured skin temperature when the significant difference between the skin temperature and the air temperature was believed to be influencing how well the skin temperature at this point was indicating the fuel

Table 7. Prediction of fuel tank temperatures at various station-stops of a Fokker F-28 flight from Winnipeg to Toronto on 1989 April 16.

LOCATION & COMMENTS	FLIGHT		REFUELLING FUEL		WING TANK FUEL			WING TANK FUEL DEDUCED FROM LOWER SURFACE	
	TIME	AIR TEMP.	WEIGHT	TEMP.	WEIGHT	MEAS. TEMP.	CALC. TEMP.	MEAS. TEMP.	CALC. TEMP.
	(min)	(°C)	(lb)	(°C)	(lb)	(°C)	(°C)	(°C)	(°C)
WPG - prior to departure					14000	10	-	4	-
Flight leg	10	-10							
YHD - upon arrival					11600	8	8.4	3	2.9
Flight leg	10	-15							
YQT - upon arrival					8700	6	6.1	1.5	1.6
Refuelling			5300	8					
YQT - prior to departure					14000	6	6.8	1.5	2.3
Flight leg	16	-24							
YAM - upon arrival					9900	2	3.0	-3	-1.0
Refuelling			1100	3					
YAM - prior to departure					11000	2	3.0	-4	-0.6
Flight leg	21	-23							
YYZ - upon arrival					6200	0	-1.2	-2	-3.2

temperature. Finally, Column 10 displays the fuel temperature predicted through the use of Eq. 26 for flight segments, and Eq. 27 after refuelling. The difference between Columns 8 and 10 is that the former is initiated upon the measured wing tank temperature, whereas the latter is initiated upon the wing tank temperature deduced from the lower wing surface temperature measurement.

Inspection of the data presented in Table 7 reveals that the calculated fuel temperatures in Columns 8 and 10 are reasonably representative of the fuel temperatures measured or estimated in Columns 7 and 9 respectively. This suggests that Eqns. 26 and 27 are appropriate means of estimating fuel temperatures in the wing tanks of the Fokker F-28.

Turning now to the flight of C-FONF on 1989 March 10, Table 8 displays the data used to predict the temperature of the fuel in the wing tanks during the station-stop at Dryden. Column 1 gives the location and approximate time for the entries which follow. Columns 2 and 3 indicate the duration and temperature of flight segments at cruise altitude. Column 4 shows the air temperature observed during the station-stop. Columns 5 and 6 exhibit the quantity and estimated temperature of the fuel uploaded to or downloaded from the aircraft's fuel tanks at a given station-stop (if applicable). These temperatures have been estimated by adjusting the measured air temperature by the relationships deduced from the data of Table 6. Finally, Columns 7 and 8 display the quantity and temperature in the F-28's wing tanks. Column 8's estimates are initialized with the predicted fuel temperature at Winnipeg, and are based upon subsequent calculations of cooling at cruise altitude by Eq. 26 and mixing during refuelling by Eq. 27.

The refuelling fuel temperature (Column 4 of Table 8) at Winnipeg (YWG) has been estimated at 0°C because the measured air temperature was steady near 0°C overnight. The fuel uploaded at Thunder Bay (YQT) was predicted to be at near -5°C based upon a minimum temperature of -7.8°C several hours earlier and an air temperature of near -3°C during the refuelling. Finally, the temperature of the fuel in the refuelling truck at Dryden was approximated by 0°C as a result of the small difference between the overnight minimum temperature (-2.3°C) and the air temperature at the time of refuelling (1.0°C). The last column in Table 8 reveals that the predicted fuel temperature in the wing tanks cooled consistently during the flight segments after departure from Winnipeg until refuelling at Dryden. In general, the fuel tank temperatures were predicted to be within about 1.5°C of the outside air temperatures at all station stops prior to the final stop at Dryden. The 3500 lb of 0°C fuel uploaded at Dryden likely warmed the wing tank temperature to about -4.7°C from the estimated -6.4°C prior to refuelling. Both of these temperatures were significantly below the ambient air temperature of between 1.0 and 0.4°C.

Table 8. Prediction of fuel tank temperatures during the flight segments of Fokker F-28 C-FONF on 1989 March 10.

LOCATION & TIME (UTC)	FLIGHT TIME (min)	FLIGHT AIR TEMP. (°C)	STATION STOP AIR TEMP. (°C)	REFUELLING FUEL WEIGHT (lb)	REFUELLING FUEL TEMP. (°C)	WING TANK FUEL WEIGHT (lb)	WING TANK FUEL TEMP. (°C)
YWG: Refuelling			0.1	7100	0		
YWG: 13:30 - Prior to departure			0.1			16000	0.0
Flight leg	7	-27					
YHD: 14:19 - Upon arrival			-1.8			12800	-1.5
Flight leg	9	-27					
YQT: 15:32 - Upon arrival			-4.2			9600	-3.3
YQT: Refuelling			-3	6000	-5		
YQT: After Refuelling						15600	-4.0
YQT: Download fuel			-3	-2800	-4.0		
YQT: 16:55 - Prior to departure			-2.6			12800	-4.0
Flight leg	13	-27					
YHD: 17:40 - Upon arrival			1.0			9500	-6.4
YHD: 17:45 - Refuelling			1.0	3500	0		
YHD: 18:10 - Prior to departure			0.4			13000	-4.7

4.2 Evaluating the Rate of Freezing of the Precipitation Layer

With a knowledge of the likely fuel tank temperature while C-FONF was on the ground at Dryden, we are now ready to evaluate the heat flux terms in Eq. 4 to determine the net heat flux, and from this, the time required to freeze the water in the precipitation layer.

It was explained in Section 3 that since the precipitation layer was formed by falling wet snowflakes, it must have been at the freezing temperature as it was being formed. Thus for the first term in Eq. 4, $q_a = 0$. The wind speeds recorded by the AES observer between 17:40 and 18:10 UTC varied between 0 and 4 kt. Using this latter value (equivalent to about 2 m·s^{-1}), it becomes apparent from comparison to values in Table 5 that at such low wind speeds, the third, fourth and sixth terms (q_v, q_k and q_s, respectively) are all near zero.

Between 17:40 and 18:00 UTC, the water-equivalent precipitation rates estimated from the transmissometer's measurements and "corrected" through the use of the procedure of Section 2, were between 0.02 and 0.22 mm·h^{-1}. Between 18:00 and 18:10 UTC, these precipitation rates are believed to have varied between 1.1 and 4.5 mm·h^{-1}. These four values are equivalent to mass fluxes of 5.6×10^{-6}, 6.1×10^{-5}, 3.1×10^{-4} and 1.3×10^{-3} kg·m^{-2}·s^{-1}. Utilizing Eq. 12, the heat released in freezing these partially-melted snowflakes (q_m) is thus 0.2, 2.0, 10.4 and 41.8 J·m^{-2}·s^{-1} respectively.

With a wind speed of 2 m·s^{-1} and thus a wing Reynold's number of $Re_c = 5.2 \times 10^5$, Eq. 20 may be used to determine the wing Nusselt Number ($Nu_c = 1950$). From Eq. 17 we can then calculate the value of the convective heat transfer coefficient ($h_C = 13.4$ W·m^{-2}·K^{-1}). Since the Dryden air temperature was observed to be near 0.7°C during the period of heaviest snowfall, Eq. 14 leads us to an estimate of the value of the convective heat flux for this wind speed and temperature ($q_c = -9.4$ J·m^{-2}·s^{-1}).

The Dryden dew point temperature at 18:00 UTC was noted to be -3.0°C. Using Eq. 16 gives an estimate of the evaporative heat flux ($q_e = 25.8$ J·m^{-2}·s^{-1}).

Finally, the flux of heat conducted into the wing of the aircraft may be estimated with the following relationship:

$$q_i = \frac{t_p - t_f}{\dfrac{T_p}{2k_p} + \dfrac{T_s}{k_s} + \dfrac{T_f}{2k_f}} \tag{28}$$

where t_p and t_f are the temperatures of the precipitation layer (0°C) and the wing tank fuel (-4.7°C) respectively. The thicknesses of the precipitation layer, the aluminum skin of the wing and a suitable volume of tank fuel are given by T_p, T_s and T_f respectively. The thermal conductivity of the three layers are represented by k_p, k_s and k_f respectively.

In Eq. 28, the conduction is assumed to occur between the midpoints of the two outer layers.

Since it was assumed above that the density of the precipitation layer was 400 kg·m^{-3}, then the thickness of the near 0.55 kg·m^{-2} layer of precipitation as estimated in Section 2 would have been T_p = 1.38 mm of wet snow. The thermal conductivity of snow has been taken to be k_p = 0.47 W·m^{-1}·K^{-1}. The thickness of the aluminum skin used in these calculations is T_s = 4 mm. Since the thermal conductivity of the aluminum, estimated at k_s = 138 W·m^{-1}·K^{-1} (see, for example, the SAE Aerospace Applied Thermodynamics Manual), is so much greater than that of the snow or the fuel, this thickness estimate will play little part in the accuracy of the overall calculation of conductive heat flux.

It is necessary to ensure that the fuel layer is sufficiently thick that it is able to absorb the heat which might be transferred to it from the precipitation layer without significantly changing its mean temperature. Assuming again that 10% of the precipitation layer is water and the remainder snow, then the heat per unit area which must be removed to freeze the water is equal to the product of: the melted fraction of snow (0.1); the latent heat of fusion (L_f = 3.34×10^5 J·kg^{-1}); and the mass per unit area of the precipitation layer (0.55 kg·m^{-2}). This product is equal to 1.84×10^4 J·m^{-2}. Now, since the specific heat capacity of JP4 fuel is c_p = 1.93×10^3 J·kg^{-1}·K^{-1}, and the density of JP4 is approximately 789 kg·m^{-3}, then the thickness of a layer of fuel which will be warmed by 1°C in absorbing the heat from the freezing of the precipitation layer will be T_f = 12 mm. The thermal conductivity of JP4 has been taken to be k_f = 0.14 W·m^{-1}·K^{-1} (see, for example, Kays and Crawford, 1980). In addition to the layers mentioned above, there is also a layer of plastic-like material which lines the inside of the F-28's wing fuel tanks. Since this layer is likely on the order of 5 mm or less, and since the thermal conductivity of this layer is likely near that of Nylon or Teflon (both having the same conductivity as the JP4 fuel), this layer will have only a small effect upon the thermal heat flux between the precipitation layer and the fuel. Inserting all of the appropriate values from above into Eq. 28 gives a conductive heat flux of q_i = 106 J·m^{-2}·s^{-1}.

All of the above heat flux terms may now be utilized to solve for the net heat flux into or out of the precipitation layer. These data are displayed in Table 9. Column 2 of this table displays the water-equivalent snowfall rates representative of the ranges between 17:40 to 18:00 UTC and between 18:00 and 18:10 UTC. Column 3 gives the assumed water fraction of the precipitation layer formed by the accumulation of falling wet snowflakes. Columns 4 through 7 exhibit the values of the heat flux terms which contribute to the net heat flux. Column 8 shows the net heat flux while the time estimated to completely freeze the water fraction of the wet snow in the precipitation layer is given in Column 9.

As the mass flux of the falling wet snowflakes increases from 5.6×10^{-5} kg·m^{-2}·s^{-1} to 1.3×10^{-3} kg·m^{-2}·s^{-1} (Case 8 through Case 11), the heat which must be extracted to freeze the water fraction of the incoming wet snowflakes increases (Column 4 of Table 9).

Table 9. Derivation of the time required to freeze the layer of precipitation on the wings of C-FONF as a result of various snowfall rates and estimates of the initial water fraction of the layer.

CASE	PRECIP. RATE	INITIAL WATER FRACTION OF LAYER	CONTRIBUTING HEAT FLUX TERMS				NET HEAT FLUX	TIME TO TOTALLY FREEZE PRECIP. LAYER
	R	k_m	q_m	q_c	q_e	q_i	q_f	τ
	(mm h^{-1} water equiv.)		(W·m^{-2})	(W·m^{-2})	(W·m^{-2})	(W·m^{-2})	(W·m^{-2})	(s)
8	0.02	0.1	-0.2	-9.4	25.8	106	122.20	151
9	0.22	0.1	-2.0	-9.4	25.8	106	120.40	153
10	1.1	0.1	-10.4	-9.4	25.8	106	112.00	165
11	4.5	0.1	-41.8	-9.4	25.8	106	80.60	229
12	2.7	0.1	-25.4	-9.4	25.8	106	97.00	190
13	2.7	0.2	-50.9	-9.4	25.8	53.9	19.40	1900
14	2.7	0.3	-76.3	-9.4	25.8	36.1	-23.80	-
15	2.7	0.1	-25.4	-9.4	25.8	53.9	44.90	411
16	2.7	0.1	-25.4	-9.4	25.8	36.1	27.10	681

With all of the other heat flux terms remaining constant for these cases, the predicted net heat flux gradually decreases. This results in increasing estimates of the time required to totally freeze the water fraction of the precipitation layer. However, the longest time required (Case 11, 229 s), is still significantly shorter than the 600 s period between the commencement of heavier snowfall (18:00 UTC) and the approximate time of take-off (18:10 UTC).

In order to provide a baseline for the other cases which follow, another set of calculations was performed (Case 12). Here the water-equivalent snowfall rate was chosen to be the mean value (2.7 mm·h^{-1}) over the time interval 18:00 to 18:10 UTC. The time required to freeze the layer is estimated at 190 s.

In an effort to evaluate the sensitivity of the predicted time to freeze the water fraction of the precipitation layer to changes in the estimated water fraction of the falling snowflakes, another two sets of calculations (Cases 13 and 14) were performed. In

Case 13, it was assumed that the falling snowflakes were 20% water by mass. As a result of the doubled heat required to freeze the greater water fraction of the falling wet snowflakes, the net heat flux decreased to 19.4 $J \cdot m^{-2} \cdot s^{-1}$ and the time required to freeze the precipitation layer rose significantly to 1900 s. A water fraction of 0.3 (Case 14) led to a net heat flux of -23.8 $J \cdot m^{-2} \cdot s^{-1}$. These two cases demonstrate that as the water fraction of the falling snowflakes increases, this not only increases the heat which must be removed to freeze the falling flakes, it also increases the heat needed to be removed to freeze the precipitation layer. The combination of effects leads to a very rapidly increasing time to freeze the precipitation layer, eventually resulting in a predicted inability of the wing tank fuel to remove enough of the heat from the precipitation layer to allow it to freeze at all.

Finally, in order to determine the effect upon these calculations of an increase in the total thickness of the precipitation layer, Case 12 was repeated with layers of doubled and tripled thickness (Cases 15 and 16). In the first of these two cases, as a result of the increased amount of heat which must be transferred to the wing tank fuel, the thickness of the fuel layer must be increased to maintain a small increase of temperature as a result of this heat transfer. This results in an approximately 50% decrease in the conductive heat flux (Column 8). The net heat flux is thus 44.9 $J \cdot m^{-2} \cdot s^{-1}$ and the time to freeze the precipitation layer increases to 411 s from 190 s. In the final set of calculations (Case 16), the thickness of the fuel layer which absorbs the heat from the precipitation layer is increased yet again. This further reduces the net heat flux, and results in an estimate of the time to freeze the water fraction of the precipitation layer of 681 s.

From these cases, it is evident that increasing the assumed water fraction of the falling wet snowflakes dramatically increases the time required to freeze the precipitation layer. In fact, with a snowflake water fraction of 0.3, there would no longer be conduction of heat from the precipitation layer to the wing fuel tanks, and the water in the wet snow would not freeze at all. On the other hand, increasing the depth of the precipitation layer from about 1.4 to 4.1 mm of wet snow increases the time to freeze the precipitation layer significantly, but would still allow most of the layer to freeze in the 600 s interval during the heavier snowfall (18:00 to 18:10 UTC). Further increases in the precipitation layer thickness would permit only some lower fraction of the layer to freeze, with the upper portion remaining wet snow.

5.0 DISCUSSION AND SUMMARY

The estimated thickness of wet snow which would have accumulated on the wings of C-FONF during its station-stop at Dryden on 1989 March 10 is 1.38 mm. This value has been determined from analyses of the visibility data recorded by the AES observer at the Dryden Airport, and by a transmissometer located near the runway. The relationship used to estimate precipitation rate from visibility is an empirical one, and the data from which it was derived show considerable scatter. The main uncertainty in the relationship

is due to the variation in terminal velocity of the snowflakes because of variations in their size and wetness (and thus density). Since the relationship has been derived for "normal" snow, it may be expected that if the snowflakes are wet, then they will fall faster than "normal". This would permit the snowflakes to accumulate more quickly at the ground than would "normal" snowflakes, while obstructing the visibility to the same extent. Therefore, it is expected that despite the efforts in Section 2 to "calibrate" the visibility to precipitation rate relationship, unusually wet snowflakes may have contributed to a greater depth of precipitation than that estimated above.

The extensive calculations described in Section 3 lead to the conclusion that an insufficient amount of cooling to freeze the precipitation layer would have been provided by the mechanisms of: adiabatic cooling of the air as it accelerated over the wing; and evaporative cooling as a result of the comparatively dry air near the ground at the time of take-off. In general, the adiabatic cooling of the air just outside of the boundary layer plus the evaporative cooling caused by less than saturated air were more or less offset by the frictional heating of the boundary layer in combination with the heat required to freeze the partially-melted snowflakes impacting on the wing. Any impinging snowflakes during the take-off roll would thus have likely met a partially wetted precipitation layer surface, and this fact, in combination with the fact that the snowflakes themselves would likely have been somewhat wet, leads to the conclusion that many of these snowflakes would have stuck to the forward portions of the precipitation layer during the take-off roll.

The investigation of the contribution of the conductive heat flux from the precipitation layer on the wing to the wing fuel tanks shows that, under certain circumstances and in combination with the other heat flux terms, sufficient cooling might have resulted in a complete freezing of the water fraction of the precipitation layer during the 10 min interval of the heavier snowfall rate while the aircraft was on the ground (18:00 to 18:10 UTC). The assumed value of the falling snowflake's water fraction has been shown to significantly alter the time required to freeze the precipitation layer. The thickness of the precipitation layer has also exhibited a strong influence upon the freezing time. Given that the depth of the wet snow on the wings was likely greater than the best estimate of 1.38 mm calculated from the available data, it seems probable that the heat conduction into the wing fuel tanks would have permitted a lower portion of the water in the wet snow layer to have frozen, while leaving some upper portion in a partially liquid state. Because the density of the wet snow was between that of dry snow (100 kg·m^{-3}) and ice (near 920 kg·m^{-3}), this layer was composed of a lattice of deformed and coagulated ice crystals interspersed with air pockets and water. As the water froze in the lower portion of this layer, it would likely have left a very rough interface between the lower and upper portions of the precipitation layer. As the aircraft rolled down the runway, the remaining water in the upper portion of the precipitation layer might have been forced to drain away, possibly carrying with it some of the ice in the upper portion of the layer. The resulting very rough surface on the wings could have had a significant impact on the aerodynamic performance of the aircraft. It is interesting to note that the

thermal conductivity of the aluminum skin of the aircraft is much greater than that of the wet snow, the air or the fuel in the wing tanks. As a result, the aluminum skin might have conducted heat away from the precipitation layer even further forward on the wing than the location of the wing spar forming the forward wall of the wing tanks. Thus the hypothesized rough precipitation layer surface may have extended forward to the more aerodynamically critical portions of the wing.

6.0 REFERENCES

Houghton, E. L. and Brock, A. E. 1970. Aerodynamics for Engineering Students. Second Edition. Edward Arnold (Publishers) Ltd., London.

Kays, W. M. and Crawford, M. E. 1980. Convective Heat and Mass Transfer. 2nd Edition. McGraw-Hill Book Company, New York, NY.

King, W. D. 1985. Air Flow and Particle Trajectories around Aircraft Fuselages. Part III: Extensions to Particles of Arbitrary Shape. Journal of Atmospheric and Oceanic Technology **2** (4): 539-547.

Makkonen, L. 1984. Modeling of Ice Accretion on Wires. Journal of Climate and Applied Meteorology **23** (6).

Makkonen, L. 1989. Estimation of Wet Snow Accretion on Structures. Cold Regions Science and Technology **17**: 83-88.

Mellor, M. and Mellor, A. 1988. Some Characteristics of Falling Snow. Cold Regions Science and Technology **15**: 201-206.

Oleskiw, M. M. 1982. A Computer Simulation of Time-Dependent Rime Icing on Airfoils. Ph.D. Thesis, University of Alberta, Edmonton.

Pais, M. R., Singh, S. N. and Zou, L. 1988. Determination of the Local Heat-Transfer Characterisitics on Simulated Smooth Glaze Ice Accretions on a NACA 0012 Airfoil. AIAA 26th Aerospace Sciences Meeting, Reno, Nevada, January 1988. American Institute of Aeronautics and Astronautics, Washington, D. C.

SAE Committee AC-9, Aircraft Environmental Systems, 1969. SAE Aerospace Applied Thermodynamics Manual. 2nd Edition. Society of Automotive Engineers, Inc., New York, NY.

Stallabrass, J. R. 1987. Measurements of the Concentration of Falling Snow. *In* Snow Property Measurement Workshop. Chateau Lake Louise, April, 1985. *Edited by* P. R. Kry. National Research Council Canada, Ottawa. pp. 389-410.

Walker, J. E. 1952. Fuel Systems for Turbine-Engined Aircraft. Journal of the Royal Aeronautical Society: 657-679.

Žukauskas, A. and Žiugžda, J. 1985. Heat Transfer of a Cylinder in Crossflow. *Translated by* E. Bagdonaite. *Edited by* G. F. Hewitt. Hemisphere Publishing Corporation, Washington, D. C.

REPORT DOCUMENTATION FORM/FORMULAIRE DE DOCUMENTATION DE RAPPORT

REPORT No./ NO DU RAPPORT 1 IME-CRE-TR-003	REPORT No./ NO DU RAPPORT 2 32124	SECURITY CLASSIFICATION/ CLASSIFICATION DE SECURITÉ 3 ___ Top Secret/Très secret
DISTRIBUTION/DIFFUSION ___ Controlled/Controlée 4 _XX_ Unlimited/Illimitée		___ Secret ___ Confidential/Confidentiel ___ Protected/Protégée _XX_ Unclassified/Non classifiée

DECLASSIFICATION: DATE OR REASON/DÉCLASSEMENT: DATE OU RAISON 5

TITLE, SUBTITLE/TITRE, SOUS-TITRE 6   Freezing Precipitation on Lifting Surfaces

AUTHOR(S)/AUTEUR(S) 7   M. M. Oleskiw

SERIES/SÉRIE 8   Technical Report

CORPORATE AUTHOR/PERFORMING ORGANIZATION/ AUTEUR D'ENTREPRISE/AGENCE D'EXÉCUTION   National Research Council of Canada 9   Institute for Mechanical Engineering

SPONSORING OR PARTICIPATING AGENCY/AGENCE DE SUBVENTION OU PARTICIPATION   Commission of Inquiry into the Air Ontario Crash at Dryden, Ontario 10   P.O. Box 687, Adelaide Station, Toronto, ON M5C 2J8

DATE 11 1991/09	FILE/DOSSIER 12 3741-4	SPECIAL CODE/ CODE SPÉCIALE 13 REA00	PAGES 14 31(vi)	FIGURES 15 0	REFERENCES 16 12

NOTES
 	
17   This report was requested by Mr. D. J. Langdon, Chief, Systems Engineering, Canadian Aviation
        Safety Board in a letter dated 1989 June 20. The request was made on behalf of Mr. J. Jackson,
        Investigator in Charge, Commission of Inquiry into the Air Ontario Crash at Dryden, Ontario

DESCRIPTORS (KEY WORDS)/MOTS-CLÉS 18   ICE, ICING, DEICE, DEICING, ANTIICING, SNOW, ATMOSPHERIC PRECIPITATION

SUMMARY/SOMMAIRE 19   Please see Abstract.

ADDRESS/ADDRESSE
        Dr. R.M.W. Frederking, Head
        Cold Regions Engineering
        Institute for Mechanical Engineering
        Montreal Road, Ottawa, K1A 0R6, Canada
20   (613) 993-2439

Appendix 7

Human Factors Aspects of the Air Ontario Crash at Dryden, Ontario: *Analysis and Recommendations to the Commission of Inquiry*

Robert L. Helmreich, Ph.D.

December 12, 1990

Human Factors Aspects of the Air Ontario Crash at Dryden, Ontario:
Analysis and Recommendations to the
Commission of Inquiry into the Air Ontario Crash at Dryden, Ontario

Robert L. Helmreich, Ph.D
NASA/University of Texas Aerospace Crew Research Project[1]

Austin, Texas
December 12, 1990

Introduction and Overview

At the request of the *Commission of Inquiry into the Air Ontario Crash at Dryden, Ontario*, evidence assembled in the course of investigation into the causes of the crash was examined in terms of human factors and organizational issues. Material reviewed included reports of the Operations Group and the Human Performance Group, interviews with relevant personnel, and sworn testimony presented before the Commission. When viewed from a research perspective, the body of facts suggests an operational environment that allowed an experienced crew to reach a flawed decision regarding the safety of take-off during snowfall with accumulating contamination of the aircraft's wings.

The absence of direct evidence from voice or flight recorders initially seems to be a serious hindrance to the investigative effort. In fact, the lack of this type of evidence has resulted in a more extensive exploration of broader issues, including regulatory and organizational factors than might otherwise have been conducted. Because of the depth of the investigation, the lessons to be gained from this in-depth investigation may prove to be of value for the governance of flight operations and the training of crews.

It may be useful to outline the background for the author's opinions. They grow out of more than twenty years experience conducting research into the multiple determinants of human behavior and performance under the sponsorship of agencies such as the National Science Foundation, the Office of Naval Research, the National Aeronautics and Space Administration, and the Federal Aviation Administration. Current investigations are under the auspices of the NASA/University of Texas Aerospace Crew Research Project, directed by the author. Included in the project are investigations of personality factors relative to pilot and Astronaut selection, group dynamics, aircraft characteristics such as automation, and organizational issues such as the development and influence of subcultures (Helmreich & Wilhelm, 1990; Helmreich, in press).

Another central element of the research is evaluation of the effectiveness of training in *Crew Resource Management* (*CRM*: Helmreich, 1991). *CRM* training is aimed at improving crew coordination, decision making, situational awareness, and interpersonal communications. It stresses the importance of utilizing all available resources inside and outside the cockpit and the development of an effective team including cabin crewmembers in the process. The

concept of *CRM* is becoming widely accepted and is an integral part of training in many organizations. Only recently, however, has empirical research demonstrated that such training can affect flightcrew behaviour (Helmreich, Chidester, Foushee, Gregorich, & Wilhelm, 1990; Helmreich, Wilhelm, Gregorich, & Chidester, 1990).

Underlying the research is the fact that the behaviour of flightcrews in any given situation is determined by a number of simultaneously operating factors. These include: 1) the regulatory environment - operational standards and supervision; 2) the organizational environment - the culture and behavioural norms of the organization including morale, policies and standards, organizational stability and change, and available resources; 3) the physical environment - meteorological and operating conditions and the aircraft, including its condition and capabilities; 4) the crew environment - interpersonal coordination and communications including cockpit, cabin, and ground personnel, and individual characteristics of crewmembers - training, experience, motivation, personality, attitudes, fatigue, and stress both from the immediate operational situation and significant personal life events (Foushee & Helmreich, 1988; Helmreich, 1990). Figure 1 shows graphically the environments surrounding flight operations. Events and circumstances exemplifying these categories will be discussed as they relate to the Dryden crash and possible reasons for the actions of the crew of Air Ontario Flight 363.

The results of this analysis suggest that the concatenation of multiple factors from each category allowed the crew to decide to take off with contaminated wings. According to this view, no single factor taken in isolation would have triggered the crew's behaviour prior to and during take-off, but in combination they provided an environment in which a serious procedural error could occur. This array of contributory influences without a single, proximal cause warrants classification of the accident as a system failure. The analysis will attempt to define these influences and their inter-relationships. Observations and suggested counter-measures will also be provided.

Figure 1. Flightcrew Environments: Factors Influencing Behaviour

Crew

Physical Environment

Organizational Environment

Regulatory Environment

RLH 11/27/90

History of the Trip. The crew reported in at Winnipeg at approximately 0630CST Monday, March 6, for a five day trip in Fokker F-28, registration CFONF, involving six legs per day ending at 1530CST. The trip schedule and crew pairings are shown in Figure 2. Captain George Morwood had flown with the two flight attendants before, but none had flown with First Officer Keith Mills. After flying the Monday, March 6 sequence, Captain Morwood was displaced Tuesday by Captain Robert Nyman and Wednesday by Captain Alfred Reichenbacher. He resumed the trip for Thursday, March 9 and Friday, March 10.

On March 10, the crew checked in at Winnipeg at approximately 0640 and discovered that the Auxiliary Power Unit (APU) was inoperative. The aircraft departed for Dryden at 0749, approximately 10 minutes late after waiting for de-icing. It was further delayed at Dryden by poor weather at Thunder Bay. At Thunder Bay the flight was refueled on the basis of a passenger load of 55. However, an additional 10 passengers were added, placing the aircraft over the computed maximum allowable gross weight for take off. After some debate over course of action, the aircraft was defueled and the additional passengers retained. The flight departed Thunder Bay 64 minutes late and arrived at Dryden 1130CST. The aircraft was refueled at Dryden with an engine running because there were no ground start facilities there. Contrary to Air Ontario policy stated in the cabin manual, passengers remained on board during refueling.

During the stop at Dryden snow was falling and accumulating on the wings. First Officer Mills commented on the radio to Kenora at 1200, "...quite puffy snow, looks like its going to be a heavy one". Shortly after beginning to taxi, a passenger asked Flight Attendant Katherine Say when the plane was going to be de-iced. The flight attendants did not inform the flightcrew of these expressed concerns about the need to de-ice.

The flight was delayed for approximately four minutes while a light aircraft landed. At 1207CST the flight was cleared to Winnipeg and at 1209 First Officer Mills transmitted that the flight was about to take off. The aircraft lifted off but never left ground effect and crashed into trees beginning 126 meters from the end of the runway. The aircraft was destroyed by impact and fire. Both pilots, one flight attendant, and twenty-one passengers were killed. Forty-four passengers and one crew member survived with injuries. The chronology for March 10 is shown in Figure 3.

Figure 2. Trip Routing March 6 - 10, 1989
Air Ontario Line for Morwood/Mills

Segments	Crew
Winnipeg-Dryden	MAR 6 - Morwood/Mills
Dryden-Thunder Bay	Say/Hartwick
Thunder Bay-Dryden	MAR 7 - Nyman/Mills
Dryden-Winnipeg	Say/Hartwick
Winnipeg-Thunder Bay	MAR 8 - Reichenbacher/Mills
Thunder Bay-Winnipeg	Say/Hartwick
	MAR 9 - Morwood/Mills
	Say/Hartwick
	MAR 10 - Morwood/Mills
	Say/Hartwick

Figure 3. Air Ontario Flights 362/363
March 10, 1989

Segment	Times	Delay
Winnipeg-Dryden	0749-0819CST	13 min
Dryden-Thunder Bay	0850-0932CST	20 min
Thunder Bay-Dryden	1104-1130EST	64 min
Dryden - crash	1203-(1211)CST	

RLH 10/24/90

I. The Regulatory Environment.

The crew of Air Ontario 363 was governed by the regulations and practices of Transport Canada. Several aspects of the current regulations provided an indirect, deleterious influence on the crew's operational environment. These allowed the development of a situation which failed to provide safeguards in this case against flawed decisions concerning landing and take-off in Dryden under adverse weather conditions. The following issues are cited as relevant to the accident.

I(a). **The failure to provide clear guidance for organizations and crews regarding the need for de-icing.** The regulatory requirement in effect at the time of the accident prohibited aircraft from commencing a flight "...when the amount of frost, snow, or ice adhering to the wings, control surfaces, or propellor of the aeroplane may adversely affect the safety of the flight". As noted in the *Commission of Inquiry into the Air Ontario Crash at Dryden Ontario Interim Report* (1989), "...there are no existing Transport Canada-approved guidelines which dispatchers or flight and ground crews may use to assist them in making a reasoned judgment as to what amount of contamination to an aircraft's lifting surfaces would adversely affect the safety of flight". In the absence of guidelines, idiosyncratic views of the degradation caused by differing amounts of contamination could prevail. There were also no formal requirements for training in the effects of icing contamination and associated phenomena such as "cold soaking", and the differential susceptibility of different aircraft types to icing effects.

I(b). **A lack of rigour in regulating and monitoring the operations of Air Ontario, Inc., following its merger and during the initiation of jet service in the F-28.** Transport Canada allowed the F-28 operation to continue passenger service for a number of months without an approved Minimum Equipment List and an accepted Aircraft Operating Manual specifying standard operating procedures. Closer monitoring of the initiation of this service would have revealed other significant operational problems including inconsistent content in manuals (i.e., different manuals in the cockpit and conflicts between cabin and cockpit manuals) and problems in weight and balance computations. It would have been especially important at this time to conduct extensive line observations of crew performance in the F-28. Testimony of Transport Canada witnesses identifies a lack of resources for the enforcement of safety regulations and monitoring of flight operations.

I(c). An audit of Air Ontario operations that was delayed and incomplete in scope. Evidence from several airline mergers that have been observed in the U.S. suggests that they create conditions which warrant increased regulatory surveillance. There are always disruptions in operational effectiveness surrounding the joining of disparate operations that call for increased efforts directed toward monitoring operations and ensuring compliance with appropriate safety standards. Strikes have also been observed to create major operational problems, even after their settlement, and to interfere with effective crew-management communications. A national audit of Air Ontario was scheduled for February, 1988. While the airworthiness, passenger safety, and dangerous goods portion of the audit were completed as scheduled, the flight operations portion was postponed until July, 1988 and again until November, 1988, when it was completed. The combination of a merger, a strike, and the introduction of a new aircraft type, would seem to have mandated an extensive audit of the operation. It is noteworthy that the audit that was conducted failed to examine the most significant operational change in the organization, the initiation of jet service in the F-28. Testimony by the leader of the audit indicates that he was inexperienced in audit procedures, was directing his first audit, and had a limited staff. The statement that examination of crew training records forms the heart of an audit certainly reflects an honest opinion. However, from the author's research experience, an alternative view can be proposed that the observable behaviour of crews in line operations is the key to understanding the level of safety and effectiveness in flight operations.

I(d). The failure to require effective training and licensing requirements for flight dispatchers and to establish regulations governing dispatch and flight following. Transport Canada had no formal requirements for the training and licensing of dispatchers and allowed a carrier such as Air Ontario to operate with a pilot self-dispatch system. While the arrangement at Air Ontario was in compliance with regulations, it practiced much less rigorous control of operations than its parent organization, Air Canada.

I(e). The lack of clear criteria for the qualifications and training of airline management, Check Airmen, and Air Carrier Inspectors. In times of rapid organizational change frequent shifts in operational conditions and practices are common as is substantial turnover in managerial positions. While organizations normally strive to maintain the highest possible level of experience and competence, in the absence of formal rules, compromises are frequent. It is suggested that more clearly defined guidelines could help organizations recognize situations

where they need outside expertise to increase the safety and effectiveness of operations. In evaluating personnel, both the extent and quality of experience can serve as indicators of whether there are sufficient qualifications to direct and evaluate operations effectively. In the case of a new operation such as the initiation of F-28 service, such determinations may be difficult for those directly involved to make.

One persistent problem in the standardization of air carrier operations is the fact that regulatory inspectors and Check Airmen monitoring line operations are normally limited to working within a single aircraft type. The implication of this is that procedural variances that develop between the aircraft fleets of an organization fail to be detected by individuals who are restricted to dealing with a single component of the organization. Several airlines are adopting the policy of having evaluators monitor crew coordination and effectiveness across aircraft types to gain insight into type differences and developing subcultures.

II. The Organizational Environment.

A number of factors surrounding the nature and operation of Air Ontario created an environment conducive to operational error. At the highest level, Air Canada, despite owning controlling interest, *failed* to require Air Ontario to operate to Air Canada standards and failed to provide resources to achieve these standards. Similarly, a number of decisions and practices at Air Ontario served to allow an operation with significant safety-related deficiencies to develop and continue. The focus of this discussion is not on faulting organizations for failing to go beyond regulatory requirements. Rather, it is to discuss the *operational impact* of the organizational setting and practices that were present at this time. The factors to be discussed have been observed to impact operations in other air carriers facing similar constraints. It should be noted, however, that organizations undergoing such transformations might not be in a position to recognize their safety implications from within.

II(a). **Lack of operational support from Air Canada.** During the period of initiation of F-28 service, Air Canada owned a seventy-five percent, controlling interest in Air Ontario which operated under shared ("AC") flight designators. Air Canada has long experience in jet transport operations and stringent requirements for dispatch and flight following. The resources of this organization would have been highly valuable in smoothing the transition to the merged carrier and initiating jet service in the F-28. According to testimony, there were

financial reasons (maintaining independent operations and pay scales) for maintaining a separation between the two carriers and there was no regulatory requirement for sharing resources and standards.

II(b). The disruptive impact of mergers and strikes. Mergers among air carriers have become increasingly frequent in recent years. In the course of our investigations, research into crew attitudes and behaviour has been conducted in several airlines which were the results of one or more mergers. As part of the research, crewmember attitudes toward management of the flightdeck are assessed using a survey instrument, the *Cockpit Management Attitudes Questionnaire (CMAQ)* (Helmreich, 1984; Gregorich, Helmreich, & Wilhelm, 1990). Attitudes regarding flightdeck management have been validated as predictors of crew performance and were derived from research implicating them as relevant in many accidents and incidents (Helmreich, Foushee, Benson, & Russini, 1986). The data show significant differences in attitudes as a function of previous organizational membership in each organization we have studied - in one case nearly a decade after a merger.[2] The results clearly indicate the existence of enduring subcultures within organizations. The issues measured by the CMAQ are shown in Appendix I. It is our premise that when cultural factors support the maintenance of differing attitudes about the appropriate conduct of flight operations, the effectiveness of flightcrew performance is likely to be compromised. Degani and Wiener (1990), in their study of normal checklist usage in air carrier operations, suggest that the stresses of merger can result in crews retaliating against management by disregarding mandated checklist procedures. The process of combining seniority lists from merging organizations also frequently results in poor relations among crewmembers from the different airlines. We have found that pejorative nicknames are often employed to label crewmembers from the opposite side of mergers.

Similarly, our data indicate that labour-management strife can have a deleterious effect on crewmembers' morale and attitudes toward their organizations. While there is no evidence to suggest that a crash has resulted directly from the impact of a strike, there is no doubt that the negative climate fostered by poor pilot-management relations is not conducive to effective team performance. In several airlines, even some years after a strike, relations among pilots and between pilots and managements remain poor.

---

2. A report on the impact of mergers with the organizations involved de-identified is under preparation for release in 1991.

Evidence from Air Ontario personnel supports the existence of differing sub-cultures in Austin Airways and Air Ontario with occasional categorization of former Austin Airways personnel as "Bush Pilots" who could be assumed to have informal, operational practices at variance with those of former Air Ontario flightcrews. The F-28 program was disproportionately managed by former Austin Airways personnel who could have influenced the operation in the direction of Austin Airways norms. The dominance of Air Ontario flight operations management by Austin Airways personnel also created ill-will among some former Air Ontario pilots. Morale problems and poor relations among crewmembers can interfere with effective teamwork and crew coordination.

One finding from our research into Crew Resource Management training is that it can serve to reduce differences in attitudes about flightdeck management between subcultures and between crew positions. Air Ontario management had looked into such training. Captain Robert Nyman, Director of Flight Operations, testified that the *CRM* courses available did not appear to fit the Air Ontario operation. Both the Chief Pilot and Chief Training Pilot attended a *CRM* course presented in Toronto by a major airline and reported it to be both of limited value and expensive.

II(c). **High personnel turnover following the merger.** In the period between the merger of the two carriers and the accident, there were substantial changes in personnel. Part of the operation was sold and the size of the combined organization was reduced from eight hundred to approximately six hundred. There was also turnover in two critical areas of management, Vice President of Flight Operations and Director of Flight Operations. Similarly, the position of Safety Officer was filled, became vacant due to a resignation, and subsequently re-filled. The lack of continuity in management could have impeded needed supervision of operational issues such as the introduction of a new aircraft type and standardization of operations following the merger. Programs such as *CRM* cannot alleviate operational problems associated with a lack of management stability and consistent direction.

II(d). **Lack of organizational experience in jet operations.** Air Ontario as an organization did not have experience in jet transport operations. At the time of the introduction of the F-28, efforts were made to acquire outside expertise in management and representations to this effect were made to Transport Canada. Ultimately, Captain Claude Castonguay, who had substantial jet transport operational experience (including in the F-28) was hired, but resigned after one

month. Six months later he was called back to perform two line indoctrinations. In his letter of resignation, Captain Castonguay stated, "So much as I would like to keep working to establish your FK28 program, I have concluded that I cannot function in my duties as Check Pilot when I do not get the support I need." No one was subsequently hired from outside the organization to fill this role, leaving Air Ontario to manage the process with internal resources.

II(e). Deficiencies in Systems Operation Control (SOC) practices. Air Ontario operated with a dispatching system that consisted partly of full flight following and partly of pilot self dispatch. Although this system was permitted by current Transport Canada regulations, it failed to provide crews with the same level of support and resources given crews in the parent organization, Air Canada.

In the absence of regulations mandating formal training and licensing for dispatchers, Air Ontario primarily employed on the job training for dispatch personnel. For the introduction of the F-28, brief training in the operation of this type of aircraft was provided only for duty managers. In contrast, Air Canada provides its dispatchers with more formal training and operational guidelines - including rules that would forbid dispatching an aircraft with an inoperative APU into a station such as Dryden with no ground start capabilities. That the Air Ontario system was deficient is indicated by observed errors in flight releases such as fuel load calculations using wrong parameters. Indeed, the flight release for CFONF contained errors on the day of the accident.

II(f). Lack of standard operating procedures and manuals for the F-28. Service was initiated without a specific Air Ontario operating manual for the F-28. There was also no approved Minimum Equipment List for some months after passenger service began. There were inconsistencies between cockpit and cabin manuals provided crews. For example, the cabin manual required passenger disembarkation for refueling with an engine running while there was no parallel rule in the cockpit manual. Crews thus lacked formal organizational guidelines either from resources available on the flightdeck or from SOC.

II(g). Inconsistencies/deficiencies in training F-28 crewmembers. Initial training of F-28 crewmembers, including both ground school and simulator training, was contracted with Piedmont Airlines. Piedmont itself was involved in a merger with USAir which decided to achieve standardization of the merged operation by shifting all former Piedmont personnel to

USAir procedures and manuals. There were several implications of this organizational environment for Air Ontario crews. The first was that some received training from the Piedmont F-28 manual while those training later worked with the USAir manual. Since Air Ontario had not developed its own manuals, some individuals returned with the Piedmont Manual and others with that of USAir. While Air Ontario stated that the Piedmont Manual was its standard, this was not clearly communicated to crews and no efforts were made to provide all crews with the same manual. Air Ontario also failed to receive updates to the manuals it was using. Although the Fokker Aircraft Flight Manual was carried in the aircraft, there was a lack of training involving this manual and there were discrepancies between the Fokker and Piedmont manuals, for example in computing corrections for runway contamination. A second result of the Piedmont merger was a scarcity of simulator time for completing the training of Air Ontario crews. Because of this, a number of pilots were trained in the aircraft by newly qualified Air Ontario pilots rather than in the Piedmont simulator. Even with highly experienced instructors, there is an industry consensus that simulator training provides broader and more effective training.

Crewmembers surveyed by the Safety Officer following the accident generally reported their Line Indoctrination at Air Ontario to be "fair" in quality. One deficiency noted was a failure to define clearly the duties of the pilot flying and the pilot not flying.

II(h). Leadership of the F-28 program. Captain Joseph Deluce was selected as Project Manager and Chief Pilot for the F-28 and Convair 580. Captain Deluce had numerous responsibilities including line flying during the strike which preceded aircraft delivery and conducting training and line indoctrination in the F-28 for new crewmembers. He also carried Chief Pilot responsibilities for both fleets. Captain Deluce had limited operational experience in both the F-28 and the Convair 580. Airlines typically choose individuals with substantial experience in an aircraft type to be Chief Pilot.

One incident that may have had a significant impact on crewmember attitudes was the removal of an F-28 crew from a line trip to meet with the Chief Pilot for allegedly writing up too many maintenance discrepancies on the aircraft. The perception of other crewmembers of such an event would likely be of a lack of leader support for optimal operating conditions and a strong pressure to operate at all costs.

II(i). **The informal culture at Air Ontario.** One of the more striking findings to emerge from our research into flightcrew behaviour has been the discovery of significant differences between aircraft fleets within organizations in attitudes regarding flightdeck management and in ratings of behaviour in both line operations and Line Oriented Flight Training conducted in the simulator (Helmreich, Chidester, Foushee, Gregorich, and Wilhelm, 1990; Helmreich, 1990). These have been observed even in organizations with a strong commitment to standardization and form one of the justifications for implementing CRM training to develop common standards and values. Informal subcultures frequently tolerate or encourage practices which are at variance with organizational policies or regulatory standards.

Conditions at Air Ontario during the period of initiation of F-28 service would appear to have been conducive to the development of a non-standard subculture. These include previously noted lax regulatory supervision, high management turnover, the self-dispatch system with SOC personnel who lacked knowledge of the F-28 and were generally inexperienced, and the lack of clearly specified and enforced standard operating procedures. The reputation of being "Bush pilots" was attached to former Austin Airways pilots who formed a large percentage of the leadership of the F-28 program. Evidence of procedural variance is found in several reported practices. An example is writing mechanical problems or *snags* on paper to be passed to relieving crews instead of entering them in the aircraft logbook, thus permitting deferral of maintenance and avoiding the grounding of aircraft - a practice in violation of Transport Canada regulations. Others include the so-called "eighty knot check", a visual examination of the wing surfaces during take-off to ensure that contamination had blown off prior to rotation, and the practice of making overweight landings. A related fact is that Captain Deluce, the Chief Pilot, had been involved in at least two earlier, reported incidents involving take-offs with snow or ice contaminated surfaces. These suggest that the culture, at least among former Austin Airways crewmembers, may have allowed crews considerable leeway in making decisions about whether to take-off with surface contamination - a practice that was not proscribed by current Transport Canada regulations. It seems likely that the message communicated during training, and in the Fokker manual for the F-28, that *no* snow, ice, or frost should be present on wings may have been discounted to some extent by crews who had successfully operated (albeit in different types of aircraft) with some degree of contamination. Additionally, the Check Airmen appointed for the F-28 fleet were inexperienced in the aircraft and with jet operations and may not have been in a strong position to impose standards.

II(j). Maintenance problems with the F-28. A number of maintenance problems were encountered with the F-28. These were exacerbated by a lack of familiarity with the aircraft on the part of maintenance personnel and a shortage of spare parts. The Journey Log for the accident aircraft, CFONF, listed a number of problems between June and December, 1988, many deferred for extended periods. These included earlier problems with the Auxiliary Power Unit (APU) in August and October of 1988. On several occasions in 1989 the cabin filled with smoke with passengers aboard.

On the day of the accident, CFONF was dispatched with an inoperative APU and had three other deferred maintenance items including roll and yaw in the autopilot and a fuel gauge reading intermittently. Other discrepancies that were brought to the attention of the cockpit crew by the cabin crew prior to the first flight on March 10 included inoperative exit lights, dim cabin emergency floor lighting, missing oxygen masks, and problems closing the main door because of a missing clip.

II(k). Flight Attendant training. The practice of Flight Attendant training at Air Ontario discouraged flight attendants bringing operational issues to the attention of the flightdeck and questioning operations. Training stressed the competence of pilots and fostered a position of total reliance on the cockpit crew. Two examples of the results of this separation of cabin and cockpit can be seen on the day of the accident. These included the hot refueling of the aircraft in Dryden at variance with the cabin manual and the failure of the flight attendants to relay passenger concerns about de-icing to the flightdeck. In contrast to this lack of communication, the concepts taught in Crew Resource Management stress the importance of complete information exchange between the flightdeck and the cabin.

III. The Physical Environment

A number of negative factors were present in the operating environment facing the crew on March 10. These included an aircraft with mechanical problems including the inoperative APU and poor weather that had created an early delay for de-icing in Winnipeg and a subsequent hold in Dryden because of weather at Thunder Bay. Indeed the weather was unsettled in the entire region that day necessitating non-standard alternates at a greater than normal distance, thus increasing dispatch fuel requirements. There was also a change in the

Human Factors of the Air Ontario Crash 15

passenger manifest in Thunder Bay increasing the passenger load and necessitating defueling to meet weight restrictions for take off and landing at Dryden. At Dryden, there was no ground start equipment making it necessary to leave an engine running and forcing the Captain to hot refuel. Finally, snow was falling during the station stop in Dryden.

IV. The Crew Environment

A number of factors that were present in the crew environment of the accident flight have been identified through research in other organizations as significant stressors that can serve to reduce flightcrew effectiveness. These include both situational factors surrounding the operation and characteristics of individual crewmembers.

<u>Situational Factors</u>

IV(a). Crewmembers' unfamiliarity with the aircraft and their training experience. Both Captain Morwood and First Officer Mills were new to the F-28 and had fewer that 100 hours of operational experience in this aircraft type. After completion of ground and simulator training at Piedmont, Captain Morwood returned to flying the Convair 580 and his line transition to the F-28 was further delayed by the Air Ontario strike. First Officer Mills received his training in the aircraft rather than the simulator. For Captain Morwood, the delay in reinforcing his training on the line could have rendered him less effective initially. For First Officer Mills, the lack of opportunity to acquire skills and confidence in the simulator could have had a similar effect.

There is growing concern in the industry, based on several recent accidents in the U.S., about the safety implications of pairing crewmembers new to an aircraft soon after completion of line indoctrination, particularly under adverse weather conditions. There is obviously a significant learning curve in becoming comfortable with a new aircraft, particularly one substantially different from prior equipment. One of the basic premises of the crew concept of flight operations is that crewmembers support each other in service of the goal of safe and effective flight management. When *both* crewmembers are still acquiring familiarity with the aircraft, the margin of safety is reduced. Efforts are underway in the U.S. to set requirements for operational experience after initial training and to mandate scheduling of newly qualified crewmembers with those having substantial experience in the aircraft type.

IV(b). **Organizational background and lack of experience working together.** Several additional issues made the pairing of Captain Morwood and First Officer Mills potentially stressful. One was the fact that Morwood came from the Air Ontario organization while Mills' background was with Austin Airways. Additionally, both Morwood and Mills had been operating as Captains in their prior aircraft. Individuals accustomed to acting as pilot in command have been noted to function less effectively when paired. These factors, combined with the lack of enforced standard operating procedures (including the noted failure to specify pilot flying - pilot not flying duties in the F-28 line indoctrination), could well have reduced the effectiveness of this crew as a *team*.

This trip was also the first time that the crew had operated together and Captain Morwood was displaced for two days. Experimental simulation research conducted by NASA-Ames Research Center (Foushee, Lauber, Baetge, & Acomb, 1986) found that crew coordination and effectiveness is increased by the simple fact of working together as a team. In this study, crews who were fatigued (from a three day, multi-segment line trip) or not fatigued (coming from days off) flew an experimental simulation involving bad weather and mechanical malfunctions. The purpose of the study was to explore the effects of operationally induced fatigue on performance. The most surprising and serendipitous finding from the study was that *crews who had flown together previously performed better than crews paired for the first time whether or not they were fatigued!*

IV(c). **Delays and stresses imposed by the operating environment.** The initial segment of March 10 was delayed because of a need to de-ice the aircraft in Winnipeg. As noted, there were also major (APU) and minor mechanical problems with CFONF. In a radio communication, Captain Morwood commented "...everything else has gone wrong today." After the first leg, an additional delay was experienced because of poor weather in Thunder Bay. On arrival at Thunder Bay, additional passengers were taken aboard from a cancelled flight after refueling, making it necessary to remove fuel to meet weight requirements and causing it to depart more than an hour behind schedule. On arrival at Dryden, it was necessary to refuel with an engine running because of the lack of ground start capability. At the same time, snow was falling. As the Captain had fewer than 100 hours in the aircraft type, he required a higher RVR than a more experienced pilot would have. He may (or should have been) concerned that visibility would become below his minimum requirement prior to departure. The flight was

already running late and a number of passengers had tight connections in Winnipeg. A final delay of approximately four minutes was incurred to await the arrival of a Cessna 150 which was experiencing difficulties because of the poor weather.

Personal Factors

IV(d). Captain George Morwood. Captain George Morwood was 52 years old and had more than 24,000 hours flying time. His operational experience was entirely in Canadian operations. He had worked for the predecessor of Air Ontario and had served as a Check Pilot and Chief Pilot for the Convair 580 at Air Ontario. He trained on the F-28 at Piedmont Airlines in January and February of 1988, but did not begin line flying in the F-28 until December, 1988. At the time of the crash he had 81 hours in the aircraft. His jet experience included approximately 600 hours in the Gulfstream G-2.

According to his record and peer reports, Morwood was above average in ability. He had shown concern with safety issues in his prior management positions and was aware of icing effects, including those caused by differential temperatures of fuel and ambient air. According to his record, he had delayed or cancelled flights because of icing. Probably based on his long experience as a Check Pilot, and Chief Pilot, Captain Morwood was reported to be in the habit of operating as an "instructor" while flying. In theory, this characteristic could be an annoyance to highly experienced junior crewmembers such as First Officer Mills who had considerable experience flying as a Captain.

Captain Morwood was reported to have a strong commitment to on time operations and a high level of concern for his passengers. There were a number of delayed passengers with connecting flights in Winnipeg on March 10. In addition, Morwood had a scheduled personal trip immediately following his last flight segment. These factors could have heightened motivation to complete the scheduled flying.

IV(e). First Officer Keith Mills. Keith Mills was 35 years old and had more than 10,000 hours flight experience. He began flying for Austin Airways as DHC6 Co-pilot in 1979 and became a Captain on the Hawker-Siddely HS748 in February 1988. He completed F-28 ground training in January, 1989 and aircraft training at Air Ontario. At the time of the crash he had 65 hours in the F-28 and approximately 3,500 jet hours in the Cessna Citation.

Mills had some record of difficulties with "stick and rudder" aspects of flying, but he met all regulatory requirements for competence. His failure to receive simulator training in the F-28 and Morwood's long experience and reputation as a perpetual "instructor" may have made Mills somewhat reluctant to practice optimal crew resource management concepts and to provide operational suggestions to Captain Morwood. Mills also had a scheduled personal trip at the end of his last flight segment.

V. The Situation of March 10

The picture that emerges from examination of the regulatory and organizational environments in which this crew was operating is one of an array of factors which served to undermine their effectiveness and to increase the stress of flight operations. None of these factors taken alone is likely to *cause* an accident - as evidenced by the fact that the F-28 was operated without incident or accident for months prior to March 10. However, when these factors were combined with the particular conditions of the physical environment (the inoperative APU, lack of facilities at Dryden, weather conditions, pressures to take off, etc.) the margin of safety was clearly reduced. Factors in the crew environment such as the operational unfamiliarity of the crew with each other and the aircraft doubtless exacerbated the situation.

V(a). Environmental Stressors. In considering the crew's actions on March 10, the environmental factors that may have been perceived as stressors should be reviewed. Psychological stress can serve to reduce individual and team effectiveness especially in the areas of interpersonal communications and coordination and decision making. Relevant classes of stressors include time pressure, and frustrations associated with inadequate resources and sub-optimal operating conditions. Captain Morwood and First Officer Mills faced a number of these conditions throughout their day. It may provide a useful context for the situation at Dryden to summarize them chronologically.

> 1. On accepting the aircraft in Winnipeg, the APU was found to be unserviceable. As noted previously, there were three additional, deferred maintenance items and other items in the cabin reported by the flight attendants.

2. The marginal weather throughout the region forced an initial delay for de-icing and the adoption of a distant alternate with a consequent requirement to carry additional fuel.

3. It was necessary to plan for "hot refueling" in Dryden because an engine would have to be left running. This may have triggered additional concerns because of company policy (and a stated requirement in the Fokker Publication on Cold Weather Operation) that the aircraft could not be de-iced with the engines running. However, it is not clear whether Captain Morwood had received a company memorandum about de-icing policy for the F-28.

4. SOC dispatched the flight with a clearly erroneous Flight Release. Testimony from pilot witnesses indicated little confidence in·the SOC operation. It may have been a source of frustration or concern for the crew on this date to have been dispatched with no explicit accommodation for the unserviceable APU under adverse weather conditions.

5. Both crewmembers had fewer than 100 hours in the F-28. In addition to the stress imposed by lack of familiarity with the aircraft, Captain Morwood had more restrictive limits for visibility because of his low experience level in type. This could have added to his concerns about getting in and out of stations with poor weather.

6. The flight was delayed on its initial stop in Dryden because Thunder Bay weather was below landing limits.

7. There was considerable confusion surrounding the loading of additional passengers in Thunder Bay and the need to defuel the aircraft to meet weight restrictions. The crew had to communicate with SOC through a radio relay by Air Canada since there was no direct communications link from the flightdeck. This situation increased the delay of the flight to more than an hour on departure from Thunder Bay.

8. The fire trucks required for hot refueling were not in position on the aircraft's arrival at Dryden. This factor added to the accumulating delay and probable frustration of the crew over the disruptions surrounding the day's operations.

9. The date of the accident was the beginning of the March school break. There were many passengers with connections to make. The crew expressed concern over this in radio communications.

10. As the flight landed in Dryden, it began to snow, with the fall increasing during the stop. While the reported visibility was above minima, the actual visibility may have been at or below the Captain's minima at the time of take off.

While none of these issues alone can be considered an overwhelming stressor, taken in concert they indicate a taxing operational environment.

From the perspective of hindsight, it seems likely that a change in any one of a number of conditions might have provided the extra margin of safety needed. For example, a more stringently regulated and managed dispatch system would probably have precluded operations into Dryden on the return from Thunder Bay. An effective training program in Crew Resource Management could have resulted in a review of the operational situation involving both pilots and led to a critical evaluation of the decision to take off without de-icing. Similarly, training that encouraged cabin crewmembers to share operational concerns with flightcrews and pilots to listen to such concerns might also have triggered further consideration of the implications of accumulating contamination on the aircraft.

The issues discussed in preceding sections have an empirical basis as significant influences on flightcrew behaviour, but a weighting of each as a determinant of the outcome of Flight 363 cannot be made from the available record. Nor can the decision processes surrounding the take off from Dryden be specified in the absence of Cockpit Voice Recorder evidence. However, it is possible to envision a likely scenario for the crew's actions based on consideration of the four sets of determinants of crew behaviour described previously. It must be stressed that this represents a *post hoc* reconstruction that may be erroneous in part or whole.

VI. A Scenario for Crew Decision Making in Dryden

In retrospect, the decision to operate into Dryden on the return from Thunder Bay without a functioning APU was questionable, but understandable. The initial stop in Dryden was

uneventful, despite a delay because of weather conditions in Thunder Bay. Although the forecast for the region showed a risk of freezing precipitation, on approach to Dryden conditions were VFR. Making the stop would minimize passenger disruption. However, once on the ground in Dryden, the weather and operational situation deteriorated. At the same time, the crew had conducted a day of flying that must be considered stressful because of the mechanical problems with CFONF, increasing delays, the changed passenger load resulting in additional delay, and the crew's relative inexperience in F-28 operations. While on the ground in Dryden, the following issues faced the Crew:

1. Considerations surrounding refueling with an engine running

2. Pressures to get passengers to Winnipeg for connections

3. The inconvenience of stranding passengers in Dryden with limited facilities

4. Logistic problems surrounding de-icing with an unserviceable APU and no ground start capability

5. The need to import ground start equipment if both engines were to be shut down and consequent long delay

6. Snowfall during the stop causing both aircraft and runway contamination and deteriorating visibility that might be below minimums for the Captain

7. The implications of contamination on the aircraft

8. The implications of contamination on the runway (including conflict between Fokker and Piedmont manuals in this area)

9. The additional delay posed by the arrival of the Cessna 150

10. Planned personal trips which would be impacted by long delay in Dryden

One of the effects of psychological stress (including that imposed by time pressure) is an inability to process multiple sources of information as effectively as under more relaxed conditions. As listed in the previous section, a case can be made for the fact that the crew, and especially Captain Morwood as pilot in command, was under considerable stress by the time the flight stopped for the second time in Dryden. It may also be inferred that the operating standards of Air Ontario and the absence of formal training and organizational endorsement of

crew coordination concepts, would have tended to preclude rigorous *crew* evaluation of the operational situation.

Surrounding the decision to take off are several critical questions. One is whether the crew was aware of the safety implications of the accumulating snow. As noted, Captain Morwood had a history of concern and awareness of icing risks. He had delayed the initial flight of the day for de-icing. Testimony by a representative of Transport Canada included an incident when Captain Morwood insisted on going back to the gate in the Convair 580 for de-icing even though the Inspector had remarked that the snow seemed dry and the propellers were blowing it off the wings. Also, a 1983 letter from Air Ontario management endorsing the Captain's authority to de-ice when circumstances require was found in Captain Morwood's flight bag at the accident scene.

A second question is whether the crew was aware of the accumulation of snow on the wings at Dryden. The Captain visited the terminal during the stop in his shirt-sleeves and would have been aware of snow falling. During a conversation with SOC during this period, he commented to Ms. Mary Ward that the weather at Dryden was "going down." The cockpit crew also had the ability to observe the wings from the cockpit and the testimony of informed passengers indicated that snow was accumulating visibly there. It seems inconceivable that the crew would have been unaware of snow on the wings. The fact that Morwood inquired of the station manager at Dryden about de-icing facilities there also suggests awareness.

Despite his knowledge of icing and probable awareness of the snow gathering on the wings, it seems most likely that Captain Morwood weighed costs and benefits surrounding the issues listed above and concluded that the best course of action would be to take off expeditiously. Several things may have influenced this decision. One is that because of the multiple stressors involved in the situation and his focus on completing the trip, he failed to weigh the risks as heavily as the benefits from getting out before the weather deteriorated further. The ambiguity of regulations regarding icing could also have influenced his decision. Although it was noted that emphasis was placed in training at Piedmont on taking off with no wing contamination, he may not have felt that the issue was as serious in the F-28 as other aircraft given higher rotation speeds and additional opportunity to blow the accumulation off during take-off roll.

The role of First Officer Mills in this decision is, of course, indeterminate. However, based on considerations regarding experience and status it is not likely that he was heavily involved by Captain Morwood.

There was probably a misperception about the nature of the contamination as it relates to "cold soaking", the situation when portions of an aircraft are at a temperature below the ambient temperature because of having descended from altitudes where ambient air is colder or from heat transfer to areas containing fuel colder than the ambient temperature. Pilots interviewed by the author were primarily concerned with heat transfer at high altitudes and less aware of the phenomenon occurring on the ground due to cold fuel in wing tanks. The Piedmont manual which was used at Air Ontario addresses this phenomenon in a section on Cold-Weather Operations. It states:

> "When the tanks contain sufficient fuel of sub zero temperatures as may be the case after long flights at very low ambient temperature, water condensation or rain will freeze on the wing upper surfaces during the ground stop forming a smooth, hardly visible ice coating.
> During take off this ice may break away and at the moment of rotation enter the engine causing compressor stall and/or engine damage." (Piedmont F-28 Manual, Exhibit 307 3A-24-1)

A decision could well have been reached that the snow would blow off, given the large fluffy flakes coming down and the lack of accumulation on the tarmac surrounding the aircraft. The possibility that a layer of rough ice caused by cold soaking extended to the leading edge was probably not entertained by either Morwood or Mills.

Psychological pressure to complete the trip as scheduled, commonly referred to as "get home-itis", cannot be ruled out. Captain Morwood was clearly concerned about holiday passengers with connecting flights in Winnipeg and both he and Mills had personal trips planned after completion of the trip. Had the flight been cancelled in Dryden, it would have been necessary to fly in ground start equipment causing a lengthy delay and disruption of crew and passenger plans. Once on the ground in Dryden, the implications of a long delay doubtless had a subtle influence on the decision process.

A final chance to re-evaluate the situation was probably missed when the flight took its final delay for the landing of the Cessna 150. However, the accumulation of stress and frustration surrounding the day's operations had probably reduced the crew's effectiveness and decision making capabilities by this time.

While the Captain as Pilot in Command must bear responsibility for the decisions to land and take off in Dryden on the day in question, it seems equally clear that the aviation system failed him at the critical moment by not providing effective management, guidelines, and procedures that would assist him in such decisions.

In the following section, observations and suggested corrective measures are offered in the hope that they may provide greater resources for future crews who find themselves in stressful situations trying to evaluate multiple pieces of information and having to make choices among unpleasant, alternative courses of action.

VII. Observations

The following are corrective measures that could be taken to increase system safety and effectiveness. It is noted that the first recommendation of the Commission to Transport Canada was to remove the ambiguity from regulations surrounding wing contamination and that this was favorably received.

VII(a). **Monitoring of air carrier operations.** It would be valuable to establish guidelines for air carrier management in terms of qualifications needed for effective job performance. A similar set of standards could be established for Air Carrier Inspectors and others involved in surveillance of airline operations. Requirements for inspectors and check airmen could include training in the evaluation of human factors aspects of flight operations.

Training in the conduct of air carrier audits and requirements for qualification of audits could be strengthened. In particular, emphasis in audits should be on observation of line operations evaluating both human factors and technical proficiency.

Strengthened requirements for flight dispatch and the training of dispatchers should be developed for all airline operations.

VII(b). Winter operations. Yearly training and review of Winter operations procedures should be conducted. This should include not only general issues regarding icing, cold soaking, and de-icing procedures, but also information specific to particular aircraft types as needed.

VII(c). Common standards for major airlines and their feeder operations. Airlines operating under a common designator should maintain the same standards of training, dispatching, and performance. The need is probably greater for effective training and organizational support in smaller carriers that operate into secondary stations with fewer facilities. In many cases, pilots in regional carriers may have had less experience and less formal training. The resources of the major carriers could be highly beneficial for the safety and effectiveness of these regional carriers and could allow them to establish levels of training that they could not effect independently.

VII(d). Formal training in Crew Resource Management for all crewmembers. Accumulating experience in the U.S. and many other countries has demonstrated the importance of *CRM* training. The U.S. has encouraged this training through an Advisory Circular and it is a requirement for operating under a new Special Federal Aviation Regulation called the *Advanced Qualification Program*. Efforts are underway in the U.S. to initiate a regulatory requirement mandating *CRM* training for all air carriers operating under Parts 121 and 135 of the Federal Aviation Regulations. A copy of the *CRM Advisory Circular* and a proposed revision drafted by the author as part of a committee of the Air Transport Association are included as Appendix II and II-A. A premise of the Advisory Circular, supported by empirical research, is that a single training experience in *CRM* concepts is insufficient to provide long term changes in crew coordination and performance. Such training must be accompanied by opportunities to practice the concepts and to receive reinforcement for their use. Check Airmen and Instructors have been identified as critical to this endeavour and should be given training in the evaluation and reinforcement of human factors issues as an extension of their traditional role (Helmreich, Chidester, Foushee, Gregorich, & Wilhelm, 1989). This type of evaluation and reinforcement can and should occur both in ground training and during line checks and should center on clearly understandable exemplars of effective and ineffective performance that have come to be called *behavioural markers* of crew performance. Examples of these and a form for evaluation of crew performance (the *CRM/LOS Checklist*) are included as Appendix

III. There is a growing belief that this training can be effectively extended to cabin crews and other operational personnel. One can speculate that had both the flight attendants and cockpit crew completed *CRM* training and accepted its concepts, there might have been an exchange of information that would have precluded the take off.

VII(e). Crew oriented training and evaluation. The historical emphasis in aviation has been on individual, technical proficiency and both training and evaluation have centered on the performance of the individual pilot. However, data from accidents and incidents suggest that the *CRM*-related issues isolated in accidents and incidents involve failures of *crews* to operate effectively as *teams*. Many airlines and military units have reacted to this by increasing the emphasis in training and checking on crew-level performance. In checking line operations this is accomplished by including the performance of the crew as a unit as part of the evaluation and debriefing (for example, using the *CRM/LOS Checklist* as a template for evaluation).

Another approach being used increasingly (and required in the U.S. for carriers that will operate under the *Advanced Qualification Program*) is the use of *Line Oriented Flight Training (LOFT)* which involves complete crews training in simulators under realistic operating conditions including flight releases, air traffic communications, and facing a variety of operational problems including inflight emergencies. A key to the success of this training is that it is *non-jeopardy* meaning that crews are allowed to experiment with a variety of behaviours and approaches without placing their licenses at risk. Events are allowed to proceed without intervention by the Instructor and are usually recorded on videotape for subsequent review and debriefing. In its early development, *LOFT* required access to high fidelity simulators placing this form of training out of the reach of many organizations, especially regional and commuter airlines. However, recent research and theorizing (Franz, Prince, Salas, & Law, 1990; Helmreich, Kello, Chidester, Wilhelm, & Gregorich, 1990; Helmreich, Wilhelm, & Gregorich, 1988) suggests that low fidelity simulators and training devices may provide excellent settings for training in crew coordination and should make the technique available to almost all organizations.

VII(f). Establishment of a Safety Office in all air carriers. In addition to regulatory monitoring of air carriers, an independent Safety Office can serve an important function in isolating potential threats to safety. A Safety Officer with direct access to top management is in a position to initiate corrective action when threats to safety are uncovered. In addition to

training in investigative techniques, training in human factors, database management, and analysis would also be highly desirable for Safety Officers and their staffs.

References

Degani, A., & Wiener, E.L. (1990). *Human factors of flight-deck checklists: The normal checklist* (NASA contract report 177549). Moffett Field, CA: NASA Ames Research Center.

Foushee, H.C., & Helmreich, R.L. (1988). Group interactions and flightcrew performance. In E. Wiener & J. Nagel (Eds.), *Human factors in modern aviation*, (pp. 189-227). New York: Academic Press.

Foushee, H.C., Lauber, J.K., Baetge, N.M., & Acomb, D.B. (1986) *Crew factors in flight operations III: The operational significance of exposure to short-haul air transport operations*. Moffett Field, CA, U.S.: NASA-Ames Research Center, TM 88322.

Franz, T.M., Prince, C., Salas, E., & Law, J.R. (1990). Low fidelity flight simulation: Applications for aircrew coordination training. in press.

Gregorich, S.E., Helmreich, R.L., & Wilhelm, J.A. (1990). The structure of Cockpit Management Attitudes. *Journal of Applied Psychology, 75*, 682-690.

Helmreich, R.L. (1984). Cockpit management attitudes. *Human Factors, 26*, 583-589.

Helmreich, R.L. (1990). *Studying flightcrew interaction: The intersection of basic and applied research.* Talk presented at the dedication of the NASA-Ames Research Center Human Performance Research Laboratory. Moffett Field, CA.

Helmreich, R.L. (1991). The long and short term impact of Crew Resource Management training (pp. 81-83) In *Proceedings of the AIAA/NASA/FAA/HFS Conference: Challenges in Aviation Human Factors: The National Plan.* Vienna, VA.

Helmreich, R.L., Chidester, T.R., Foushee, H.C., Gregorich, S.E., & Wilhelm, J.A. (1989). *Critical issues in implementing and reinforcing Cockpit Resource Management Training.* Austin, NASA/UT Technical Report 89-5.

Helmreich, R.L, Chidester, T.R., Foushee, H.C, Gregorich, S.E. & Wilhelm, J.A. (1990, May). How effective is Cockpit Resource Management Training? Issues in evaluating the impact of programs to enhance crew coordination. *Flight Safety Digest,* 1-17. Arlington, VA: Flight Safety Foundation.

Helmreich, R.L., Foushee, H.C., Benson, R., & Russini, W. (1986) Cockpit resource management: Exploring the attitude-performance linkage. *Aviation, Space and Environmental Medicine, 57,* 1198-1200.

Helmreich, R.L., Kello, J.E., Chidester, T.R., Wilhelm, J.A. & Gregorich, S.E. (1990) Maximizing the operational impact of Line Oriented Flight Training (LOFT): Lessons from initial observations. NASA/UT Technical Report 90-1.

Helmreich, R.L. & Wilhelm, J.A. (1990).   Determinants of flightcrew behavior.   In *Proceedings of the International Civil Aviation Organization Human Factors Seminar (A-276 - A-286).* Leningrad, USSR.

Helmreich, R.L., Wilhelm, J.A., & Gregorich, S.E. (1988) Notes on the concept of LOFT: An agenda for research. NASA/The University of Texas at Austin Technical Report 88-1.

Helmreich, R.L., Wilhelm, J.A., Gregorich, S.E., & Chidester, T.R. (1990) Preliminary results from the evaluation of Cockpit Resource Management Training: Performance ratings of flightcrews. *Aviation, Space, and Environmental Medicine, 61,* 576-579.

FINAL REPORT
CONTENTS

VOLUME I

VOLUME II

VOLUME III

Commission of
Inquiry into the
Air Ontario Crash
at Dryden, Ontario

Commission d'enquête
sur l'écrasement d'un
avion d'Air Ontario
à Dryden (Ontario)